Title

High-throughput screening and chemoproteomic approaches to identify procaspase inhibitors

Author

Castellon, Jose Omar

Publication Date

2024

Peer reviewed|Thesis/dissertation

UNIVERSITY OF CALIFORNIA

Los Angeles

High-throughput screening and chemoproteomic approaches to identify procaspase inhibitors

A dissertation submitted in partial satisfaction of the requirements for the degree Doctor of Philosophy in Molecular Biology

by

Jose Omar Castellon

2024

ABSTRACT OF THE DISSERTATION

High-throughput screening and chemoproteomic approaches

to identify procaspase inhibitors

by

Jose Omar Castellon

Doctor of Philosophy in Molecular Biology

University of California, Los Angeles, 2024

Professor Keriann M. Backus, Chair

Caspases are a highly conserved family of cysteine-aspartyl endoproteases known for their essential roles in regulating apoptosis, inflammation, cell differentiation, and proliferation. Aside from the canonical roles in apoptosis, their functions in diverse cell functions and diseases, including neurodegenerative disease, autoimmune disorders, and cancers, remain poorly defined. Studying caspases is very difficult as they have complex activation mechanisms. Most caspases exist as inactive proenzymes. There are multiple caspase isoforms, some of which have redundant functions. Additionally, they behave differently in living cells and tissues, rendering in vitro assays ineffective, and are involved in crosstalk with other cellular processes such as autophagy and immune responses. Due to these challenges, new approaches can elucidate the biological function of specific caspases. Complementary to genetic approaches, small molecule inhibitors have emerged as useful tools for modulating caspase activity. However,

achieving high selectivity remains a central challenge for caspase-directed inhibitor development efforts due to all twelve human caspases' high sequence and structure homology. Here, using a chemoproteomics and high-throughput screening (HTS) approach, I identified lead compounds that selectively label and inhibit procaspase-2 and identified new pan-caspase reactive inhibitors. First, using a chemical-proteomic platform termed isoTOP-ABPP, I identified a highly reactive non-catalytic cysteine residue, C370, located near the active site of caspase-2. I assayed a panel of cysteine reactive electrophiles using an engineered TEV-cleavable caspase-2 construct to validate the hits against pro-caspase-2 activity. I found a selective pro-caspase-2 inhibitor that targets the non-catalytic cysteine residue and binds the monomeric form of the enzyme. I also confirmed target engagement using cellular thermal shift assays (CETSA). Next, I identified a group of caspase inhibitors using a high-throughput screening assay. From a screen of approximately 120,000 compounds, I found pifithrin-μ (PFTμ), a known p53 inhibitor, as a caspase reactive covalent inhibitor and interesting scaffold molecule. From that same group of compounds, I found that the decomposed product of compound SO265 was driving caspase inhibition in my initial screen. Target engagement was also confirmed for both compounds using CETSA. I found that PFTμ and the other pan-caspase reactive electrophiles could protect Jurkat cells from Fas ligand and staurosporine-mediated apoptosis. This study demonstrates the potential of chemoproteomics and high-throughput approaches to help identify selective caspase inhibitors.

The dissertation of Jose Omar Castellon is approved.

Robert Damoiseaux

Melody Man Hing Li

Robert Thompson Clubb

Jorge Z Torres

Keriann Marie Backus, Committee Chair

University of California, Los Angeles

2024

Table of Contents

LIST OF FIGURES

Chapter 2:

Chapter 3:

ACKNOWLEDGEMENTS

I would like to thank all those who helped me complete this research. First, I want to thank Dr. Keriann M. Backus, whose support, encouragement, and mentorship have been invaluable in shaping my research and helping me grow as an academic. I truly appreciate the time Keri has invested in my development and the insightful feedback she provided along the way. The other members of my committee – Dr. Robert Damoiseaux, Dr. Melody Man Hing Li, Dr. Robert Thompson Clubb, and Dr. Jorge Z. Torres – have generously shared their time, offered invaluable feedback, and offered encouragement that has motivated me through my time at UCLA. I also want to thank Dr. Robert Damoiseaux and everyone in the MSSR facility to express my heartfelt gratitude for the invaluable support and for the time dedicated to helping me in the screening facility.

I would also like to express my gratitude to all the current and former members of the Backus Lab for their support, guidance, assistance, and camaraderie, in particular: Brianna Hill-Payne, Dr. Maria F. Palafox, Dr. Yan Tianyang (Sunny), Dr. Heta Desai, Lisa Boatner, Nik Burton, Ashley Julio, Andrew Becker, Flowreen Shikwana, Miranda Villanueva, Alexandra Turmon, Dr. Samuel Ofori, Eli Biletch, Nitesh Perumal, Dr. Katrina Andrews, Dr. Chau Ngo, Dr. Lara Holoidovsky, Ernest Armenta, Sho Takechi, and Dr. Jian Cao. I have formed lasting friendships and will always cherish the wonderful memories we have created together. I was fortunate to work with incredibly brilliant, funny, outgoing, and caring individuals.

I sincerely thank my family and friends outside of UCLA – Pedro Castellon, Oscar Castellon, Reyna Castellon, Blaz Castellon, German Figueroa, and Tasha Figueroa – for their unwavering support from the very beginning.

Chapter 2 is a version of Castellón, J. O., Ofori, S., Burton, N. R., Julio, A. R., Turmon, A. C., Armenta, E., Sandoval, C., Boatner, L. M., Takayoshi, E. E., Faragalla, M., Taylor, C., Zhou, A. L., Tran, K., Shek, J., Yan, T., Desai, H. S., Fregoso, O. I., Damoiseaux, R., & Backus, K. M. (2024). Chemoproteomics Identifies State-Dependent and Proteoform-Selective Caspase-2 Inhibitors. Journal of the American Chemical Society, 146(22), 14972-14988. https://doi.org/10.1021/jacs.3c12240

Chapter 3 is a version of Castellón, J.O., Yuen, C., Han, B., Andrews, K.H., Ofori, S., Julio A., Boatner, L.M., Palafox M.F., Damoiseaux, R. & Backus, K.M. (2024). An activation-based high throughput screen identifies caspase-10 inhibitors. In preparation.

Curriculum Vita

Education

Expected 2024	**Ph.D.** | **University of California, Los Angeles (UCLA)** Molecular Biology Interdepartmental Doctoral Program: Biochemistry, Biophysics and Structural Biology (BBSB)
2017	**M.S.** | **California State University, Los Angeles** Chemistry and Biochemistry
2014	**B.S.** | **California State University, Channel Islands** **B.S.** Chemistry: Biochemistry Option **B.A.** Spanish Minor in Biology Certificate in Translation

Awards and Fellowships

2023 High Throughput Chemistry and Chemical Biology (HTCCB) Gordon Research Conference (GRC)

- Recipient of the Carl Storm Underrepresented Minority Fellowship (CSURM), which provided travel support to attend the HTCCB GRC,

2023 University of California Drug Discovery Consortium (UCDDC)

- Second-place poster presentation

2020 – 2021 Whitcome Fellowship

- This award is intended to recognize the student's academic accomplishments and significant research experience in biology and chemistry, providing 2 quarters of tuition/fees and an annual stipend of $25,836.

2017 – 2020 NSF Graduate Research Fellowship Program (GRFP), Fellowship Award

- Highly competitive fellowship funding five years of graduate studies ($12,000/year)
- Includes three years of stipend ($34,000/year)

2016 CSU Innovation Corps (I-Corps),

- This award is intended to guide students as entrepreneur leaders, with the help of a faculty-led team including an industry mentor and research mentor, to design a biotechnology product targeted towards industry.
- Received $2,500 microgrant used to interview and work with mentors, advisors, and potential partners.

2015 – 2017 LSAMP Bridge to Doctorate Fellowship, Cohort XII

- This award is granted to highly motivated, first-generation college graduates interested in higher education.
- The award grants $30,000 stipend plus $10,500 in tuition fees, travel, and research per year for two years.

Publications

Castellón, J.O., Yuen, C., Han, B., Andrews, K.H., Ofori, S., Julio A., Boatner, L.M., Palafox M.F., Damoiseaux, R. & Backus, K.M. (2024). An activation-based high throughput screen identifies caspase-10 inhibitors. *Submitted*.

Ofori, S., Desai, H. S., Shikwana, F., Boatner, L. M., Dominguez Iii, E. R., **Castellón, J. O.**, & Backus, K. M. (2024). Generating cysteine-trypsin cleavage sites with 2-chloroacetamidine capping [10.1039/D4CC01583E]. *Chemical Communications*. https://doi.org/10.1039/D4CC01583E

Castellón, J. O., Ofori, S., Burton, N. R., Julio, A. R., Turmon, A. C., Armenta, E., Sandoval, C., Boatner, L. M., Takayoshi, E. E., Faragalla, M., Taylor, C., Zhou, A. L., Tran, K., Shek, J., Yan, T., Desai, H. S., Fregoso, O. I., Damoiseaux, R., & Backus, K. M. (2024). Chemoproteomics Identifies State-Dependent and Proteoform-Selective Caspase-2 Inhibitors. *Journal of the American Chemical Society*, *146*(22), 14972-14988. https://doi.org/10.1021/jacs.3c12240

Cao, J., Armenta, E., Boatner, L., Desai, H., Chan, N., **Castellón, J.O.**, & Backus, K. (2020). Suzuki–Miyaura cross-coupling for chemoproteomic applications. *American Chemical Society (ACS)*. https://dx.doi.org/10.26434/chemrxiv.12055218.v1

Xu, J. H., Eberhardt, J., Hill-Payne, B., González-Páez, G. E., **Castellón, J. O.**, Cravatt, B. F., Forli, S., Wolan, D. W., & Backus, K. M. (2020). Integrative X-ray Structure and Molecular Modeling for the Rationalization of Procaspase-8 Inhibitor Potency and Selectivity. *ACS Chemical Biology*, *15*(2), 575-586. https://doi.org/10.1021/acschembio.0c00019

Chapter 1. Introduction

Caspases are cysteine-aspartyl proteases that play important roles in the regulation of apoptosis, which is a form of programmed cell death that plays an essential role in development and cellular homeostasis[1,2]. Beyond their well-known role in apoptosis, caspases are also involved in other important cellular processes, such as inflammation[3,4], cell differentiation[5-7], tissue remodeling[8], cell cycle regulation[9], proliferation[10-14], and neural protein aggregation[15]. Chemical probes, which are small molecules designed to selectively interact with a specific protein target to modulate its activity, can be used to elucidate these and other unknown biological functions of caspases. Chemical probes mitigate off-target effects by interacting specifically with their targets. They can be used to investigate caspase roles in cellular processes such as programmed cell death, inflammation, and disease mechanisms, they can act quickly, and they can be used across different biological systems, making them attractive tools not just for studying caspase function but also to study potential therapeutic targets related to a specific caspase activity.

Caspases are translated as inactive proteoforms, known as zymogens or procaspases. Internal or external cellular death stimuli trigger caspase activation, which occurs through a cascade of proteolytic cleavage events at specific aspartate residues, leading to the removal of the inhibitory pro-domain and resulting in the dimerization, conformational change, and activation of the active enzyme composed of large and small subunits. These subunits subsequently assemble into an active heterodimeric or homodimeric caspase complex, allowing the protease to target downstream substrates

and propagate the apoptotic or inflammatory signal[16-18]. In the apoptotic pathway, these activated caspases cleave various substrate targets, leading to the breakdown of organelles, proteins, and other macromolecular structures and, ultimately, the death of the cell. The functions of caspases in the apoptotic pathway have been thoroughly investigated. Still, their roles in other critical cellular mechanisms, such as regulation of inflammation in autoimmune disorders, neurodegenerative diseases, tumor progression in cancers, cellular homeostasis, and cellular differentiation processes, remain enigmatic, underlining the importance of selective small molecules.

Small chemical probes that selectively target specific caspases can help elucidate their roles in biology, like the known CRISPR inhibitors such as Azidothymidine, designed to better control or modulate gene-editing processes. Traditionally, achieving selective inhibition of caspases poses a significant challenge due to their broad functional roles, complexity of their regulation[19], high degree of structural and primary sequence similarity, and shared active site. Moreover, the diverse and context-dependent expression of caspases in different tissues adds another layer of difficulty; for example, in the development of drosophila, distinct spatial and temporal patterns were observed for caspase-3 activation in different tissues[20], different types of tumors were shown to have increased caspase-2 and caspase-8 expression levels[19] and increased caspase-9 activity has been implicated in Alzheimer's diseases[21], thus the need for inhibitors that can precisely modulate caspase activity in specific cellular environments.

Unlike other caspases, the precise role of caspase-2 in apoptosis and cell signaling remains elusive[22]. It shares characteristics of both initiator and effector caspases. Yet, its activation mechanisms[17], substrate specificity[23,24], and involvement in non-apoptotic

pathways are poorly understood[9,25,26]. Additionally, caspase-2 has been implicated in diverse cellular processes like DNA damage response[9], tumor suppression[27], and metabolic regulation[28], making it a complex and multifaceted target for study. We hypothesized that targeting a non-catalytic cysteine residue near the active site of caspase-2 could enable selective inhibition, similar to what has been observed for other caspases such as caspase-6[29]. Furthermore, I hypothesized targeting the pro-form over the active- form of caspase-2 is expected to improve selectivity over other caspases, as I have shown in our previous studies with procaspase-8[30].

As described in Chapter 2, we developed a small inhibitor library for caspase-2 consisting of a panel of various pan-cysteine reactive compounds, which effectively targeted the pro-form of caspase-2. Additionally, using high-throughput screening (HTS), we first identified potential inhibitors for procaspase-10 along with promiscuous cysteine reactive inhibitors, detailed in Chapter 3. The engagement of our selective caspase probes was validated through competitive isoTOP-ABPP mass spectrometry, activity assays, and cellular thermal shift assay (CETSA) for caspase-2. The activity of the pro-forms of both caspase-2 was analyzed using our engineered TEV-cleavable constructs. Our developed and cysteine reactive inhibitors were also shown to protect cells from intrinsic and extrinsic apoptotic stimuli.

As described in Chapter 3, we established a high-throughput screening (HTS) assay to enable the identification of inhibitors targeting procaspase-10. Caspase-10 plays a key role in the extrinsic apoptotic pathway, specifically in immune cell regulation and immune response[31-33]. Its selective inhibition could help dissect its specific functions in apoptosis and immune regulation, providing insights into its contributions to diseases

including autoimmune lymphoproliferative syndrome (ALPS)[31,34]. I first engineered a TEV activatable procaspase-10 construct, proCASP10TEV Linker, that was compatible with HTS and identified approximately 120,000 initial hit compounds. From the initial hits, 237 were found to have a Z-score of less than -3. The 237 hits were validated with a re-screen with proCASP10TEV Linker and a counter-screen with active-caspase-10 construct to determine which hits were real procaspase-10 inhibitors. From the 237 hits, I found a small number inhibiting TEV protease. I conducted a structure-activity relationship (SAR) analysis on the validated hits and found a cluster of hits with a thiadiazole chemotype that inhibited caspase-10 activity. I also identified pifithrin-μ (PFTμ), a known p53 inhibitor, as a novel caspase inhibitor. Interestingly, I found that one of the thiadiazine chemotype hits, SO265, undergoes rearrangement to an isomer followed by a formation of a disulfide active product over the span of 24 hours under ambient conditions. I was able to show that PFTμ can protect cells from FasL-mediated apoptosis, implying that it plays a role in caspase inhibition.

References

1. Nicholson, D.W., et al., *Identification and inhibition of the ICE/CED-3 protease necessary for mammalian apoptosis.* Nature, 1995. **376**(6535): p. 37-43.
2. Riedl, S.J. and Y. Shi, *Molecular mechanisms of caspase regulation during apoptosis.* Nature Reviews Molecular Cell Biology, 2004. **5**(11): p. 897-907.
3. Thornberry, N.A., et al., *A novel heterodimeric cysteine protease is required for interleukin-1βprocessing in monocytes.* Nature, 1992. **356**(6372): p. 768-774.
4. Thornberry, N.A., D.K. Miller, and D.W. Nicholson, *Interleukin-1β-converting enzyme and related proteases as potential targets in inflammation and apoptosis.* Perspectives in Drug Discovery and Design, 1995. **2**(3): p. 389-399.
5. Sordet, O., et al., *Specific involvement of caspases in the differentiation of monocytes into macrophages.* Blood, 2002. **100**(13): p. 4446-4453.
6. Lamkanfi, M., et al., *Caspases in cell survival, proliferation and differentiation.* Cell Death & Differentiation, 2007. **14**(1): p. 44-55.
7. Lippens, S., et al., *Epidermal differentiation does not involve the pro-apoptotic executioner caspases, but is associated with caspase-14 induction and processing.* Cell Death & Differentiation, 2000. **7**(12): p. 1218-1224.
8. Gorelick-Ashkenazi, A., et al., *Caspases maintain tissue integrity by an apoptosis-independent inhibition of cell migration and invasion.* Nature Communications, 2018. **9**(1).
9. Boice, A.G., et al., *Caspase-2 regulates S-phase cell cycle events to protect from DNA damage accumulation independent of apoptosis.* Oncogene, 2022. **41**(2): p. 204-219.

10. Kanderova, V., et al., *Lymphoproliferation, immunodeficiency and early-onset inflammatory bowel disease associated with a novel mutation in Caspase 8.* Haematologica, 2019. **104**(1): p. e32-e34.

11. Su, H., et al., *Requirement for Caspase-8 in NF-κB Activation by Antigen Receptor.* Science, 2005. **307**(5714): p. 1465-1468.

12. Salmena, L., et al., *Essential role for caspase 8 in T-cell homeostasis and T-cell-mediated immunity.* Genes & Development, 2003. **17**(7): p. 883-895.

13. Chun, H.J., et al., *Pleiotropic defects in lymphocyte activation caused by caspase-8 mutations lead to human immunodeficiency.* Nature, 2002. **419**(6905): p. 395-399.

14. Beisner, D.R., et al., *Cutting Edge: Innate Immunity Conferred by B Cells Is Regulated by Caspase-8.* The Journal of Immunology, 2005. **175**(6): p. 3469-3473.

15. Rissman, R.A., et al., *Caspase-cleavage of tau is an early event in Alzheimer disease tangle pathology.* Journal of Clinical Investigation, 2004. **114**(1): p. 121-130.

16. Salvesen, G.S. and V.M. Dixit, *Caspase activation: The induced-proximity model.* Proceedings of the National Academy of Sciences, 1999. **96**(20): p. 10964-10967.

17. Baliga, B.C., S.H. Read, and S. Kumar, *The biochemical mechanism of caspase-2 activation.* Cell Death Differ, 2004. **11**(11): p. 1234-41.

18. Oberst, A., et al., *Inducible Dimerization and Inducible Cleavage Reveal a Requirement for Both Processes in Caspase-8 Activation.* Journal of Biological Chemistry, 2010. **285**(22): p. 16632-16642.

19. Shalini, S., et al., *Old, new and emerging functions of caspases.* Cell Death & Differentiation, 2015. **22**(4): p. 526-539.

20. Ding, A.X., et al., *CasExpress reveals widespread and diverse patterns of cell survival of caspase-3 activation during development in vivo.* eLife, 2016. **5**: p. e10936.

21. Avrutsky, M.I. and C.M. Troy, *Caspase-9: A Multimodal Therapeutic Target With Diverse Cellular Expression in Human Disease.* Front Pharmacol, 2021. **12**: p. 701301.

22. Krumschnabel, G., et al., *The enigma of caspase-2: the laymen's view.* Cell Death & Differentiation, 2009. **16**(2): p. 195-207.

23. Eichler, M., et al., *The caspase-2 substrate p54nrb exhibits a multifaceted role in tumor cell death susceptibility via gene regulatory functions.* Cell Death & Disease, 2022. **13**(4).

24. Bouchier-Hayes, L. and D.R. Green, *Caspase-2: the orphan caspase.* Cell Death & Differentiation, 2012. **19**(1): p. 51-57.

25. Zhao, Y., S. Dhani, and B. Zhivotovsky, *Unveiling caspase-2 regulation by non-coding RNAs.* Cell Death & Disease, 2022. **13**(9).

26. Sladky, V.C. and A. Villunger, *Uncovering the PIDDosome and caspase-2 as regulators of organogenesis and cellular differentiation.* Cell Death & Differentiation, 2020. **27**(7): p. 2037-2047.

27. Ho, L.H., et al., *A tumor suppressor function for caspase-2.* Proceedings of the National Academy of Sciences, 2009. **106**(13): p. 5336-5341.

28. Machado, M.V., et al., *Caspase-2 promotes obesity, the metabolic syndrome and nonalcoholic fatty liver disease.* Cell Death & Disease, 2016. **7**(2): p. e2096-e2096.

29. Van Horn, K.S., et al., *Engaging a Non-catalytic Cysteine Residue Drives Potent and Selective Inhibition of Caspase-6.* Journal of the American Chemical Society, 2023. **145**(18): p. 10015-10021.

30. Xu, J.H., et al., *Integrative X-ray Structure and Molecular Modeling for the Rationalization of Procaspase-8 Inhibitor Potency and Selectivity.* ACS Chemical Biology, 2020. **15**(2): p. 575-586.

31. Consonni, F., et al., *Study of the potential role of CASPASE-10 mutations in the development of autoimmune lymphoproliferative syndrome.* Cell Death & Disease, 2024. **15**(5).

32. Milhas, D., et al., *Caspase-10 Triggers Bid Cleavage and Caspase Cascade Activation in FasL-induced Apoptosis.* Journal of Biological Chemistry, 2005. **280**(20): p. 19836-19842.

33. Krug, H.F., *Caspase-10 is the key initiator caspase involved in tributyltin-mediated apoptosis in human immune cells.* J Toxicol, 2012. **2012**: p. 395482.

34. Rieux-Laucat, F., F. Le Deist, and A. Fischer, *Autoimmune lymphoproliferative syndromes: genetic defects of apoptosis pathways.* Cell Death & Differentiation, 2003. **10**(1): p. 124-133.

Chapter 2. Chemoproteomics identifies state-dependent and proteoforms-selective caspase-2 inhibitors

José O. Castellón[1], Samuel Ofori[1], Nikolas R. Burton[1,2], Ashley R. Julio[1,2], Alexandra C. Turmon[1,2], Ernest Armenta[1,2], Carina Sandoval[6], Lisa M. Boatner[1,2], Evan E. Takayoshi[1,2], Marina Faragalla[1,2], Cameron Taylor[7], Ann Zhou[1,2], Ky Tran[1,2], Jeremy Shek[1,2], Tianyang Yan[1,2], Heta S. Desai[1], Oliver I. Fregoso[6], Robert Damoiseaux[4,5,7,8,9], Keriann M. Backus[1, 2,3,4,5*]

1. Biological Chemistry Department, David Geffen School of Medicine, UCLA, Los Angeles, CA, 90095, USA
2. Department of Chemistry and Biochemistry, UCLA, Los Angeles, CA 90095, USA
3. DOE Institute for Genomics and Proteomics, UCLA, Los Angeles, CA 90095, USA
4. Jonsson Comprehensive Cancer Center, UCLA, Los Angeles, CA 90095, USA
5. Eli and Edythe Broad Center of Regenerative Medicine and Stem Cell Research, UCLA, Los Angeles, CA 90095 USA
6. Department of Microbiology, Immunology, and Molecular Genetics, University of California, Los Angeles, California, USA, 90095
7. California NanoSystems Institute (CNSI), UCLA, Los Angeles, CA, 90095, United States
8. Department of Molecular and Medical Pharmacology, UCLA, Los Angeles, CA, 90095, USA

9. Department of Bioengineering, Samueli School of Engineering, UCLA, Los Angeles, CA, 90095, USA

* Corresponding Author: Keriann M. Backus, Biological Chemistry Department, David Geffen School of Medicine, UCLA, Los Angeles, CA, 90095, USA, E-mail: kbackus@mednet.ucla.edu.

ABSTRACT

Caspases are a highly conserved family of cysteine-aspartyl proteases known for their essential roles in regulating apoptosis, inflammation, cell differentiation, and proliferation. Complementary to genetic approaches, small-molecule probes have emerged as useful tools for modulating caspase activity. However, due to the high sequence and structure homology of all twelve human caspases, achieving selectivity remains a central challenge for caspase-directed small-molecule inhibitor development efforts. Here, using mass spectrometry-based chemoproteomics, we first identify a highly reactive non-catalytic cysteine that is unique to caspase-2. By combining both gel-based activity-based protein profiling (ABPP) and a *tobacco etch virus* (TEV) protease activation assay, we then identify covalent lead compounds that react preferentially with this cysteine and afford a complete blockade of caspase-2 activity. Inhibitory activity is restricted to the zymogen or precursor form of monomeric caspase-2. Focused analogue synthesis combined with chemoproteomic target engagement analysis in cellular lysates and in cells yielded both pan-caspase reactive molecules and caspase-2 selective lead compounds together with a structurally matched inactive control. Application of this focused set of tool compounds to stratify the functions of the zymogen and partially processed (p32) forms of caspase-2 provide evidence to support that caspase-2-mediated response to DNA damage is largely driven by the partially processed p32 form of the enzyme. More broadly, our study highlights future opportunities for the development of proteoform-selective caspase inhibitors that target non-conserved and non-catalytic cysteine residues.

INTRODUCTION

Programmed cell death or apoptosis is a tightly regulated biological process required for the removal of irreversibly damaged or unwanted cells. Caspases are cysteine aspartate proteases responsible for the initiation and execution of programmed cell death[1-3]. Caspase-mediated proteolysis has also been implicated in a number of non-apoptotic processes, including cellular activation[4-5], differentiation[6-8], cell proliferation[9], immune response[4, 10-12], cell cycle regulation[9, 13], and inflammation[10, 14]. Human cancers[9, 15-17], neurodegenerative diseases[18] and monogenic disorders[4, 12] have all been linked to aberrant caspase activity. Motivated by these numerous important and diverse functions, there is ongoing interest in the functional stratification of individual caspases.

Delineating the unique and overlapping functions of caspase family members has been hindered by their high sequence and structural homology[19-21] as well as compensatory functional activities—12 caspases are encoded by the human genome[22]. While genetic tools, including CRISPR-Cas9, have been successfully applied to the study of individual family members[23], such approaches are complicated by the compensatory expression of closely related caspase homologues[24].

Chemical probes are useful tools for studying protein function; complementary to genetic approaches, chemical probes offer the added advantages of producing graded effects (both agonism and antagonism) and acute application[25-26], features well suited to the study of essential genes and post translational processes. Peptide-based and active-site directed cysteine-reactive inhibitors are widely utilized to inactivate and study caspase function. Exemplary electrophilic peptides with established caspase inhibitor activity include peptide-aldehydes (e.g. DEVD-CHO)[27-28], peptide-chloromethyl ketones

and -fluoromethyl ketones (e.g. YVAD-cfk and z-VAD-fmk)[29-30], and peptide-acyloxymethyl ketones (AOMK)[31-32]. Recent studies have revealed the utility of covalent fragment electrophiles in targeting individual caspases via covalent modification of catalytic cysteine residues[33-34]. However, the overlapping substrate profiles and the generally limited inhibitor selectivity[35-36] together demonstrate the need for alternative approaches to achieve selective caspase inhibition.

Recent studies, including our own[33, 37], have revealed three alternative approaches to peptide-based caspase inhibitors. First, allosteric inhibitors have been reported that target caspase-1, -6, and -7[38-41]. Second, our recent work revealed that improved selectivity could be achieved using non-peptidic compounds that function by targeting the catalytic cysteine in the precursor or zymogen form of the enzyme[33, 37]. Third, recent studies have revealed that caspases harbor functional and ligandable non-catalytic cysteine residues that are unique to individual caspases. For example, our recent work revealed that mutation of a near active site cysteine residue (C409) in caspase-8 afforded an almost completely inactive enzyme[42]. For pro-caspase-3, nitrosylation of C163 in pro-caspase-3 blocks apoptosis in human T cells[43]. Covalent modification of C264 in Caspase-6 by enantioenriched vinyl-sulfonamide probes afforded selective blockade of enzyme activity[44]. Whether additional non-catalytic caspase cysteines can be selectively targeted by chemical probes remains an open question.

Among all caspases, caspase-2 remains particularly enigmatic. While typically annotated as an apoptosis initiating (initiator) caspase[45], caspase-2 shares substrates with executioner caspases and can be cleaved by caspase-3[46-47]. Caspase-2 is most well characterized as playing an important role in regulating cell death in response to DNA-

damage[13, 16, 48-51]. Caspase-2 acts as a tumor suppressor affording MDM2 cleavage, which promotes p53 stability[16, 50]. More broadly, caspase-2 has been linked to cell death induced by metabolic imbalance[52], endoplasmic reticulum (ER) stress[53], and a mechanism of delayed mitosis-linked cell death[54-55]. Independent of its pro-apoptotic functions, caspase-2 has also been tied to cell cycle progression[13] and regulation of cell proliferation[56], including by functioning as a checkpoint for supernumerary centrosomes[55]. Pointing towards possible therapeutic opportunities for caspase-2 selective inhibitors, caspase-2 activity has been implicated in neurodegenerative diseases, most notably in the context of Alzheimer's disease (AD) and other tauopathies, through cleavage of the tau protein, which impairs memory in a murine AD disease model[57]. Intriguingly, caspase-2 depletion has recently been reported as protective in a murine model of NAFLD/NASH[53, 58], suggestive of possible further therapeutic utility for caspase-2 inhibitors.

Here, using a high coverage cysteine chemoproteomic platform, we identified a highly reactive and ligandable non-catalytic cysteine (C370) that is unique to caspase-2. We found that covalent modification at C370 blocks caspase-2 activity in a proteoform specific manner, occurring only in the monomeric zymogen or precursor form of caspase-2. By combining gel-based activity-based protein profiling (ABPP) with a *tobacco etch virus* (TEV)[59] protease activation assay, we assessed the inhibitory activity of a panel of electrophilic compounds, which guided our discovery of active and control compounds spanning multiple electrophilic chemotypes. Protein- and cysteine-directed chemoproteomic analysis together with pulldown and gel-based thermal shift assays confirm cell-based engagement of caspase-2, with zymogen selectivity. Functional analysis points towards differential contributions of the full length and p32 forms of

caspase-2 in response to genotoxic agents. A heretofore unreported pan-caspase reactive chemotype is also revealed. Taken together, our study provides a comprehensive toolbox of chemical probes, proteomic platforms, and functional assays to guide ongoing and future proteoform-selective caspase inhibitor campaigns.

RESULTS

Mass spectrometry-based chemoproteomics identifies a highly reactive non-catalytic cysteine residue (C370) in caspase-2. Prior studies, including our own, revealed that mass spectrometry-based chemoproteomic measurements of intrinsic cysteine reactivity towards the pan-cysteine reactive probe iodoacetamide alkyne **(IAA**; **Figure 1A** and **Figure S1**) correlate with residue functionality[42, 60]. Therefore, our first step to identify functional and ligandable cysteine residues in caspase-2 was to deploy a high coverage isotopic tandem orthogonal proteolysis activity-based protein profiling (isoTOP-ABPP)[60-61] to assay caspase cysteine reactivity. Following the workflow shown in **Figure 1A**, we assayed the IAA-reactivity of cysteine residues in lysates derived from Jurkat cells, a primary acute lymphoblastic leukemia (ALL) cell line, in which many caspases show elevated expression[62]. By pairing the isoTOP-ABPP workflow with single-pot solid-phase-enhanced sample-preparation (SP3) and high field asymmetric ion mobility spectrometry (FAIMS)[63-64], we generated high coverage reactivity datasets that compared cysteine reactivity with 100 μM versus 10 μM **IAA**—highly reactive cysteines, termed “hyper-reactive” residues were classified based on the calculated isoTOP-ABPP ratio values near to zero [$Log_2(R_{heavy:light})$ = $Log_2(R_{10:1})$ = -1.0–1.0], consistent with saturation of labeling at low concentrations of iodoacetamide alkyne.

In aggregate the **IAA**-reactivity was quantified for 11457 total cysteines from 4111 total proteins (**Table S1**). Eighteen total caspase cysteines from seven caspases were quantified across all replicate experiments. Unexpectedly, given the established nucleophilicity of protease catalytic thiolate nucleophiles[65], non-catalytic cysteine (C370) in caspase-2 was found to be the most highly reactive residue and only hyper-reactive caspase cysteine across all caspase cysteines quantified (**Figure 1B** and **1C** and **Figure S2A**). As caspase activation is tightly regulated, with protease activity only unleashed during apoptosis, we also extended this analysis to cellular lysates derived from cells undergoing extrinsic [Fas-Fas ligand (FasL)-induced] apoptosis[66-67]. This analysis revealed that C370 remains highly reactive towards IAA in lysates derived from apoptotic cells (**Figure 1C** and **Figure S2B**).

C370 is highly conserved, active-site proximal, and modestly impacts the activity of recombinant active caspase-2. Both the catalytic cysteine (C320) and active-site proximal C370 in caspase-2 are highly conserved across species (**Figure S3A,B**)[1]. Additionally, C370 is uniquely found in caspase-2 (**Figure S3C**), unlike the catalytic C320, which is shared across all human caspases (**Figure S3D**). As our prior study had shown that mutation of an IAA-reactive non-catalytic cysteine in caspase-8 nearly completely abolished protein function[42], we postulated that C370 in caspase-2 may serve a similar regulatory role. To assess whether mutation of C370 adversely affected caspase-2 activity, we recombinantly expressed caspase-2. Comparison of the relative activity of wild-type active caspase-2 with C370A mutated protein revealed a modest ~10%

decrease in enzyme activity, measured under saturating conditions with the Ac-VDVAD-AFC fluorogenic substrate (**Figure 1D**).

Given the seeming contradiction between the elevated intrinsic reactivity of C370 and its seeming modest impact on the active enzyme activity (**Figure 1D**), we speculated that the C370 IAA-reactivity might be favored in the precursor or zymogen form of the enzyme. Consistent with this hypothesis, in the x-ray crystal structure of active caspase-2 (PDB: 1PYO), Cys370 appears buried (**Figure 1E,F**). Homology modeling using I-TASSER[68], revealed that in a more pro caspase-like conformation[37, 69-71], C370 is located on the C-terminal loop adjacent to the active site region (**Figure 1F**). The conformational changes caused by the 180° flip of the C-terminal loop and subsequent orientational shift of the sulfhydryl putatively affording increased solvent accessibility for C370.

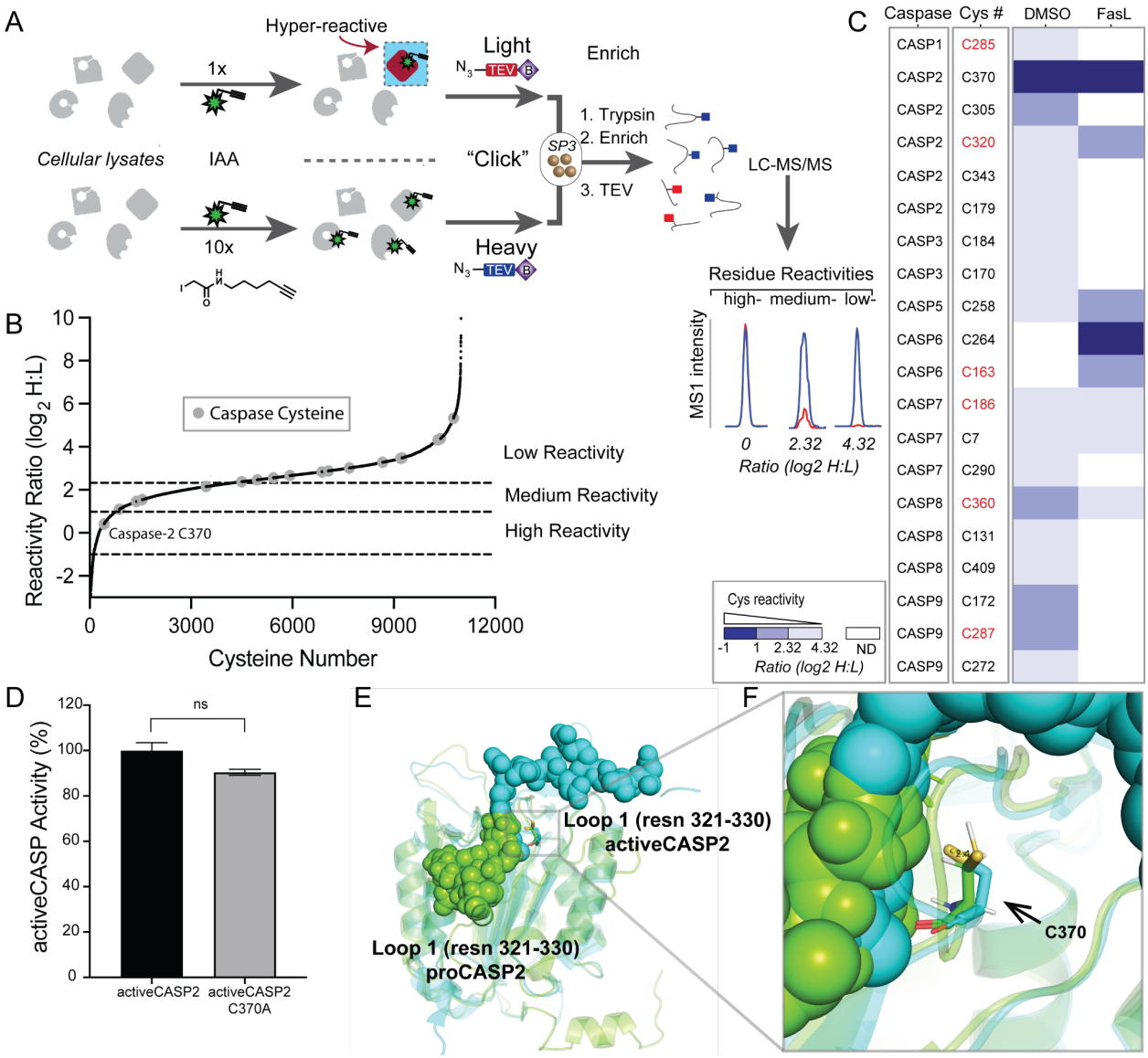

Figure 1. **Isotopic tandem orthogonal proteolysis–activity-based protein profiling (isoTOP-ABPP) to stratify the reactivity of caspase cysteine residues.** (A) IsoTOP-ABPP workflow used here, which was modified from the previously published methods[60-61] to incorporate single-pot, solid-phase-enhanced sample-preparation (SP3) cleanup[72]. Lysates are treated with either 10 or 100 μM **IAA** followed by copper-catalyzed azide-alkyne cycloaddition (CuAAC) conjugation to the previously reported isotopically labeled *tobacco etch virus* (TEV)-cleavable biotinylated peptide tags[60]. The samples are then

combined, subjected to SP3 cleanup and on-resin trypsin digest, enrichment on streptavidin resin followed by TEV proteolysis, and liquid chromatography–tandem mass spectrometry (LC-MS/MS) analysis. isoTOP-ABPP ratios (log_2 H:L) are calculated from the MS1 ion intensity ratios for heavy- versus light-labeled peptides for peptides from non-apoptotic Jurkat cells. Ratio thresholds: high" reactivity: $Log_2(R_{heavy:light})$ = -1.0 – 1.0, "medium" reactivity: $Log_2(R_{heavy:light})$ = = 1 - 2.32, "low" reactivity $Log_2(R_{heavy:light})$ = >2.32. ND-Not detected. Workflow was adapted with permission from[73]. Copyright [2019][Springer Nature]. (B) Waterfall plot showing isoTOP-ABPP reactivity analysis of cell lysates derived from viable non-apoptotic Jurkat cells. (C) Comparison of the measured isoTOP-ABPP reactivity ratios for caspase cysteines identified in analysis of vehicle treated (DMSO) and apoptotic (50 ng/μL FasL, 4h) cellular lysates. Non-apoptotic experiments (n = 6) and Apoptotic experiments (n = 5). (D) Comparison of the activity of recombinant activeCASP2 and activeCASP2_C370A using fluorogenic substrate Ac-VDVAD-AFC monitored by multimodal plate reader with percentage activity calculated from the linear range of the reaction curves. (E) Crystal structure of activeCASP2 (PDB: 1PYO; complexed with Acetyl-Leu-Asp-Glu-Ser-Asp-cho) in cyan highlighting active site adjacent loop (Loop 1) overlaid with predicted (I-TASSER[68, 74-75] structure of pro-caspase-2 in green. (F) 180° flip of loop 1 repositions the C370 Sulfhydryl. Figures were generated using Pymol[76]. For D data represents mean activity ± STDEV for two technical replicate experiments. Statistical significance was calculated with unpaired Student's t-tests, comparing activeCASP2 to activeCASP2_C370A; ns, not significant, n.s. $p>0.05$. All MS data can be found in **Table S1**. Cys shown in Red are catalytic nucleophiles.

Zymogen- and caspase-2 specific labeling of C370 by electrophilic alkyne-probes. The homology models together with previous findings that both catalytic and non-catalytic caspase cysteines are amenable to covalent modification in the protease's zymogen form[33, 42, 44] prompted us to establish a gel-based activity-based assay to further probe the labeling specificity of C370 in caspase-2. Recombinant pro-caspase-2 (proCASP2) was expressed harboring D333A and D347A mutations, which prevent caspase cleavage and activation, together with single and dual C370A and C320A mutations to assess cysteine specificity (See **Table S2** for a summary of all constructs). We then subjected each recombinant protein to labeling with **IAA** or caspase-directed **Rho-DEVD-AOMK** [Asp-Glu-Val-Asp-(2,6-dimethyl benzoyloxy)-methyl ketone] probe (**Figure S1**)[77], to assay general cysteine reactivity and caspase activity, respectively (**Figure 2A,B**). Notably, we performed these experiments with protein added to cell lysate to enhance delineation of specific versus non-specific labeling by each probe. We observed that the widely cysteine-reactive **IAA** labels both C370 and C320. In contrast with the relatively robust zymogen labeling, the active form of caspase-2 only shows trace labeling by **IAA (Figure 2B)**. Consistent with prior studies, we observed that the **Rho-DEVD-AOMK** labeled the catalytic nucleophile C320, with mutation of this residue completely blocking labeling. We were initially surprised to observe labeling of the zymogen form of the enzyme by **Rho-DEVD-AOMK**, as this probe is tailored to react with catalytically competent caspases. As prior studies have shown that the zymogen form of caspase-2 exists as a mixture of inactive monomer and catalytically competent dimeric forms[45], this observed labeling may be rationalized in part by a mixed population of active and inactive enzyme.

Given the established value of cysteine-reactive probes as tool compounds, and even as lead candidates for potential therapies, we next set out to determine whether more elaborated compounds featuring more attenuated electrophiles could label C370 selectively. To this end, we obtained a small panel of structurally diverse aliphatic and aromatic cysteine-reactive alkyne-containing scout fragments, including newly synthesized analogues (**1-4**) and previously reported compounds (**KB18**, **KB19**, **KB61**)[33] (**Figure 2A** and **Figure S1**). We labeled our panel of recombinant caspase-2 proteins with these additional cysteine-reactive probes (**Figure 2B**). In contrast with active caspase-2, which labeled poorly with nearly all probes tested, we found that the D333A, D347A mutant form of the protein (zymogen-like) labeled robustly with a number of probes. Mutation of C370A nearly completely blocked labeling, which supports our hypothesis that the primary reactive cysteine in the zymogen protein is the non-catalytic C370 residue, which was further supported by the strong probe labeling of the C320A mutated protein. C370 was labeled robustly by most chloroacetamide probes, including **1** and **2**. As chloroacetamides generally show heighted proteome-wide reactivity, we also tested several acrylamide probes (**3**, **4**, **KB18**) and gratifyingly found that acrylamide **3** labeled caspase-2 at a level comparable to many of the chloroacetamide compounds.

Given the aforementioned catalytic activity of pro-caspase-2 (proCASP2), we next sought to assess whether modifications to C370 in the zymogen form of caspase-2 by **3** would impact activity. Pre-treatment of proCASP2 with **3** partially blocked enzyme activity in a cysteine-dependent manner (**Figure 2C**). While zymogen forms of caspases generally show low activity[78], the addition of kosmotropes (e.g. sodium citrate) can increase activity[79-80]. Consistent with these prior studies, we found that addition of both

dithiothreitol (DTT) and sodium citrate afforded increased activity of the D330A, D347A mutant enzyme (**Figure S4**), as assayed using the fluorogenic substrate Ac-VDVAD-AFC[81]. We also observed that C370A mutation afforded a substantial decrease in zymogen activity (**Figure 2C**), in contrast to our analysis of activeCASP2 C370A (**Figure 2D**). Treatment of activeCASP2 with **3** afforded no significant inhibition, consistent with a model whereby **3** labels the zymogen form of caspase-2 (**Figure 2D**).

The partial inhibition of caspase-2 by **3** can be rationalized by either incomplete labeling of the protein or by an allosteric inhibitory mechanism, where C370 modification affords only partial inactivation. Caspase-2 labeling by **3** saturated at approximately 25 μM, which would align with complete labeling (**Figure S5**). However, bottom-up LC-MS/MS analysis of recombinant protein labeled by **3** (100 μM) revealed only partial modification under conditions of excess probe (**Figure S6** and **Table S3**). These data point to only partial modification of caspase-2 as the likely explanation for the incomplete inhibition—we do note that we cannot rule out the possible gas phase lability of the acrylamide modification during MS/MS analysis as an alternative explanation for the observed partial labeling[82].

Based on our prior cysteine chemoproteomic datasets[33, 83-84], caspase cysteines generally react poorly with acrylamide-substituted compounds. Therefore, we postulated that the acrylamide in **3** might offer the additional benefit of improved caspase selectivity. As expected, no substantial labeling was observed for **3**-treated proCASP8 and proCASP10, as analyzed by gel-based ABPP (**Figure 2E**). Furthermore, only modest inhibition of activeCASP8 was observed after treatment with **3** (**Figure 2F**).

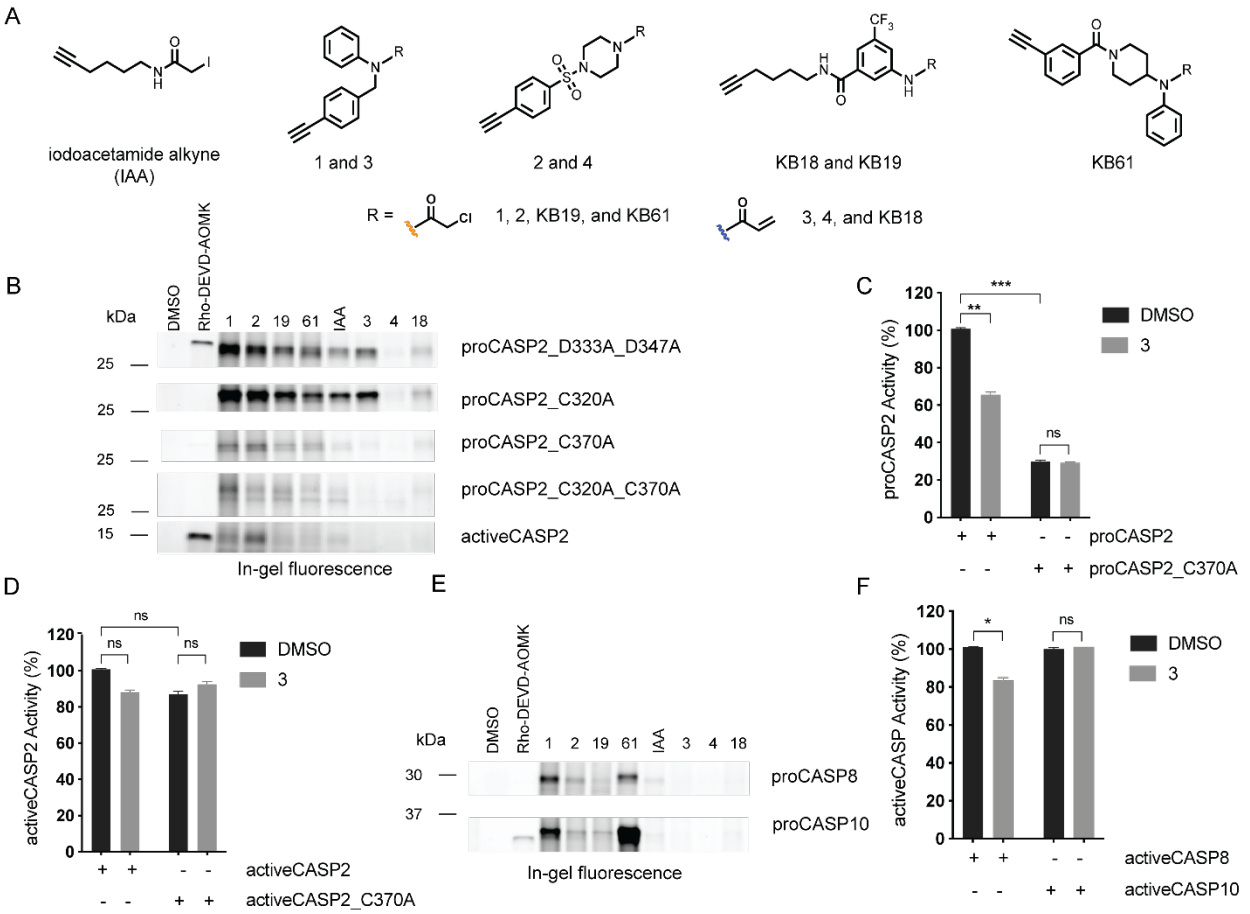

Figure 2. Alkyne probe 3 preferentially labels C370 over other caspase cysteines to afford partial blockade in pro-caspase activity. (A) Structures of cysteine reactive clickable probes including previously reported **IAA**[60] and **KB18**, **KB19**, and **KB61**[33], as well as compounds **1**–**4,** unique to this study. (B) Gel-based ABPP analysis of recombinant caspase-2 constructs harboring the indicated mutations in Jurkat whole cell lysates treated for 1h with the indicated compounds (10 μM for all click probes except for IAA, which was analyzed at 1 μM, and **Rho-DEVD-AOMK** at 2 μM). (C) Assessment of compound-induced changes in protease activity for proCASP2 and proCASP2_C370A proteins subjected to **3** (100 μM, 2h, 30 °C) followed by multimode plate reader fluorescence analysis of caspase activity using the fluorogenic substrate Ac-VDVAD-AFC

(1 μM) under kosmotropic conditions (sodium citrate)[79-80]. (D) Relative activities of activeCASP2 in the absence (Black) or presence of **3** (Gray) (100 μM) assessed using fluorogenic substrate Ac-VDVAD-AFC. (E) Gel-based ABPP analysis of recombinant pro-caspase-8 (proCASP8) and pro-caspase-10 (proCASP10) subjected to the indicated compounds (10 μM for all click probes except for IAA, which was analyzed at 1 μM, and **Rho-DEVD-AOMK** at 2 μM). (F) Relative protease activities of activeCASP8 and activeCASP10 in the absence (Black) or presence of **3** (Gray) (100 μM, 2h, 30 °C) assessed using fluorogenic substrate Ac-VDVAD-AFC. For **Figure 2D**, **2E** and **2F**, experiments were performed in triplicate. Full length gels shown in **Figure S7** and **S8**. For C, D, F Data represent mean values and standard deviation. Statistical significance was calculated with unpaired Student's t-tests, ns, not significant, * $p<0.05$, ** $p<0.01$, ** *$p<0.001$, ns $p>0.05$.

Assessment of the scope of chemotypes that label Caspase-2 at C370. Given the challenges associated with lead optimization for electrophilic compounds, including idiosyncratic structure–activity relationship (SAR) that can be complicated by difference in pre- and post-alkylation binding poses, and the absence of high-resolution co-crystal structures, we opted to pursue multiple parallel lines of SAR analysis, including synthesis of analogues of **3 (Figure 3A)** and broadening the chemotypes evaluated by obtaining a small panel of putative electrophilic scaffolds (**Figure S1**, **P01**, **P02**, **P03, P04, P04, P05,** and **P06**). Gel-based ABPP analysis revealed that methylphenyl propiolate **P01**, beta-nitrostyrene **P03**, and nitrovinyl benzodioxole **P06** all label C370 (**Figure S9**). As the potency of these compounds compares favorably to **3**, with near complete competition of

C370 at 10 μM dose (**Figure S10**), we additionally chose to synthesize and test a focused set of methyl phenylpropiolate **P01** analogues (**Figure 3A** and **Figure S1**).

Using a gel-based ABPP screening format, we compared the potency of library members **5-16** (**Figure 3B)**. We find that the N-phenyl-N-benzyl analogue modifications to the benzyl moiety (e.g. methyl ester **9** and benzimidazole **11**) show similar (~20 μM) apparent IC50 values (**Figure 3C**). Replacement of the aniline portion with a more electron withdrawing chloropyrimidine group **10** (**Figure 3C**) afforded an increase in potency (apparent IC50 11.0 μM). Naphthyl compound **12** showed no appreciable competition of probe labeling for caspase-2, indicating that large modifications to the aniline ring are not tolerated. For the **P01** analogues, we find that benzyl, phenyl, and isopropyl ester modifications decrease compound potency, consistent with a potential steric clash with the bulkier substituents (**Figure S10)**. Curiously, the bulky tert-butyl pyridine analogue **6** did not suffer from decreased potency, hinting that the pyridine species may alter the electrophilicity and/or binding pose relative to the non-heterocyclic analogues. **P01** analogues **7** and **8**, which feature larger aromatic substituents (quinoline and carbazole, respectively) both maintained caspase-2 labeling, with the carbazole analogue showing modestly decreased potency.

We then extended our SAR analysis to assess labeling of recombinant proCASP8, proCASP10 and activeCASP2, activeCASP3, activeCASP8, and activeCASP9 (**Figure 3B** and **Figure S11-S16)**. Gratifyingly, none of the compound **3** analogues (**9-12**) showed any appreciable caspase-8/10 labeling. In contrast, we were surprised to observe, given our aforementioned observations that caspase catalytic cysteines generally react poorly with Michael acceptors, that **P01** together with analogues **5** and **6** afford marked labeling

of both proCASP8 and proCASP10 (**Figure 3B** and **Figure S11**, **Figure S12 and Figure S13**). The bulkier analogues **7** and **8** showed, respectively, partial and near complete selectivity for C370 over the catalytic cysteines in caspase-8 and caspase-10 (**Figure 3B** and **Figure S11**). These same compounds did not block labeling of recombinant activeCASP3 as visualized using the **Rho-DEVD-AOMK** probe (**Figure S14**). No inhibition was observed for recombinant activeCASP8, activeCASP9, or activeCASP3 enzyme activity, and only modest 20% inhibition of activeCASP2 was detected (**Figure S15** and **S16**). Together these data support that **P01** engages multiple procaspases, whereas other analogues show considerable selectivity for proCASP2, and none of the compounds tested considerably inhibit any of the the evaluated recombinant active caspases.

To assess whether these selectivity profiles extended to endogenous caspases, we next subjected our compound library to competitive isoTOP-ABPP analysis in Jurkat cell lysates, following the workflow shown in **Figure S17**, as has been reported previously[33]. While we initially struggled to consistently detect C370, we found that the use of a FAIMS device during acquisition (**Figure S18**) afforded a marked increase in coverage of a number of quantified caspase cysteines, including C370. This observation aligns with prior reports of online gas phase fractionation improving coverage for both cysteine chemoproteomics[85] as well as other low abundance ions[63, 86-87]. In aggregate across 10 compounds screened, we quantified 11190 cysteines from 3998 proteins and 20 total cysteines from six caspases (**Figure 3D** and **Table S3**). Notably we only detect caspase-6 peptides containing C264 a handful of datasets, which is consistent with

previous reports indicating difficulties with detecting this peptide from endogenous protein[44].

Gratifyingly and consistent with our gel-based ABPP analysis, we observed that compounds **P01, 6-9,** and **11)** all afford high precursor intensity ratios for peptides harboring C370, consistent with compound modification at C370. Inactive control compound **12** showed no appreciable labeling for any caspase cysteine detected. Again, consistent with our gel-based analysis we observe that a number of the **P01 analogues** are reactive towards initiator caspase-8 and -9 catalytic cysteines. This finding further supports the likelihood of this chemotype as broadly caspase reactive.

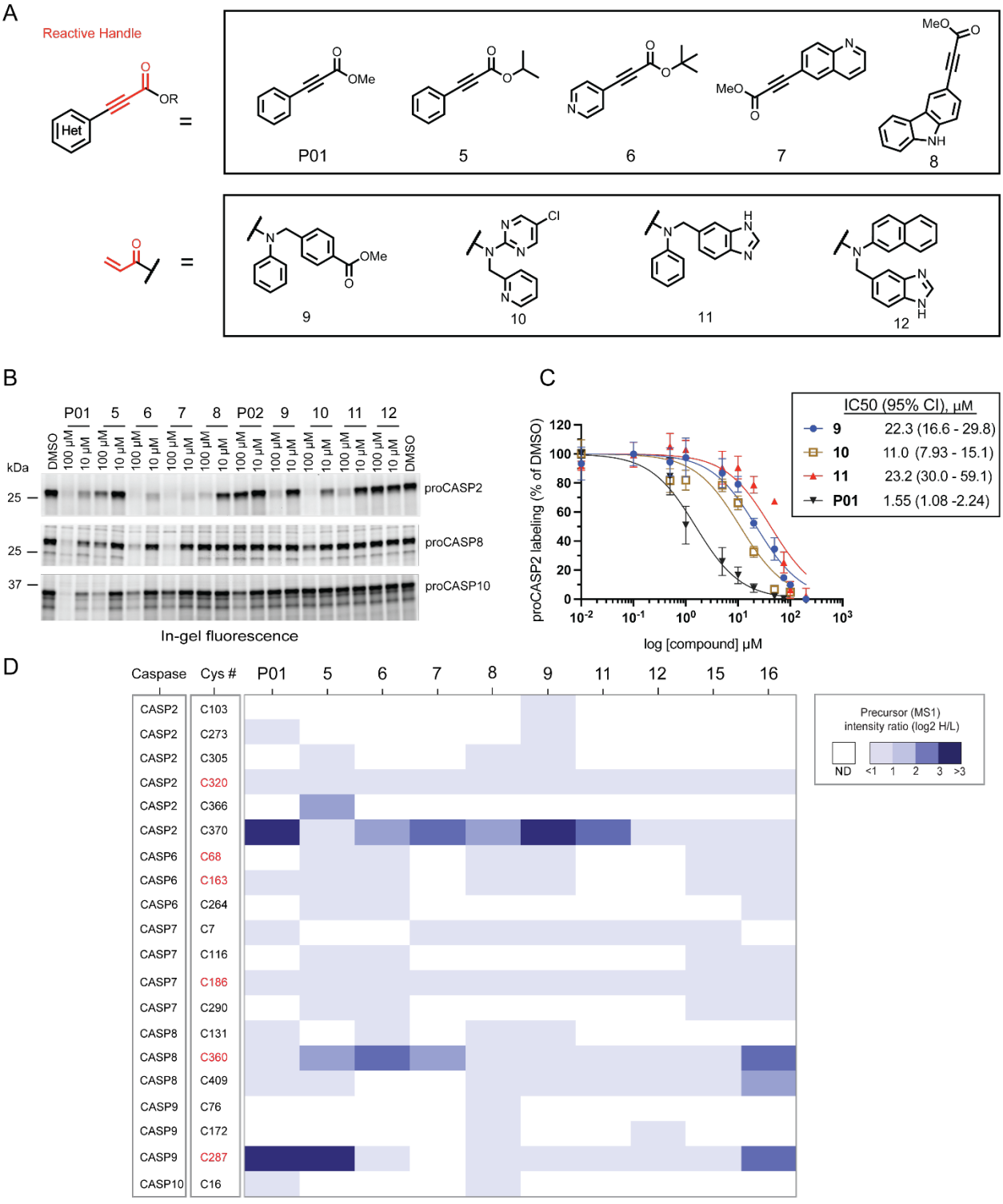

Figure 3. **Fragment electrophiles selectively label proCASP2 at C370**. (A) Structures of electrophilic compound library of **3** and **P01** analogues. (B) Gel-based ABPP analysis

of the indicated recombinant proteins in whole cell lysates treated for 1h with the indicated compounds followed by click conjugation to compound **3** (10 μM) for proCASP2 and **KB61 (**10 μM) for proCASP8 and proCASP10. Full length gel images in supporting information **Figure S11** (C) Apparent IC50 curve for blockade of **3** labeling of proCASP2 by the indicated compounds. CI, 95% confidence intervals. (D) Caspase cysteines quantified in competitive isoTOP-ABPP analysis of Jurkat cell lysates treated with **P01**, **5** and **6** (25 μM) and **7**, **8**, **9**, **11**, **12**, **14**, **15**, and **16** (100 μM). Competition ratios are calculated from the mean quantified precursor intensity (log_2H/L) for DMSO (H, heavy) versus compound-treatment (L, light). Cysteines shown in Red are catalytic residues. ND-Not detected. For C, data represent mean values ± standard deviation of the mean for at least three independent experiments. For D, experiments were conducted in at least two biological replicates. All MS data can be found in **Table S3**.

Establishing TEV-protease activatable caspase-2. Our functional studies using recombinant proCASP2 **(Figure 2C**) hinted that C370 labeling afforded inhibition of the pro-enzyme. However, these assays were complicated by the relatively low overall activity of the pro-enzyme, particularly in the absence of a kosmotropic agent (i.e. citrate). Therefore, our next step was to establish an assay that could test whether labeling of C370 in the inactive form of the enzyme would inhibit the active enzyme. We were motivated by previous reports that utilized engineered *tobacco etch virus* (TEV) protease-activatable caspase constructs[88-90] for cell-based studies. To test whether this technology would extend to *in vitro* caspase-2 inhibition studies, we generated proCASP2TEV and proCASP2TEV_C370A by replacing both caspase-2 cleavage sites (D333 and D347) with TEV (ENLYFQG) cleavage motifs (**Figure S19)**. Gratifyingly, upon addition of TEV

protease, we observed marked TEV-dependent increased catalytic activity (**Figure 4A**) and near complete conversion to active caspase-sized species as detected by gel-based ABPP (**Figure 4B,C** and **Figure S20**,**S21**). The activation was rapid, occurring within 5-10 minutes, and only required modest (2.5 μM) concentrations of TEV protease to achieve complete activation. Comparison of the kinetic parameters of proCASP2TEV and activeCASP2 revealed that the introduction of the TEV cleavage motifs afforded no substantial change in k_{cat} or K_m (**Figure 4D**). Consistent with our proCASP2 constructs, we found that proCASP2TEV was labeled efficiently by both **Rho-DEVD-AOMK** and **3**, with the latter showing C370-specific labeling, as assayed by gel-based ABPP (**Figure 4B,C** and **Figure S21B** and **Figure S22**). DEVD-Rho labeling was only detectable for the 18 kDa cleavage product, which contains C320, whereas **3**-labeling was only observed for the 12 kDa cleavage product, which harbors C370 (arrows in **Figure 4C).** This striking probe-dependent labeling pattern provides additional evidence supporting the specificity of **3** for C370.

Autoactivation complicates TEV-dependent inhibition assays. Motivated by the TEV-dependent high activity of our engineered construct, we next asked whether treatment with our lead caspase-2 electrophilic compounds would block TEV dependent activity. We subjected our lead construct proCASP2TEV to treatment with excess of compounds **P01**, **8**, **9**, and **10** (100 μM), followed by activation by TEV protease in the presence of excess DTT (5 mM) to quench unreacted compound—as TEV protease is a cysteine protease, addition of DTT is required to prevent TEV catalytic cysteine alkylation, which could result in spurious measures of inhibition. Surprisingly, we observed minimal compound-dependent inhibition, both in the presence and absence of TEV protease

(**Figure S23**). In contrast, gel-based ABPP analysis revealed comparable labeling of proCASP2TEV to that observed for our proCASP2 constructs (**Figure S24, S25**).

Somewhat perplexed by the apparent inconsistency between the inhibition data and the gel-based ABPP analysis, we speculated that the recombinant protein might harbor a mixture of proteoforms, including both compound-sensitive and insensitive species. Our previous observation of the partial labeling of the C370 peptide by **3** (**Figure S6**) in proCASP2 was consistent with this hypothesis. Also consistent with this hypothesis, we observed that proCASP2TEV and proCASP2TEV_C370A exhibit autocleaving properties as indicated by the presence of an 18 kDa **Rho-DEVD-AOMK**-reactive form of caspase-2 detected in the immobilized metal affinity chromatography (IMAC)-purified protein (**Figure S26)** and observed TEV-independent activity (**Figure S27**). In contrast, autocleavage of proCASP2 and proCASP2_C370A was not detected (**Figure S28**). In light of these confounding factors, we opted to pursue a tryptophan scanning mutagenesis strategy[91-92]. We generated the C370W mutated protein to test whether genetic introduction of a bulky residue, which mimics small molecule labeling[93], would afford a complete blockade of enzyme activity. The proCASP2TEV_C370W protein, which was obtained in high yield and purity (**Figures S29**), showed no detectable activity (**Figure 4E**).

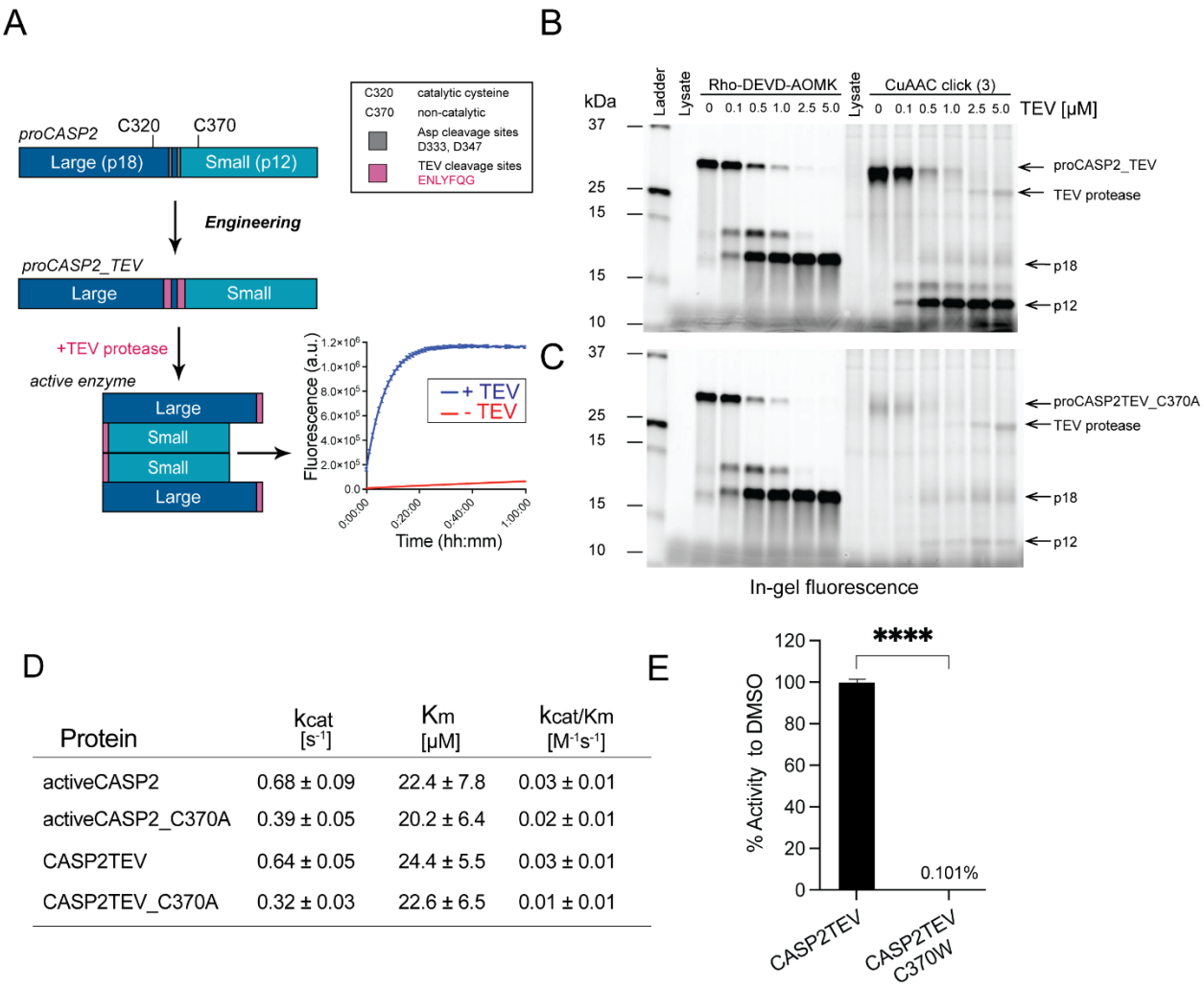

Protein	kcat [s^{-1}]	Km [μM]	kcat/Km [$M^{-1}s^{-1}$]
activeCASP2	0.68 ± 0.09	22.4 ± 7.8	0.03 ± 0.01
activeCASP2_C370A	0.39 ± 0.05	20.2 ± 6.4	0.02 ± 0.01
CASP2TEV	0.64 ± 0.05	24.4 ± 5.5	0.03 ± 0.01
CASP2TEV_C370A	0.32 ± 0.03	22.6 ± 6.5	0.01 ± 0.01

Figure 4. **TEV-cleavable proCASP2 is activated by TEV protease with minimal effects on enzyme kinetics**. (A) Replacement of caspase-2 cleavage sites (D333 and D347) with TEV (ENLYFQG) cleavage motifs affords engineered proCASP2TEV and proCASP2TEV_C370A proteins, which exhibit TEV-dependent increase in caspase activity towards Ac-VDVAD-AFC fluorogenic substrate. (B) Gel-based ABPP analysis of (B) proCASP2TEV and (C) proCASP2TEV_C370A, which were treated with either **Rho-DEVD-AOMK** (1 μM final concentration) or compound **3** (10 μM final concentration) for 1h, followed by activation with TEV protease at increasing concentrations and click

conjugation to Rho-Azide for **3**-treated samples. For quantitation and coomassie staining refer to **Figures S20** and **S21**. (D) Calculated Michaelis−Menten kinetic parameters using Ac-VDVAD-AFC substrate, including 95% confidence intervals, for proCASP2TEV following activation with TEV protease andactiveCASP2. (E) Relative activity of proCASP2TEV and proCASP2TEV_C370W proteins assessed using Ac-VDVAD-AFC substrate following activation with TEV protease. For E, data represents mean values ± standard deviation of the mean for three independent experiments. Statistical significance was calculated with unpaired Student's t-tests, **** $p<0.005$.

Preferential labeling of the monomeric form of pro-caspase-2. Most initiator caspases (e.g. caspase-8, -9 and -10) exist primarily in an inactive monomeric state, with dimerization resulting in rapid activation[78]. While proCASP2 is thought to function as an initiator caspase, unique among caspases, its physiological pro-enzyme form (with CARD pro-domain) exists as a mixture of monomeric and dimeric states[45]. Therefore, we hypothesized that our recombinant pro-caspase, which lacks the CARD domain, might also exist as a mixture of oligomeric states. We subjected our proCASP2TEV and proCASP2TEV_C370A proteins to size exclusion chromatography (SEC), which revealed an elution profile for recombinant proCASP2TEV consistent with a mixed population of putative monomer, dimer, and a cleavage product (~ 25.0 kDa; **Figure 5A, 5B**). SEC analysis of proCASP2TEV_C370A revealed two major species matching the molecular weights of monomeric and dimeric caspase-2 (**Figure 5C, 5D**). Notably, both proCASP2TEV and proCASP2TEV_C370A samples also harbored trace amounts of putative active caspase-2 species (~18 kDa bands), which were not visualized by

Coomassie staining but were detectable by the Rho-DEVD-AOMK activity-based probe (**Figure 5B, 5D**). Similarly, mixed putative monomer and dimer populations were observed for gel filtration analysis of the proCASP2 and proCASP2_C370A constructs (**Figure S30** and **Figure S31**), with the exception of the presence of previously noted ~25 kDa intermediate species that was only observed for proCASP2_TEV.

Somewhat unexpectedly, we observe striking elution-dependent difference in the relative intensities of caspase-2 labeling by Rho-DEVD-AOMK. While proCASP2_TEV was observed to be a roughly 1:1 mixture of caspase-2 monomer and dimer, we observed ~three-fold more labeling relative to protein abundance for the dimer-containing fractions (0.30 - 0.45) compared to the monomer-harboring fractions 0.48 - 0.55) (**Figure 5E**). These findings support that monomeric caspase-2 is generally less active towards the Rho-DEVD-AOMK activity-based probe. The distinct SAR of the monomer and dimer proteins was further illustrated by our gel-based ABPP analysis of size-exclusion isolated fractions labeled by either probe **3** or Rho-DEVD-AOMK, which revealed the preferential labeling of the monomeric protein by probe **3** and dimer protein by Rho-DEVD-AOMK (**Figure 5F**).

Guided by these observations, we next asked whether these isolatable forms of caspase-2 would behave differently both in terms of measured catalytic activity and inhibition by our C370-reactive compounds. Comparative TEV-dependent activity was observed for both caspase-2 monomer/dimer species (**Figure 5G**). Consistent with our previous observation of partial inhibition of proCASP2 by **3 (Figure 2C),** the dimeric fractions only exhibited partial inhibition by **compound 9**. In contrast**,** the monomeric fractions showed near complete inhibition by **9** (**Figure 5G**)**.** Extension of this analysis to

our panel of electrophilic compounds, revealed, for the monomeric fractions, near complete inhibition of proCASP2TEV for all compounds that showed caspase-2 labeling as detected by gel-based ABPP (**Figure 5H**).

Given that we had observed a putative cysteine-mutant-dependent increase in the fraction of monomeric protein detected by gel filtration for the proCASP2TEV_C370A protein (**Figure 5C**), we additionally wondered whether compound labeling at C370 might similarly afford an increase in monomeric caspase-2. Consistent with this model, filtration analysis after compound labeling revealed a shift in the protein elution profile towards increased monomeric species (**Figure S32**). Alongside our inhibition and gel-based analysis data, this finding supports that compound labeling at C370 favors the monomeric zymogen form of caspase-2.

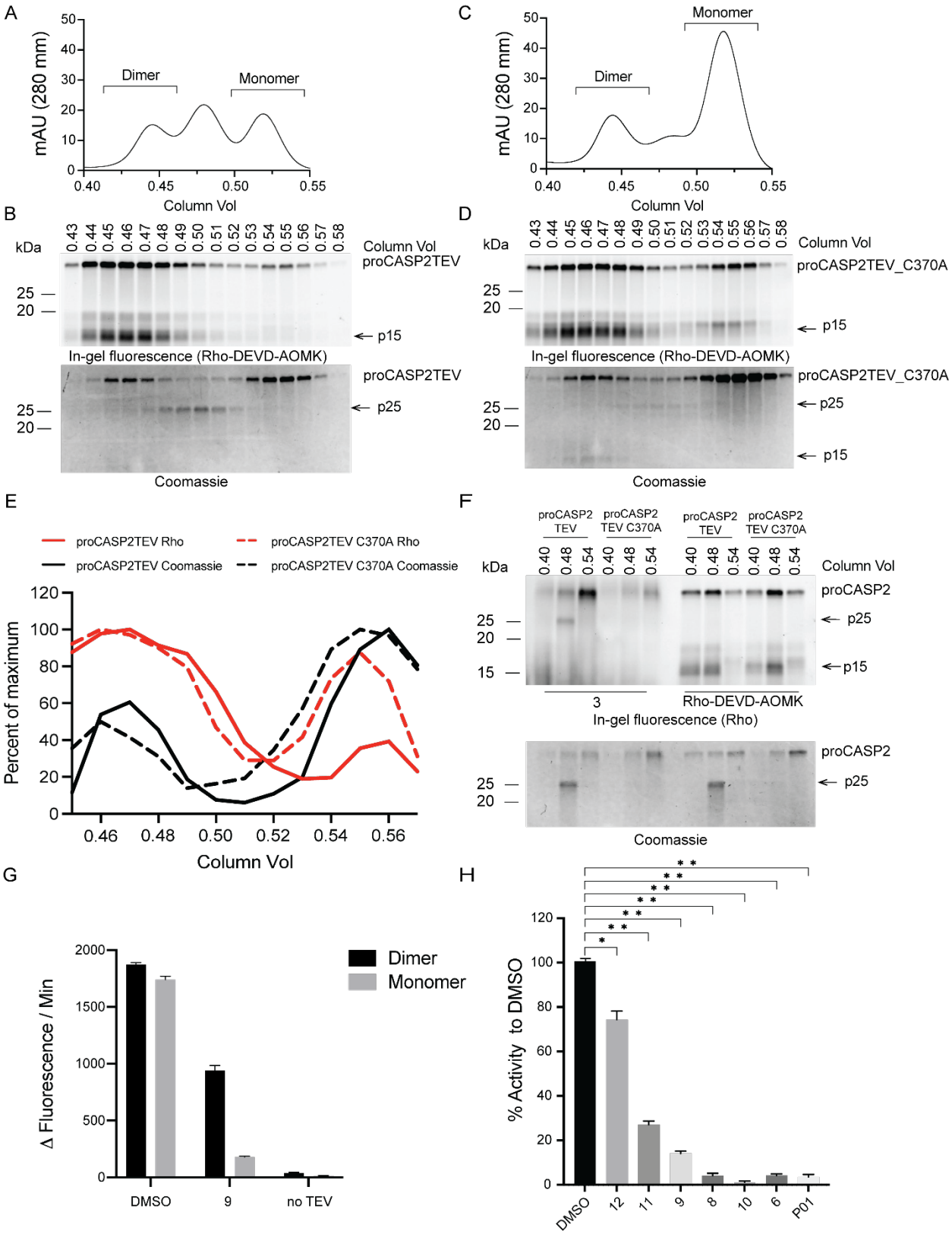
A
mAU (280 mm)
Dimer
Monomer
Column Vol
B
kDa
Column Vol
proCASP2TEV
p15
In-gel fluorescence (Rho-DEVD-AOMK)
proCASP2TEV
p25
Coomassie
C
mAU (280 mm)
Dimer
Monomer
Column Vol
D
kDa
Column Vol
proCASP2TEV_C370A
p15
In-gel fluorescence (Rho-DEVD-AOMK)
proCASP2TEV_C370A
p25
p15
Coomassie
E
proCASP2TEV Rho
proCASP2TEV C370A Rho
proCASP2TEV Coomassie
proCASP2TEV C370A Coomassie
Percent of maximum
Column Vol
F
proCASP2 TEV
proCASP2 TEV C370A
kDa
Column Vol
proCASP2
p25
p15
3
Rho-DEVD-AOMK
In-gel fluorescence (Rho)
Coomassie
G
Δ Fluorescence / Min
Dimer
Monomer
DMSO
9
no TEV
H
% Activity to DMSO
DMSO
12
11
9
8
10
6
P01

Figure 5. **State-dependent inhibition of caspase-2.** (A-D) Gel filtration analysis of (A,B) proCASP2TEV (C,D) proCASP2TEV_C370A showing (A,C) the UV absorbance at 280 nm (A280) for each sample and (B,D) gel-based ABPP analysis of the indicated fractions labeled with **Rho-DEVD-AOMK** (1 μM)**.** (E) Percent of maximum dimeric and monomeric fractions of proCASP2TEV and proCASP2TEV C370A. Relative band intensities were determined for coomassie bands (black) and **Rho-DEVD-AOMK**-labeled bands (red). Percent components of total dimer and monomer forms calculated from the area under the curve (AUC) of dimeric column volume fractions (0.40 - 0.46) and monomeric column volume fractions (0.50 - 0.55) for proCASP2TEV activity assessed by labeling with **Rho-DEVD-AOMK** and total protein assessed with coomassie staining. (F) Gel-based ABPP analysis of the indicated gel filtration fractions for of proCASP2TEV and proCASP2TEV_ C370A with either **Rho-DEVD-AOMK** or **3,** with the latter samples conjugated to Rho-azide by click chemistry. (G) Relative activity of monomeric versus dimeric fractions of proCASP2TEV subjected to the indicated treatment by either compound **9** (100 μM, 1h, 30 ℃) or vehicle (DMSO) followed by addition of TEV protease or vehicle and activity analysis under kosmotropic conditions using **Ac-VDVAD-AFC** fluorogenic substrate. (H) Measured percent activity for monomeric fractions of proCASP2TEV treated with the indicated compounds (100 μM, 1h, 30 ℃) followed by addition of TEV protease and kosmotropic buffer. For B, D, and F Arrows indicate cleaved or processed caspase. For G and H data represent mean values and ± standard deviation of the mean, n = 3 and statistical significance was calculated with unpaired Student's t-tests, * $p<0.05$, ** $p<0.01$.

In cell engagement of C370 is achieved by both broadly caspase reactive and caspase-2 selective compounds. As we postulated that the caspase-2 monomer-dimer equilibrium is likely sensitive to protein concentration, we next wondered whether caspase-2 sensitivity to compound labeling would be maintained in cell-based treatments. Using our established isoTOP-ABPP workflow (**Figure S17**), we subjected Jurkat cells to labeling with both active and inactive compounds followed by lysis, IAA labeling, enrichment, sequence specific proteolysis, and LC-MS/MS analysis. In aggregate, we identified 9089 cysteines from 3506 proteins (**Table S5**). As with our lysate-based labeling, we achieved high caspase coverage, quantifying 21 total cysteines from eight caspases (**Figure 6A**). The SAR observed across the library screen was generally comparable to that observed for our lysate-based labeling studies. Compound **P01** did, however, show modestly increased ratios for our cell-based analysis across all detected caspase cysteines. Of note, we excluded compound **10** from cell-based analysis due to observed general cytotoxicity, which we ascribe to the presence of two putative electrophilic sites in the scaffold.

To further confirm that caspase-2 was directly labeled by our inhibitors in cell-based experiments, we also opted to subject cells to protein-directed ABPP analysis[94]. In this experiment cells were treated with either vehicle DMSO or compound **9,** following which both groups were treated with click probe **3**. After conjugation to biotin-azide, enrichment on streptavidin resin, and on-resin tryptic digest, LC-MS/MS analysis and label-free quantitation (LFQ) using FragPipe Analyst[95] revealed significant enrichment and off-competition of caspase-2 by probes **3** and **9**, respectively (**Figure 6B**). Of the 3080 identified proteins, caspase-2 was one of the top enriched proteins out of the 140

significantly off-competed proteins (log2(FC) >2, adjusted p-value < 0.05). None of the other caspases detected in this experiment were significantly off-competed by compound **9**, which provides further evidence of the selectivity of this compound for caspase-2 (**Figure 6B**).

Guided by our prior work using small molecule inhibitors to delineate the relative involvement of caspase-8 and -10 in initiating extrinsic apoptosis[33] and the widespread use of the pan-caspase inhibitor DEVD-fmk for pinpointing caspase-dependent processes, we assessed compound-dependent changes to apoptosis. We observe that the broadly caspase reactive **P01** afforded a near completed blockade of both intrinsic and extrinsic apoptosis, induced with staurosporine (STS) and FasL, respectively (**Figure 6C, Figure S33**). Compound **5**, which was observed to potently label catalytic cysteines in caspase-8 and -9 initiator caspases as well as C370 in caspase-2, also afforded a partial blockade of extrinsic apoptosis and near complete blockade of intrinsic apoptosis**.** While caspase-2 selective inhibitors, including compound **9** and **11**, robustly labeled C370 *in situ* as measured by isoTOP-ABPP, these compounds did not impact FasL- nor STS-induced apoptosis (**Figure 6C** and **Figure S33**). These findings align with the established functions of caspase-8/9/3 as the primary drivers of these forms of apoptosis.

Caspase-2 is activated in response to DNA-damage and loss of caspase-2 has been shown to decrease activation of apoptosis in response to DNA damaging agents[13, 16, 48-51]. However, apoptosis can proceed in the absence of caspase-2, which complicates delineating caspase-2 activity from that of other caspases. To aid in assessing the activity of our compounds in affecting caspase-2 mediated cellular response to DNA damage, we opted to pursue two parallel lines of inquiry. First, we generated U2OS cells

stably expressing shRNAs targeting caspase-9, which we expected to be the likely caspase responsible for any compensatory activity upon caspase-2 inactivation. Immunoblot analysis revealed robust depletion of caspase-9 for one of the three sHRNAs together with minimal changes to expression for the scrambled shRNA, both for caspase-9 together with other caspases analyzed (**Figure S34**). We then subjected the knockdown cell lines to etoposide followed by immunoblot analysis to assess altered cleavage of caspase-2 in response to caspase-9 knockdown (**Figure 6D**). Strikingly, we observe the rapid cleavage of partially processed caspase-2 (p32) within 1 hour of treatment with etoposide, with no appreciable difference observed for the caspase-9 expressing cells compared to the caspase-9 knockdown cells, respectively (**Figure 6D**, **Figure S35**). These data are consistent with caspase-2 processing occurring independently of caspase-9. Intriguingly, we observe maximal caspase-2 cleavage within 4 hours of treatment, with the signal for cleaved caspase-2 generally decreasing at later timepoints. These data align with the generally rapid cellular response to DNA damage.

Guided by this rapid activation, we opted to subject our U2OS cells to immunoblot analysis following comparatively short 3h treatment with etoposide (**Figure S36**). We find that many of the compounds that engage caspase-2, including **5**, **8** and **9**, afford somewhat decreased PARP1 cleavage. The less selective caspase inhibitors retained this activity at longer 10h etoposide treatment times (**Figure S37**, **S38**). Intriguingly, treatment with these compounds also leads to a modest decrease in the immunoblot signal for caspase-2, caspase-8, and caspase-9, suggestive of compound-induced changes in protein abundance. We do also observe increased PARP cleavage for cells simultaneously treated with etoposide and a subset of our compounds, the cause of which

remains to be elucidated (**Figure S38**). Somewhat unexpectedly, we did not observe substantial compound-induced protection for processing of the p32 form of caspase-2, either for the 3h or 10h etoposide incubations.

We expect that the partially processed p32 caspase observed in non-apoptotic cells, both here and in prior reports, should exist primarily as a protein dimer and thus should be relatively insensitive to our small molecules, consistent with our recombinant protein analysis. To test this hypothesis, we subjected cell lysates treated with either active compound **9** or inactive compound **12** followed by cellular thermal shift assay (CETSA) analysis[96], which revealed marked stabilization of the full length protein upon treatment with compound **9** together with no change in stability of the p32 proteoform (**Figure 6E**) and no stabilization for compound **12** (**Figure S39**). Streptavidin pulldown analysis recapitulated this finding–capture and competition of the full-length protein was observed using compounds **3** and **9**, whereas no signal was detected for the p32 proteoform (**Figure 6F**). These data provide further evidence of in cell preferential engagement of the full-length caspase-2 proteoform. Quantification of phosphorylated H2AX (γ-H2AX[97]) and p53-binding protein 1 (GFP-53BP1[98]) after treatment with etoposide (**Figure S40** respectively) revealed that compound treatment afforded no substantial decrease in either γ-H2AX or GFP-53BP1 signal (**Figure 6G**). Taken together these data are consistent with the C370-inhibitor refractory partially processed p32 form of caspase-2 being primarily responsible for the caspase-2 protease-mediated response to DNA damaging agents.

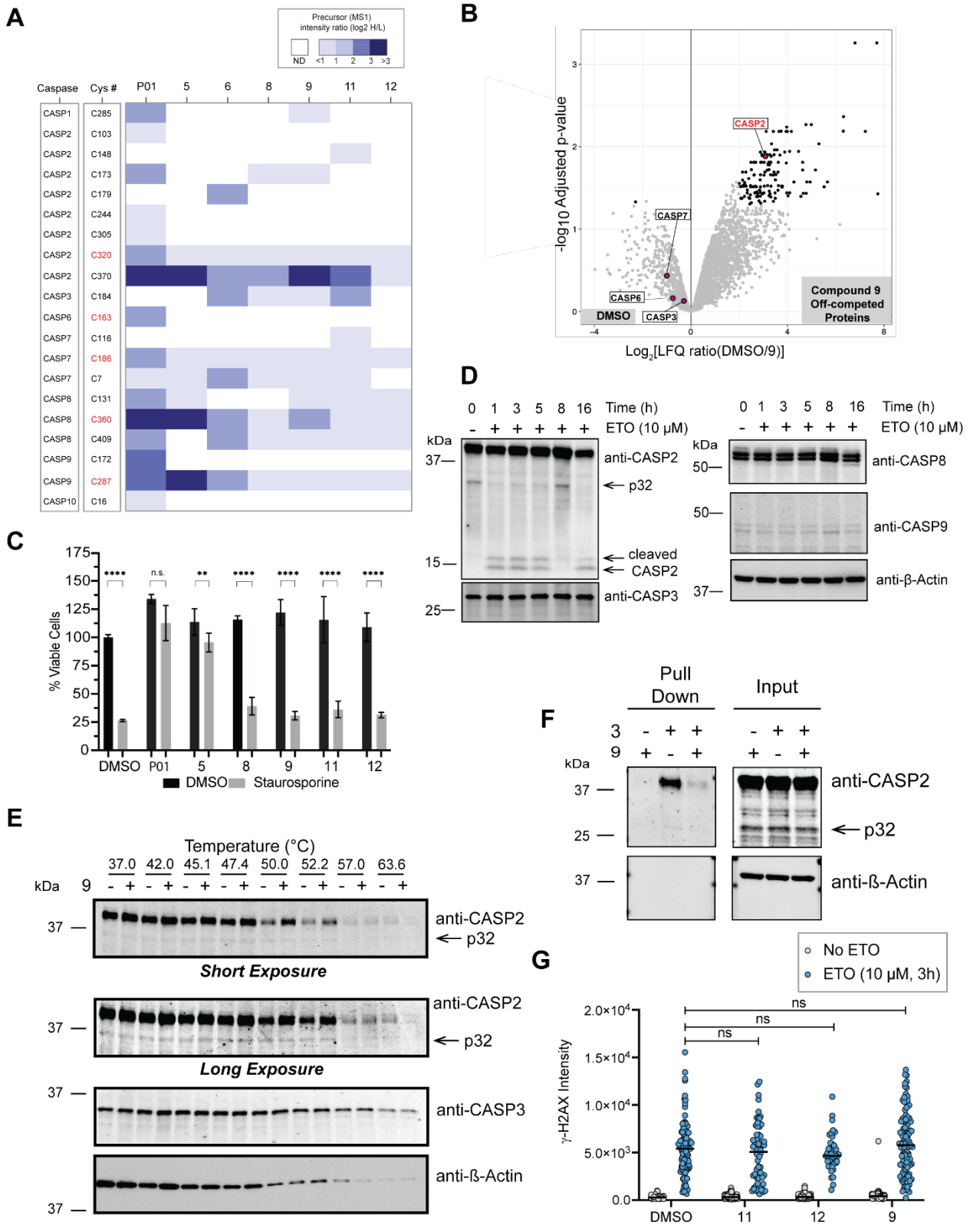
A
Precursor (MS1) intensity ratio (log2 H/L)
ND <1 1 2 3 >3
Caspase Cys # P01 5 6 8 9 11 12
CASP1 C285
CASP2 C103
CASP2 C148
CASP2 C173
CASP2 C179
CASP2 C244
CASP2 C305
CASP2 C320
CASP2 C370
CASP3 C184
CASP6 C163
CASP7 C116
CASP7 C186
CASP7 C7
CASP8 C131
CASP8 C360
CASP8 C409
CASP9 C172
CASP9 C287
CASP10 C16
B
-log10 Adjusted p-value
Log2[LFQ ratio(DMSO/9)]
CASP2
CASP7
CASP6
CASP3
DMSO
Compound 9 Off-competed Proteins
C
% Viable Cells
DMSO P01 5 8 9 11 12
DMSO Staurosporine
n.s.
D
Time (h) 0 1 3 5 8 16
ETO (10 μM) - + + + + +
kDa
anti-CASP2
p32
cleaved CASP2
anti-CASP3
anti-CASP8
anti-CASP9
anti-β-Actin
E
Temperature (°C)
37.0 42.0 45.1 47.4 50.0 52.2 57.0 63.6
kDa 9
anti-CASP2
p32
Short Exposure
Long Exposure
anti-CASP3
anti-ß-Actin
F
Pull Down
Input
3 - + +
9 + - +
kDa
anti-CASP2
p32
anti-ß-Actin
G
No ETO
ETO (10 μM, 3h)
γ-H2AX Intensity
ns
DMSO 11 12 9

Figure 6. **In situ labeling of caspase-2 by electrophilic lead compounds and blockade of extrinsic and intrinsic apoptosis by promiscuous caspase inhibitors.** (A) Caspase cysteines quantified in competitive isoTOP-ABPP analysis of Jurkat cells treated with **P01**, **5**, **6** (25 μM) and **8**, **9**, **10**, **11**, and **12** (100 μM). Competition ratios are calculated from the mean quantified precursor intensity (log_2 H/L) for DMSO (H, heavy) versus compound-treatment (L, light). * indicates catalytic cysteine residue. Experiments were conducted in at least two biological replicates. ND-Not detected. (B) Protein-directed ABPP analysis of U2OS cells treated with compound 9 (100 μM) or vehicle (DMSO) for 1h followed by compound 3 (20 μM) for 1h with proteomic analysis using LFQ and FragPipe Analyst[95]. (C) Comparison of effects of the indicated compounds [1h pre-treatment with **P01**, **5**, and **6** (25 μM) and **8**, **9**, **10**, **11**, and **12** (100 μM)] on staurosporine (STS, 1μM, 4h)-induced apoptosis of Jurkat cells assayed by CellTiter-Glo®. Viability experiments were performed in biological triplicate. (D) Immunoblot analysis of caspase-9 shRNA knockdown U2OS cell line JC1 (see **Figure S34** for confirmation of knockdown) subjected to etoposide (10 μM) for the indicated treatment times. (E) CETSA analysis of U2OS cell lysate treated with compound **9** or compound **12** (100 μM) for 1h followed by immunoblot. (F) U2OS cells were treated with either vehicle (DMSO) or compound **9** (100 μM) for 1h followed by compound **3** (20 μM) for 1h. Following lysis, treated samples were subjected to click-enabled pulldown on streptavidin resin followed by immunoblot analysis. (G) U2OS cells were treated with the indicated compounds (100 μM) for 1h followed by etoposide (10 μM) for 3h were stained for y-H2AX and relative intensity was quantified with ImageJ[99]. All MS data can be found in **Table S5**. For C data represent

mean values and standard deviation, n=3. Statistical significance was calculated with unpaired Student's t-tests, * $p<0.05$, ** $p<0.01$, *** $p<0.005$. ****$p<0.001$. NS $p>0.05$.

DISCUSSION

Despite being the most evolutionarily conserved caspase, caspase-2 remains enigmatic, implicated in numerous cellular processes, spanning DNA damage response, tumor suppression, response to oxidative stress, and has even been linked to nonalcoholic steatohepatitis (NASH)[53], alzheimer's[57, 100], and Huntington's diseases[101]. Thus, there is an increasing interest in the development of caspase-2 selective chemical probes with use for both functional biology and early-stage drug development, demonstrated by recent reports of selective peptide-based inhibitors[102-103]. Here, using a high coverage, FAIMS-enabled chemoproteomics approach, we identify a ligandable, potentially druggable, non-catalytic and active site proximal cysteine (C370). By combining gel-based ABPP and a novel TEV-activation assay, we identify both caspase-2 selective and broadly caspase-reactive lead compounds. We find that covalent modification of C370 occurs in recombinant protein and in cells in a proteoform-selective manner, as demonstrated by the observed zymogen-selectivity and preferential labeling of the monomeric form of caspase-2. The development of proteoform context-dependent small molecule ligands is a burgeoning area, spanning molecular glue degrader molecules[104] to the recently reported DNA-dependent ligands[105]. Our study adds to this toolbox by guiding the discovery and functional characterization of state-dependent targetable cysteine residues in cysteine proteases.

While chemoproteomic analysis confirmed robust engagement of C370 for both cell- and lysate-based analysis, only the more promiscuous caspase lead compounds afforded marked protection from extrinsic and intrinsic apoptosis, including DNA-damage mediated processes. Genetic approaches have linked this latter pathway to caspase-2[13, 16, 50-51]. Thus, we ascribe the disconnect between chemical inhibition and genetic depletion, to the activity of the partially processed p32 form of caspase-2 which we found was generally resistant to covalent modification of C370. We cannot, however, rule out compensatory activities of other caspases or non-catalytic functions of caspase-2, for example activities of its CARD domain[106]. As caspase-2 forms comparatively stable homodimers[45], we cannot rule out the alternative possibility that a small fraction of full length dimerized caspase-2, which is resistant to covalent modification of C370, could be responsible for the observed sensitivity to etoposide-mediated apoptosis. Delineating these possibilities would benefit from the development of the pairing of induced dimerization strategies[107] and caspase-2 directed degrader molecules or through the use of the DTAG system[108].

Our findings contribute to the growing body of evidence regarding the presence of ligandable non-catalytic cysteine residues in other caspases, including the recently targeted cysteine residue C264 in caspase-6[44]. As demonstrated by the blockbuster success of targeting such conserved non-catalytic cysteines in kinases[109-111], non-catalytic cysteines represent an exciting, yet still largely untapped opportunity for high selectivity caspase inhibitor development campaigns. However, despite our best efforts, we were unable to progress our best lead compounds beyond modest low micromolar potency. Despite this limitation, our use of a structurally matched inactive control

compound **12**, allowed us to demonstrate that C370 does exhibit SAR towards electrophilic lead compounds. These findings provide a strong foundation for future efforts, likely enabled by caspase-2 co-crystal structures, to further increase the potency of caspase-2 directed leads. As C370 is uniquely found in caspase-2, these molecules are expected to retain high caspase-2 selectivity.

CONCLUSION

Identification of proteoform selective molecules is an area of rapidly emerging interest[33, 112-116]. As shown by type II inhibitors that target inactive forms of kinases[117-119], we expect that targeting pro-caspases should emerge as a general strategy to selectively inactivate individual caspases in cells. An additional feature of pro-caspase inhibitors is that, when compared with active caspase inhibitors, they should fully block downstream caspase activation—active caspase inhibitors are ill equipped to block the rapid caspase activation (<30 min)[120]— and subsequent cleavage of effector caspases that is observed during apoptosis. However, and pointing towards a potential limitation of such pro-caspase-directed molecules, some caspases, such as caspase-2 exist as partially activated species in proliferating, non-apoptotic cells. Thus, as we have shown here for the p32 form of caspase-2, pro-caspase directed inhibitors may fail to engage the physiologically relevant caspase species, and therefore may prove less useful as tool compounds in these contexts. Thus, we expect that our study together with the development of future chemoproteomic platforms incorporate additional dimensionality (e.g. spliceform or protein molecular weights) will provide a roadmap for the production of such state-dependent chemical probes.

Looking more broadly towards the rapidly evolving area of covalent inhibitor development, our finding that the methylphenylpropiolate scaffold **P01** exhibits widespread cysteine reactivity, both towards caspases and more broadly, points towards untapped opportunities for its use as a scout electrophile. In contrast to similar chloroacetamide scout electrophiles, which have proven challenging to progress to more potent chemical probes, we expect this chemotype should progress more readily towards more attenuated acrylamide leads, both for caspases, and across the cysteinome.

Acknowledgments

This study was supported by National Institutes of Health DP2 GM146246-02 (K.M.B.), Beckman Young Investigator Award (K.M.B.), UCLA DOE Institute (DE-FC02-02ER63421), NSF GRFP (1000235263), TRDRP T31DT1800 (T.Y.), NIGMS System and Integrative Biology 5T32GM008185-33 (L.M.B.), and UCLA's Cellular and Molecular Biology (CMB) Training Program T32GM007185 (E.A.). The UCLA Molecular Screening Shared Resource is supported by Jonsson Comprehensive Cancer Center, award number P30CA016042 by the National Cancer Institute of the National Institutes of Health. We thank all members of the Backus lab for their helpful suggestions and Dennis Wolan for providing plasmids and for the Rho-DEVD-AOMK probe. GFP-53BP1 U2OS reporter cell line was kindly provided to OIF by Claudia Lukas (University of Copenhagen, Denmark)[98].

Conflicts of Interest

The authors declare no financial or commercial conflict of interest.

ASSOCIATED CONTENT

Supplementary Methods and Supplementary Figures S1-S40 and Tables S2, S6-S8 (PDF)

Table S1: Proteomic datasets for isoTOP-ABPP detection of hyperreactive cysteines (xlsx)

Table S3: Proteomic datasets for isoTOP-ABPP ligandability analysis for cell lysates (xlsx)

Table S4: Proteomic datasets for comparison of FAIMS versus no FAIMS acquisition and recombinant protein labeling (xlsx)

Table S5: Proteomic datasets for isoTOP-ABPP ligandability analysis for cells and for Protein-directed ABPP in cells (xlsx)

Table S9: Sequences of shRNAs used (xlsx)

The MS data have been deposited to the ProteomeXchange Consortium (http://proteomecentral.proteomexchange.org) via the PRIDE[121] partner repository with the dataset identifiers PXD042362, PXD051381, and PXD046269.

References

1. Kumar, S., et al., *Induction of apoptosis by the mouse Nedd2 gene, which encodes a protein similar to the product of the Caenorhabditis elegans cell death gene ced-3 and*

the mammalian IL-1 beta-converting enzyme. Genes & Development, 1994. **8**(14): p. 1613-1626.

2. Yuan, J., et al., *The C. elegans cell death gene ced-3 encodes a protein similar to mammalian interleukin-1 beta-converting enzyme.* Cell, 1993. **75**(4): p. 641-52.
3. Wang, L., et al., *Ich-1, an Ice/ced-3-related gene, encodes both positive and negative regulators of programmed cell death.* Cell, 1994. **78**(5): p. 739-750.
4. Chun, H.J., et al., *Pleiotropic defects in lymphocyte activation caused by caspase-8 mutations lead to human immunodeficiency.* Nature, 2002. **419**(6905): p. 395-399.
5. Alam, A., et al., *Early Activation of Caspases during T Lymphocyte Stimulation Results in Selective Substrate Cleavage in Nonapoptotic Cells.* The Journal of Experimental Medicine, 1999. **190**(12): p. 1879-1890.
6. Fujita, J., et al., *Caspase activity mediates the differentiation of embryonic stem cells.* Cell Stem Cell, 2008. **2**(6): p. 595-601.
7. Baena-Lopez, L.A., et al., *Non-apoptotic Caspase regulation of stem cell properties.* Semin Cell Dev Biol, 2018. **82**: p. 118-126.
8. Madadi, Z., et al., *The non-apoptotic role of caspase-9 promotes differentiation in leukemic cells.* Biochimica Et Biophysica Acta. Molecular Cell Research, 2019. **1866**(12): p. 118524.
9. Sakthivel, D., et al., *Caspase-2 is essential for proliferation and self-renewal of nucleophosmin-mutated acute myeloid leukemia.* bioRxiv: The Preprint Server for Biology (Cancer Biology), Posted May 30, 2023: p. DOI:2023.05.29.542723 (accessed 2024-04-01).

10. Thornberry, N.A., et al., *A novel heterodimeric cysteine protease is required for interleukin-1βprocessing in monocytes.* Nature, 1992. **356**(6372): p. 768-774.
11. Salmena, L., et al., *Essential role for caspase 8 in T-cell homeostasis and T-cell-mediated immunity.* Genes & Development, 2003. **17**(7): p. 883-895.
12. Wang, J., et al., *Inherited Human Caspase 10 Mutations Underlie Defective Lymphocyte and Dendritic Cell Apoptosis in Autoimmune Lymphoproliferative Syndrome Type II.* Cell, 1999. **98**(1): p. 47-58.
13. Boice, A.G., et al., *Caspase-2 regulates S-phase cell cycle events to protect from DNA damage accumulation independent of apoptosis.* Oncogene, 2022. **41**(2): p. 204-219.
14. Martinon, F. and J. Tschopp, *Inflammatory caspases and inflammasomes: master switches of inflammation.* Cell Death & Differentiation, 2007. **14**(1): p. 10-22.
15. Oliver, T.G., et al., *Caspase-2-mediated cleavage of Mdm2 creates a p53-induced positive feedback loop.* Molecular Cell, 2011. **43**(1): p. 57-71.
16. Terry, M.R., et al., *Caspase-2 impacts lung tumorigenesis and chemotherapy response in vivo.* Cell Death & Differentiation, 2015. **22**(5): p. 719-730.
17. Eskandari, E. and C.J. Eaves, *Paradoxical roles of caspase-3 in regulating cell survival, proliferation, and tumorigenesis.* Journal of Cell Biology, 2022. **221**(6): p. e202201159.
18. Rissman, R.A., et al., *Caspase-cleavage of tau is an early event in Alzheimer disease tangle pathology.* J Clin Invest, 2004. **114**(1): p. 121-30.
19. Fuentes-Prior, P. and Guy S. Salvesen, *The protein structures that shape caspase activity, specificity, activation and inhibition.* Biochemical Journal, 2004. **384**(Pt 2): p. 201-232.

20. Chéreau, D., et al., *Structural and Functional Analysis of Caspase Active Sites.* Biochemistry, 2003. **42**(14): p. 4151-4160.

21. McLuskey, K. and Jeremy C. Mottram, *Comparative structural analysis of the caspase family with other clan CD cysteine peptidases.* Biochemical Journal, 2015. **466**(Pt 2): p. 219-232.

22. Julien, O. and J.A. Wells, *Caspases and their substrates.* Cell Death and Differentiation, 2017. **24**(8): p. 1380-1389.

23. Lee, B.L., et al., *ASC- and caspase-8-dependent apoptotic pathway diverges from the NLRC4 inflammasome in macrophages.* Scientific Reports, 2018. **8**(1): p. 3788.

24. Zheng, T.S. and R.A. Flavell, *Divinations and Surprises: Genetic Analysis of Caspase Function in Mice.* Experimental Cell Research, 2000. **256**(1): p. 67-73.

25. Hartung, I.V., et al., *Expanding Chemical Probe Space: Quality Criteria for Covalent and Degrader Probes.* Journal of Medicinal Chemistry, 2023. **66**(14): p. 9297-9312.

26. Garbaccio, Robert M. and Emma R. Parmee, *The Impact of Chemical Probes in Drug Discovery: A Pharmaceutical Industry Perspective.* Cell Chemical Biology, 2016. **23**(1): p. 10-17.

27. Garcia-Calvo, M., et al., *Inhibition of human caspases by peptide-based and macromolecular inhibitors.* The Journal of Biological Chemistry, 1998. **273**(49): p. 32608-32613.

28. Nicholson, D.W., et al., *Identification and inhibition of the ICE/CED-3 protease necessary for mammalian apoptosis.* Nature, 1995. **376**(6535): p. 37-43.

29. Enari, M., H. Hug, and S. Nagata, *Involvement of an ICE-like protease in Fas-mediated apoptosis.* Nature, 1995. **375**(6526): p. 78-81.

30. Slee, E.A., et al., *Benzyloxycarbonyl-Val-Ala-Asp (OMe) fluoromethylketone (Z-VAD.FMK) inhibits apoptosis by blocking the processing of CPP32.* The Biochemical Journal, 1996. **315 (Pt 1)**(Pt 1): p. 21-24.

31. Thornberry, N.A., et al., *Inactivation of Interleukin-1.beta. Converting Enzyme by Peptide (Acyloxy)methyl Ketones.* Biochemistry, 1994. **33**(13): p. 3934-3940.

32. Kato, D., et al., *Activity-based probes that target diverse cysteine protease families.* Nature Chemical Biology, 2005. **1**(1): p. 33-38.

33. Backus, K.M., et al., *Proteome-wide covalent ligand discovery in native biological systems.* Nature, 2016. **534**(7608): p. 570-574.

34. Cuellar, M.E., et al., *An electrophilic fragment screening for the development of small molecules targeting caspase-2.* European Journal of Medicinal Chemistry, 2023. **259**: p. 115632.

35. Talanian, R.V., et al., *Substrate Specificities of Caspase Family Proteases *.* Journal of Biological Chemistry, 1997. **272**(15): p. 9677-9682.

36. Pop, C. and G.S. Salvesen, *Human Caspases: Activation, Specificity, and Regulation *.* Journal of Biological Chemistry, 2009. **284**(33): p. 21777-21781.

37. Xu, J.H., et al., *Integrative X-ray Structure and Molecular Modeling for the Rationalization of Procaspase-8 Inhibitor Potency and Selectivity.* ACS Chemical Biology, 2020. **15**(2): p. 575-586.

38. Hardy, J.A., et al., *Discovery of an allosteric site in the caspases.* Proceedings of the National Academy of Sciences, 2004. **101**(34): p. 12461-12466.

39. Tubeleviciute-Aydin, A., et al., *Identification of Allosteric Inhibitors against Active Caspase-6.* Sci Rep, 2019. **9**(1): p. 5504.

40. Vance, N.R., L. Gakhar, and M.A. Spies, *Allosteric Tuning of Caspase-7: A Fragment-Based Drug Discovery Approach.* 2017. **56**(46): p. 14443-14447.

41. Scheer, J.M., M.J. Romanowski, and J.A. Wells, *A common allosteric site and mechanism in caspases.* Proceedings of the National Academy of Sciences, 2006. **103**(20): p. 7595-7600.

42. Palafox, M.F., et al., *From chemoproteomic-detected amino acids to genomic coordinates: insights into precise multi-omic data integration.* Molecular Systems Biology, 2021. **17**(2): p. e9840.

43. Jiang, Z.L., et al., *S-nitrosylation of caspase-3 is the mechanism by which adhesion fibroblasts manifest lower apoptosis.* Wound Repair and Regeneration, 2009. **17**(2): p. 224-229.

44. Van Horn, K.S., et al., *Engaging a Non-catalytic Cysteine Residue Drives Potent and Selective Inhibition of Caspase-6.* Journal of the American Chemical Society, 2023. **145**(18): p. 10015-10021.

45. Baliga, B.C., S.H. Read, and S. Kumar, *The biochemical mechanism of caspase-2 activation.* Cell Death & Differentiation, 2004. **11**(11): p. 1234-1241.

46. Olsson, M., J. Forsberg, and B. Zhivotovsky, *Caspase-2: the reinvented enzyme.* Oncogene, 2015. **34**(15): p. 1877-1882.

47. Bouchier-Hayes, L. and D.R. Green, *Caspase-2: the orphan caspase.* Cell Death Differ, 2012. **19**(1): p. 51-7.

48. Lim, Y., L. Dorstyn, and S. Kumar, *The p53-caspase-2 axis in the cell cycle and DNA damage response.* Experimental & Molecular Medicine, 2021. **53**(4): p. 517-527.

49. Sohn, D., W. Budach, and R.U. Jänicke, *Caspase-2 is required for DNA damage-induced expression of the CDK inhibitor p21(WAF1/CIP1).* Cell Death Differ, 2011. **18**(10): p. 1664-74.

50. Oliver, T.G., et al., *Caspase-2-mediated cleavage of Mdm2 creates a p53-induced positive feedback loop.* Mol Cell, 2011. **43**(1): p. 57-71.

51. Tinel, A. and J. Tschopp, *The PIDDosome, a protein complex implicated in activation of caspase-2 in response to genotoxic stress.* Science, 2004. **304**(5672): p. 843-6.

52. Wilson, C.H., et al., *Caspase-2 deficiency enhances whole-body carbohydrate utilisation and prevents high-fat diet-induced obesity.* Cell Death & Disease, 2017. **8**(10): p. e3136.

53. Kim, J.Y., et al., *ER Stress Drives Lipogenesis and Steatohepatitis via Caspase-2 Activation of S1P.* Cell, 2018. **175**(1): p. 133-145.e15.

54. Dawar, S., et al., *Caspase-2-mediated cell death is required for deleting aneuploid cells.* Oncogene, 2017. **36**(19): p. 2704-2714.

55. Fava, L.L., et al., *The PIDDosome activates p53 in response to supernumerary centrosomes.* Genes & Development, 2017. **31**(1): p. 34-45.

56. Ho, L.H., et al., *A tumor suppressor function for caspase-2.* Proceedings of the National Academy of Sciences of the United States of America, 2009. **106**(13): p. 5336-5341.

57. Zhao, X., et al., *Caspase-2 cleavage of tau reversibly impairs memory.* Nature Medicine, 2016. **22**(11): p. 1268-1276.

58. Machado, M.V., et al., *Reduced lipoapoptosis, hedgehog pathway activation and fibrosis in caspase-2 deficient mice with non-alcoholic steatohepatitis.* Gut, 2015. **64**(7): p. 1148-57.

59. Kapust, R.B., et al., *The P1' specificity of tobacco etch virus protease.* Biochemical and biophysical research communications, 2002. **294**(5): p. 949-955.

60. Weerapana, E., et al., *Quantitative reactivity profiling predicts functional cysteines in proteomes.* Nature, 2010. **468**(7325): p. 790-795.

61. Weerapana, E., A.E. Speers, and B.F. Cravatt, *Tandem orthogonal proteolysis-activity-based protein profiling (TOP-ABPP)--a general method for mapping sites of probe modification in proteomes.* Nature Protocols, 2007. **2**(6): p. 1414-1425.

62. Abraham, R.T. and A. Weiss, *Jurkat T cells and development of the T-cell receptor signalling paradigm.* Nat Rev Immunol, 2004. **4**(4): p. 301-8.

63. Saba, J., et al., *Enhanced sensitivity in proteomics experiments using FAIMS coupled with a hybrid linear ion trap/Orbitrap mass spectrometer.* J Proteome Res, 2009. **8**(7): p. 3355-66.

64. Hebert, A.S., et al., *Comprehensive Single-Shot Proteomics with FAIMS on a Hybrid Orbitrap Mass Spectrometer.* Analytical Chemistry, 2018. **90**(15): p. 9529-9537.

65. Arad, D., R. Langridge, and P.A. Kollman, *A simulation of the sulfur attack in catalytic pathway of papain using molecular mechanics and semiempirical quantum mechanics.* Journal of the American Chemical Society, 1990. **112**(2): p. 491-502.

66. Itoh, N., et al., *The polypeptide encoded by the cDNA for human cell surface antigen Fas can mediate apoptosis.* Cell, 1991. **66**(2): p. 233-243.

67. Suda, T., et al., *Molecular cloning and expression of the Fas ligand, a novel member of the tumor necrosis factor family.* Cell, 1993. **75**(6): p. 1169-78.

68. Yang, J., et al., *The I-TASSER Suite: protein structure and function prediction.* Nature Methods, 2015. **12**(1): p. 7-8.

69. Elliott, J.M., et al., *Crystal Structure of Procaspase-1 Zymogen Domain Reveals Insight into Inflammatory Caspase Autoactivation.* Journal of Biological Chemistry, 2009. **284**(10): p. 6546-6553.

70. Chai, J., et al., *Crystal Structure of a Procaspase-7 Zymogen: Mechanisms of Activation and Substrate Binding.* Cell, 2001. **107**(3): p. 399-407.

71. Thomsen, N.D., J.T. Koerber, and J.A.J.P.o.t.N.A.o.S. Wells, *Structural snapshots reveal distinct mechanisms of procaspase-3 and-7 activation.* 2013. **110**(21): p. 8477-8482.

72. Hughes, C.S., et al., *Single-pot, solid-phase-enhanced sample preparation for proteomics experiments.* Nature Protocols, 2019. **14**(1): p. 68-85.

73. Backus, K.M., *Applications of Reactive Cysteine Profiling.* Curr Top Microbiol Immunol, 2019. **420**: p. 375-417.

74. Roy, A., A. Kucukural, and Y. Zhang, *I-TASSER: a unified platform for automated protein structure and function prediction.* Nat Protoc, 2010. **5**(4): p. 725-38.

75. Zhang, Y., *I-TASSER server for protein 3D structure prediction.* BMC Bioinformatics, 2008. **9**: p. 40.

76. Schrödinger L, D.W., *The PyMOL Molecular Graphics System*. 2020: Schrödinger, LLC.

77. Vickers, C.J., G.E. González-Páez, and D.W. Wolan, *Selective detection and inhibition of active caspase-3 in cells with optimized peptides.* J Am Chem Soc, 2013. **135**(34): p. 12869-76.

78. Salvesen, G.S. and V.M. Dixit, *Caspase activation: The induced-proximity model.* Proceedings of the National Academy of Sciences, 1999. **96**(20): p. 10964-10967.

79. Kruspig, B., et al., *Citrate kills tumor cells through activation of apical caspases.* Cell Mol Life Sci, 2012. **69**(24): p. 4229-37.

80. Boatright, K.M., et al., *A unified model for apical caspase activation.* Mol Cell, 2003. **11**(2): p. 529-41.

81. Ito, A., et al., *Possible involvement of cytochrome c release and sequential activation of caspases in ceramide-induced apoptosis in SK-N-MC cells.* Biochimica Et Biophysica Acta, 1999. **1452**(3): p. 263-274.

82. Browne, C.M., et al., *A Chemoproteomic Strategy for Direct and Proteome-Wide Covalent Inhibitor Target-Site Identification.* J Am Chem Soc, 2019. **141**(1): p. 191-203.

83. Cao, J., et al., *Multiplexed CuAAC Suzuki-Miyaura Labeling for Tandem Activity-Based Chemoproteomic Profiling.* Anal Chem, 2021. **93**(4): p. 2610-2618.

84. Boatner, L.M., et al., *CysDB: a human cysteine database based on experimental quantitative chemoproteomics.* Cell Chem Biol, 2023. **30**(6): p. 683-698.e3.

85. Yan, T., et al., *SP3-FAIMS Chemoproteomics for High-Coverage Profiling of the Human Cysteinome*.* Chembiochem, 2021. **22**(10): p. 1841-1851.

86. Hebert, A.S., et al., *Comprehensive Single-Shot Proteomics with FAIMS on a Hybrid Orbitrap Mass Spectrometer.* Anal Chem, 2018. **90**(15): p. 9529-9537.

87. Ziegler, A.R., et al., *FAIMS-enabled N-terminomics analysis reveals novel legumain substrates in murine spleen.* bioRxiv: The Preprint Server for Biology (Biochemistry), Posted July 19, 2023: p. DOI:2023.07.18.549248 (accessed 2024-04-01).

88. Morgan, C.W., et al., *Turning on caspases with genetics and small molecules.* Methods Enzymol, 2014. **544**: p. 179-213.

89. Julien, O., et al., *Quantitative MS-based enzymology of caspases reveals distinct protein substrate specificities, hierarchies, and cellular roles.* Proc Natl Acad Sci U S A, 2016. **113**(14): p. E2001-10.

90. Gray, D.C., S. Mahrus, and J.A. Wells, *Activation of specific apoptotic caspases with an engineered small-molecule-activated protease.* Cell, 2010. **142**(4): p. 637-46.

91. Sharp, L.L., J. Zhou, and D.F. Blair, *Tryptophan-scanning mutagenesis of MotB, an integral membrane protein essential for flagellar rotation in Escherichia coli.* Biochemistry, 1995. **34**(28): p. 9166-71.

92. Vallée-Bélisle, A. and S.W. Michnick, *Visualizing transient protein-folding intermediates by tryptophan-scanning mutagenesis.* Nat Struct Mol Biol, 2012. **19**(7): p. 731-6.

93. Taylor, I.R., et al., *Tryptophan scanning mutagenesis as a way to mimic the compound-bound state and probe the selectivity of allosteric inhibitors in cells.* Chem Sci, 2020. **11**(7): p. 1892-1904.

94. Cravatt, B.N., E.; Hayward, R.; DeMeester, K.; Ogasawara, D.; Dix, M.; Nguyen, T.; Ashby, P.; Simon, G.; Schreiber, S.; Melillo, B., *Comprehensive Mapping of Electrophilic Small Molecule-Protein Interactions in Human Cells.* ChemRxiv Posted Jun 04, 2023: p. DOI:10.26434/chemrxiv-2023-s446 (accessed 2023-08-01).

95. Hsiao, Y., et al., *Analysis and visualization of quantitative proteomics data using FragPipe-Analyst.* bioRxiv: The Preprint Server for Biology (Bioinformatics), Posted March 11, 2024: p. 10.1101/2024.03.05.583643 (accessed 2024-04-01).

96. Jafari, R., et al., *The cellular thermal shift assay for evaluating drug target interactions in cells.* Nat Protoc, 2014. **9**(9): p. 2100-22.

97. Sandoval, C., K. Nisson, and O.I. Fregoso, *HIV-1 Vpr-induced DNA damage activates NF-κB through ATM-NEMO independent of cell cycle arrest.* bioRxiv: The Preprint Server for Biology (Microbiology), Posted May 23, 2023: p. 10.1101/2023.05.23.541990 (accessed 2024-04-15).

98. Bekker-Jensen, S., et al., *Dynamic assembly and sustained retention of 53BP1 at the sites of DNA damage are controlled by Mdc1/NFBD1.* J Cell Biol, 2005. **170**(2): p. 201-11.

99. Schneider, C.A., W.S. Rasband, and K.W. Eliceiri, *NIH Image to ImageJ: 25 years of image analysis.* Nature Methods, 2012. **9**(7): p. 671-675.

100. Pozueta, J., et al., *Caspase-2 is required for dendritic spine and behavioral alterations in J20 APP transgenic mice.* Nature communications, 2013. **4**: p. 1939.

101. Hermel, E., et al., *Specific caspase interactions and amplification are involved in selective neuronal vulnerability in Huntington's disease.* Cell Death & Differentiation, 2004. **11**(4): p. 424-438.

102. Bosc, E., et al., *Genuine selective caspase-2 inhibition with new irreversible small peptidomimetics.* Cell Death & Disease, 2022. **13**(11): p. 959.

103. Poreba, M., et al., *Potent and selective caspase-2 inhibitor prevents MDM-2 cleavage in reversine-treated colon cancer cells.* Cell Death Differ, 2019. **26**(12): p. 2695-2709.

104. Ito, T., et al., *Identification of a primary target of thalidomide teratogenicity.* Science, 2010. **327**(5971): p. 1345-50.

105. Won, S.J., et al., *Redirecting the pioneering function of FOXA1 with covalent small molecules.* bioRxiv: The Preprint Server for Biology (Biochemistry), Posted March 21, 2024.: p. 10.1101/2024.03.21.586158 (accessed 2024-03-30).

106. Bouchier-Hayes, L. and S.J. Martin, *CARD games in apoptosis and immunity.* EMBO Rep, 2002. **3**(7): p. 616-21.

107. Robeson, A.C., et al., *Dimer-specific immunoprecipitation of active caspase-2 identifies TRAF proteins as novel activators.* Embo j, 2018. **37**(14).

108. Nabet, B., et al., *The dTAG system for immediate and target-specific protein degradation.* Nature Chemical Biology, 2018. **14**(5): p. 431-441.

109. Zhang, J., P.L. Yang, and N.S. Gray, *Targeting cancer with small molecule kinase inhibitors.* Nature Reviews Cancer, 2009. **9**(1): p. 28-39.

110. Zhao, Z. and P.E. Bourne, *Progress with covalent small-molecule kinase inhibitors.* Drug Discovery Today, 2018. **23**(3): p. 727-735.

111. Abdeldayem, A., et al., *Advances in covalent kinase inhibitors.* Chemical Society Reviews, 2020. **49**(9): p. 2617-2687.

112. Cravatt, B.F., *Activity-Based Protein Profiling – Finding General Solutions to Specific Problems.* Israel Journal of Chemistry, 2023. **63**(3-4): p. e202300029.

113. Kemper, E.K., et al., *Global profiling of phosphorylation-dependent changes in cysteine reactivity.* Nat Methods, 2022. **19**(3): p. 341-352.

114. Ostrem, J.M., et al., *K-Ras(G12C) inhibitors allosterically control GTP affinity and effector interactions.* Nature, 2013. **503**(7477): p. 548-51.

115. Dhawan, N.S., A.P. Scopton, and A.C. Dar, *Small molecule stabilization of the KSR inactive state antagonizes oncogenic Ras signalling.* Nature, 2016. **537**(7618): p. 112-116.

116. Dai, S.A., et al., *State-selective modulation of heterotrimeric Gαs signaling with macrocyclic peptides.* Cell, 2022. **185**(21): p. 3950-3965.e25.

117. Wang, W., D. Krosky, and K. Ahn, *Discovery of Inactive Conformation-Selective Kinase Inhibitors by Utilizing Cascade Assays.* Biochemistry, 2017. **56**(34): p. 4449-4456.

118. Ayala-Aguilera, C.C., et al., *Small Molecule Kinase Inhibitor Drugs (1995–2021): Medical Indication, Pharmacology, and Synthesis.* Journal of Medicinal Chemistry, 2022. **65**(2): p. 1047-1131.

119. Schindler, T., et al., *Structural mechanism for STI-571 inhibition of abelson tyrosine kinase.* Science, 2000. **289**(5486): p. 1938-42.

120. Tyas, L., et al., *Rapid caspase-3 activation during apoptosis revealed using fluorescence-resonance energy transfer.* EMBO Rep, 2000. **1**(3): p. 266-70.

121. Perez-Riverol, Y., et al., *The PRIDE database and related tools and resources in 2019: improving support for quantification data.* Nucleic Acids Res, 2019. **47**(D1): p. D442-d450.

SUPPORTING INFORMATION

Chemoproteomics identifies state-dependent and proteoform-selective caspase-2 inhibitors

José O. Castellón[1], Samuel Ofori[1], Nikolas R. Burton[1,2], Ashley R. Julio[1,2], Alexandra C. Turmon[1,2], Ernest Armenta[1,2], Carina Sandoval[6], Lisa M. Boatner[1,2], Evan E. Takayoshi[1,2], Marina Faragalla[1,2], Cameron Taylor[7], Ann Zhou[1,2], Ky Tran[1,2], Jeremy Shek[1,2], Tianyang Yan[1,2], Heta S. Desai[1], Oliver I. Fregoso[6], Robert Damoiseaux[4,5,7,8,9], Keriann M. Backus[1, 2,3,4,5]

1. Biological Chemistry Department, David Geffen School of Medicine, UCLA, Los Angeles, CA, 90095, USA

2. Department of Chemistry and Biochemistry, UCLA, CA 90095, USA

3. DOE Institute for Genomics and Proteomics, UCLA, Los Angeles, CA 90095, USA ;

4. Jonsson Comprehensive Cancer Center, UCLA, Los Angeles, CA 90095, USA

5. Eli and Edythe Broad Center of Regenerative Medicine and Stem Cell Research, UCLA, Los Angeles, CA 90095 USA

6. Department of Microbiology, Immunology, and Molecular Genetics, University of California, Los Angeles, California, USA

7. California NanoSystems Institute (CNSI), UCLA, Los Angeles, CA, 90095, United States

8. Department of Molecular and Medical Pharmacology, UCLA, Los Angeles, CA, 90095, USA

9. Department of Bioengineering, Samueli School of Engineering, UCLA, Los Angeles, CA, 90095, USA

* Corresponding Author: Keriann M. Backus, Biological Chemistry Department, David Geffen School of Medicine, UCLA, Los Angeles, CA, 90095, USA, E-mail: kbackus@mednet.ucla.edu.

Table of Contents

1. Supplementary Figures

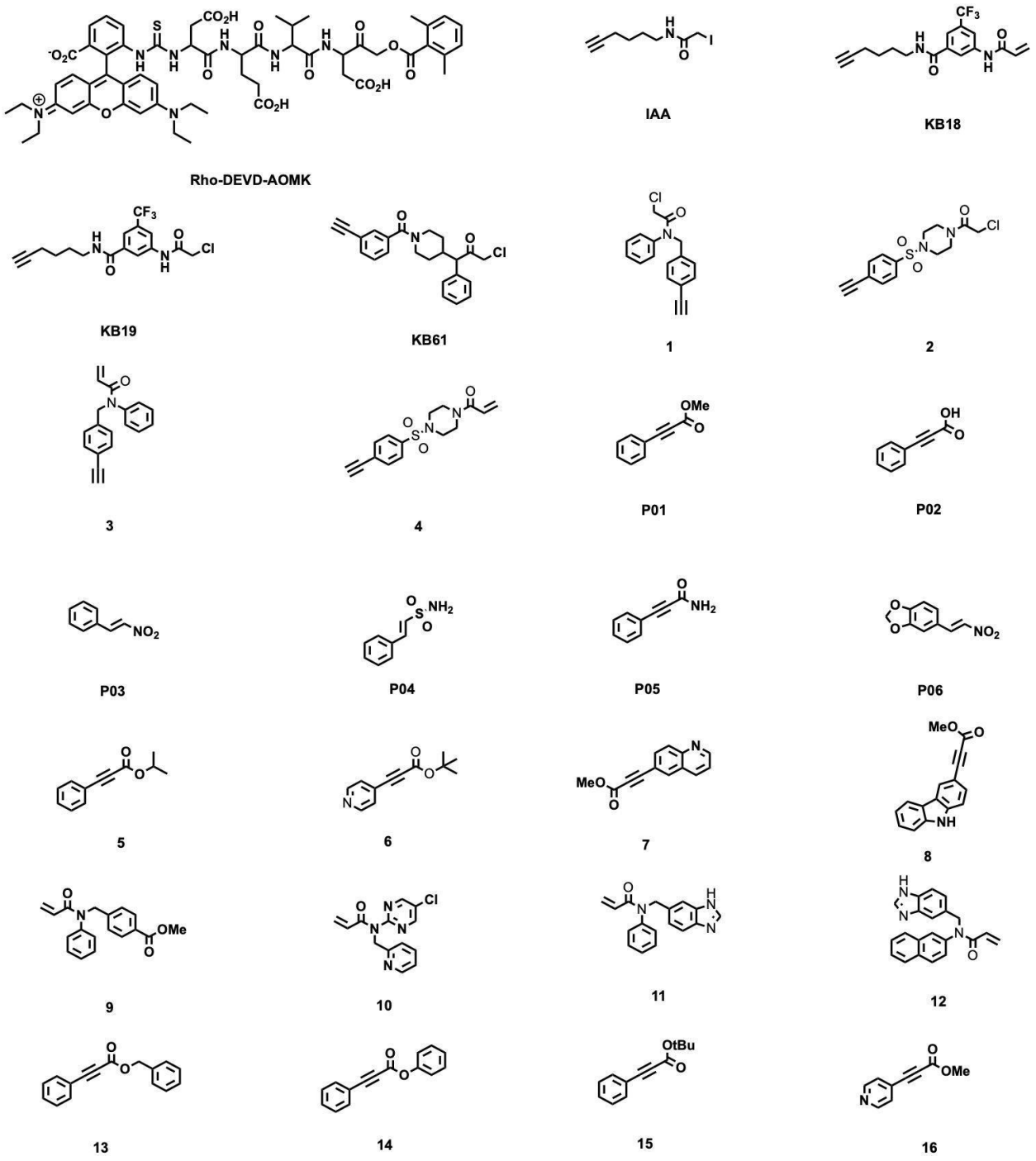

Figure S1. **Structures of compounds used in this study**, including previously reported compounds **KB18**, **KB19**, and **KB61** reported by Backus, KM., et al. 2016[1], **Rho-DEVD-**

AOMK probe generated by Wolan *et al*.,[1] iodoacetamide alkyne (**IAA**) first reported by Weerapana et al.,[2] and purchased compounds **P01** (Fisher Scientific, AC334590050), **P02** (Fisher Scientific, P06105G), **P03** (Combi-blocks, QB-5712), (**P04** (Combi-blocks, ST-8644), **P05** (Combi-blocks, QC-2990) and **P06** (Combi-blocks, QF-4549).

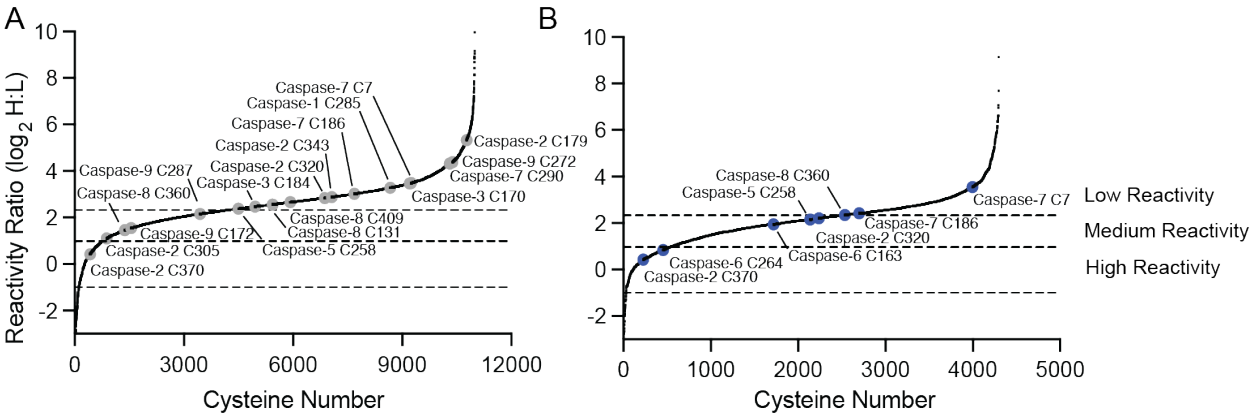

Figure S2. **Isotopic tandem orthogonal proteolysis–activity-based protein profiling (isoTOP-ABPP) reactivity analysis of (A) non-apoptotic cell lysates and (B) apoptotic lysates.** Cell lysates obtained for Jurkat cells treated with FasL (50 ng/μL FasL, 4h) and subjected to isoTOP-ABPP ABPP[2-3] comparing concentration-dependent cysteine labeling by **IAA (**10 μM vs 100 μM, 1h) analysis following the workflow shown in **Figure 1A**. IsoTOP-ABPP ratio ($R_{10:1}$) reactivity thresholds, calculated from the MS1 ion intensity ratios: "high" reactivity: $Log_2(R_{heavy:light})$ = -1.0 – 1.0, "medium" reactivity: $Log_2(R_{heavy:light})$ = = 1 - 2.32, "low" reactivity $Log_2(R_{heavy:light})$ = >2.32. Non-apoptotic experiments (n=6). Apoptotic experiments (n = 5). All MS data can be found in **Table S1**.

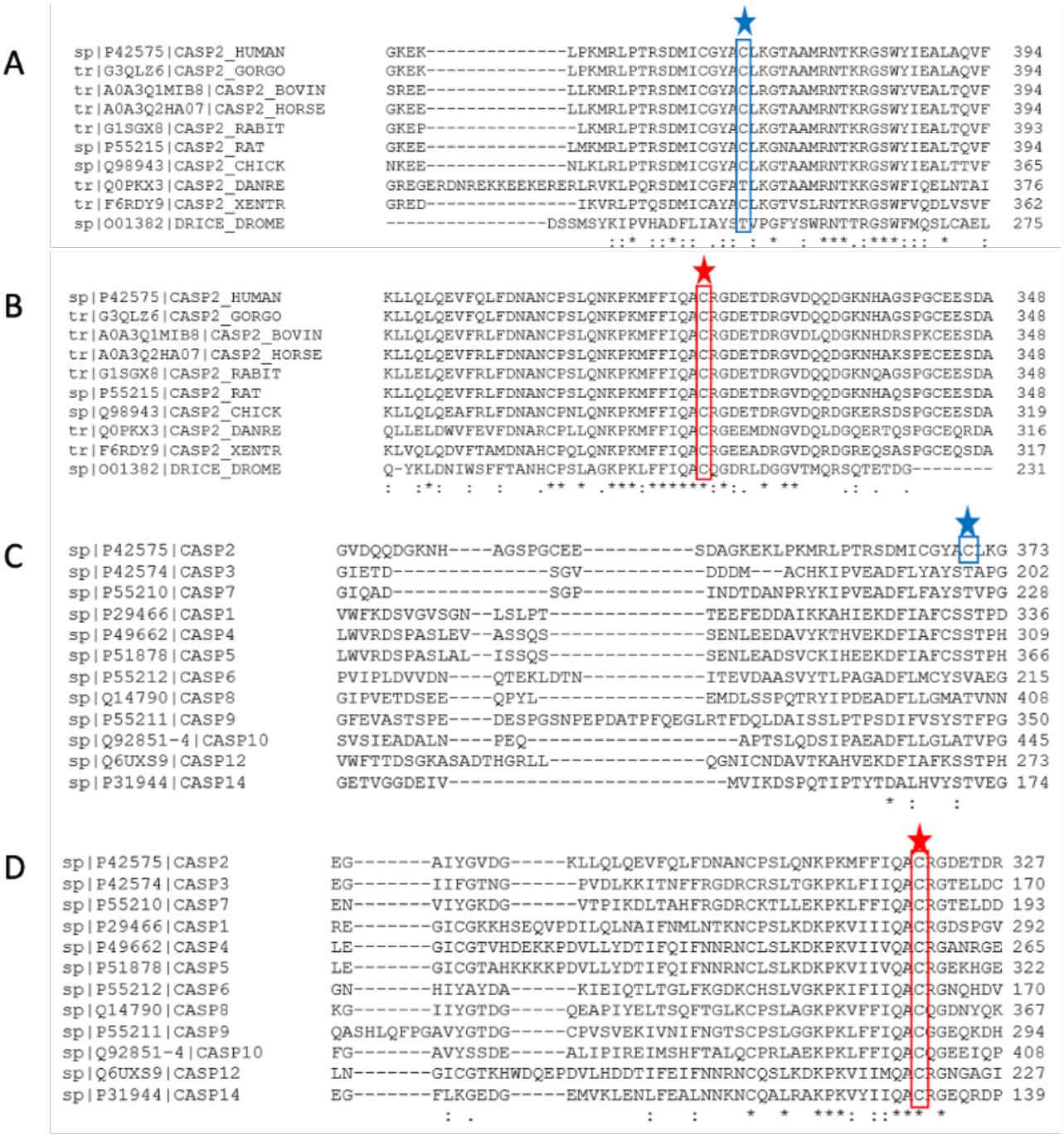

Figure S3. C370 is highly conserved and unique to caspase-2. (A,B) Model organism caspase-2 orthologue protein sequence alignments (Clustal Omega.[4-5] (A) C370 in blue and (B) catalytic C320 in red. (C,D) Protein sequence alignment of 12 human caspases. (C) C370 in blue and (D) Catalytic C320 in red.

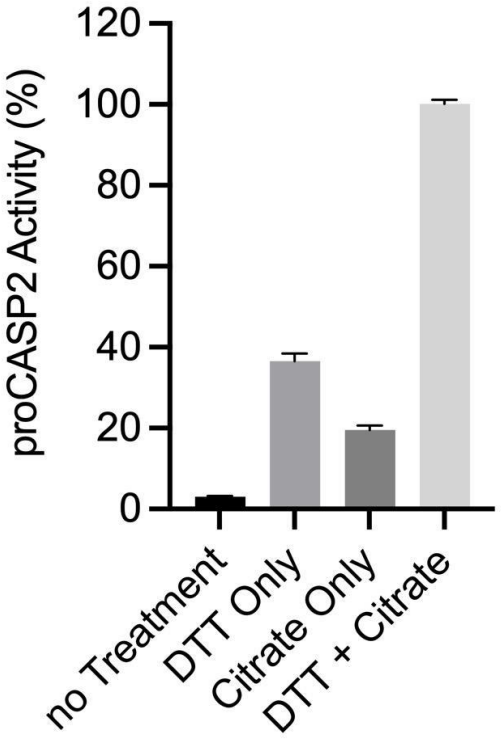

Figure S4. Assessment of recombinant proCASP2 (D333A, D347A) activity sensitivity to additives. Additives: DTT (10 mM pre-treatment for 30 mins) and citrate (333 mM added immediately prior to assay). Activity of recombinant proCASP2 (1 μM recombinant protein in PBS supplemented with 333 mM citrate buffer pH 7.4) monitored using fluorogenic substrate Ac-VDVAD-AFC (10 μM substrate) and fluorescence

emission spectra (λ_{ex} = 400 nm and λ_{em} = 505 nm) monitored by multimodal plate reader with percentage activity relative to DTT+Citrate conditions calculated from the linear range of the reaction curves. Data represent mean values ± STDEV for three technical replicate experiments.

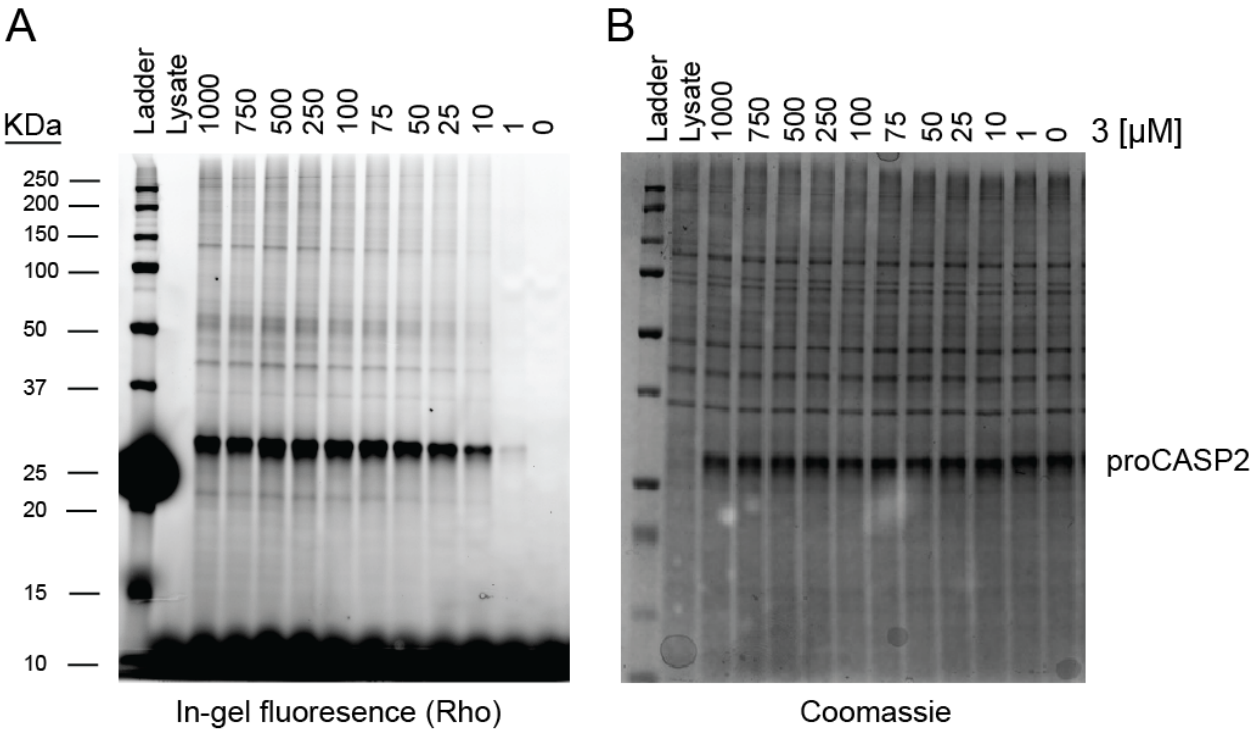

Figure S5. Dose-dependent labeling of proCASP2 by alkyne probe 3. Gel-based ABPP analysis of recombinant proCASP2 in cell lysates subjected to labeling a dose range of **3** for 1h followed by click conjugation to rhodamine azide and SDS-PAGE analysis. (A) In-gel fluorescence and (B) Coomassie InstantBlue visualization of protein loading.

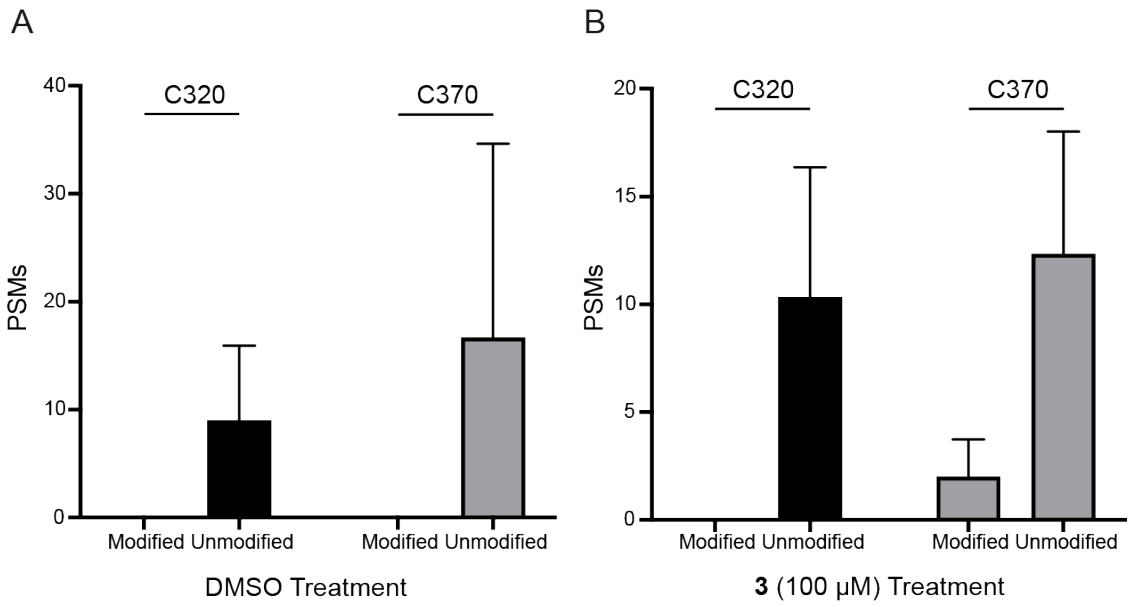

Figure S6. **Bottom-up proteomic analysis of recombinant proCASP2 labeled by 3**. Recombinant proCASP2 in PBS was treated with either (A) DMSO vehicle or (B) compound **3** (100 μM final concentration) for 1h at 30℃ followed by sample cleanup (SP3), sequence specific digest and LC-MS/MS analysis. Data represent mean values ± STDEV for three biological replicates. All MS Data can be found in **Table S4.**

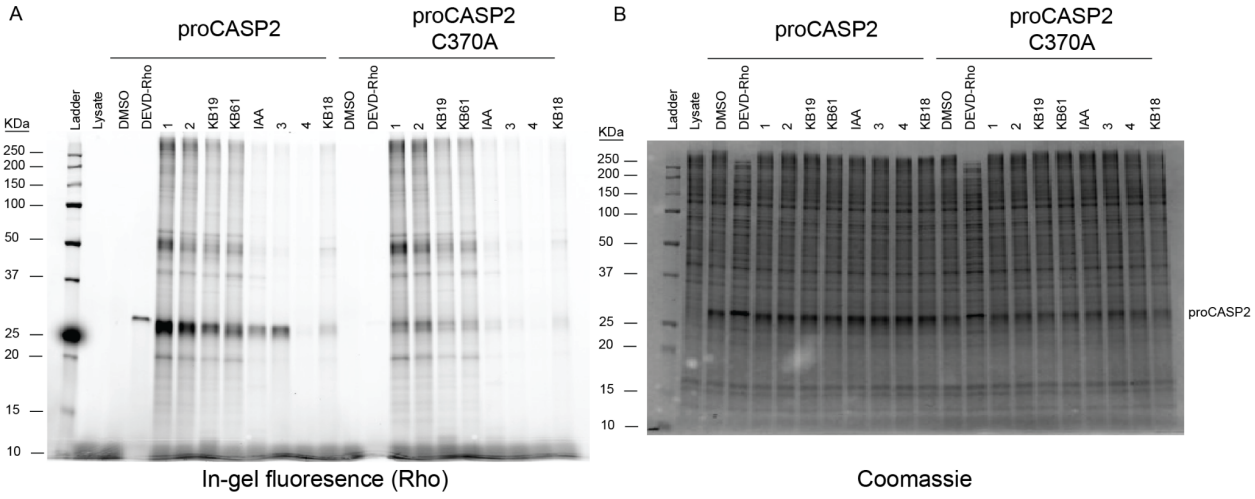

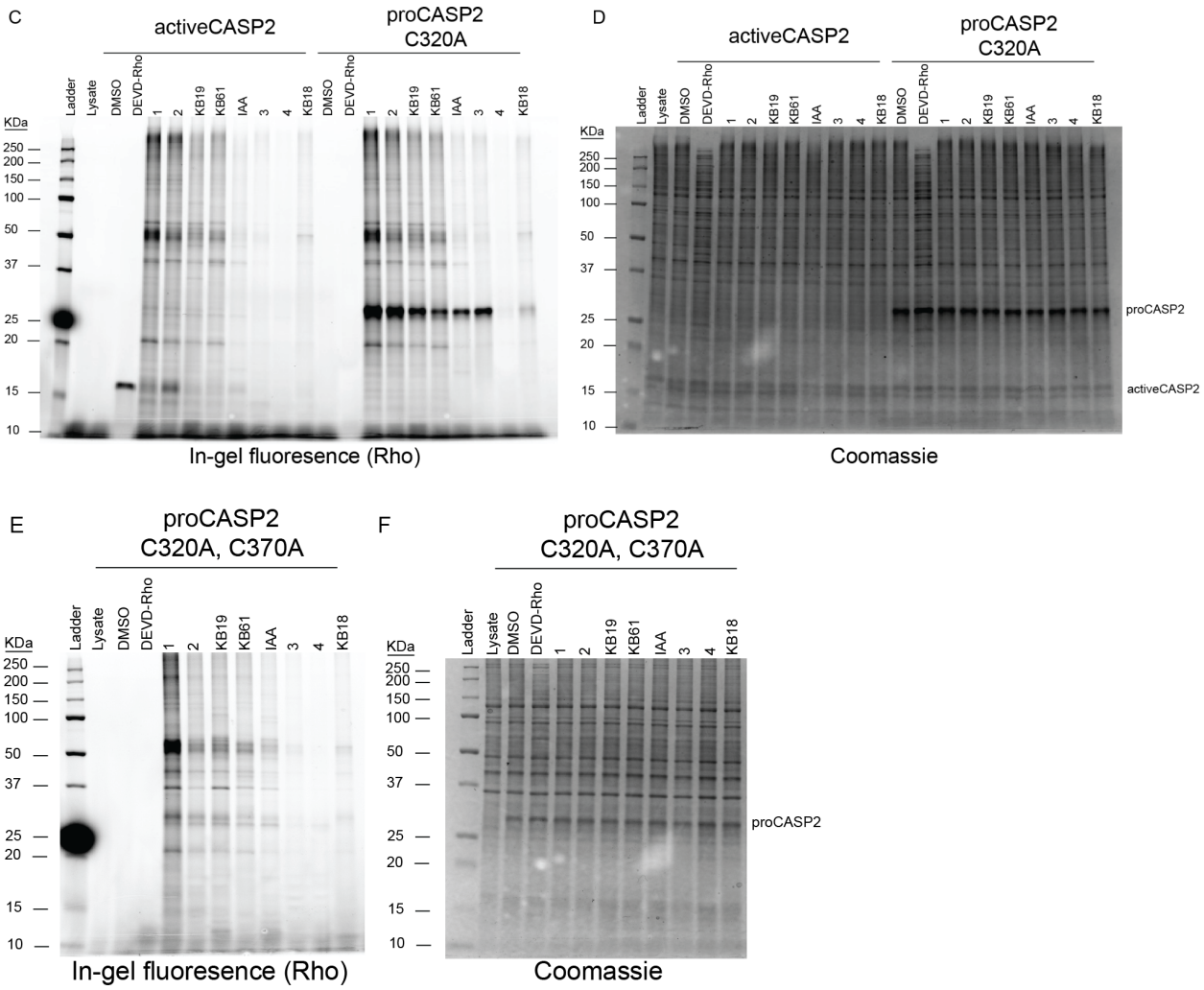

Figure S7. Full length gels for Figure 2B, labeling of proCASP2 by alkyne probes. Gel-based ABPP analysis of recombinant caspase-2 constructs harboring the indicated mutations in whole cell lysates treated for 1h with the indicated compounds (10 μM for all click probes, 2 μM final for **Rho-DEVD-AOMK** and 2 μM final for **IAA**), followed by click conjugation to rhodamine azide for alkyne probes and in-gel analysis. (A,C,E) in-gel fluorescence and (B,D,F) Coomassie InstantBlue visualization of protein loading for (A,B) proCASP2 and proCASP2_C370A (C, D) activeCASP2 and proCASP2_C320A, (E, F) proCASP2_C320A,C370A and proCASP2_C320A.

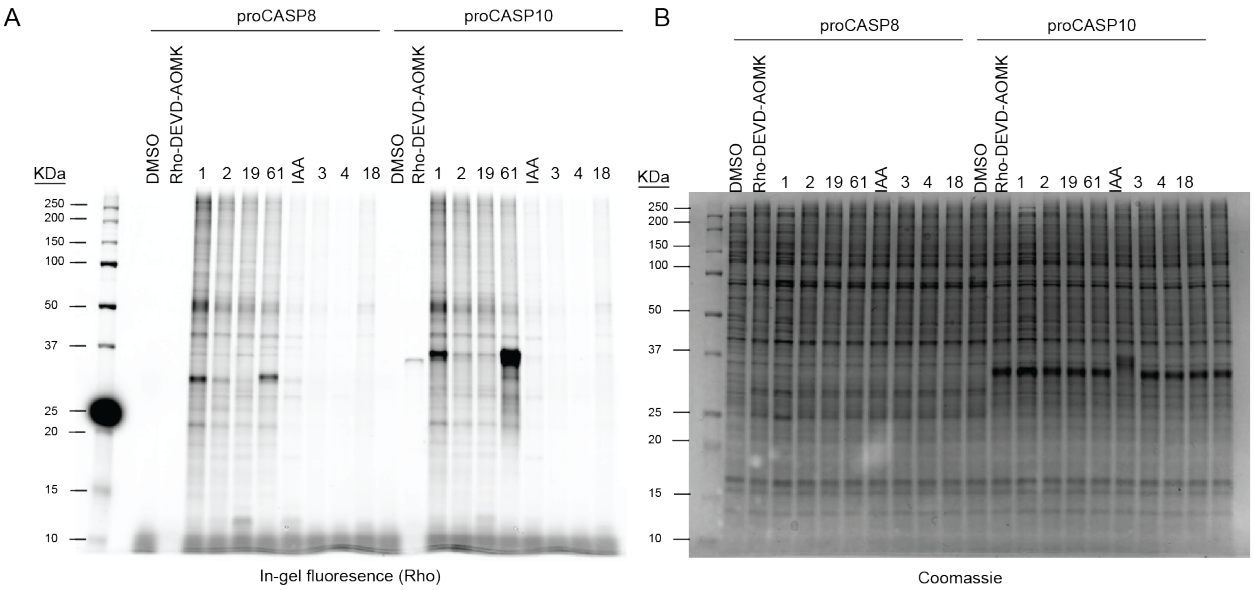

Figure S8. Full length gels for Figure 2E, labeling of proCASP8 and proCASP10 by alkyne probes. Gel-based ABPP analysis of recombinant proCASP8 and proCASP10 in Jurkat cell lysates treated for 1h with the indicated compounds (10 μM for all click probes and 2 μM final for **Rho-DEVD-AOMK**), followed by click conjugation to rhodamine azide for alkyne probes and in-gel analysis. (A) in-gel fluorescence and (B) Coomassie InstantBlue visualization of protein loading.

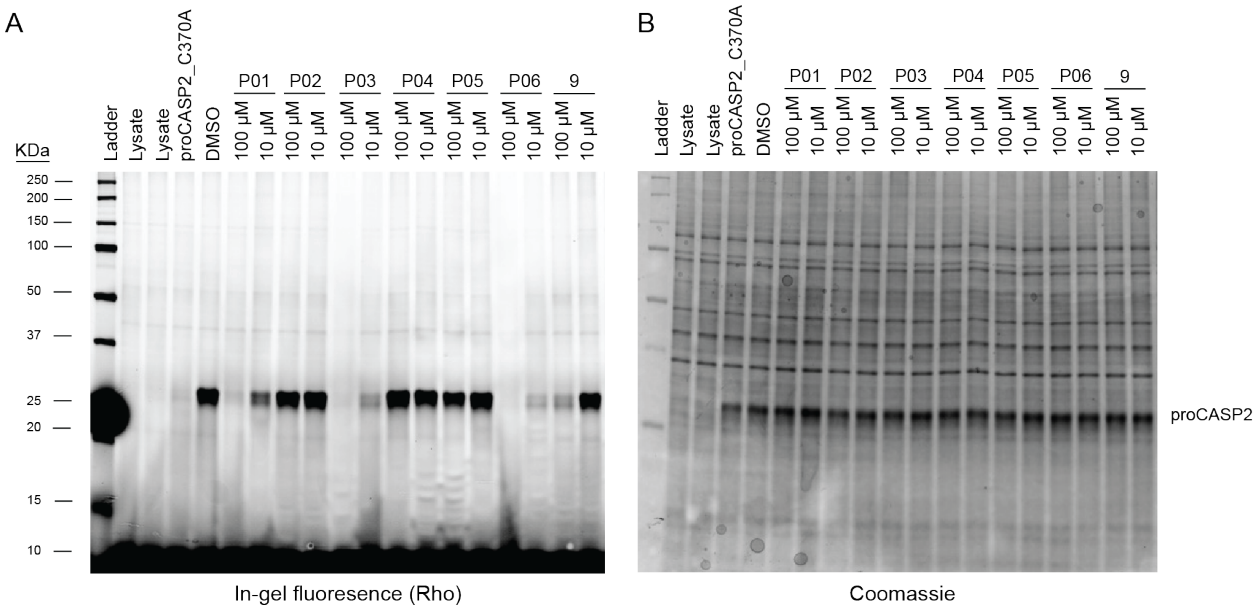

Figure S9. Competitive gel-based ABPP analysis of proCASP2 labeling by diverse electrophilic fragments. Recombinant proCASP2 in Jurkat cell lysates treated for 1h with the indicated compounds at the indicated concentrations, followed by **3** (10 µM, 1h), click conjugation to rhodamine azide and in-gel analysis. (A) in-gel fluorescence and (B) Coomassie InstantBlue visualization of protein loading.

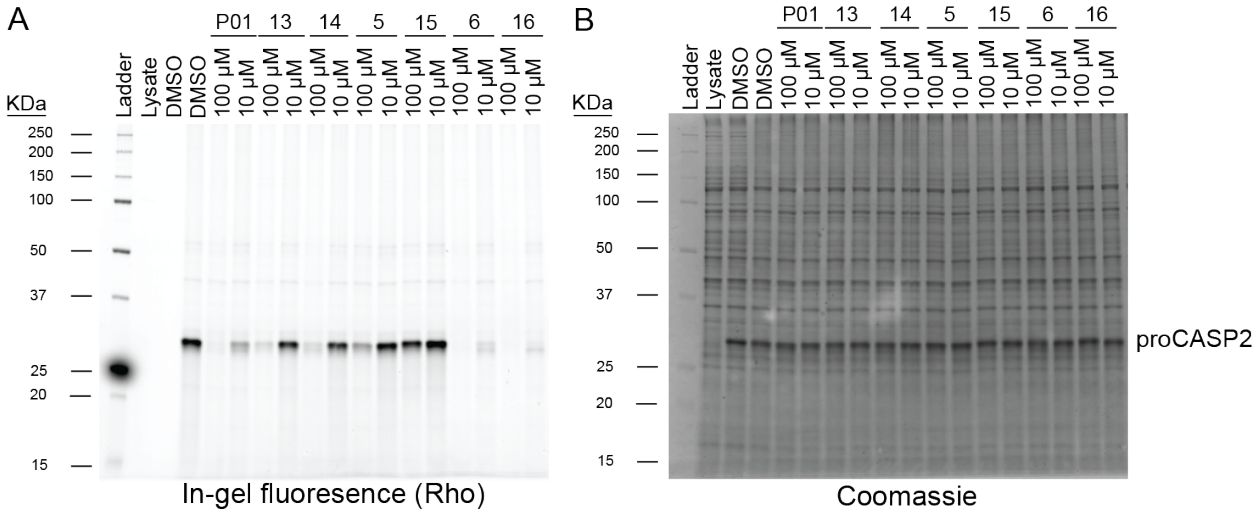

Figure S10. **Competitive gel-based ABPP analysis of proCASP2 labeling by methyl phenylpropiolate (P01) analogues.** Recombinant proCASP2 in Jurkat cell lysates treated for 1h with the indicated compounds at the indicated concentrations, followed by **3** (10 μM, 1h), click conjugation to rhodamine azide and in-gel analysis. (A) in-gel fluorescence and (B) Coomassie InstantBlue visualization of protein loading.

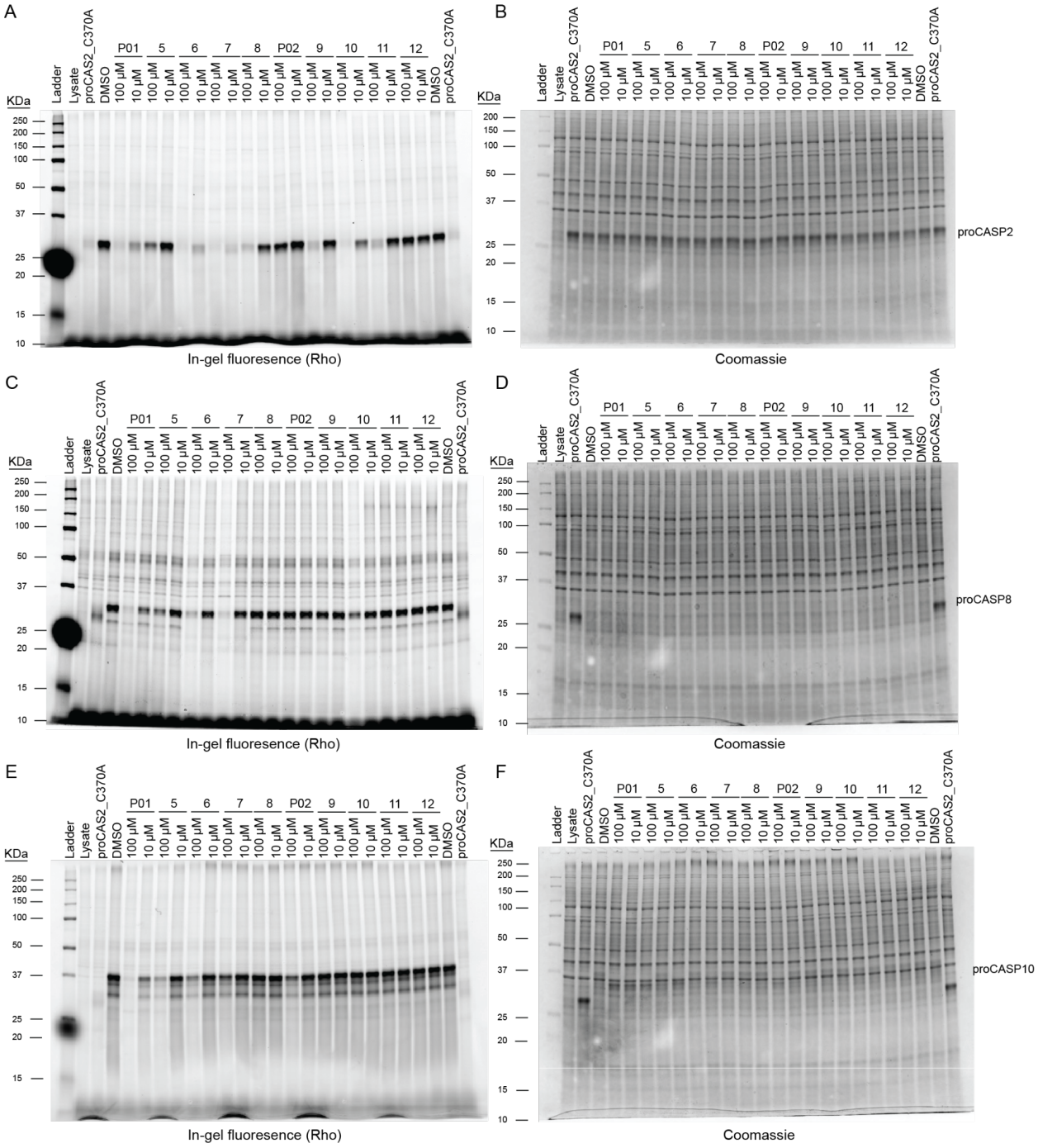

Figure S11. Competitive gel-based ABPP analysis of procaspases labeling by electrophilic fragments. Gel-based ABPP analysis of recombinant (A,B) proCASP2, (C,D) proCASP8, and (E,F) proCASP10 in whole cell lysates treated for 1h with the indicated compounds at the indicated concentrations, followed by either **3** (10 µM, 1h)

for proCASP2 or **KB61** (10 μM, 1h) for proCASP8 and proCASP10, click conjugation to rhodamine azide and in-gel analysis. (A,C,E) in-gel fluorescence and (B,D,F) Coomassie InstantBlue visualization of protein loading.

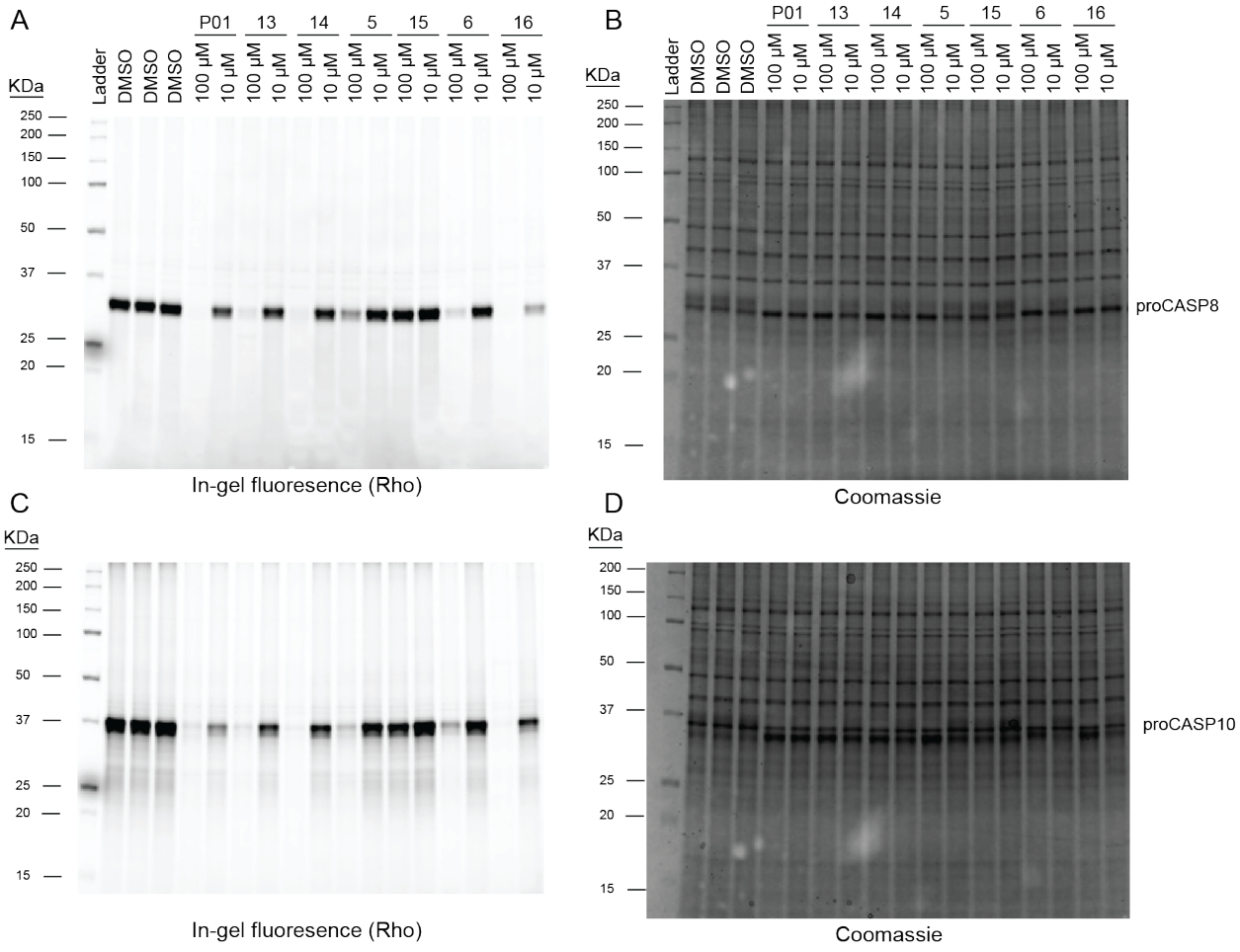

Figure S12. **Competitive gel-based ABPP analysis of proCASP8 and proCASP10 labeling by electrophilic fragments.** Gel-based ABPP analysis of recombinant (A,B) proCASP8 and (C,D) proCASP10) in whole cell lysates treated for 1h with the indicated compounds at the indicated concentrations, followed by **KB61** (10 μM, 1h) for proCASP8 and proCASP10, click conjugation to rhodamine azide and in-gel analysis. (A,C) in-gel fluorescence and (B,D) Coomassie InstantBlue visualization of protein loading.

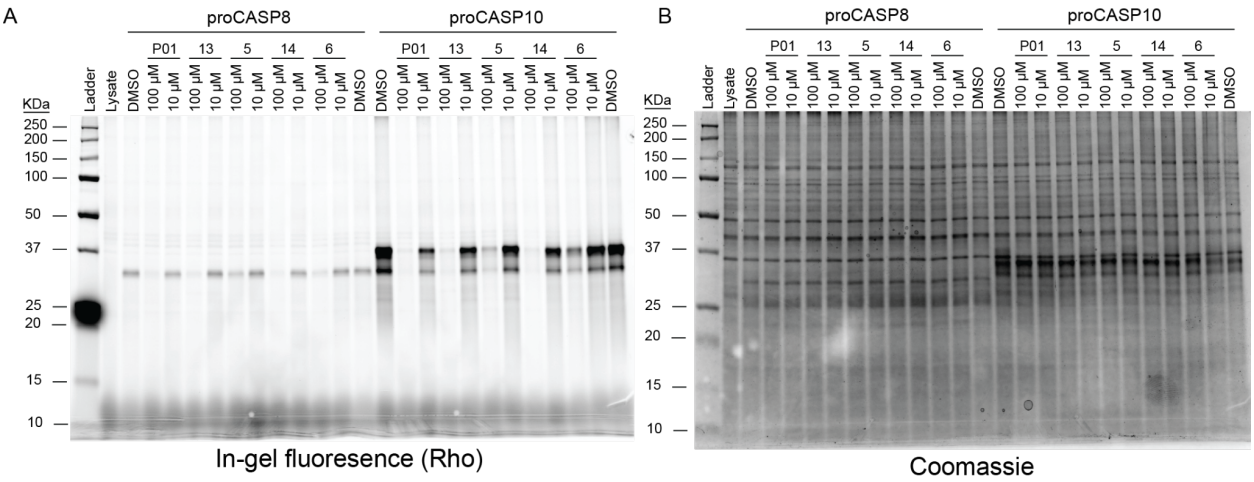

Figure S13. **Competitive gel-based ABPP analysis of proCASP8 and proCASP10 labeling by P01 analogues.** The indicated procaspases in whole cell lysates were treated for 1h with the indicated compounds at the indicated concentrations, followed by **KB61** (10 µM, 1h), click conjugation to rhodamine azide and in-gel analysis. (A) in-gel fluorescence and (B) Coomassie InstantBlue visualization of protein loading.

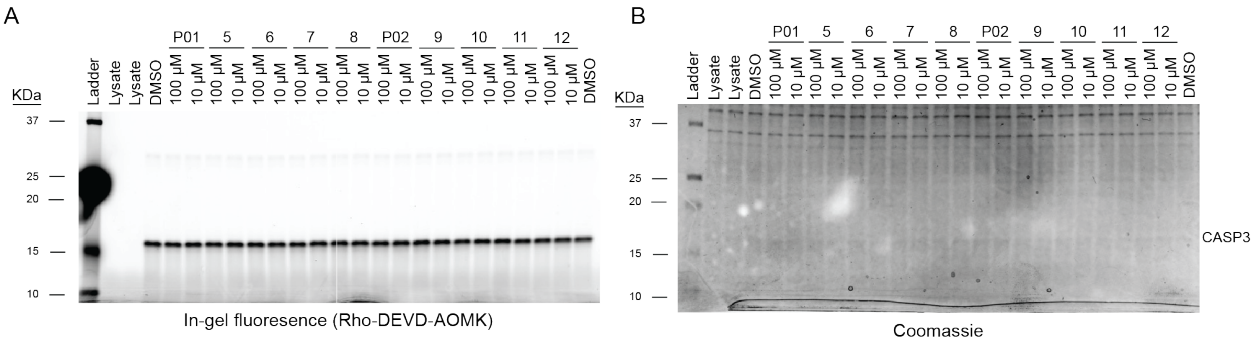

Figure S14. **Competitive gel-based ABPP analysis of activeCASP3 labeling by electrophilic fragments.** ActiveCASP3 in whole cell lysates was treated for 1h with the indicated compounds at the indicated concentrations, followed by **Rho-DEVD-AOMK** (0.2 μM), and in-gel analysis. (A) in-gel fluorescence and (B) Coomassie InstantBlue visualization of protein loading.

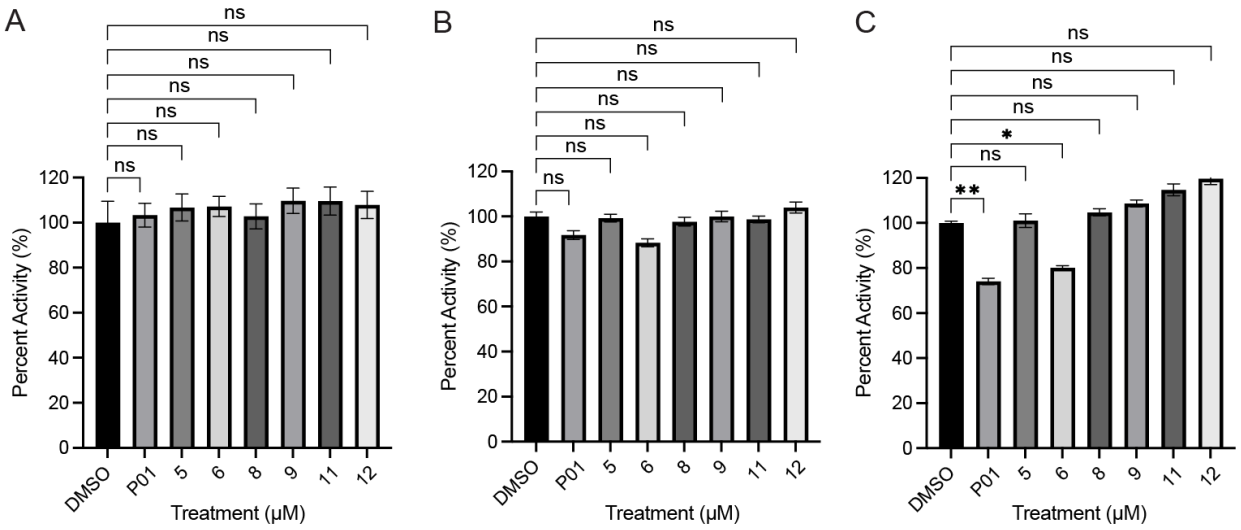

Figure S15. **Assessment of recombinant (A) activeCASP3, (B) activeCASP8, and (C) activeCASP9 activity after incubation with electrophilic fragments.** Relative activity of recombinant protein (100 nM) following 1h incubation with the indicated compounds at either 25 μM (**P01**, **5** and **6**) or 100 μM (**8**, **9**, **11**, and **12**). Activity assessed using fluorogenic substrate Ac-VDVAD-AFC (10 μM) with fluorescence emission spectra (λ_{ex} = 400 nm and λ_{em} = 505 nm) monitored by multimodal plate reader with percentage activity relative to DMSO calculated from the linear range of the reaction curves. Data represent

mean values ± STDEV for three technical replicates. Statistical significance was calculated with unpaired Student's t-tests, n.s., not significant, * $p<0.05$, ** $p<0.01$, n.s. $p>0.05$.

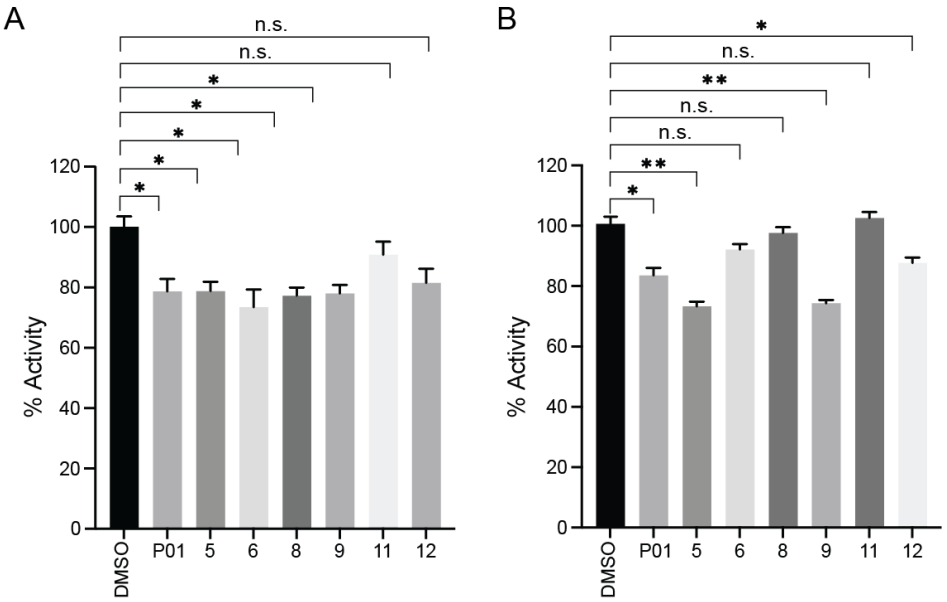

Figure S16. Assessment of recombinant (A) activeCASP2 and (B) activeCASP2_C370A sensitivity to electrophilic fragments. Relative activity of recombinant protein (100 nM) following 1h incubation with the indicated compounds at either 25 μM (**P01**, **5**, and **6**) or 100 μM (**8**, **9**, **11**, and **12**). Activity of recombinant protein assessed using fluorogenic substrate Ac-VDVAD-AFC (10 μM) with fluorescence emission spectra (λ_{ex} = 400 nm and λ_{em} = 505 nm) monitored by multimodal plate reader with percentage activity relative to DMSO calculated from the linear range of the reaction curves. Data represent mean values ± STDEV for three technical replicates. Statistical

significance was calculated with unpaired Student's t-tests, n.s., not significant, * $p<0.05$, ** $p<0.01$, n.s. $p>0.05$.

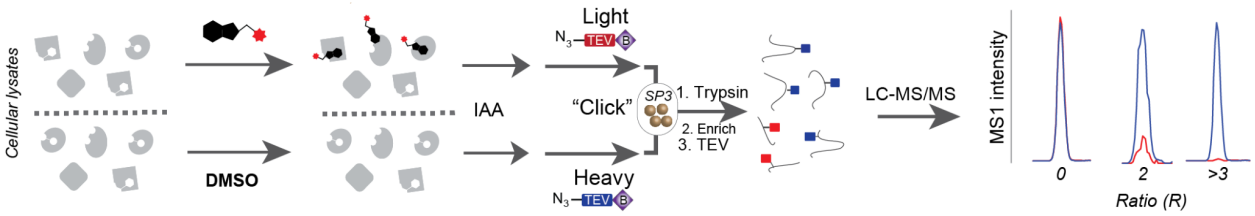

Figure S17. Workflow for competitive isoTOP-ABPP analysis of electrophilic fragments. IsoTOP-ABPP workflow used here, which was modified from the previously published method to incorporate single-pot, solid-phase-enhanced sample-preparation (SP3) cleanup.[6-7] Jurkat lysates are treated with either compound (100 μM) or vehicle (DMSO) followed by **IAA** cysteine capping at 200 μM final concentration for 1h. Samples were subjected to Cu(I)-catalyzed azide–alkyne cycloaddition (CuAAC) conjugation to isotopically labeled tobacco etch virus (TEV)-cleavable biotinylated peptide tags.[2] The samples are then combined, subjected to SP3 cleanup, enrichment on streptavidin and sequential trypsin and TEV digests, the combined samples were acquired by LC-MS/MS and the relative areas for the MS1 chromatographic peaks quantified. IsoTOP-ABPP ratios (R = $\log_2$DMSO:compound) are calculated from the MS1 ion intensity ratios for heavy- versus light-labeled peptides. Competition H:L ratios (R = $\log_2$H:L) ≥ 2 designate fragment electrophile labeling sites.

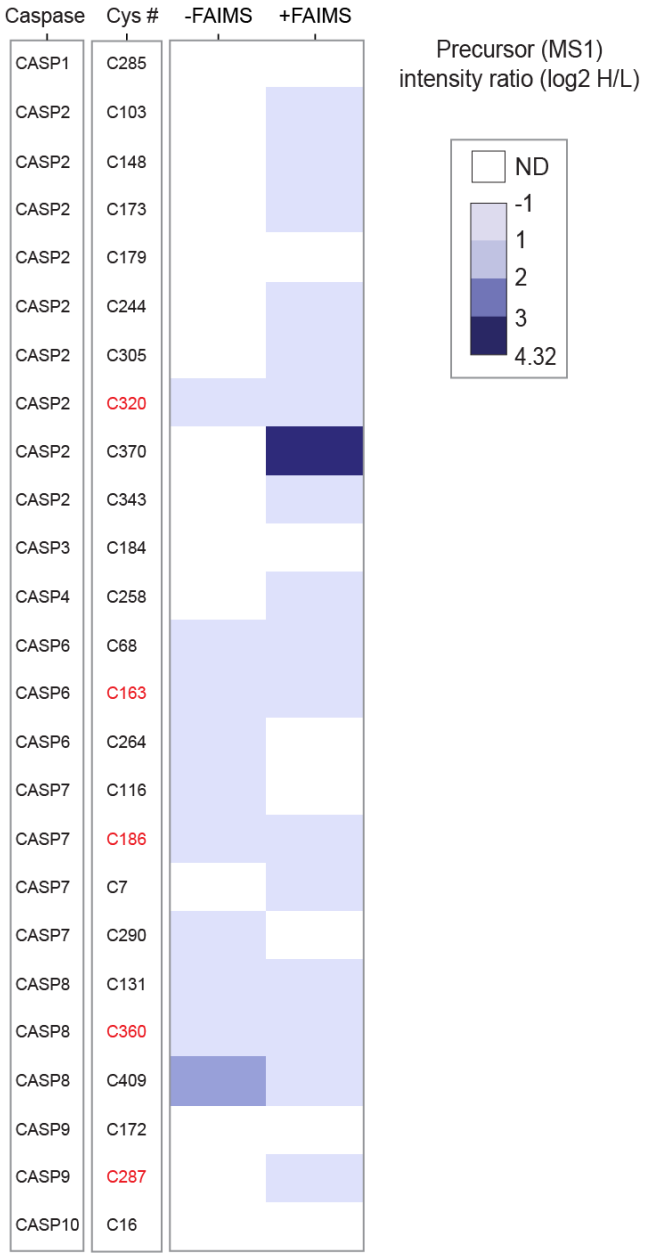

Figure S18. Assessment of impact of FAIMS acquisition on caspase peptide coverage. Competitive isoTOP-ABPP samples prepared as shown in **Figure S17** with

Jurkat lysates treated with **9** (100 μM for 1h) or vehicle (DMSO). Shown are the mean values for precursor ion intensity ratios for biological replicates (n = 2) acquired ± FAIMS. MS Data can be found in **Table S4 (7901 total peptides and 3272 total proteins)**. * Indicate catalytic cysteine residues.

```
proCASP2           DNANCPSLQNKPKMFFIQACRGDETDRGVDQQ-----DGKNHAGSPGCEES          346
proCASP2TEV        DNANCPSLQNKPKMFFIQACRGDETDRGVDQQENLYFQGKNHAGSPGCEES          351
proCASP2TEV_C370A  DNANCPSLQNKPKMFFIQACRGDETDRGVDQQENLYFQGKNHAGSPGCEES          351
                   ******************************       *************

proCASP2           D-----AGKEKLPKMRLPTRSDMICGYACLKGTAAMRNTKRGSWYIEALAQVFSERA   398
proCASP2TEV        ENLYFQGGKEKLPKMRLPTRSDMICGYACLKGTAAMRNTKRGSWYIEALAQVFSERA   403
proCASP2TEV_C370A  ENLYFQGGKEKLPKMRLPTRSDMICGYAALKGTAAMRNTKRGSWYIEALAQVFSERA   403
                         .********************.****************************
```

Figure S19. **Sequences of engineered proCASP2TEV cleavable constructs**. Sequence alignments of truncated caspase-2 UniProtKB-1 isoform (truncated residue from D301 and earlier) aligned with the indicated proCASP2TEV cleavable constructs. Highlighted in yellow is the catalytic cysteine residue, C320 and the non-catalytic cysteine residue, C370. Highlighted in green are the protease cleavable residues D333 and D347 that were replaced with a TEV recognition sequence, ENLYFQG.

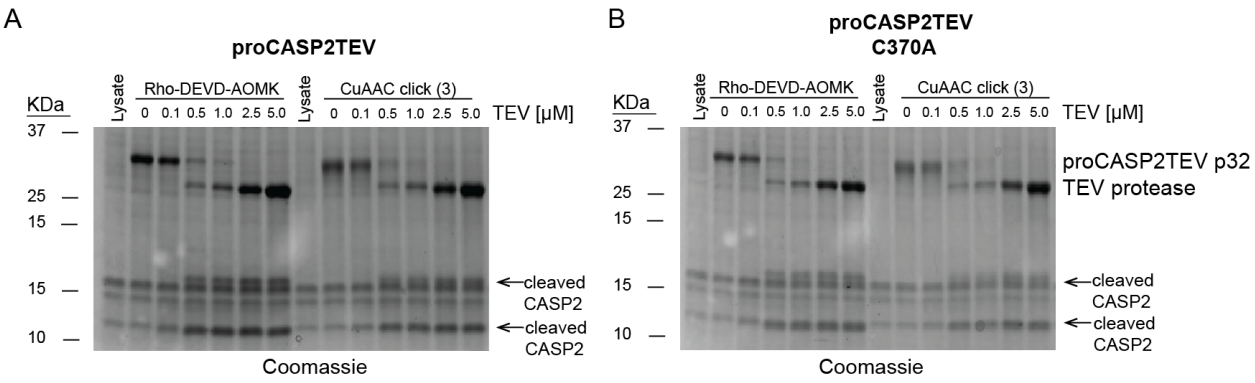

Figure S20. **InstantBlue™ coomassie protein staining of ABPP gels shown in Figure 4B,C.** (A) proCASP2TEV and (B) proCASP2TEV_C370A.

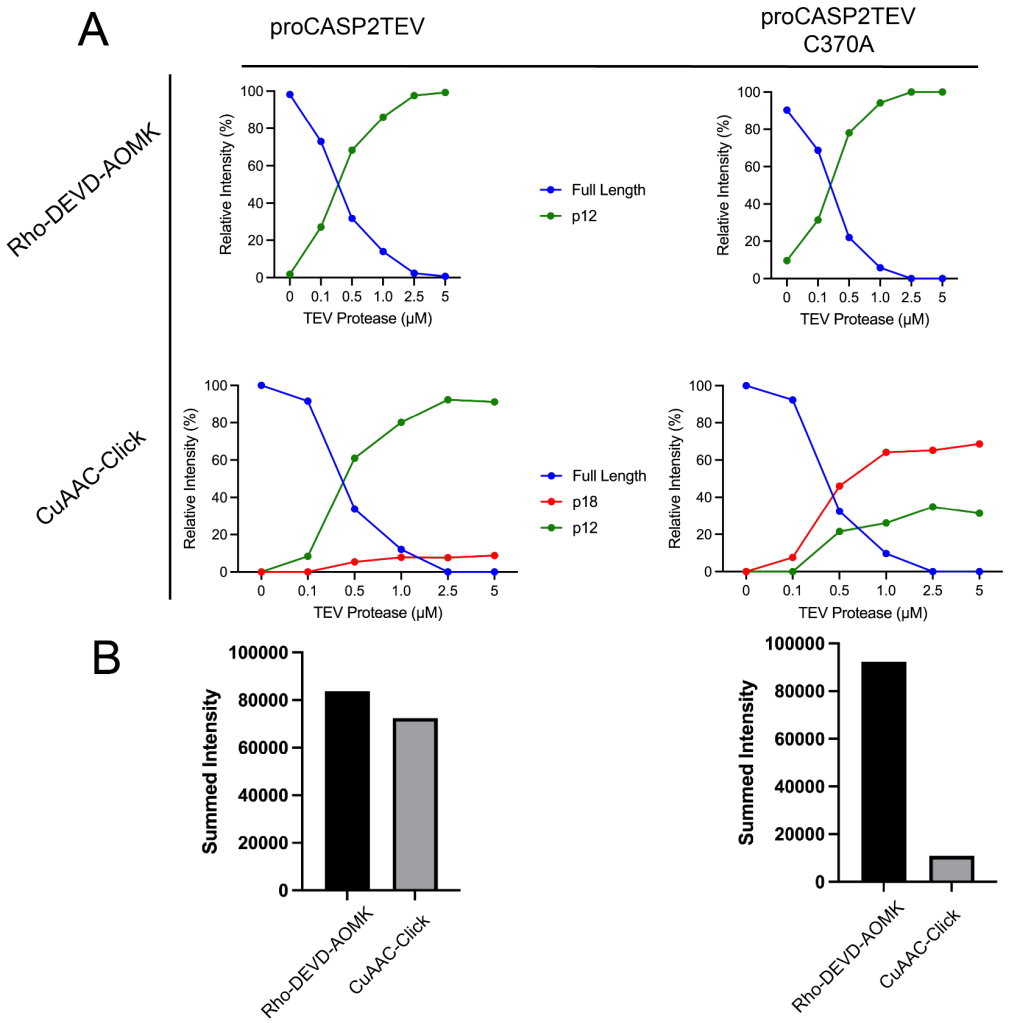

Figure S21. Quantification of relative in gel fluorescence band intensities (rhodamine) for ABPP gels labeled with Rho-DEVD-AOMK and **3** shown in **Figure 4B,C**. (A) Intensities normalized to aggregate band intensity are shown for the full-length (p35) and cleaved proCASP2TEV (p18 and p12) bands. (B) Summed intensities for all bands quantified in A for proCASP2_TEV (left) and proCASP2_TEV_C370A (right).

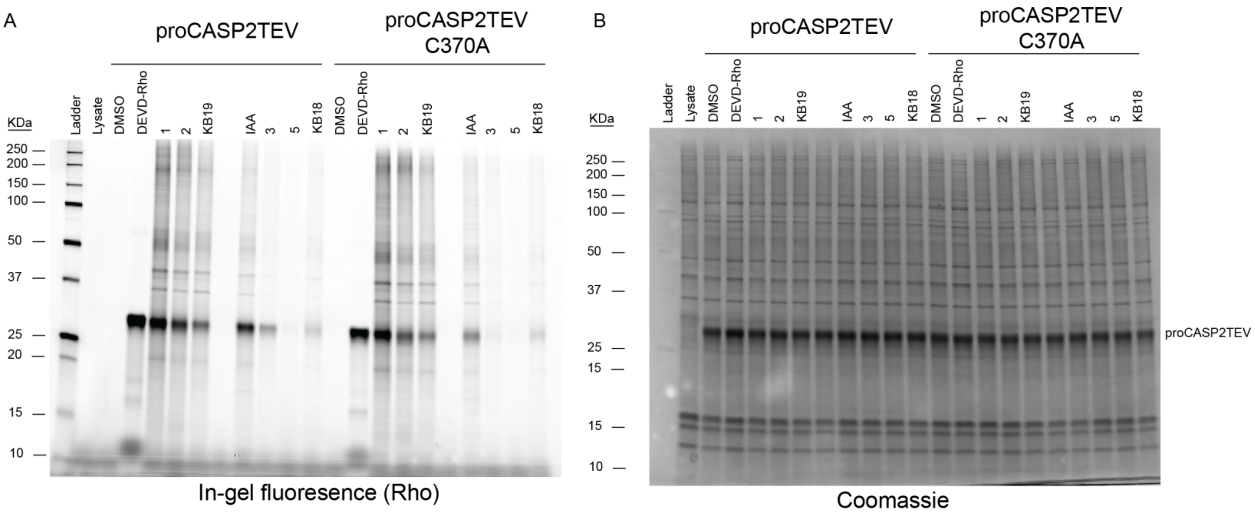

Figure S22. Click compound 3 does not label proCASP2TEV_C370A. Labeling of **proCASP2TEV and proCASP2TEV_C370A by alkyne probes.** Gel-based ABPP analysis of the indicated procaspases in whole cell lysates treated for 1h with the indicated compounds (10 μM for all click probes and 2 μM final for Rho-DEVD-AOMK), click conjugation to rhodamine azide and in-gel analysis. (A) in-gel fluorescence and (B) Coomassie InstantBlue visualization of protein loading.

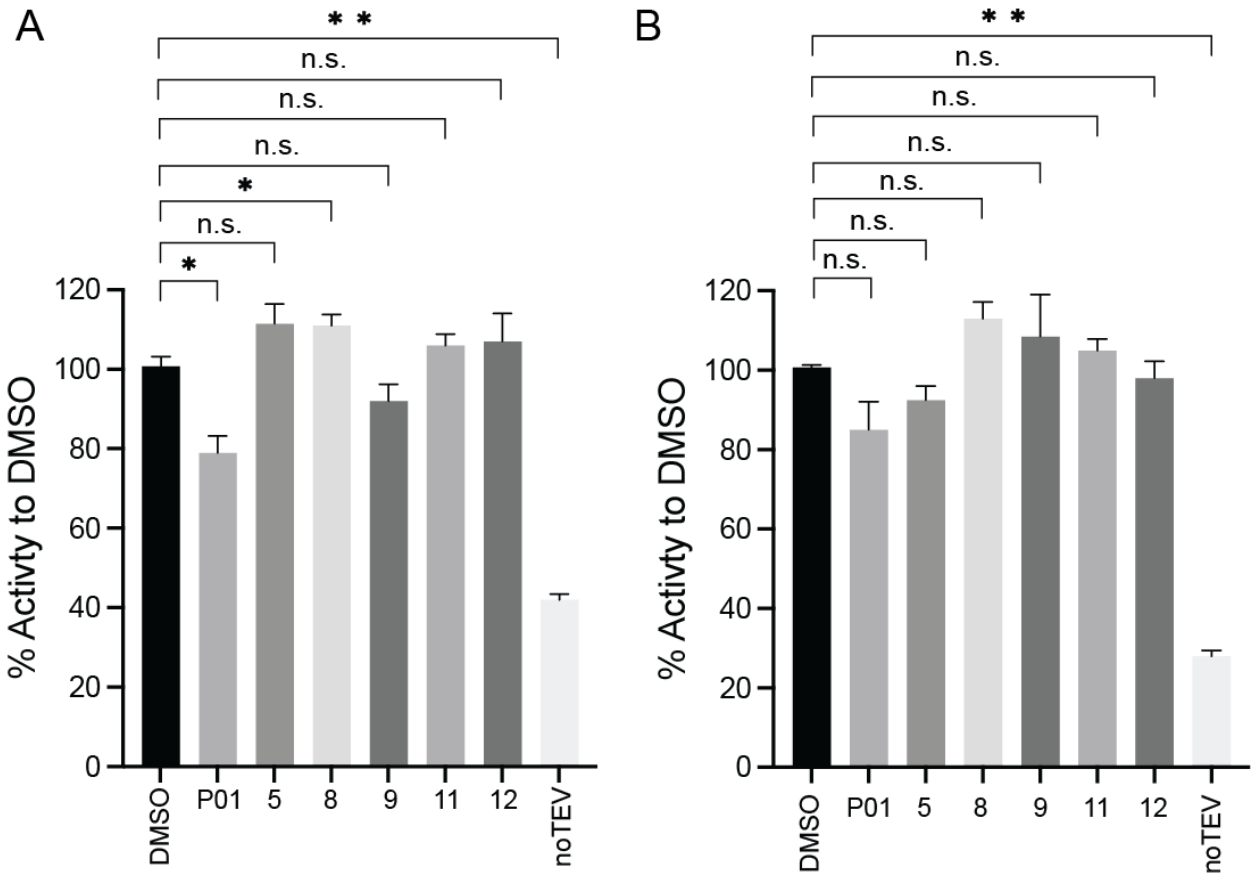

Figure S23. Activity of proCASP2TEV and proCASP2TEV_C370A with P01 analogues showing little to no inhibition prior to size exclusion chromatography (SEC) separation of monomer and dimer species. Recombinant (A) proCASP2TEV and (B) proCASP2TEV_C370A (100 nM) were treated with DMSO vehicle or the indicated compounds at 100 μM concentration (**8**, **9**, **11**, **12**) or 25 μM (**P01** and **5**) for 1h followed by addition of TEV protease (2 μM). Subsequently, samples were then treated with 5 μM Ac-VDVAD-AFC 5 mM DTT, and 333 mM citrate in PBS and analyzed via spectrophotometer monitoring 7-amino-4-trifluoromethylcoumarin (AFC) release by substrate cleavage was detected at λ_{ex} = 400 nm and λ_{em} = 505 nm every minute after substrate incubation for 1h. Percent activities calculated from the slope of the linear range calculated from the reaction progress curves. Experiments were performed in triplicates

with mean relative activity compared to DMSO ± STDEV shown. Statistical significance was calculated with unpaired Student's t-tests, n.s., not significant, * p<0.05, ** p<0.01, n.s. p>0.05.

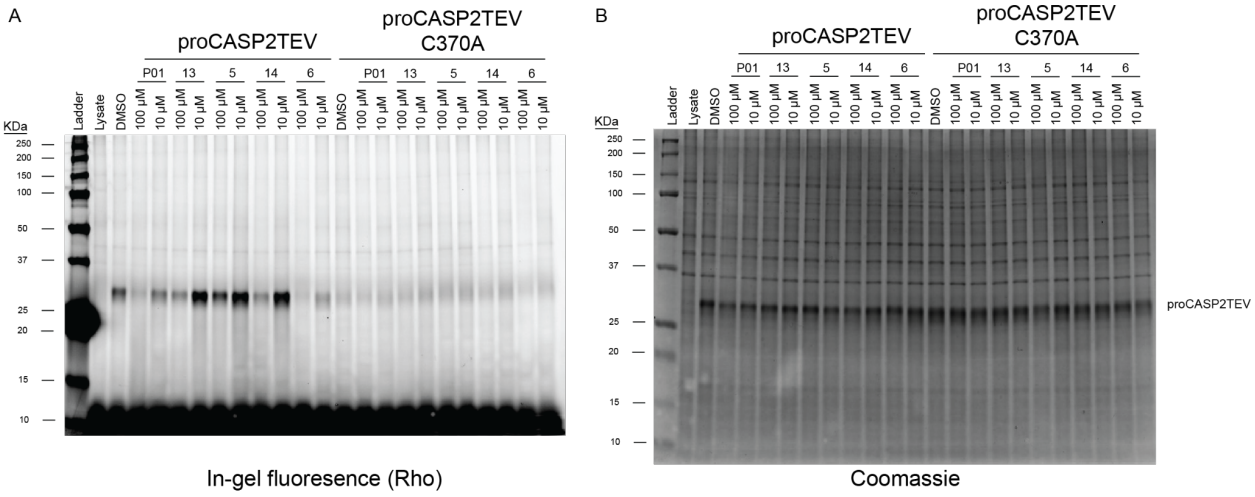

Figure S24. **P01 analogues do not compete for labeling of compound 3 similar to proCASP2 ABPP assay.** The indicated procaspases in whole cell lysates were treated for 1h with the indicated compounds at the indicated concentrations, followed by **3** (10 µM, 1h), click conjugation to rhodamine azide and in-gel analysis. (A) in-gel fluorescence and (B) Coomassie InstantBlue visualization of protein loading.

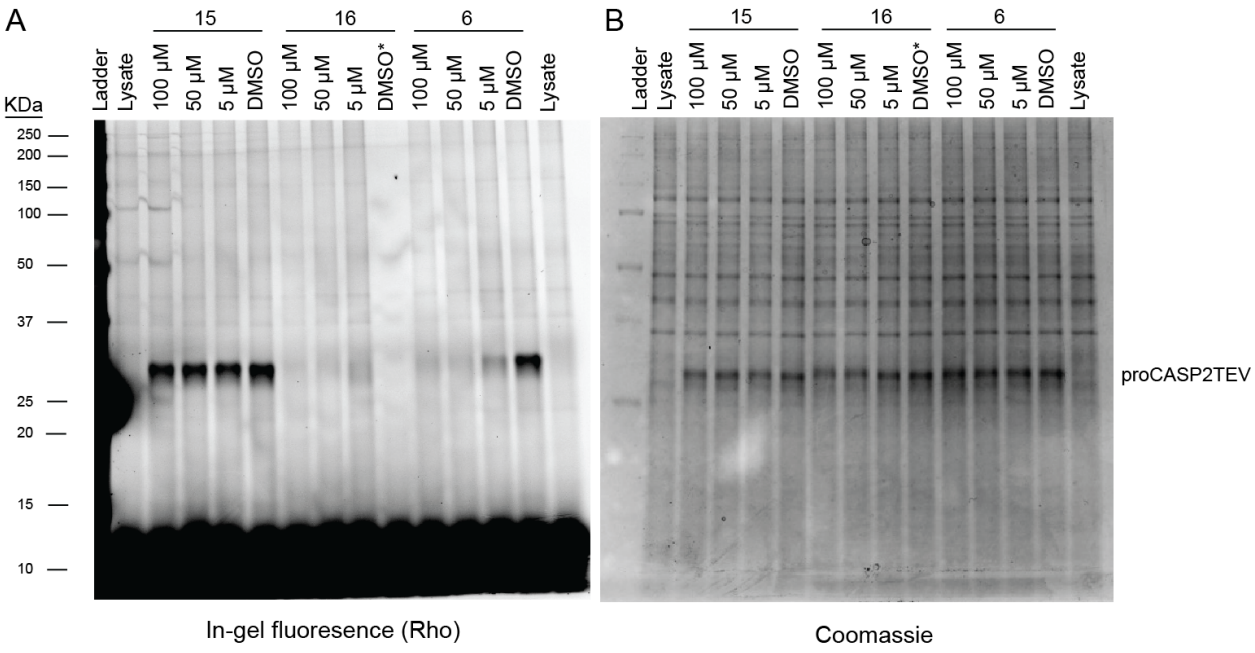

Figure S25. **Dose-dependent labeling by electrophilic fragments for proCASP2TEV.** proCASP2TEV in whole cell lysates were treated for 1h with the indicated compounds at the indicated concentrations, followed by **3** (10 µM, 1h), click conjugation to rhodamine azide and in-gel analysis. (A) in-gel fluorescence and (B) Coomassie InstantBlue visualization of protein loading. *DMSO indicates no treatment with compound **3**.

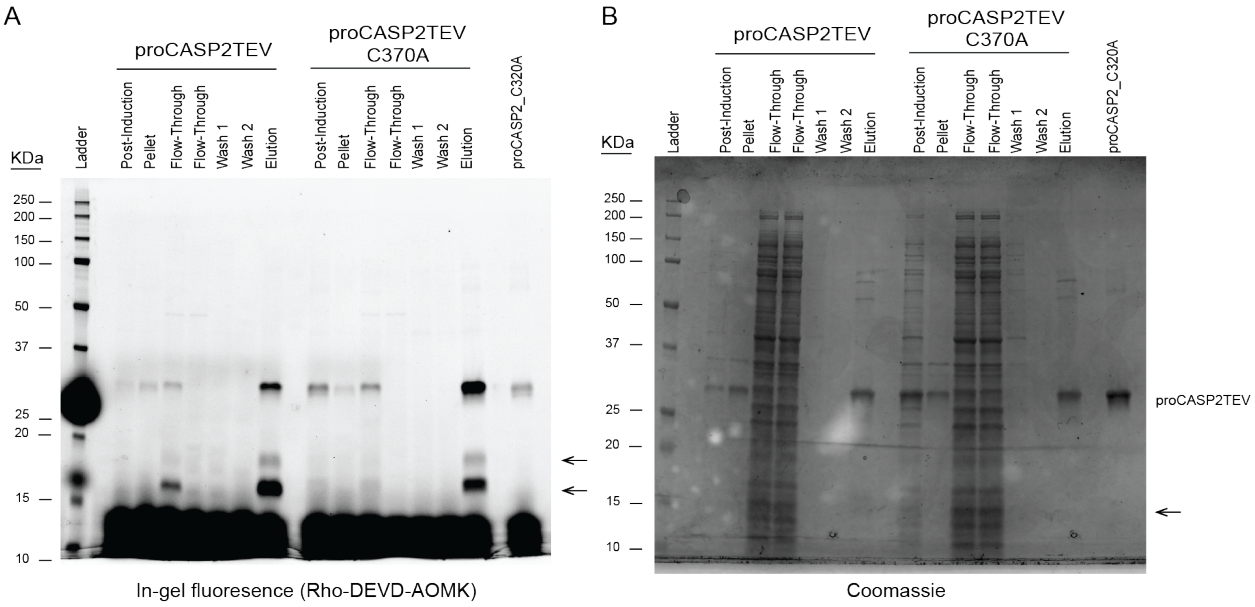

Figure S26. **Gel-Based ABPP assessment of recombinant proCASP2TEV and proCASP2TEV_C370A auto-cleaving properties**. Protein purification after IPTG induction and overexpression in BL21 (DE3) *E.coli* cells. Lysate or eluant from each purification step was labeled by **Rho-DEVD-AOMK** (2 µM, 1h) followed by (A) in-gel fluorescence and (B) Coomassie InstantBlue visualization of protein loading. Arrows indicate cleaved caspase-2 as labeled by **Rho-DEVD-AOMK**.

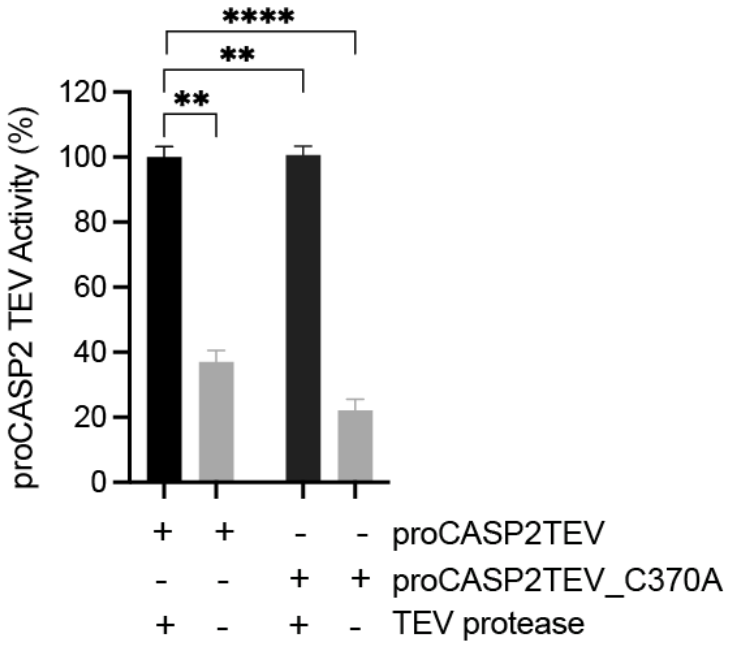

Figure S27 . **TEV-induced activity of proCASPTEV proteins.** Activity of recombinant protein assessed using fluorogenic substrate Ac-VDVAD-AFC (10 μM substrate) with fluorescence emission spectra (λ_{ex} = 400 nm and λ_{em} = 505 nm) monitored by multimodal plate reader with percentage activity relative to +TEV protease samples calculated from the linear range of the reaction curves. Data represent mean values ± STDEV for three technical replicates. Statistical significance was calculated with unpaired Student's t-tests, ** p<0.001, ****p<0.0001.

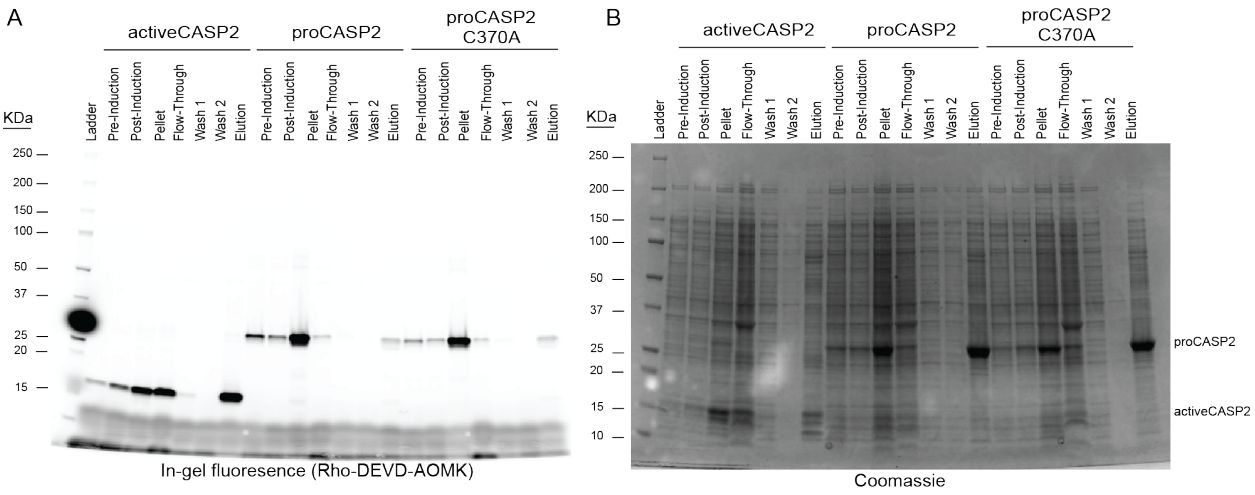

Figure S28 . Gel-Based ABPP assessment of recombinant activeCASP2, proCASP2, and proCASP2_C370A auto-cleaving properties. Protein purification after IPTG induction and overexpression in BL21 (DE3) *E.coli* cells. Lysate or eluant from each purification step was labeled by **Rho-DEVD-AOMK** (2 µM, 1h) followed by (A) in-gel fluorescence and (B) Coomassie InstantBlue visualization of protein loading.

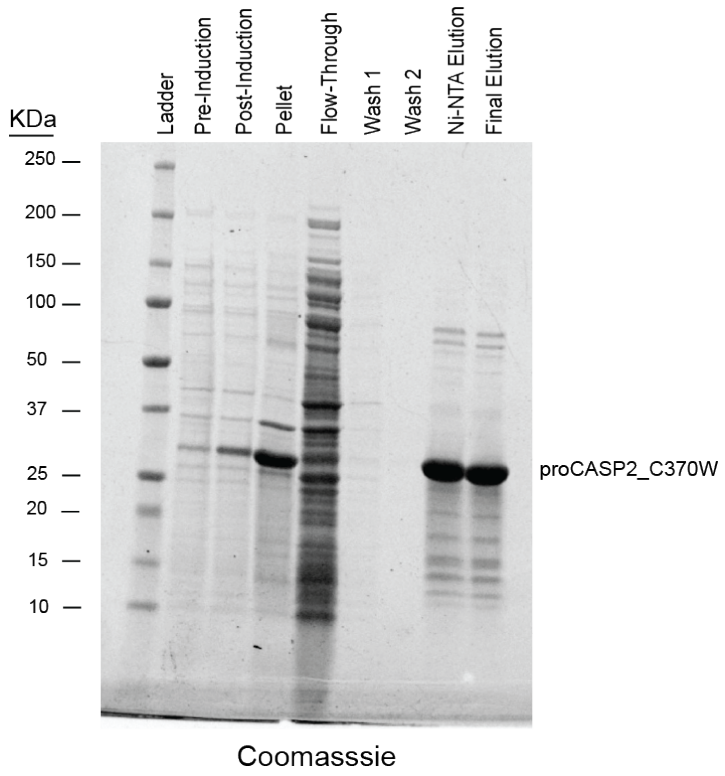

Figure S29. Gel-Based ABPP assessment of recombinant proCASP2_C370W auto-cleaving properties. Protein purification after IPTG induction and overexpression in BL21 (DE3) *E. coli* cells. Lysate or eluant from each purification step was visualized by Coomassie InstantBlue.

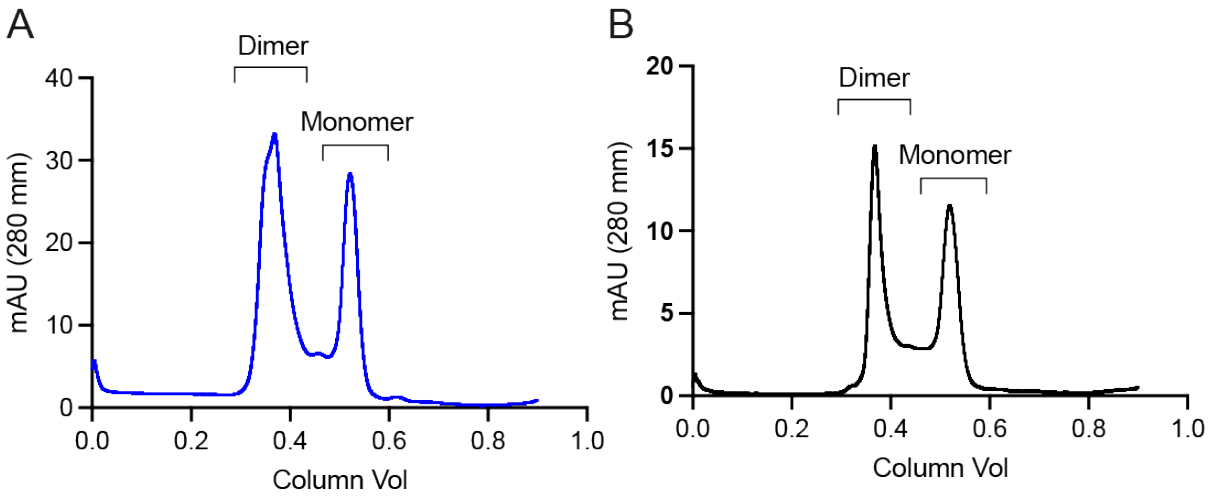

Figure S30. **Gel-filtration analysis of recombinant proCASP2 and proCASP2_C370A**. Superdex 75 gel filtration fast protein liquid chromatography (FPLC) elution profiles of recombinant proCASP2 constructs. (A) proCASP2 and (B) proCASP2_C370A, with peaks corresponding to molecular weights consistent with dimeric (column volumes 0.30 - 0.45) and monomeric (column volumes 0.48 - 0.55) proteins.

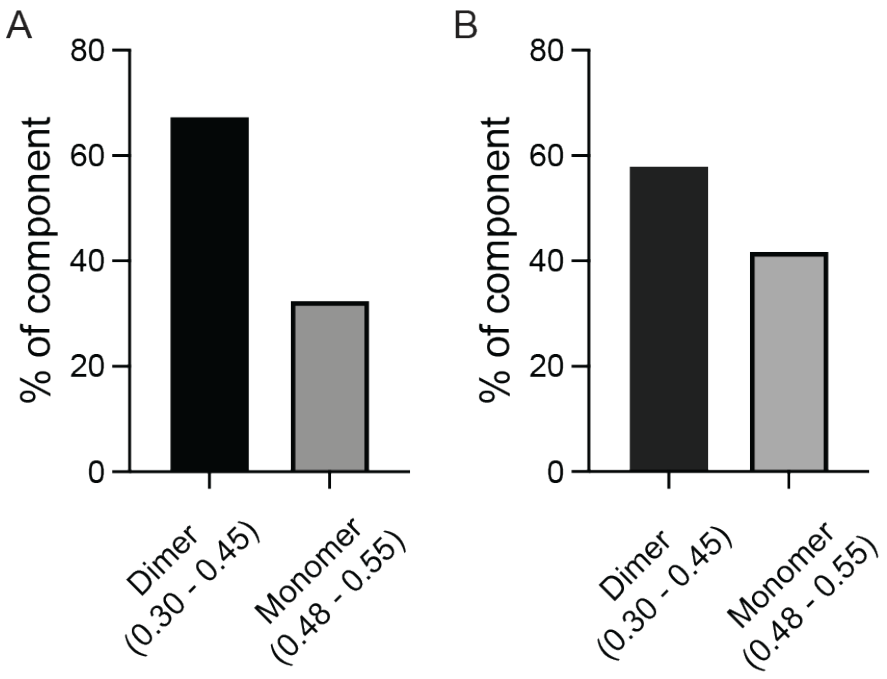

Figure S31. Quantification of the relative peak areas for Figure S28. Percent of dimer and monomer (% of component) for (A) proCASP2 and (B) proCASP2_C370A. Percent of component was determined by area-under-the-curve (AUC) calculations (AUC integrated measurement tool from GraphPad Prism 9) of dimeric gel filtration column volume fractions (0.30 - 0.45) and monomeric fractions (0.48 - 0.55) from proCASP2 (0.3 mg/mL).

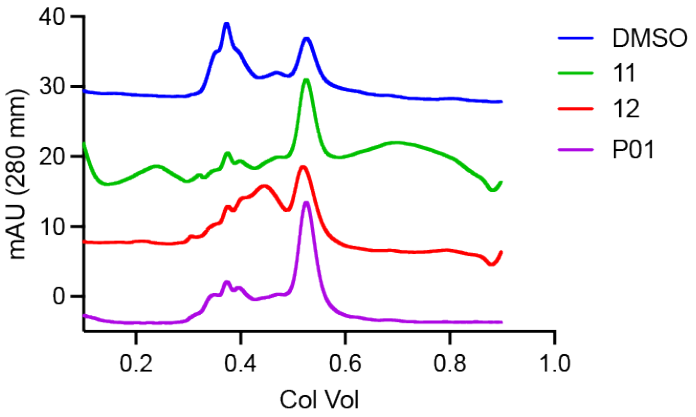

Figure S32. Assessment of compound-induced changes to proCASP2TEV gel filtration elution profile. proCASP2TEV was treated for 1h with the indicated compounds (100 µM, 30 °C, 1h) followed by Superdex 75 gel filtration fast protein liquid chromatography (FPLC).

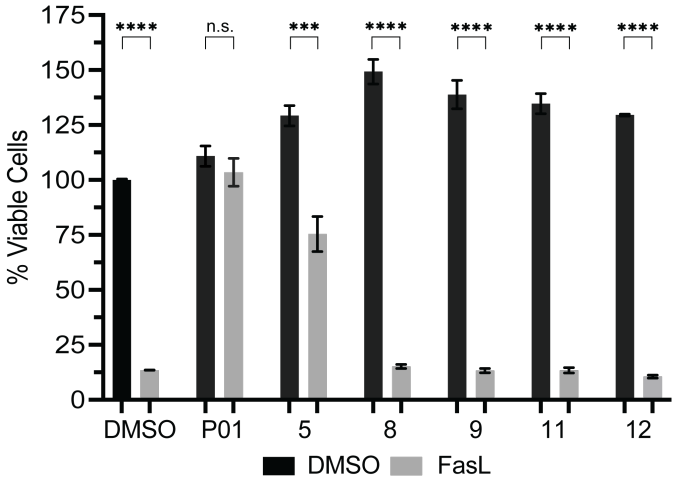

Figure S33. Assessing compound-induced protection from FasL-induced apoptosis. 1h pre-treatment with P01, 5, and 6 (25 µM) and 8, 9, 10, 11, and 12 (100 µM) followed by FasL (50 ng/mL, 4h)-induced apoptosis apoptosis of Jurkat cells assayed by CellTiter-Glo® Data represent mean values and standard deviation, n=3.

Statistical significance was calculated with unpaired Student's t-tests, * p<0.05, ** p<0.01, *** p<0.005. ****p<0.001. NS p>0.05.

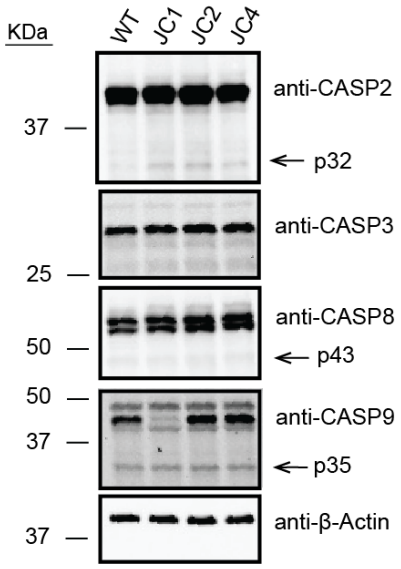

Figure S34. Immunoblot analysis of U2OS cells engineered to overexpress shRNAs targeting caspase-9 (JC1, JC2) or scrambled (JC4).

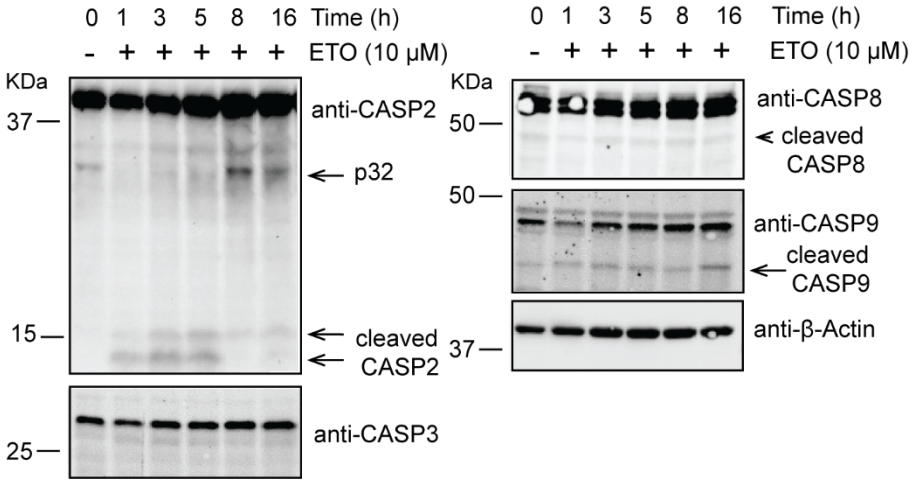

Figure S35. **Assessing time-dependent activation of caspase-2 in response to etoposide**. U2OS cells treated with 10 μM etoposide and cells were harvested at the indicated time points followed by immunoblot analysis for the indicated proteins.

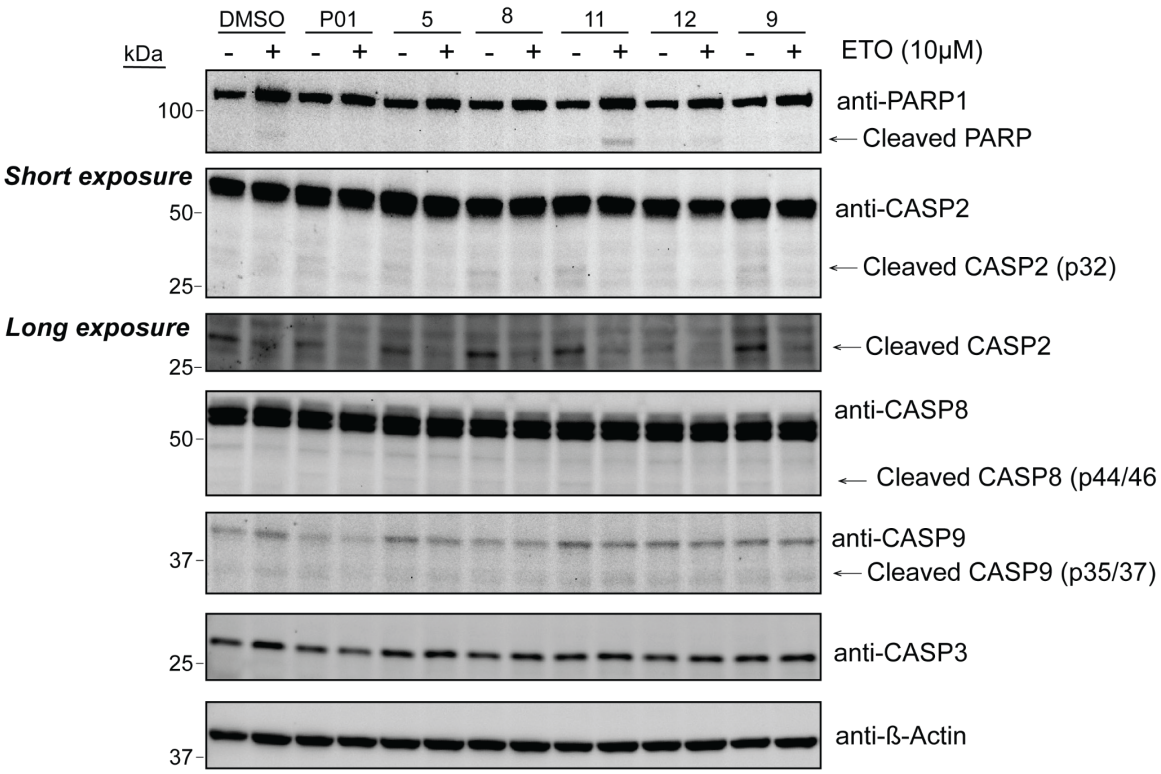

Figure S36. **Assessing compound-induced protection from shorter 3h treatment with etoposide genotoxic agent.** U2OS cells were subjected to 1h pre-treatment with P01, and 5 (25 μM) and 9, 11, and 12 (100 μM)] followed by etoposide (10 μM, 3h)-induced apoptosis.

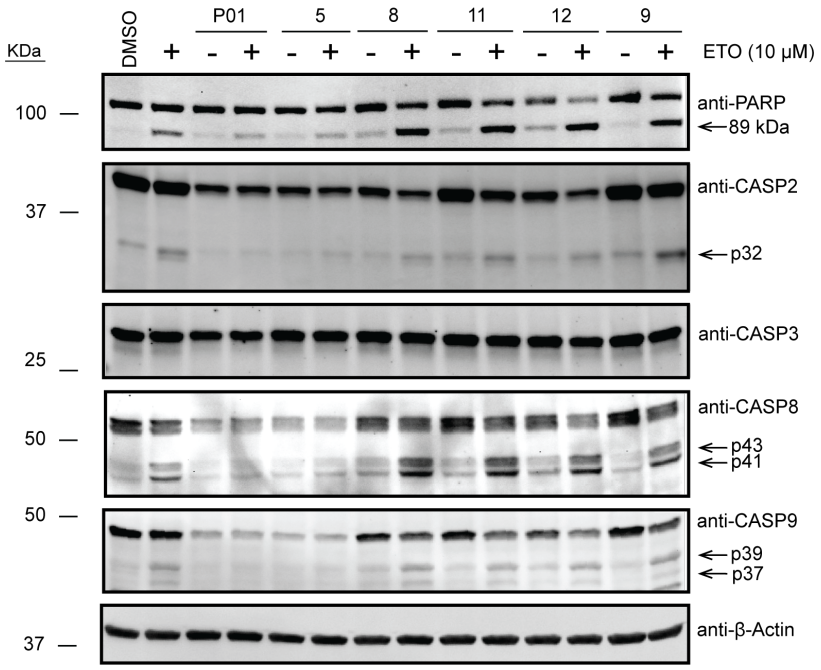

Figure S37. **Assessing compound-induced protection from longer 10h treatment with etoposide genotoxic agent.** 1h pre-treatment with **P01** and **5** (25 μM) and **8**, **11**, and **12** (100 μM) followed by etoposide (10 μM, 10h)-induced apoptosis with cleavage of PARP, CASP2, CASP8, and CASP9 visualized by immunoblot.

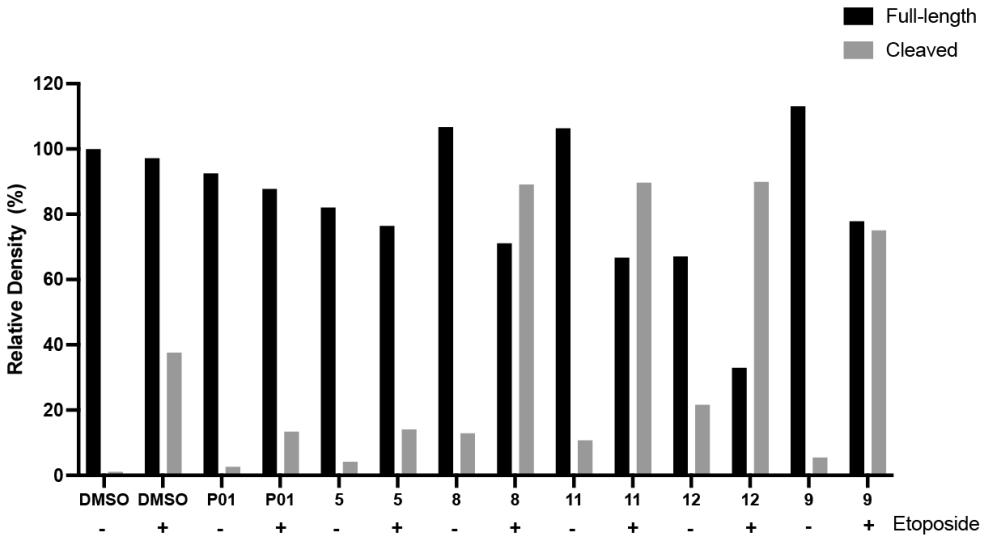

Figure S38. Quantification of relative PARP cleavage for immunoblot shown in Figure S37.

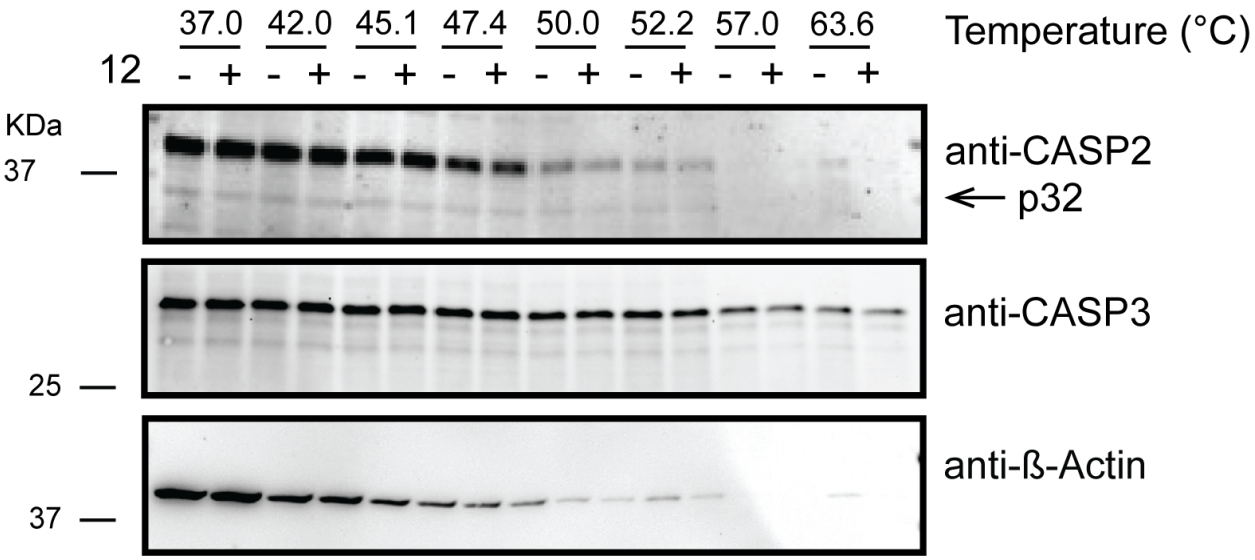

Figure S39. CETSA analysis for U2OS cell lysates treated with compound **12** (100 µM).

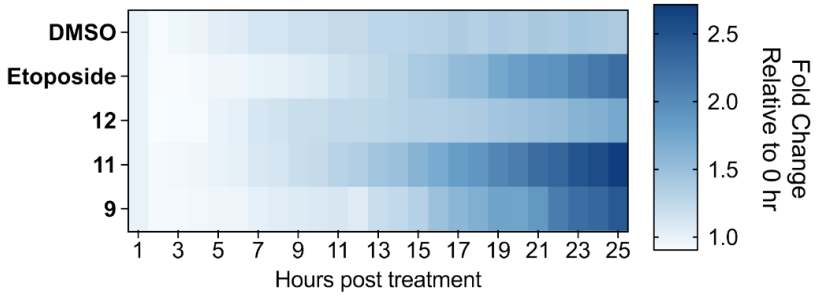

Figure S40. U2OS GFP-53BP1[8] etoposide treatment in the presence or absence of electrophilic compounds. Cells were treated with 10 nM etoposide or 10 nM DMSO 1h prior to addition of either 100 µM **12**, **11**, or **9**. Plates were imaged on a Sartorius SX5 IncuCyte at every 1h time point over the course of the next 24 hours. Heatmap represents fold change of well green fluorescence intensity as compared to time point zero.

2. Supplementary Tables

Table S1, S3-5. Datasets corresponding to each figure, provided in the attached supplementary files (.xlsx).

Table S2. Summary list of recombinant pET23B caspase-2 plasmids (Residues 170-452) used in this study.

Construct	Mutation	Source
activeCASP2	n/a	Current study
activeCASP2_C370A	C370A	Current study
activeCASP2_C320A	C320A	Current study
activeCSP2C320A_C370A	C320A, C370A	Current study
proCASP2_D326A	D326A, D333A, D347A	Current study
proCASP2	D333A, D347A	Current study
proCASP2_C370A	C370A, D333A, D347A	Current study
proCASP2TEV	D333ENLYFQG, D347ENLYFQG	Current study
proCASP2TEV_C370A	D333ENLYFQG, D347ENLYFQG, C370A	Current study

Table S6. Summary list of recombinant caspase-8 and caspase-10 as well as purchased caspase-3 constructs used in this study.

Construct	Mutation	Source
activeCASP3	n/a	Vickers, C.J., *et al*. 2013 [9]

activeCASP8	n/a	Backus, K.M., *et al*. 2016[10]
activeCASP10	n/a	Backus, K.M., *et al*. 2016[10]
proCASP8	D347A, D384A, C409S, C433S	Backus, K.M., *et al*. 2016[10]
proCASP10	D415A	Backus, K.M., *et al*. 2016[10]

Table S7. Files in Proteomics Identification Database (PRIDE) datasets. PRIDE IDENTIFIERS:PXD042362, PXD051381, and PXD046269.

Figure	File name	Compound	Experiment
Figure 1B	2020-10-07-JOC-70min_FAIMS_3cv_-35_-45_-60_OTIT_SP3_B2-4.csv_results.raw		isoTOP_nonApop
	2020-10-07-JOC-70min_FAIMS_3cv_-35_-45_-60_OTIT_SP3_B3-5.csv_results.raw		isoTOP_nonApop
	2020-10-07-JOC-70min_FAIMS_3cv_-35_-45_-60_OTIT_SP3_S1-1.csv_results.raw		isoTOP_nonApop
	2020-10-07-JOC-70min_FAIMS_3cv_-35_-45_-60_OTIT_SP3_S2-2.csv_results.raw		isoTOP_nonApop
	2020-10-07-JOC-70min_FAIMS_3cv_-35_-45_-60_OTIT_SP3_S3-3.csv_results.raw		isoTOP_nonApop
	2020-12-05-kb-70min_FAIMS_100micron_3cv_-35_-45_-55--OTIT_JOC_7.csv_results.raw		isoTOP_nonApop
	2020-12-05-kb-70min_FAIMS_100micron_3cv_-35_-		isoTOP_no

	45_-55--OTIT_JOC_8.csv_results.raw		nApop
Figure 1C	2020-10-24-JOC-70min_FAIMS_3cv_-35_-45_-60_OTIT_1-2-rerun-1.csv_results.raw		isoTOP_Apop
	2020-10-24-JOC-70min_FAIMS_3cv_-35_-45_-60_OTIT_1-3-rerun-2.csv_results.raw		isoTOP_Apop
	2020-10-24-JOC-70min_FAIMS_3cv_-35_-45_-60_OTIT_2-3.csv_results.raw		isoTOP_Apop
	2020-10-24-JOC-70min_FAIMS_3cv_-35_-45_-60_OTIT_3-4.csv_results.raw		isoTOP_Apop
	2020-12-05-kb-70min_FAIMS_100micron_3cv_-35_-45_-55--OTIT_JOC_1.csv_results.raw		isoTOP_Apop
	2020-12-05-kb-70min_FAIMS_100micron_3cv_-35_-45_-55--OTIT_JOC_2.csv_results.raw		isoTOP_Apop
	2020-12-6-kb-70min_FAIMS_100micron_3cv_-35_-45_-55--OTIT-JOC_3		isoTOP_Apop
Figure 3E	2022-05-04-KB-JOC_isoTOP_EA312_6_quant.raw	6	isoTOP_lysates
	2021-08-03-KB-ET-EA312-4-steep.raw	6	isoTOP_lysate
	2022-05-15-KB-JOC_isoTOP_EA326_1_quant.raw		isoTOP_lys

		5	ates
	2022-05-15-KB-JOC_isoTOP_EA326_2_quant.raw	5	isoTOP_lysates
	2022-04-27-KB-JOC_isoTOP_EA329C_10_quant.raw	15	isoTOP_lysates
	2022-05-04-KB-JOC_isoTOP_EA329C_9_quant.raw	15	isoTOP_lysates
	2022-05-04-KB-JOC_isoTOP_EA329D_7_quant.raw	16	isoTOP_lysates
	2022-05-04-KB-JOC_isoTOP_EA329D_8_quant.raw	16	isoTOP_lysates
	2021-12-30-KB-JOC-338-A-2_quant.raw	7	isoTOP_lysates
	2021-12-30-KB-JOC-338-B-6_quant.raw	7	isoTOP_lysates
	2021-12-9-KB-JOC-70min-isoTOP-EA339-8_quant.raw	8	isoTOP_lysates
	2021-12-9-KB-JOC-70min-isoTOP-EA339-7_quant.raw	8	isoTOP_lysates
	2022-09-18-KB-FAIMS-JOC-isoTOP-lysate-SO339-	8	isoTOP_lys

	8.pep.raw		ates
	2021-12-9-KB-JOC-70min-isoTOP-MPP-4.raw	P01	isoTOP_lysates
	2021-12-9-KB-JOC-70min-isoTOP-MPP-3.raw	P01	isoTOP_lysates
	2021-12-9-KB-JOC-70min-isoTOP-SO22-2_quant.raw	10	isoTOP_lysates
	2022-05-04-KB-JOC_isoTOP_SO22_5_quant.raw	10	isoTOP_lysates
	2022-09-18-KB-FAIMS-JOC-isoTOP-lysate-SO86-1.raw	12	isoTOP_lysates
	2022-09-18-KB-FAIMS-JOC-isoTOP-lysate-SO86-2.raw	12	isoTOP_lysates
	2022-09-18-KB-FAIMS-JOC-isoTOP-lysate-SO103-4.raw	11	isoTOP_lysates
	2022-09-23-KB-FAIMS-JOC-isoTOP-lysate-SO103-3_rerun091822.raw	11	isoTOP_lysates
	2022-09-23-KB-FAIMS-JOC-isoTOP-lysate-SO139-5_rerun091822.raw	9	isoTOP_lysates
	2022-09-23-KB-FAIMS-JOC-isoTOP-lysate-SO139-	9	isoTOP_lys

	6_rerun091822.raw		ates
Figure S7	2021-09-12-KB-JOC-DMSO-1.raw		Recombinant protein
	2021-09-1-KB-JOC-DMSO-2.raw		Recombinant protein
	2021-09-1-KB-JOC-DMSO-3.raw		Recombinant protein
	2021-09-1-KB-JOC-AZ12-1.raw	3	Recombinant protein
	2021-09-1-KB-JOC-AZ12-2.raw	3	Recombinant protein
	2021-09-1-KB-JOC-AZ12-3.raw	3	Recombinant protein
Figure S18	2022-06-18-KB-noFAIMS-JOC--IsoTOP-SO139_RT_5.raw	9	isoTOP
	2022-06-18-KB-noFAIMS-JOC--IsoTOP-SO139_RT_6.raw	9	isoTOP
	2022-09-23-KB-FAIMS-JOC-isoTOP-lysate-SO139-5_rerun091822.raw	9	isoTOP
	2022-09-23-KB-FAIMS-JOC-isoTOP-lysate-SO139-	9	isoTOP

	6_rerun091822.raw		
Figure 6A	2022-09-10-KB-FAIMS-JOC-isoTOP-incell-MPP_frozen_2.raw	P01	isoTOP_in-cell
	2022-09-09-KB-FAIMS-JOC-isoTOP-incell-MPP_frozencells_3_rerun0828.raw	P01	isoTOP_in-cell
	2022-09-09-KB-FAIMS-JOC-isoTOP-incell-MPP_freshcells_4_rerun0828.raw	P01	isoTOP_in-cell
	2022-12-07-KB-JOC-isoTOP_incell_SO22_9.raw	10	isoTOP_in-cell
	2022-12-07-KB-JOC-isoTOP_incell_SO22_10.raw	10	isoTOP_in-cell
	2022-12-06-KB-JOC-isoTOP_incell_SO86_1.raw	12	isoTOP_in-cell
	2022-12-06-KB-JOC-isoTOP_incell_SO86_2.raw	12	isoTOP_in-cell
	2022-12-06-KB-JOC-isoTOP_incell_SO103_3.raw	11	isoTOP_in-cell
	2022-12-06-KB-JOC-isoTOP_incell_SO103_4.raw	11	isoTOP_in-cell
	2022-12-06-KB-JOC-isoTOP_incell_SO139_5.raw	9	isoTOP_in-

			cell
	2022-12-08-KB-JOC-isoTOP_incell_SO139_6_rerun.raw	9	isoTOP_in-cell
	2023_02_14_KB_FAIMS_incell_isoTOP_EA339_JOC_1.raw	8	isoTOP_in-cell
	2023_02_14_KB_FAIMS_incell_isoTOP_EA339_JOC_2.raw	8	isoTOP_in-cell
	2023_02_14_KB_FAIMS_incell_isoTOP_EA339_JOC_3.raw	8	isoTOP_in-cell
	2023_02_14_KB_FAIMS_incell_isoTOP_EA312_JOC_4.raw	6	isoTOP_in-cell
	2023_02_14_KB_FAIMS_incell_isoTOP_EA312_JOC_5.raw	6	isoTOP_in-cell
	2023_02_14_KB_FAIMS_incell_isoTOP_EA312_JOC_6.raw	6	isoTOP_in-cell
	2023_02_14_KB_FAIMS_incell_isoTOP_EA326_JOC_7.raw	5	isoTOP_in-cell
	2023_02_14_KB_FAIMS_incell_isoTOP_EA326_JOC_8.raw	5	isoTOP_in-cell
	2023_02_14_KB_FAIMS_incell_isoTOP_EA326_JOC_	5	isoTOP_in-

	9.raw		cell
Figure 6B	2023-12-30-KB-NoFAIMS-AZ12-LFQ-JOC_1.raw	3	Protein-ABPP
	2023-12-30-KB-NoFAIMS-AZ12-LFQ-JOC_2.raw	3	Protein-ABPP
	2023-12-30-KB-NoFAIMS-AZ12-LFQ-JOC_3.raw	3	Protein-ABPP
	2023-12-30-KB-NoFAIMS-AZ12-LFQ-JOC_4.raw	3 and 9	Protein-ABPP
	2023-12-30-KB-NoFAIMS-AZ12-LFQ-JOC_5.raw	3 and 9	Protein-ABPP
	2023-12-30-KB-NoFAIMS-AZ12-LFQ-JOC_5.raw	3 and 9	Protein-ABPP

Table S8. List of caspase-2 primer sequences used in this study.

Purpose	**Primer Sequence**	
Subclone Caspase-2 into pET23b	5'-AA**CATATG**GGTCCTGTCTGCCTTCAGGTG-3'	Forward

(Residues 170-452)		
Subclone Caspase-2 into pET23b	5'-AA**CTCGAG**TGTGGGAGGGTGTCC-3'	Reverse
Mutation C370A	5'-GCGGCTATGCCGCCCTCAAAGGGACTGCCGCCATGCGG-3'	Forward
	3'-GTCCCTTTGAGGGCGGCATAGCCGCATATCATGTCTG-5'	Reverse
Mutation C320A	5'-CTTCATCCAGGCCGCCCGTGGAGATGAGACTGATCG-3'	Forward
	3'-CATCTCCACGGGCGGCCTGGATGAAGAACATTTTTG-5'	Reverse
Mutation D333A	5'-GAGATGAGACTGCTCGTGGGGTTGACCAACAAGCTGGAAAGAACCACG-3'	Forward
	5'-GTGGAGATGAGACTGCTCGTGGGGTTGACCAACAAGCTGGAAAGAACCACGCAGG-3'	Reverse
Mutation D347A	5'-CCCCTGGGTGCGAGGAGAGTGCTGCCGGTAAAGAAAAGTTG-3'	Forward
	5'CAACTTTTCTTTACCGGCAGCACTCTCCTCGCACCCAGGGG	Reverse

	-3’	
Mutation C370W	5'-GCGGCTATGCCTGGCTCAAAGGGACTGCCGCCATGCGG-3'	Forward
	3'-CAGTCCCTTTGAGCCAGGCATAGCCGCATATCATGTCTG-5'	Reverse
ENLYFQG insertion	5'-GAAAATCTCTACTTCCAGGGCGGTAAAGAAAAGTTGCCG-3'	Forward
	3'-CTTTACCGCCCTGGAAGTAGAGATTTTCACTCTCCTCGC-5'	Reverse

Table S9. Lentivirus vector and shRNA sequences for caspase-9 knockdown cells, provided in the attached supplementary files (.xlsx).

3. Biology Methods

Cell lines, culture conditions

Jurkat cells were cultured in Roswell Park Memorial Institute (RPMI) media (Fisher Scientific, 11875119) with 10% fetal bovine serum (Avantor Seradigm Lot # 214B17) and 100U/mL penicillin and 100U/mL streptomycin at 37℃ and 5% CO_2. Jurkat cells were obtained from ATCC (TIB-152). Cell culture reagents including RPMI 1640 media, trypsin-EDTA and penicillin/streptomycin (Pen/Strep) were purchased from Fisher Scientific.

Mycoplasma testing

Mycoplasma testing was conducted monthly using the MycoAlert® kit (LT07-703, Lonza Rockland, Rockland, ME) following the manufacturer's instructions.

Cell Harvesting

Suspension cells were centrifuged at 1,400 *g* for 5 minutes and the supernatant was aspirated. The pellets were then washed in 10 mL PBS and centrifuged at 1,400 *g* for 5 minutes. PBS wash was repeated, and the subsequent pellet was then resuspended in 1 mL PBS in a microcentrifuge tube and centrifuged at 1,400 *g* for 5 minutes. The supernatant was aspirated, and the cells were stored at -80 ℃.

Cell Lysis

Jurkat lysates used for competitive ABPP gel analysis were lysed using an Ultrasonic Probe Sonicator at Power 2 for 10 pulses, 1 second pulse, 1 second off on ice. For western blotting samples, cells were reconstituted and lysed using cold 100 µL of 0.3% 3-[(3-Cholamidopropyl) dimethylammonio]-1-propanesulfonate (CHAPS) buffer in PBS.

The reconstituted cell pellet was left to incubate with the CHAPS buffer on ice for 15 min. The samples were then harvested by centrifugation (1,400 x g, 10 min) and the clarified supernatant was then transferred to a new tube.

Plasmids

Caspase-2 (Residues 170-452) was subcloned into pET23b (+) and the point mutations and insertions generated by site-directed mutagenesis using the primer sequences listed in Table S8. Plasmids were propagated in chemically competent TOP10 cells.

Protein Concentration

Protein concentrations were determined using a Bio-Rad DC protein assay kit following the manufacturer's instructions using reagents from Bio-Rad Life Science (DC Reagent A and B, 5000113 and 5000114).

isoTOP-ABPP proteomic sample preparation

Cell processing: Apoptotic Jurkat cells (treated with 50 ng/mL FasL for 4h) or non-apoptotic Jurkat cells (treated with DMSO for 4 h) were harvested at 1.0 x10^6 cells/mL and harvested by centrifugation (1,400 x *g*). Collected cells were then resuspended in 10 mL of cold PBS and subsequently harvested by centrifugation (1,400 x *g*), and this wash step was repeated 2 cycles. Cell pellets were then reconstituted in 500 µL of cold PBS and subjected to Ultrasonic Probe Sonicator lysis (Power 2, 10x pulses; 1 second pulse, 1 second off) on ice. Lysate concentrations were then adjusted to 2 mg/mL.

Electrophilic fragment and IA-alkyne labeling: For cysteine reactivity analysis, 200 µL lysates (2 mg/mL) were then labeled with either 10 µM or 100 µM iodoacetamide alkyne (**IAA**) for 1h at ambient temperature. For lysate-based compound screening, samples were treated with either DMSO or fragment electrophiles at 25 µM (**P01**, **5**, **6**) or 100 µM (**3**, **7-16**) for 1h followed by subsequent labeling with 200 µM **IAA** for 1h. For the in-cell treated samples, 10 ml of 1.2 x 10^6 cells/mL were treated with DMSO or electrophilic fragments (25 or 100 µM) for 1h. Cells were subsequently harvested as detailed for *Cell Harvesting* and lysed as detailed for *Cell Lysis*. Samples were prepared in at least biological duplicate.

Click chemistry: Samples were subjected to bioorthogonal copper(I)-catalyzed azide-alkyne cycloaddition (CuAAC)[11] or "click" conjugation to previously reported isotopically labeled *tobacco etch virus* (TEV)-cleavable biotinylated peptide tags[2]. To 200 µL cell lysates (2 mg/mL), samples were combined with a premixed cocktail of click reagents consisting of TEV tags (4µl of 5 mM stock, final concentration= 100 µM), TCEP (4 µl of fresh 50 mM stock in water, final concentration 1 mM), TBTA (12 µl of 1.7 mM stock in DMSO/t-butanol 1:4, final concentration = 100 µM), and CuSO4 (4 µl of 50 mM stock in water, final concentration = 1 mM). After 1h, the samples were then combined pairwise (400 µL total) and treated with 40 µL of 10% SDS (1% SDS final) followed by 0.5 µL of benzonase (Fisher Scientific, 707464). Samples were left to incubate for 30 min at 37 ℃. Following benzonase treatment, samples were subjected to Single-Pot Solid-Phase-enhanced sample-preparation (SP3).

Single-Pot Solid-Phase-enhanced sample-preparation (SP3): Following the previously reported protocol[6], for each 400 µL sample (400 µg protein), 40 µL Sera-Mag SpeedBeadsTM Carboxyl Magnetic Beads, hydrophobic (Thermo Scientific™, 09-981-123) and 40 µL Sera-Mag SpeedBeadsTM Carboxyl Magnetic Beads, hydrophilic (Thermo Scientific™, 09-981-121) were gently mixed and washed with 1 mL distilled water. Beads were combined using a magnetic rack (Sergi Lab Supplies, 1005a) and water was carefully aspirated. Washes were repeated for a total of 3 times. 80 µL of mixed beads were then added to the 400 µL of combined samples. The bead-sample mixture was then incubated for 5 min at ambient conditions with shaking (1000 rpm). 200 proof ethanol was added to each sample such that each sample contained ≥55% ethanol by volume (for 480 µL of combined sample/SP3 beads, 600 µL of ethanol was added). The samples were incubated for 5 min at ambient conditions with shaking (1000 rpm). The beads were then washed three times with 600 µL 80 % ethanol in water. After washes, ethanol was removed using the magnetic rack, and beads were then resuspended in 200 µL 0.5 % SDS in PBS containing 2 M urea. 10 µL of 200 mM DTT (10 µM final concentration) was then added to each sample and the samples incubated at 65 °C for 15 min. Following reduction, 10 µL of 400 mM iodoacetamide (20 µM final concentration) was added to each sample and the samples incubated for 30 min at 37 °C with shaking at 300 rpm. Subsequently, 600 µL of 200 proof ethanol was added to each sample, and the samples were incubated for 5 min at ambient conditions with shaking (500 rpm). Beads were then washed three times with 80 % ethanol in water. Samples were then diluted with 150 µL 2 M urea in PBS followed by the addition of reconstituted MS grade trypsin (2 µg, Promega, V5111). The samples were subjected to water bath sonication for

1 min and subsequently left to digest overnight (16 - 18hr) at 37℃ and shaking at 200 rpm. The digested peptide solution and SP3 beads were then transferred into 15 mL falcon tubes. Peptides were then rebound to SP3 beads via the addition of 3.8 mL of 100% acetonitrile for a final percentage of ≥95% acetonitrile by volume and the peptides were subjected to shaking at 1000 rpm for 10 minutes at ambient temperature. Beads were collected using a magnet and solution was discarded. Samples were washed with 1 mL of 100% acetonitrile three times. Digested peptides were then eluted with 100 µL of 2% DMSO in water, shaking at 1000 rpm for 30 min at 37 °C. Supernatant was collected in a 1.5 mL centrifuge tube on ice after separating SP3 beads with a magnetic rack. SP3 beads were resuspended with an additional 100 µL of 2% DMSO in water, shaking at 1000 rpm for 45 min at 37℃. Supernatant was collected after separating SP3 beads with a magnetic rack and combined with the previous elution volume (200 µL total).

Streptavidin Enrichment: Pierce™ Streptavidin Agarose resin (Thermo Scientific™, PI20353) (100 µL of resin) was first washed 3x in 10 mL of PBS by centrifugation at 1,800 x *g* for 3 min per wash. Solution was aspirated, making sure not to disturb spun down resin. After washing, resin was resuspended in 1 mL PBS/sample and re-distributed into 1.5 mL microcentrifuge tubes. The 200 µL peptide elution from previously prepared SP3 method was then added to the 1 mL of PBS/streptavidin resin. Samples were enriched by rotation for 2h at ambient conditions. After enrichment, the resin was collected by centrifugation at 1,400 x g for 5 min, and supernatant was aspirated and discarded. The resin was then subjected to washes 2x in 1 mL of PBS and 2x in 1 mL of water by centrifugation at 1,400 x g for 5 min per wash. After carefully aspirating and discarding

the water, the resin/peptide slurry was then treated with a TEV protease following the "Tev digestion" protocol.

Tev Digest: Following streptavidin enrichment, samples were resuspended in 75 µL TEV buffer (50 mM Tris, pH 8, 0.5 mM EDTA, 1 mM DTT). To the resuspended samples, 1.5 µL TEV protease (2 mg/mL or 70 µM; MacroLab, UC Berkeley) was added and the reactions were rotated for 7h at 30°C. The samples were then harvested by centrifugation (3,000 x *g*, 1 min) and the supernatant was collected. Samples were then subjected to a final cleanup following the "Sample cleanup" protocol.

Sample Cleanup: The collected peptides were then desalted using Pierce™ C18 100 µL Tips (Thermo Scientific™, 87784) following the manufacturer's protocol. Briefly, 10 mL of the following four solutions were prepared; A) 100% acetonitrile, B) 50:50 acetonitrile:ultra pure water, C) Ultra pure water with 0.1% trifluoroacetic acid, and D) 60% acetonitrile with 0.1% trifluoroacetic acid in ultrapure water. Each C18 100 µL tip was first equilibrated with 100 µL with solution A for a total of two times followed by equilibration with solution B for a total of two times. The tips were then washed with 100 µL of solution C for a total of three times. Finally, 100 µL of samples were loaded into the tips and subsequently washed 2x with solution C. Samples were then eluted with 100 µL of solution D. Following desalting, each 100 µL sample was dried by speedvac and reconstituted in 20 µL of 5% acetonitrile and 1% formic acid in water.

Recombinant proCASP2 proteomic sample preparation

25 µL recombinant purified proCASP2 (0.5 mg/mL) was first treated with 10 mM DTT followed by buffer exchange using Zeba desalting columns. Samples were treated with DMSO or compound **3** (100 µM) for 1h at 30 ℃. Samples were then subjected to *SP3 clean-up* using 5 µL of mixed SP3 beads. 30 µL beads/sample were then washed with 200 proof ethanol, followed by 2x 80% ethanol in water, and reduced with 10 µL of 200 mM DTT (10 mM final concentration) in samples reconstituted with 200 µL of 2M urea in 0.5% SDS in PBS. Samples were then incubated with 10 µL of 400 mM iodoacetamide (20 mM final concentration) and subjected to on-bead Trypsin digest following the SP3 protocol. Reconstituted samples in 100 µL of 2% DMSO in water were analyzed by LC-MS/MS.

Protein-directed ABPP proteomics analysis

Jurkat cells (10 million) were treated with either DMSO (*n* = 3) or 100 µM compound 9 (*n* = 3) for 1 h, then all conditions were treated with 20 µM alkynye probe 1 h. Cells were then harvested, lysed by sonication (power 2, 10 pulses, 1 second on/1 second off, 2 rounds), and lysate concentration normalized to 2 mg/mL by DC assay. 200 µL of each lysate was then subject to CuAAC 'click' biotinylation by treatment with 24 µL of premixed cocktail of click reagents (12 µL 1.7mM TBTA per sample, 4 µL 50mM copper sulfate per sample, 4 µL 50mM biotin-azide per sample, 4 µL 50mM TCEP per sample). Samples were then cleaned via SP3 clean-up. 20 µL Sera-Mag SpeedBeads Carboxyl Magnetic Beads per sample, hydrophobic (GE Healthcare, 65152105050250, 50 µg/µL, total 1 mg) and 20 µL Sera-Mag SpeedBeads Carboxyl Magnetic Beads per sample, hydrophilic (GE Healthcare, 45152105050250, 50 µg/µL, total 1 mg) were mixed and washed with water

three times and resuspended in 40 µL of water per sample (240 µL total). 40 µL of the bead slurry was then transferred to each lysate sample and incubated for 5 minutes at room temperature with shaking (1000 rpm). 500 µL of absolute ethanol was added to each sample and incubated for 10 minutes at room temperature with shaking (1000 rpm). The beads were then washed (3x, 400 µL 80% ethanol) with a magnetic rack. Proteins were eluted from SP3 beads with 100 µL of 0.2% SDS in PBS for 30 min at 37°C with shaking (1000 rpm). The elution was repeated with 100 µL of 0.2% SDS in PBS and the elution fractions from the same sample combined. Streptavidin resin (Thermo Scientific, Cat. No. 20353) was then prepared by washing 50 µL of streptavidin resin per sample in 10mL PBS and collecting resin by centrifugation at 1800 *g* for 5 minutes, PBS aspirated, and resin resuspended in 1 mL PBS per sample. 1mL of streptavidin slurry was added to each sample and samples rotated at room temperature for 1.5 hours. Streptavidin resin was collected via centrifugation at 1500 *g* for 2 minutes and washed 1 time with 1 mL 0.2% SDS in PBS, 3 times with 1 mL PBS, and 3 times with 1 mL molecular biology-grade water. Resin was then resuspended in 200 µL 6M urea. DTT was added to each sample to a final concentration of 10 mM and incubated at 65°C for 15 minutes. Iodoacetamide was then added to each sample to a final concentration of 20 mM and incubated at 37°C for 30 minutes. Urea was diluted to ~2M, resin collected via centrifugation at 1500 *g* for 2 minutes, supernatant aspirated, and resin resuspended in 150 µL 2M urea in PBS. Then, 3 µL of 1 mg/mL trypsin was added to each sample and samples were subject to digestion for 12-16 hours at 37°C and 200 rpm. Resin was then spun down and supernatant transferred to a new tube (containing digested peptides). Resin was washed with an additional 50 µL of molecular biology-grade water, spun down, and supernatant added to

the previous peptide fraction. Trifluoroacetic acid (TFA) was added to the samples to a final concentration of 0.5%. Samples were then cleaned with Pierce C18 spin tips (Thermo Fisher, Cat. No. 87784) according to the manufacturer's protocol. The samples were dried (SpeedVac) and reconstituted with mass spectrometry buffer (5% acetonitrile and 1% formic acid in molecular biology-grade water) and analyzed by LC-MS/MS. See the 'Data analysis' section for details on data processing.

Immunoblot-based streptavidin pull-down

U2OS cells were grown to 90% confluency, then treated with either vehicle DMSO or 100 μM compound 9 for 1h, followed by treatment with either vehicle DMSO or 20 μM click probe 3 for 1 h. Then, the same protocol as detailed in "Protein-directed ABPP proteomics analysis" was followed up until the elution from streptavidin resin. Briefly, cells were lysed by sonication, lysate concentrations normalized, compound 3-labeled proteins conjugated to biotin-azide via CuAAC, samples cleaned via SP3 clean-up, biotinylated proteins enriched on streptavidin, and non-biotinylated proteins washed away from streptavidin resin. 50 μL of each sample was saved and set aside prior to CuAAC to serve as the 'input' samples on the immunoblot. Then, proteins bound to streptavidin were eluted using 35 μL 4X SDS loading dye (BioRad 4X Laemmli Sample Buffer + 2-mercaptoethanol) and heated at 95°C for 10 minutes. The samples were resolved by SDS-PAGE gel followed by transfer to a nitrocellulose membrane. Membranes were then blocked in 5% milk in 1x Tris-Buffer Saline, 0.1% Tween® 20 (TBST) for 1h and probed with the indicated antibodies diluted in 5% milk in TBST. The membrane was incubated with primary antibody overnight at 4 °C with rocking, then washed (3x5 min TBST), and

incubated with secondary antibody (IRDye 800CW, 1:10,000) for 1h at ambient temperature. Blots were washed (3x5 min TBST) and visualized on a BioRad ChemiDoc Imaging System.

Cellular thermal shift assay (CETSA)

Freshly lysed U2OS cell lysates were spun down at 18k x g and 4°C for 10 minutes to remove any insoluble cell debris then diluted to a final concentration of 2.8 mg/mL. These lysates were then labeled with either DMSO, compound **9**, or compound **12** (100 µM) for 1h at ambient temperature. Next each sample was split into 8 PCR tubes (50 µL for each specified temperature). These lysates were then heated using a Bio-Rad PCR thermal cycler (T100) at the specified temperatures for 5 minutes immediately followed by an indefinite hold at 4°C. After heating the lysates were transferred back to 1.5 mL microcentrifuge tubes and centrifuged at 21.1k x g and 4°C for 45 minutes. After centrifugation 30 µL of the soluble portion of each sample was carefully pipetted into fresh tubes and 10 µL of 4x loading dye (Bio-Rad) was added. Samples were resolved by SDS-PAGE (Bio-Rad 4-20% Criterion Stain-Free™) and gel was imaged using Bio-Rad Chemidoc Stain-Free setting for protein loading. The gel was then transferred to nitrocellulose membrane (Bio-Rad) and blotted with indicated antibodies as detailed below.

Proteomics acquisition

The samples were analyzed by liquid chromatography tandem mass spectrometry (LC-MS/MS) using a Thermo Scientific™ Orbitrap Eclipse™ Tribrid™ mass spectrometer

(Thermo Scientific™) coupled to an Easy-nLC™ 1200 pump and to a High Field Asymmetric Waveform Ion Mobility Spectrometry (FAIMS) Interface. Peptides were fractionated online using a 16 cm long, 100 µM inner diameter (ID) fused silica capillary packed in-house with bulk C18 reversed phase resin (particle size, 1.9 µm; pore size, 100 Å; Dr. Maisch GmbH). The 70-minute water-acetonitrile gradient was delivered using a EASY-nLC™ 1200 system at different flow rates (Buffer A: water with 3% DMSO and 0.1% formic acid and Buffer B: 80% acetonitrile with 3% DMSO and 0.1% formic acid). The detailed 70 minute gradient includes 0 – 5 min from 3 % to 10 % at 300 nL/min, 5 – 15 min from 10 % to 20 % at 220 nL/min, 15 – 64 min at 20 to 47% at 220nL/min, 64-66 min from 47 % to 95 % at 250 nL/min, and 66 to 70 min at 95% buffer B in buffer A. Data was collected with charge exclusion (1, 8,>8). Data was acquired using a Data-Dependent Acquisition (DDA) method consisting of a full orbitrap MS1 scan (Resolution = 120,000) followed by sequential MS2 scans (Resolution = 15,000) to utilize the remainder of the 1 second cycle time. Precursor isolation window was set to 1 m/z and high energy c-trap dissociation (HCD) normalized collision energy was set to 30%. Run time 70 minutes Injection volume 5 µL. For data acquired using a FAIMS device 3 compensation voltages (CV; -35, -45, -55V) were used as determined in our previous study[9].

Data analysis

For isoTOP ABPP experiments, the Proteomic workflow of FragPipe and its collection of tools were set as default. FragPipe output data was then compiled using our in-house python script. Custom python scripts were implemented to compile modified_peptide_label_quant.tsv (quantification) outputs from FragPipe (v19.0).[12-14]

These scripts were used to calculate an average of median logged ratios for each peptide, cysteine and protein per replicate and experiment condition. As a preprocessing step, logged ratios from singleton peptides were removed before further analysis, and unpaired heavy or light-identified peptides were kept by setting ratios to $\log_2(20)$ or $\log_2(1/20)$. Median heavy over light ratios for the same cysteine residue from cysteine peptides of different charges and miss cleavages in the same replicate were computed. Then, for each experimental condition (apoptotic vs nonapoptotic, DMSO vs treatment, etc.), an average of medians was calculated to obtain a final "average_of_medians" metric. This "average_of_medians" value was utilized to compare the isotopical quantification of the same peptide/cysteine/protein across various experimental conditions or across replicates within the same experiment. For the protein-directed ABPP analysis quantified using label-free quantification, significantly enriched and off-competed proteins were identified using MSFragger Analyst[15], with imputation using Perseus,{Tyanova, 2016}{Tyanova, 2018} normalization and Benjamini-Hochberg correction to generate adjusted p-values, which were plotted against the average fold-change of each protein to generate the volcano plot. Proteins with a $\log_2$(fold-change) > 2 and adjusted p-value < 0.05 are considered significantly enriched.

Protein, peptide, and cysteine identification. RAW files were searched with MSFragger (v3.7) and FragPipe (v19.0). The proteomic workflow and its collection of tools was set as default and PTMprophet was enabled[15] . Precursor and fragment mass tolerance was set as 20 ppm. Missed cleavages were allowed up to 1. Peptide length was set 7 - 50 and peptide mass range was set 500 - 5000. For identification, cysteine residues were searched with differential modification C+. For ligandability quantification, MS1

labeling quant was enabled with Light set as C+521.30745 and Heavy set as C+527.3213. MS1 intensity ratio of heavy and light labeled cysteine peptides were reported with Ionquant (v1.8.10). Calibrated and deisotoped spectrum files produced by FragPipe were retained and reused for this analysis. The MS search data have been deposited to the ProteomeXchange Consortium via the PRIDE partner repository with the dataset identifiers PXD042403 and PXD046269. File details can be found in **Table S7**. Custom python scripts were implemented to compile labeled peptide datasets. Unique proteins, unique cysteines, and unique peptides were quantified for each dataset. Unique proteins were established based on UniProt protein IDs. Unique peptides were found based on sequences containing a modified cysteine residue. Unique cysteines were classified by an identifier consisting of a UniProt protein ID and the amino acid number of the modified cysteine (ProteinID_C#); residue numbers were found by aligning the peptide sequence to the corresponding UniProt protein sequences found in protein.fas FragPipe output files. For cases where multiple cysteines were labeled on the same peptide, a new identifier for each modified cysteine residue number was created. Multiplexed peptide identifiers were reported as ProteinID_C#1 and ProteinID_C#2, instead of ProteinID_C#1_C#2.

Protein expression and purification

The sequence encoding caspase-2, lacking the prodomain (residue numbers 32-121) was subcloned into the pET23b(+) with a c-terminal hexa his-tag. Point mutations (C320A, C370A, D333A, D347A) were created by PCR-based site-directed mutagenesis. Plasmids were propagated in TOP10 chemically competent cells. Single colonies from TOP10 grown cells were collected in 5 mL of LB supplemented with 100 µg/ml ampicillin

and grown overnight (16h). Cells were harvested the following day and subjected to Zyppy Plasmid Miniprep following the manufacturer's protocol (Zymo Research, D4037). Following sequencing of plasmids, validated plasmids were transformed to BL21(DE3) *e.coli* cells. Single colonies were picked from an LB agar plate and grown in 10 mL of LB media supplemented with 100 µg/mL ampicillin. The cell culture was then transferred and grown in 1 L of Miller LB medium at 37 °C to an optical density (OD600) of 0.5. The culture was then cooled to 18 °C, induced with 1 mM isopropyl-β-D-galactopyranoside (IPTG), and incubated for an additional 4h at 18 °C. The cells were centrifuged at 8,000 x *rpm* for 45 min minutes and the cell pellet was measured. The cells were resuspended in 10 mL per 1 g of cells in lysis buffer (100 mM Tris pH 7.5, 100 mM NaCl, 25 mM Imidazole). The resuspended cells were passed through a microfluidizer (Avestin Emulsiflex C3 Homogenizer; 8,000 psi x2 rounds) to ensure lysis. The cell debris was removed by centrifugation (20,000 x *g*, 45 min*)* and the supernatant was resuspended with 1 mL of Hispur Ni-NTA agarose resin (Thermo Scientific™, PI88222). The sample was washed with two rounds of lysis buffer (2 x 50 mL). His-tagged caspase-2 was eluted from the resin using an elution buffer with high imidazole concentration (100 mM Tris pH 7.5, 100 mM NaCl, 250 mM Imidazole). The eluted sample was concentrated (Amicon Ultra Centrifugal Filter Unit, 4 mL 10 kDa, Fisher Scientific, UFC801024) and buffer exchanged via PD10 desalting column (Cytiva, GE17-0851-01) into storage buffer (20 mM Tris pH 7.5, 50 mM NaCl, 5 mM DTT). Recombinant TEV protease was purchased from the Berkeley MacroLab QB3, where it was was expressed as a double mutant (L56V / S135G) pRK793 plasmid in Rosetta2(DE3)pLysS cells (TEV-DM-Prk793 L56V/ S135G) and

stored in 25 mM HEPES pH 7.5, 400 mM NaCl, 10% glycerol, 1 mM DTT. Recombinant proCASP8 and proCASP10 were purified as reported previously.[10]

Reduction and Zeba desalting

Before gel-based ABPP analysis, all recombinant protein samples were first treated with 5 mM DTT for 15 minutes followed by buffer exchange using Zeba desalting columns to ensure that all caspase protein was fully reduced prior to analysis. Samples were buffer exchanged using the Zeba Desalting Columns 7K MWCO (Thermo Scientific, 89882) following the manufacturer's desalting procedure. Briefly, Zeba columns were first harvested by centrifugation in a 1.5 mL microcentrifuge tube using a variable-speed bench-top microcentrifuge at 1,500 x *g* for 1 minute. The columns were prepared by first loading 300 µL of PBS followed by centrifugation at 1,500 x *g* for 1 minute. The washes were repeated 2 more times. 100 µL of treated or non-treated samples were then loaded onto the desalting column, harvested by centrifugation at 1,500 x *g* for 1 minute and collected in a fresh 1.5 mL microcentrifuge tube.

Gel-based ABPP.

Recombinant proteins were first subjected to *Reduction and Zeba desalting*. Subsequently recombinant proteins were added to 1 mg/mL Jurkat cell lysates to a final concentration of 2 µM recombinant protein. 25 µL of the cell lysate-recombinant protein mixture was then treated with 100 µM or 10 µM of electrophiles (**P01-P06, 5-16**) for 1h at ambient conditions or 30℃. The samples were then incubated for 1h with 1 µL of 250 µM click probes (**IAA, KB18, KB19, KB61, 1-4**) at a final concentration of 10 µM. Samples

were then subjected to either click conjugation to rhodamine azide in 3 µL of click mix containing TBTA (1.5 µL of 1.7 mM for a final concentration of 100 µM), $CuSO_4$ (0.5 µL of 50 mM for a final concentration of 1 mM), Rhodamine-azide (0.5 µL of 1.25 mM for a final concentration of 25 µM), and TCEP (0.5 of µL 50 mM for a final concentration of 1 mM) or activity-based probe **Rho-DEVD-AOMK (2** µM **)** Next, 10 µL of 4x laemmli loading dye (BioRad, 1610747) was added and the samples were denatured at 95°C for 5 minutes. Samples were resolved by SDS-PAGE and imaged using a BioRad ChemiDoc Imaging System. Coomassie InstantBlue (Fisher Scientific, ISB1L) was used for visualization of protein loading.

TEV activation Gel based ABPP

Purified recombinant caspase-2 TEV cleavable constructs (proCASP2TEV and proCASP2TEV_C37A) at 2 µM final concentration in 1 mg/mL Jurkat lysates were first treated with either compound **3** or **Rho-DEVD-AOMK** at 10 µM final concentration for 1h at ambient conditions. proCASPTEV constructs were then activated with TEV protease (2 mg/mL stock) at increasing final concentrations (0 µM, 0.1 µM, 0.5 µM, 1.0 µM, 2.5 µM, 5.0 µM) for 1h at ambient conditions. Samples treated with compound **3** were then subjected to 'click' conjugation to rhodamine azide as prepared in the "Gel based ABPP" section and visualized by SDS-PAGE in-gel fluorescence using a BioRad ChemiDoc Imaging System. Coomassie InstantBlue was used for visualization of protein loading.

Determining in vitro apparent IC_{50} values

Purified recombinant caspase-2 protein was spiked into 1 mg/mL cell lysates to make a final concentration of 2 μM recombinant protein. This mixture was aliquoted into 25 μL samples and treated with 1 μL of electrophile (final concentration of 0.1 μM, 1.0 μM, 2.5 μM, 5.0 μM, 10 μM, 20 μM, 50 μM, 75 μM, and 100 μM) for one 1h at ambient temperature. These samples were then treated with 1 μL of 250 μM compound **3** to a final concentration of 10 μM. Following incubation with the alkyne probe, 3 μL click mix was added as prepared in the "Gel based ABPP" sectionand reaction was allowed to proceed at ambient temperature for 1h. Next, 10 μL of 4x laemmli loading dye was added and the samples were denatured at 95℃ for 5 minutes. Samples were resolved by SDS-PAGE and imaged using a BioRad ChemiDoc Imaging System. Images were analyzed using ImageJ and plotted in GraphPad Prism 9 to obtain a final IC_{50} value. The percentage of labeling was determined by quantifying the integrated optical intensity of each individual band after subtracting the background signal for each fluorescent gel following the "Quantification of Gel Bands by ImageJ" protocol. Nonlinear regression analysis was used to determine the IC50 values from the dose-response curve generated in GraphPad Prism 9.

Quantification of Gel Bands by an Image J

Raw TIFF files were opened on ImageJ.[16] Bands were selected with a rectangle as region of interest (ROI). After all bands were selected and registered, the Band/Peak Quantification macro was started. Selected lanes were plotted followed by manually drawing baseline for each selected lane. Quantification of peak area was then determined using the wand tool.

Enzyme activity assay

Enzymatic activity of pro-caspase and active-caspase constructs (1 μM recombinant protein, 5 mM DTT and 333 mM citrate in PBS) were determined using the fluorescent caspase-2 substrate Ac-VDVAD-AFC(Cayman Chemicals, item number 37351) at 10 μM final concentration. Caspase and substrate buffers were mixed and immediately ran on the plate reader. 7-amino-4-trifluoromethylcoumarin (AFC) released by substrate cleavage was detected at λ_{ex} = 400 nm and λ_{em} = 505 nm using a multimodal Synergy H1 microplate reader (BioTek). Reads were collected every minute after substrate addition. Percent activities were calculated from the slope of the linear range determined from the reaction progress curves. Graphpad Prism (Version Prism 9.5.1) was used to obtain K_m and k_{cat} values by fitting reaction velocities into the Michaelis-Menten equation using varied fluorogenic substrate Ac-VDVAD-AFC concentrations of 100, 75, 50, 20, 10, 5, 2.5 and 1.0 μM.

Compound inhibition assays

Recombinant protein was first treated with 5 mM DTT for 15 minutes followed by buffer exchange using Zeba desalting columns (Thermo Scientific, 89882) as described in *Reduction and Zeba desalting.* Subsequently, 1 μM recombinant caspase-2, caspase-3, caspase-8 and caspase-10 were treated with electrophiles at indicated final concentrations (i.e. 10 μM, 100 μM, etc.) for 1h (2h for figure 2C, 2D, and 2F) at 30°C. Samples were then treated with 10 μM fluorogenic caspase-3/-7 substrate, Ac-VDVAD-AFC (Cayman , 37351) and 333 mM citrate in PBS. Reaction progress curves from

cleaved substrate fluorescence were then monitored by a multimodal plate reader as described in *Enzyme activity assay.*

Size Exclusion

Ni-NTA agarose-purified recombinant caspase-2 proteins were subjected to fast protein liquid chromatography (FPLC) using a prepackaged gel filtration column consisting of a HiLoad Superdex 75 prep grade (pg) (GE Healthcare Life Sciences) column and a NGC medium-pressure chromatography system and BioFrac collector from Bio-Rad (NGC10 Chromatography System). Column was pre-equilibrated with 1 column volume (120 mL total volume) degassed Size exclusion buffer (20 mM Tris, 50 mM NaCl, 1 mM DTT) following which analytes loaded using a 1 mL sample loop were subjected chromatography (0.5 mL/min). 1mL fractions were collected for 1 column equivalent volume (120 mL total volume). For compound treatment, recombinant protein at 0.3 mg/mL was first treated with 100 μM of compound (**P01**, **3**, **11**, **12**) at 30 ℃ for 1 h. Percent of component was determined by area-under-the-curve (AUC) calculations (AUC integrated measurement tool from GraphPad Prism 9) of the UV absorbance spectra (mAU) at 280 nm for the dimeric gel filtration column volume fractions (0.30 - 0.45) and monomeric fractions (0.48 - 0.55) from each recombinant protein sample (0.3 mg/mL).

CellTiter-Glo® Cell viability analysis

Jurkat cells in complete RPMI 1640 media (100 μL of 1.0 x10^6 cells/mL) were added to a 96-well white/clear bottom tissue culture treated plate using a multichannel pipette. To each well, samples were treated with either vehicle (2 μL of DMSO), or compound (2 μL

of 1.25 mM stock in DMSO for a final concentration of 25 μM for **P01** and **5**, or 2 μL of 5 mM stock for a final concentration of 100 μM for **8**, **9**, **11**, and **12**). Following 1h incubation, staurosporine (STS; Fisher Scientific; S-9300-10MG), or mega FasL (AdipoGen; AG-40B-0130-C010) were added to reach concentrations of 1 μM, or 50 ng/mL, respectively. Equal volume of DMSO or buffer was used for vehicle-treated samples. After incubation for either 4h in the case of the FasL and STS or 10h for etoposide, 100 μL of CellTiter-Glo® 2.0 Cell Viability Assay (Promega, G9242) was added to each well and the relative luminescence (RLU) measured. Percent cell viability was calculated relative to the DMSO treated Jurkat cells. Samples were analyzed in three biological replicates.

Lentivirus Packaging and Transduction

Plasmids of interest (**Table S9**) were normalized to a concentration of 20 ng/μL in 900 μL of AE Buffer and plated in 100 mm TC-treated cell culture dishes (Greiner). 108 μL of TransIT-LT1 (Mirus) was added to 4.5 mL of OptiMEM (Gibco). Next, pCMV-VSVg and pCMV-d8.91 were added to a 4 ng/μL concentration and the OptiMEM solution was plated into the cell culture dish containing normalized plasmid of interest and allowed to incubate at room temperature for 20 minutes. HEK 293T cells were then seeded into the dish at 18 x 10^6 cells per dish in 8.1 mL of DMEM (with FBS and PSG) and incubated at 37°C and 5% CO_2 for 24 hours.

After 24 hours, the media was exchanged for fresh DMEM and allowed to incubate at 37°C and 5% CO_2 for an additional 24 hours. After 48 hours, the supernatant was harvested and centrifuged 750 x G for 10 minutes. The virus was concentrated using Lenti-X Concentrator (Takara) according to manufacturer's suggestion and reconstituted

at a 100X in complete cell culture media. Aliquots of 200 µL were then stored at -80°C for later use.

Wells were pre-coated with 64 µg/mL RetroNectin (Takara) prior to addition of viral concentrate and then were incubated at 37 °C and 5% CO_2 for 6 hr. U2OS cells were then seeded at a target density of 0.5 - 2.5 x10^4 cells/cm^2 in DMEM (with 10% FBS, 1:100 Lentiboost (Sirion) and no antibiotics) and allowed to incubate at 37 °C and 5% CO_2 for 16 hr prior to a media change (DMEM with 10% FBS and no antibiotics). GFP-fluorescence was used to monitor transduction efficiency for 2-3 days after which 0.5 µg/mL puromycin was used to select for the transfected cells over the course of 7 days.

SDS-PAGE

To 8 mL of Jurkat cells at a density of 1.3 x 10^6 cells/mL in fresh complete RPMI 1640 media was added 2 mL of compound stocks prediluted in FBS-free RPMI media. For compounds assayed at 100 µM, 20 µL of 50 mM stock added to the 2 mL of FBS-free media, and for compounds assayed at 25 µM, 5 µL of 50 mM stock added to the 2 mL of FBS-free media. After compound addition, the cell suspensions were incubated for 1h at 37°C following which 4 µL of 25 mM stock of etoposide (ETO) [Cayman Chemical, 33419-42-0] or DMSO for a final concentration of 10 µM. Following the 1h compound incubation + 10h ETO incubation, the cells were harvested (1,400 x *g*, 3 min), washed 2x with cold PBS (1,400 x *g*, 3 min), and cell pellets were collected in 1.5 mL microcentrifuge tubes. Cell pellets were lysed using 3-[(3-Cholamidopropyl) dimethylammonio]-1-propanesulfonate (CHAPS) buffer [0.3% CHAPS in PBS; 100 µL; 30 minutes on ice] and centrifuged (1,400*g*, 10 min). The clarified supernatant was then transferred to a new

tube. The concentration of the cell lysates were determined using DC Protein Assay (BioRad) and the samples were diluted to 3.8 mg/mL. Samples were then treated with 4x SDS loading buffer and boiled at 95 ℃ for 5 min.

Western Blotting

Samples resolved by SDS-PAGE gel were either wet transferred to an activated PVDF membrane (35 Volts for 90 min at 4°C) or semi-dry (Bio-Rad Turbo Transfer System) to a nitrocellulose membrane. Membranes were then blocked in 5% milk in 1x Tris-Buffer Saline, 0.1% Tween® 20 (TBST) for 1h. After blocking membranes were then incubated with the indicated antibodies diluted in 5% milk in TBST. The primary antibodies and dilutions used are as follows: anti-PARP (Cell Signaling, 9532, 1:1,000), anti-CASP3 (Cell Signaling, 9662, 1:1,000), anti-CASP8 (cleaved form, Cell Signaling, 9746, 1:1,000), anti-CASP8 (pro-form, Cell Signaling, 4970, 1:1,000), anti-actin (Cell Signaling, 3700, 1:5,000), anti-CASP2 (ProteinTech, 10436-1-AP, 1:1,000), and anti-CASP9 (Cell Signaling, 9502, 1:1,000). Blots were incubated with primary antibody overnight at 4 °C with rocking, then washed (3x5 min TBS), and incubated with secondary antibody (IRDye 800CW or IRDye 647CW, 1:10,000) for 1h at ambient temperature. Blots were washed (3x5 min TBT) and visualized on a BioRad ChemiDoc Imaging System.

IncuCyte Live Cell Imaging

U2OS cells expressing GFP-53BP1 (kindly provided by Claudia Lukas (University of Copenhagen, Denmark[8]) were seeded in a 12-well plate at a density of 400,000 cells/well and allowed to adhere at 37°C and 5% CO_2. The following day, cells were treated with

either DMSO (10 nM) or Etoposide (10 nM) for 1 hr, after which compound (100 μM) was added and the plate placed into the imager 30 mins before the 0 hr time point read. An IncuCyte SX5 Live-Cell Imaging and Analysis System (Sartorius) was used for data acquisition. At each subsequent 1 hr time point, 9 images per well were taken using the 10X objection with phase contrast and green fluorescence. Analysis was performed using the IncuCyte 2023A software. In brief, the green integrated intensity per well was normalized to 0 hr time point per condition, each condition was prepared in 2-replicates within a plate. Images that were unfocused were removed from the analysis set prior to averaging intensity and calculating standard deviation for each well.

Immunofluorescence microscopy

Sterilized coverslips were placed in each well of a 24 well plate and coated with poly-d-lysine for 30 minutes at 37°C. Coverslips were washed with sterile water (3x 500 μL) and allowed to dry for 4 hours. U2OS cells were then seeded on coverslips at a density of 60,000 cells/well and allowed to adhere to coverslips overnight, then treated with the indicated compounds for the indicated time points. Media was aspirated and each well washed 1 time with 500 μL DPBS, followed by fixation with 3.7% formaldehyde in DPBS for 15 minutes at room temperature. Each well was then washed 2 times with 500 μL DPBS and permeabilized with 500 μL 0.1% TritonX in DPBS for 6 minutes at room temperature. Cells were then washed 3 times with 500 μL of DPBS and blocked in 1% FBS in DPBS for 30 minutes at room temperature. Cells were then incubated with 300 μL primary antibody in 0.1% FBS in PBS overnight at 4°C. Cells were then washed 2 times with 500 μL 0.1% Tween20 in PBS and 1 time with 500 μL PBS. Cells were then incubated

with 300 µL secondary antibody (AlexaFluor 549) for 1 hour at room temperature. Cells were then stained with 500 µL 1 µg/mL DAPI stain for 5 minutes. Cells were then washed 2 times with 500 µL PBS and mounted onto glass slides. Samples were left to set in the dark for 24 hours. Slides were then imaged on a Zeiss LSM880 confocal microscope at 63X oil objective. For each condition, 3 representative images were taken. Quantification of fluorescence intensity was done on ImageJ software using particle picker. Unpaired student's t-test was performed to generate p-value between control and treatment groups.

Statistics

Statistical significance was calculated with unpaired two-tailed Student's t-test using GraphPad Prism 9. Data are shown as mean ± SDEV. *P* values of <0.05 were considered significant.

4. Chemistry Methods

General Methods. All solution-phase reactions were performed in oven-dried glassware under an atmosphere of dry N_2 except where water was used as a solvent. Reactions were monitored by thin-layer chromatography, and plates were visualized by fluorescence quenching under UV light or by staining with iodine.

For compounds that required purifications, purifications were done via silica gel flash column chromatography with silica gel P60 (SiliCycle) as the stationary phase. Typical stationary phase column loadings are as follows: column height of 250 mm, column diameter of 100 mm, 100-200 mesh silica gel, Eluents used were hexanes/Ethyl acetate, Methanol/CH_2Cl_2, Petroleum ether/Ethyl acetate or hexanes/CH_2Cl_2.

Other reagents were purchased from Sigma-Aldrich (St. Louis, MO), Alfa Aesar (Ward Hill, MA), EMD Millipore (Billerica, MA), Fisher Scientific (Hampton, NH), Oakwood Chemical (West Columbia, SC), Combi-blocks (San Diego, CA) and Cayman Chemical (Ann Arbor, MI) and used without further purification. ^{1}H NMR and ^{13}C NMR spectra for characterization of new compounds and monitoring reactions were collected in $CDCl_3$, CD_3OD, CD_6CO or DMSO-d_6 (Cambridge Isotope Laboratories, Cambridge, MA) on a Bruker AV 400 MHz spectrometer or Bruker AV 500 MHz in the Department of Chemistry & Biochemistry at University of California, Los Angeles. All chemical shifts were reported in the standard notation of parts per million using the peak of residual proton signals of the deuterated solvent as an internal reference. Coupling constant units are in Hertz (Hz). Splitting patterns were indicated as follows: br, broad; s, singlet; d, doublet; t, triplet; q, quartet; m, multiplet; dd, doublet of doublets; dt, doublet of triplets. Low-resolution mass

spectroscopy was performed on an Agilent Technologies InfinityLab LC/MSD single quadrupole LC/MS (ESI source).

Purchased electrophilic fragments (P01-P06) were obtained from the following vendors: P01 (Fisher Scientific, AC334590050), **P02** (Fisher Scientific, P06105G), **P03** (Combi-blocks, QB-5712), (**P04** (Combi-blocks, ST-8644), **P05** (Combi-blocks, QC-2990) and **P06** (Combi-blocks, QF-4549).

General procedure 1:

To an oven-dried flask with a stir bar was charged the aldehyde (1 equiv.), anhydrous CH_2Cl_2 , the amine (1.1 equiv.), and acetic acid (1.2 equiv.). Sodium triacetoxyborohydride was added (1.5 equiv.) in three separate portions over the course of 1.5 h. The reaction was allowed to stir for 16 h. under nitrogen. The reaction was then quenched with water and extracted three times with DCM. Organic layers were washed with brine, dried over anhydrous Na_2SO_4, and concentrated *in vacuo* to give the crude product, which was purified by silica gel flash column chromatography to give the titled compound.

General procedure 2:

To a solution of the amine (1.1 equiv.) and the aldehyde (1.0 equiv.) in anhydrous MeOH (1.0 mL) was added AcOH (1.0 equiv.*)*. The reaction was stirred at 25 °C for 3 h. $NaBH_3CN$ (2.0 equiv.) was added at 0 °C. The reaction was stirred at 25 °C for another 1 h. LCMS showed the reaction was completed. The residue was poured into ice-water.

The aqueous phase was extracted three times with ethyl acetate.The combined organic phase was washed with brine, dried with anhydrous Na_2SO_4, filtered and concentrated in vacuo and purified by silica gel flash column chromatography to give the titled compound.

General procedure 3:

The amine (1 equiv.) was added to a round bottom flask with a stir bar and dissolved in DCM with stirring. Triethylamine (2 equiv.) was added, and the reaction was cooled to 0 ˚C. Chloroacetyl chloride (2 equiv.) was added dropwise to the flask, and the reaction was allowed to warm to room temperature as it stirred for 2 h. The reaction was washed with water, extracted with ethyl acetate, dried over Na_2SO_4 and purified by silica gel flash column chromatography to give the titled compound.

General procedure 4:

The amine (1 equiv.) was added to a round bottom flask with a stir bar and dissolved in DCM. Triethylamine (1 equiv.) was added, and the reaction was cooled to 0 ˚C. Acryloyl chloride (2 equiv.) was added dropwise to the flask, and the reaction was allowed to warm to room temperature as it stirred for 2 h. The reaction was washed with water, extracted with ethyl acetate, dried over Na_2SO_4 and purified silica gel flash column chromatography to give the titled compound.

General procedure 5:

To a round bottom flask equipped with a reflux condenser, the ester (1 equiv.) was dissolved in 3M HCl and allowed to reflux for 24 h. The reaction was cooled, extracted

three times with DCM. The combined organic layers were washed with brine, dried over Na_2SO_4, , filtered and concentrated *in vacuo* to give the titled compound.

General procedure 6:

Aryl iodide (1 equiv.), Cs_2CO_3 (2 equiv.) , $Pd(PPh_3)_4$ (0.05 equiv.), and CuI (0.05 equiv.) were added to an over-dried pressure tube and dissolved in THF, the reaction was heated to 80 °C and then propiolate (2 equiv.) was added dropwise and the mixture was allowed to stir for 24 h at 80 °C. The crude mixture was then diluted with DCM and filtered through a bed of celite. The mixture was then washed with water, extracted with DCM, dried with anhydrous sodium sulfate, filtered, and concentrated *in vacuo*. The product was then purified by silica gel flash column chromatography to give the titled compound.

General procedure 7:

To a round bottom flask was added the carboxylic acid (1 equiv.) and the alcohol (1 equiv.) which were then dissolved in CH_2Cl_2 and cooled in an ice bath. DCC (1.05 equiv.) dissolved in CH_2Cl_2 was added to the above solution in one portion under vigorous stirring and stirred for 20 min. DMAP (0.05 equiv.) was then added and the reaction mixture was allowed to warm to room temperature and stirred for 19 h. The precipitated N,N-dicyclohexylurea was filtered off and the solvent was concentrated. The crude material was then purified via silica gel flash column chromatography to give the titled compound.

Synthesis of *N*-(4-ethynylbenzyl)aniline (S01)

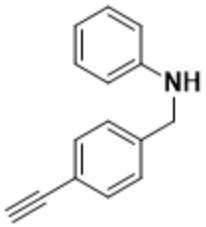

Prepared according to general procedure 1, using Aniline (737 **μ**l, 8.06 mmol) as the amine; 4-ethynylbenzaldehyde (0.937 g, 7.2 mmol) as the aldehyde . Product: off white solid (748 mg, 50%)

^{1}H NMR (400 MHz, $CDCl_3$) : δ 7.39 (d, J = 8.3 Hz, 2H), 7.36 – 7.28 (m, 3H), 7.18 (d, J = 8.4 Hz, 2H), 6.99 (dd, J = 7.9, 1.5 Hz, 2H), 6.43 (d, J = 18.8 Hz, 1H), 6.09 – 5.99 (m, 1H), 5.56 (d, J = 12.3 Hz, 1H), 4.96 (s, 2H), 3.05 (s, 1H). **^{13}C NMR (101 MHz, $CDCl_3$) :** δ 165.64, 141.61, 138.19, 132.23, 129.56, 128.71, 128.43, 128.29, 127.99, 121.14, 83.47, 52.93.

LC-MS (ESI, m/z): calcd for $C_{15}H_{14}N^+$ $[M+H]^+$ 208.1; found 208.1

Synthesis of 2-chloro-*N*-(4-ethynylbenzyl)-*N*-phenylacetamide (1)

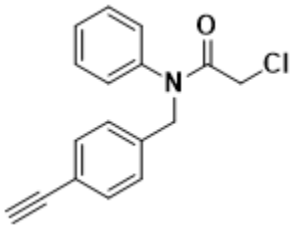

Prepared according to general procedure 3, using N-(4-ethynylbenzyl)aniline (500 mg, 1 eq, 2.4 mmol) as the amine source. Yield: 479.1 mg, 70%.

^{1}H NMR (400 MHz, $CDCl_3$) : δ 7.40 (d, J = 8.2 Hz, 2H), 7.35 (d, J = 1.5 Hz, 3H), 7.16 (d, J = 8.2 Hz, 2H), 7.01 (dd, J = 5.7, 3.8 Hz, 2H), 4.88 (s, 2H), 3.84 (s, 2H), 3.07 (s, 1H). **^{13}C NMR (101 MHz, $CDCl_3$)** : δ 166.32, 140.66, 137.37, 132.31, 129.99, 128.97, 128.21, 121.51, 83.32, 53.48, 41.95.

HRMS (ESI-TOF, m/z): calcd for $C_{17}H_{15}ClNO^+$ $[M+H]^+$ 284.0842; found 284.0836

Synthesis of 1-((4-ethynylphenyl)sulfonyl)piperazine (S02)

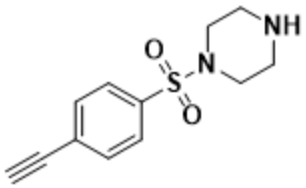

4-(4-Ethynylbenzenesulfonyl)-piperazine-1-carboxylic acid tert-butyl ester (100 mg, 0.285 mmol) was added to a round bottom flask with a stir bar, and dissolved in DCM (3 mL) with stirring and cooled to 0 ˚C. Trifluoroacetic acid (3 mL) was added to the reaction dropwise and the reaction was allowed to warm to room temperature as it stirred for 1h. The reaction was washed with water, extracted with ethyl acetate, dried over anhydrous Na_2SO_4 worked up to yield 59.4 mg of pure 1-((4-ethynylphenyl)sulfonyl)piperazine (59.4 mg, 99%).

LC-MS (ESI, m/z): calcd for $C_{12}H_{15}N_2O_2S^+$ $[M+H]^+$ 251.09; found 251.1

Synthesis of 2-chloro-1-(4-((4-ethynylphenyl)sulfonyl)piperazin-1-yl)ethan-1-on (2)

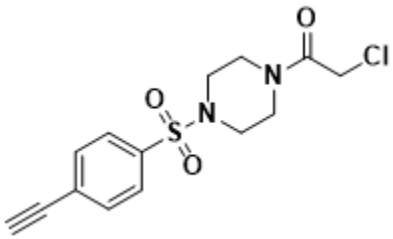

Prepared according to general procedure 3, using 4-(4-Ethynylbenzenesulfonyl)-piperazine-1-carboxylic acid tert-butyl ester (35 mg, 1 eq, 0.140 mmol) as the amine source. Product: off white solid (30.5 mg, 66%)

^{1}H NMR (400 MHz, $CDCl_3$) : δ 7.72 – 7.69 (m, 2H), 7.65 (d, J = 8.6 Hz, 2H), 4.00 (s, 2H), 3.67 (dt, J = 49.0, 4.9 Hz, 4H), 3.29 (s, 1H), 3.08 (dt, J = 24.8, 4.8 Hz, 4H). **^{13}C NMR (101 MHz, $CDCl_3$) :** δ 165.12, 135.33, 132.90, 127.59, 81.70, 81.32, 45.93, 45.75, 45.57, 41.43, 40.50.

HRMS (ESI-TOF, m/z): calcd for $C_{14}H_{16}ClN_2O_3S^+$ $[M+H]^+$ 327.0492; found 327.0489

Synthesis of *N*-(4-ethynylbenzyl)-*N*-phenylacrylamide (3)

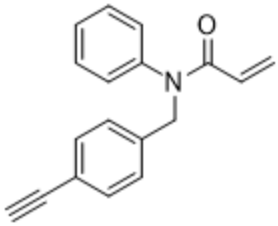

Prepared according to general procedure 4, using N-(4-ethynylbenzyl)aniline, **S01** (500 mg, 1 eq, 2.4 mmol) as the amine source. Yield: 116.2 mg , 50%.

^{1}H NMR (400 MHz, $CDCl_3$) : δ 7.39 (d, J = 8.3 Hz, 2H), 7.36 – 7.30 (m, 3H), 7.18 (d, J = 8.4 Hz, 2H), 7.03 – 6.95 (m, 2H), 6.44 (d, J = 2.0 Hz, 1H), 6.03 (dd, J = 16.8, 10.3 Hz, 1H), 5.56 (dd, J = 10.2, 2.0 Hz, 1H), 4.96 (s, 2H), 3.05 (s, 1H).**^{13}C NMR (101 MHz, $CDCl_3$)** : δ 165.64, 141.61, 138.19, 132.23, 129.56, 128.71, 128.43, 128.29, 128.24, 127.99, 121.14, 83.47, 52.93.

HRMS (ESI-TOF, m/z): calcd for $C_{17}H_{15}ClNO^+$ $[M+H]^+$ 262.1231; found 262.1227

Synthesis of 1-(4-((4-ethynylphenyl)sulfonyl)piperazin-1-yl)prop-2-en-1-one (4)

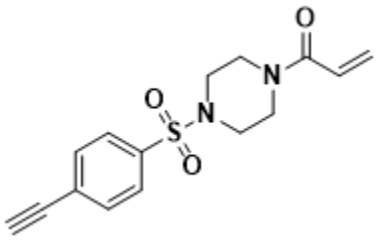

Prepared according to general procedure 4, using 1-((4-ethynylphenyl)sulfonyl)piperazine,**(S02)** (25.6 mg, 1 eq, 0.102 mmol) as the amine source. Product: off white solid (19 mg, 60%)

^{1}H NMR (400 MHz, $CDCl_3$) : δ 7.70 (d, J = 8.6 Hz, 2H), 7.64 (d, J = 8.6 Hz, 2H), 6.46 (dd, J = 16.8, 10.5 Hz, 1H), 6.25 (dd, J = 16.8, 1.7 Hz, 1H), 5.69 (s, 1H), 3.70 (d, J = 50.5 Hz, 4H), 3.28 (s, 1H), 3.05 (s, 4H). **^{13}C NMR (101 MHz, $CDCl_3$) :** δ 165.34, 135.29, 129.00, 127.62, 127.47, 126.72, 81.72, 81.24.

HRMS (ESI-TOF, m/z): calcd for $C_{15}H_{17}N_2O_3S^+$ $[M+H]^+$ 305.0960; found 305.0953

Synthesis of isopropyl 3-phenylpropiolate (5)

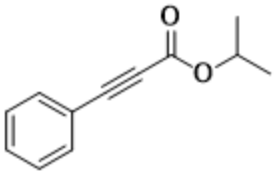

Prepared according to general procedure 7 using 3-phenylpropiolic acid (151 mg, 1.03 mmol) and propan-2-ol (61.9 mg, 1.03 mmol) as the carboxylic acid and alcohol respectively. Yield: 152 mg, 84%.

^{1}H NMR (400 MHz, $CDCl_3$) 1H NMR (400 MHz, Chloroform-d) δ 7.58 (dd, J = 8.3, 1.3 Hz, 2H), 7.47 – 7.41 (m, 1H), 7.40 – 7.33 (m, 2H), 5.16 (p, J = 6.3 Hz, 1H), 1.34 (d, J = 6.3 Hz, 6H).**^{13}C NMR (101 MHz, $CDCl_3$)** δ 153.67, 132.95, 130.52, 128.54, 119.75, 85.65, 81.07, 70.04, 21.74.

HRMS (ESI-TOF, m/z): calcd for $C_{12}H_{13}O_2^+$ $[M+H]^+$ 189.0915; found 189.0927

Synthesis of tert-butyl 3-(pyridin-4-yl)propiolate (6)

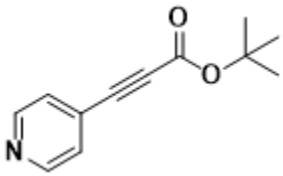

Prepared according to general procedure 6 using 4-iodopyridine (40 mg, 0.2mmol) and tert-butyl propiolate (50 mg, 0.4 mmol) as the aryliodide and alkyl propiolate respectively. Yield: 8 mg, 20%.

^{1}H NMR (400 MHz, $CDCl_3$) δ 8.09 (d, J = 8.4 Hz, 2H), 7.65 (d, J = 8.4 Hz, 2H), 1.55 (s, 9H). **^{13}C NMR (101 MHz, DMSO-d_6)** δ 151.11 , 150.04 , 132.67 , 76.37 , 75.71 , 27.25 .

HRMS (ESI-TOF, m/z): calcd for $C_{12}H_{14}NO_2^+$ $[M+H]^+$ 204.1025; found 204.1020

Synthesis of methyl 3-(quinolin-6-yl)propiolate (7)

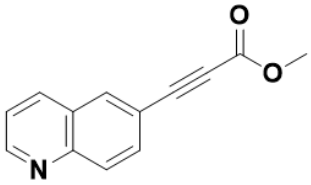

Prepared according to general procedure 6 using 6-iodoquinoline (40 mg, 0.2 mmol) and methyl propiolate (50 mg, 0.4 mmol) as the aryliodide and alkyl propiolate respectively. Yield: 4.2 mg (14%).

^{1}H NMR (400 MHz, $CDCl_3$) δ 8.98 (s, 1H), 8.17 (s, 1H), 8.13 (d, J = 5.9 Hz, 2H), 7.82 (d, J = 10.5 Hz, 1H), 7.53 – 7.45 (m, 1H), 3.87 (s, 3H). **^{13}C NMR (101 MHz, $CDCl_3$)** δ 154.25, 151.74, 136.57, 133.94, 132.25, 129.82, 122.19, 118.02, 85.58, 81.27, 52.97.

HRMS (ESI-TOF, m/z): calcd for $C_{13}H_{10}NO_2^+$ $[M+H]^+$ 212.0712; found 212.0718

Synthesis of methyl 3-(9H-carbazol-3-yl)propiolate (8)

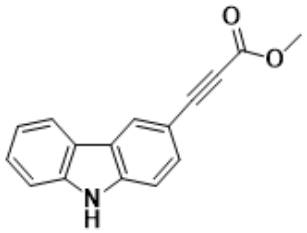

Prepared according to general procedure 6 using 3-iodo-9H-carbazole (60 mg, 0.2 mmol) and methyl propiolate (30 mg, 0.4 mmol) as the aryliodide and alkyl propiolate respectively. Yield: 9 mg, 18%

^{1}H NMR (400 MHz, $CDCl_3$) 8.40 (s, 1H), 8.03 (d, J = 7.8 Hz, 1H), 7.67 (dd, J = 8.6, 1.7 Hz, 1H), 7.45 (ddd, J = 8.3, 7.3, 1.2 Hz, 1H), 7.04 (d, J = 8.6 Hz, 1H), 6.91 (s, 1H), 6.13 (s, 1H), 3.75 (s, 3H).

^{13}C NMR (101 MHz, $CDCl_3$) δ 140.67, 139.89, 134.31, 134.16, 129.22, 127.44, 126.79, 125.98, 122.21, 120.73, 120.50, 111.83, 109.89, 82.96, 52.81.

HRMS (ESI-TOF, m/z): calcd for $C_{16}H_{12}O_2^+$ $[M+H]^+$ 250.0868; found 250.0879

Synthesis of methyl 4-((phenylamino)methyl)benzoate (S03)

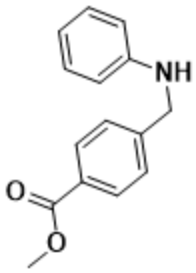

Prepared according to general procedure 1, using Aniline (1.25 mL, 13.6 mmol) as the amine; 4-methylformylbenzoate (2.00 g, 12.2 mmol) as the aldehyde . Product: brown oil. Yield: 2.79 g, 95%.

^{1}H NMR (400 MHz, $CDCl_3$) : δ 8.01 (d, J = 8.3 Hz, 2H), 7.44 (d, J = 8.4 Hz, 2H), 7.18 (dd, J = 8.5, 7.4 Hz, 2H), 6.74 (t, J = 7.3 Hz, 1H), 6.66 – 6.60 (m, 2H), 4.41 (s, 2H), 3.91 (s, 3H). **^{13}C NMR (400 MHz, $CDCl_3$) :** δ 166.97, 147.76, 144.98, 129.98, 129.34, 129.13, 127.18, 117.91, 112.96, 52.10, 48.04.

LC-MS (ESI, m/z): calcd for $C_{15}H_{16}NO_2^+$ $[M+H]^+$ 242.1; found 242.1

Synthesis of methyl 4-((N-phenylacrylamido)methyl)benzoate (9)

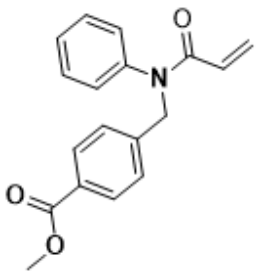

Prepared according to general procedure 4 – under nitrogen – using 4-((phenylamino)methyl)benzoate (1.47g, 6.10 mmol) as the amine source. Product: yellow oil. Yield: 1.69 g, 94%.

^{1}H NMR (400 MHz, $CDCl_3$) : d 7.94 (d, *J* = 8.3 Hz, 2H), 7.26-7.35 (m, 5H), 6.99 (dd, *J* = 7.9, 2.2 Hz , 2H), 6.44 (*J* = 16.7, 2.0 Hz), 6.04 (dd, *J* = 16.8, 6.5 Hz, 1H), 5.5 (dd, *J* = 10.3, 2 Hz, 1H), 5.0 (s, 2H), 3.9 (s, 3H). **^{13}C NMR (400 MHz, $CDCl_3$) :** δ 169.79, 166.85, 141.57, 140.53, 130.03, 129.85, 129.57, 129.02, 128.88, 128.09, 52.18, 41.81.

HRMS (ESI-TOF, m/z): calcd for $C_{18}H_{18}NO_3^+$ $[M+H]^+$ 296.1287; found 296.1279

Synthesis of 5-chloro-N-(pyridin-2-ylmethyl)pyrimidin-2-amine (S04)

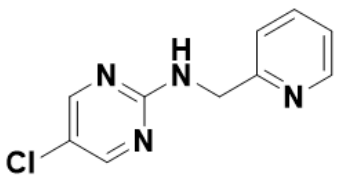

Prepared according to general procedure 2, using 5-chloropyrimidin-2-amine (266.1 mg, 1.1 eq, 2.05 mmol) as the amine; picolinaldehyde (200 mg,1 eq, 1.87 mmol) as the aldehyde . Product: off white (356.1 mg, 86.4%)

^{1}H NMR (400 MHz, $CDCl_3$) : δ 8.58 (s, 1H), 8.23 (s, 2H), 7.77 (s, 1H), 7.42 (d, J = 7.9 Hz, 1H), 7.33 – 7.27 (m, 1H), 6.45 (s, 1H), 4.78 (s, 2H). **^{13}C NMR (101 MHz, $CDCl_3$) :** δ 160.11, 156.69, 156.13, 147.46, 138.00, 122.35, 119.35, 77.16, 45.88.

LC-MS (ESI, m/z): calcd for $C_{10}H_{10}ClN_4^+$ $[M+H]^+$ 221.1; found 221.1

Synthesis of N-(5-chloropyrimidin-2-yl)-N-(pyridin-2-ylmethyl)acrylamide (10)

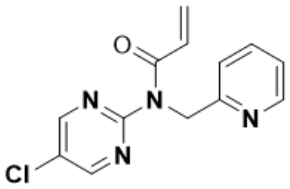

Prepared according to general procedure 4, using 5-chloro-N-(pyridin-2-ylmethyl)pyrimidin-2-amine, **S04** (200 mg, 1 eq, 0.91 mmol) as the amine source. Product: pale yellowish oil (152 mg, 61%)

^{1}H NMR (400 MHz, $CDCl_3$) : δ 8.57 (s, 2H), 8.52 (s, 1H), 7.63 (d, J = 17.2 Hz, 1H), 7.28 (s, 2H), 7.14 (s, 1H), 6.80 (dd, J = 16.8, 10.3 Hz, 1H), 6.52 – 6.44 (m, 1H), 5.75 (dd, J = 10.3, 1.7 Hz, 1H), 5.51 (s, 2H). **^{13}C NMR (101 MHz, $CDCl_3$) :** δ 167.55, 157.11, 156.38, 148.91, 136.99, 130.48, 128.05, 126.39, 122.12, 121.31, 51.42.

HRMS (ESI-TOF, m/z): calcd for $C_{13}H_{12}ClN_4O^+$ $[M+H]^+$ 275.0670; found 275.0698

Synthesis of tert-butyl 5-formyl-1H-benzo[d]imidazole-1-carboxylate (S05)

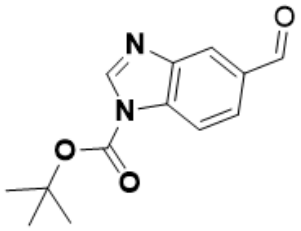

To a mixture of 3H-benzimidazole-5-carbaldehyde (500.00 mg, 3.42 mmol, 1.00 *eq*) and Et_3N (692.37 mg, 6.84 mmol, 948.45 uL, 2.00 *eq*) in DCM (5.00 mL) was added Boc_2O (1.49 g, 6.84 mmol, 1.57 mL, 2.00 *eq*) in one portion at 25 °C .The mixture was stirred at 25 °C for 16h. TLC (PE:EA=5:1,Rf =0.43) and LCMS showed the reaction was completed. The mixture was concentrated in a vacuum. The reaction mixture was filtered and the filterate was concentrated. The residue was purified by silica gel flash column chromatography to yield the titled compound (800 mg, 95%)

^{1}H NMR (400 MHz, $CDCl_3$) : δ 10.11 (s, 1H), 8.53 (s, 1H), 8.31 – 8.10 (m, 1H), 7.91 (dd, J = 2.2, 1.0 Hz, 1H), 1.73 (s, 9H). **^{13}C NMR (101 MHz, $CDCl_3$) :** δ 191.65, 147.50, 145.02, 143.79, 133.75, 133.30, 125.95, 125.45, 123.71, 121.24, 117.15, 115.06, 86.70, 28.06.

LC-MS (ESI, m/z): calcd for $C_{13}H_{15}N_2O_3^+$ $[M+H]^+$ 247.1; found 247.1

Synthesis of tert-butyl 5-((phenylamino)methyl)-1H-benzo[d]imidazole-1-carboxylate (S06)

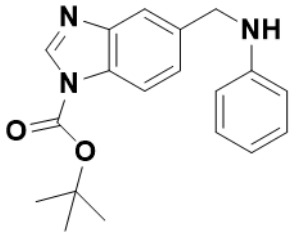

Prepared according to general procedure 2, using aniline (74.88 mg, 804.03 umol, 73.41 uL) as the amine; tert-butyl 6-

formylbenzimidazole-1-carboxylate, **S05** (180.00 mg, 730.93 umol) as the aldehyde . Product: yellow oil (240 mg, 91.4%)

^{1}H NMR (400 MHz, $CDCl_3$) : δ 8.40 (s, 1H), 8.03 (s, 1H), 7.73 (d, J = 8.2 Hz, 1H), 7.36 (dd, J = 8.3, 1.6 Hz, 1H), 4.82 (s, 2H), 1.69 (s, 9H). **^{13}C NMR (101 MHz, $CDCl_3$) :** δ 147.99, 143.55, 142.28, 138.54, 131.59, 123.53, 123.53, 120.55, 112.99, 85.75, 53.45, 28.07.

LC-MS (ESI, m/z): calcd for $C_{19}H_{22}N_3O_2^+$ $[M+H]^+$ 324.1; found 324.1

Synthesis of tert-butyl 5-((N-phenylacrylamido)methyl)-1H-benzo[d]imidazole-1-carboxylate (S07)

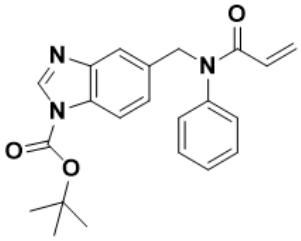

Prepared according to general procedure 4, using tert-butyl 5-((phenylamino)methyl)-1H-benzo[d]imidazole-1-carboxylate, **S06** (200 mg, 0.62 mmol) as the amine source. Product: yellow oil; and *used as is without further characterisation* (140 mg, 60%)

LC-MS (ESI, m/z): calcd for $C_{22}H_{24}N_3O_3^+$ $[M+H]^+$ 378.2; found 378.2

Synthesis of N-((1H-benzo[d]imidazol-5-yl)methyl)-N-phenylacrylamide (11)

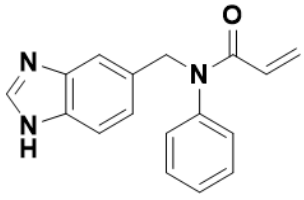

TFA (5mL.) was added to a solution of tert-butyl 5-((N-phenylacrylamido)methyl)-1H-benzo[d]imidazole-1-carboxylate, **S07** (100 mg) in DCM (20 mL) at 18° C. The resulting mixture was

stirred at 18 °C for 3 h. Upon completion, the reaction mixture was concentrated in vacuo to yield the crude. To this crude was added 10 mL of saturated sodium bicarbonate solution stirred for 15 mins, next extracted into DCM and purified by purified by silica gel flash column chromatography to yield the titled compound (57mg, 73.5%).

^{1}H NMR (400 MHz, $CDCl_3$) : δ 7.99 (s, 1H), 7.52 (d, J = 8.7 Hz, 2H), 7.31 (s, 3H), 7.12 (s, 1H), 6.99 (s, 2H), 6.41 (d, J = 18.8 Hz, 1H), 6.13 – 5.99 (m, 1H), 5.55 (d, J = 10.3 Hz, 1H), 5.09 (s, 2H). **^{13}C NMR (101 MHz, $CDCl_3$) :** δ 166.27, 142.10, 141.63, 132.47, 129.96, 129.21, 128.77, 128.43, 124.17, 116.43, 115.58, 77.16, 54.07.

HRMS (ESI-TOF, m/z): calcd for $C_{17}H_{16}N_3O^+$ $[M+H]^+$ 278.1248; found 278.1255

Synthesis of tert-butyl 6-((naphthalen-2-ylamino)methyl)-1H-benzo[d]imidazole-1-carboxylate (S08)

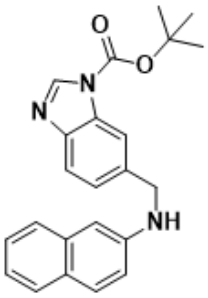

Prepared according to general procedure 2, using naphthalen-2-amine (200 mg, 1.88 mmol) as the amine; 5-formyl-1H-benzo[d]imidazole-1-carboxylate, **S05** (304.5 mg, 2.07 mmol) as the aldehyde . Product: off-white solid (268.5 mg, 88.5%)

^{1}H NMR (400 MHz, $CDCl_3$) : δ 8.42 (d, J = 8.2 Hz, 1H), 8.11 – 7.91 (m, 1H), 7.84 – 7.74 (m, 1H), 7.65 (dd, J = 11.7, 8.5 Hz, 2H), 7.57 (dd, J = 8.0, 2.7 Hz, 1H), 7.45 (dd, J = 16.1, 7.5 Hz, 1H), 7.39 – 7.30 (m, 1H), 7.19 (ddt, J = 8.1, 6.8, 1.2 Hz, 1H), 6.95 (dd, J = 8.8, 2.3 Hz, 1H), 6.85 (s, 1H), 4.58 (d, J = 6.8 Hz, 2H), 1.66 (d, J = 27.3 Hz, 9H). **^{13}C NMR (101 MHz, $CDCl_3$) :** δ 148.03, 144.50, 142.21, 135.12, 129.02, 127.64,

126.05, 126.02, 124.91, 123.96, 122.17, 120.70, 119.53, 117.90, 114.52, 113.36, 85.73, 48.69, 28.02.

LC-MS (ESI, m/z): calcd for $C_{23}H_{24}N_3O_2^+$ $[M+H]^+$ 374.1; found 374.1

Synthesis of tert-butyl 6-((N-(naphthalen-2-yl)acrylamido)methyl)-1H-benzo[d]imidazole-1-carboxylate (S09)

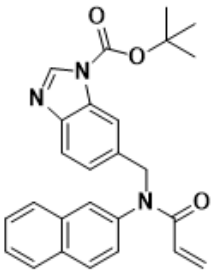

Prepared according to general procedure 4, using tert-butyl 6-((naphthalen-2-ylamino)methyl)-1H-benzo[d]imidazole-1-carboxylate, **S08** (200 mg, 0.54 mmol) as the amine source. Product: yellow oil; and *used as is without further characterisation* (180 mg, 78.6%)

LC-MS (ESI, m/z): calcd for $C_{26}H_{26}N_3O_3^+$ $[M+H]^+$ $C_{26}H_{26}N_3O_3^+$; found 428.1

Synthesis of N-((1H-benzo[d]imidazol-6-yl)methyl)-N-(naphthalen-2-yl)acrylamide (12)

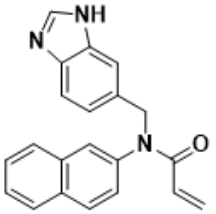

Prepared according to general procedure 2, using tert-butyl 6-((N-(naphthalen-2-yl)acrylamido)methyl)-1H-benzo[d]imidazole- 1-carboxylate, **S09** (200 mg, 1 eq, 0.84 mmol) as the amine source. Product: off-white oil (24 mg, 17.4%)

^{1}H NMR (400 MHz, $CDCl_3$) : δ 8.01 (s, 1H), 7.86 – 7.76 (m, 2H), 7.71 (d, J = 9.3 Hz, 1H), 7.64 – 7.45 (m, 5H), 7.19 – 7.09 (m, 2H), 6.44 (d, J = 18.7 Hz, 1H), 6.08 (dd, J = 16.7, 10.3 Hz, 1H), 5.52 (d, J = 12.1 Hz, 1H), 5.18 (s, 2H).

^{13}C NMR (400 MHz, $CDCl_3$) : δ 165.93, 139.07, 133.41, 132.43, 132.32, 129.62, 128.86, 128.13, 127.94, 126.87, 126.11, 123.98, 53.67.

HRMS (ESI-TOF, m/z): calcd for $C_{21}H_{18}N_3O^+$ $[M+H]^+$ 328.1450; found 328.1441

Synthesis of benzyl 3-phenylpropiolate (13)

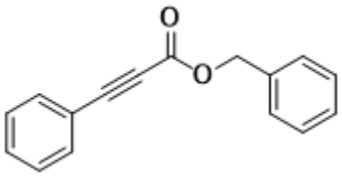

Prepared according to general procedure 7 using 3-phenylpropiolic acid (150 mg, 1.03 mmol) and benzyl alcohol (111 mg, 1.03 mmol) as the carboxylic acid and alcohol respectively. Yield: 208 mg, 86%.

^{1}H NMR (400 MHz, $CDCl_3$) δ 7.58 (dd, J = 8.3, 1.4 Hz, 2H), 7.48 – 7.33 (m, 8H), 5.27 (s, 2H).

^{13}C NMR (101 MHz, $CDCl_3$) δ 153.91, 134.93, 133.03, 130.70, 128.58, 119.56, 86.75, 80.51, 67.73.

HRMS (ESI-TOF, m/z): calcd for $C_{16}H_{13}O_2^+$ $[M+H]^+$ 237.0916; found 237.0957

Synthesis of phenyl 3-phenylpropiolate (14)

Prepared according to general procedure 7 using 3-phenylpropiolic acid (151 mg, 1.03 mmol) and phenol (96.9 mg, 1.03 mmol) as the carboxylic acid and alcohol respectively. Yield:134 mg, 83%

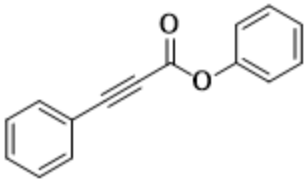

^{1}H NMR (400 MHz, $CDCl_3$) δ 7.64, 7.62, 7.51, 7.49, 7.47, 7.44, 7.42, 7.41, 7.40, 7.39, 7.30, 7.28, 7.26, 7.21, 7.21, 7.19, 7.18. **^{13}C NMR (101 MHz, $CDCl_3$)** δ 152.36, 150.17, 133.20, 131.05, 129.60, 128.68, 126.42, 121.48, 119.28..

HRMS (ESI-TOF, m/z): calcd for $C_{15}H_{11}O_2^+$ $[M+H]^+$ 223.0759; found 223.0767

Synthesis of tert-butyl 3-phenylpropiolate (15)

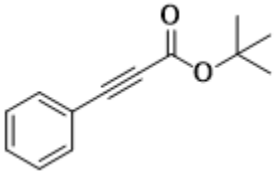

Prepared according to general procedure 6 using 3-phenylpropiolic acid (40 mg, 0.2 mmol) and tert-butyl alcohol (50 mg, 0.4 mmol) as the aryliodide and alkyl propiolate respectively. Yield: 8 mg, 20%

^{1}H NMR (400 MHz, $CDCl_3$) δ 7.60 – 7.54 (m, 2H), 7.45 – 7.39 (m, 1H), 7.39 – 7.32 (m, 2H), 1.54 (s, 9H). **^{13}C NMR (101 MHz, $CDCl_3$)** δ 153.15, 132.86, 130.30, 128.48, 119.99, 83.79, 83.52, 82.03, 28.08.

HRMS (ESI-TOF, m/z): calcd for $C_{13}H_{15}O_2Na^+$ $[M+Na]^+$ 225.0892; found 225.0893

Synthesis of methyl 3-(pyridin-4-yl)propiolate (16)

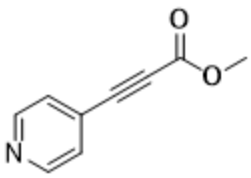

Prepared according to general procedure 6 using 4-iodopyridine (40 mg, 0.2 mmol) and methyl propiolate (50 mg, 0.4 mmol) as the aryliodide and alkyl propiolate respectively. Yield: 4.2 mg, 14%.

^{1}H NMR (400 MHz, $CDCl_3$) δ 8.71 – 8.63 (m, 2H), 7.46 – 7.39 (m, 2H), 3.86 (s, 3H).**^{13}C NMR (101 MHz, $CDCl_3$)** δ 153.65, 149.98, 127.93, 126.13, 83.53, 82.48, 53.15.

HRMS (ESI-TOF, m/z): calcd for $C_9H_8NO_2^+$ $[M+H]^+$ 161.0470; found 161.0471

5. NMR Spectra

^{1}H NMR of ***N*-(4-ethynylbenzyl)aniline (S01)** in $CDCl_3$

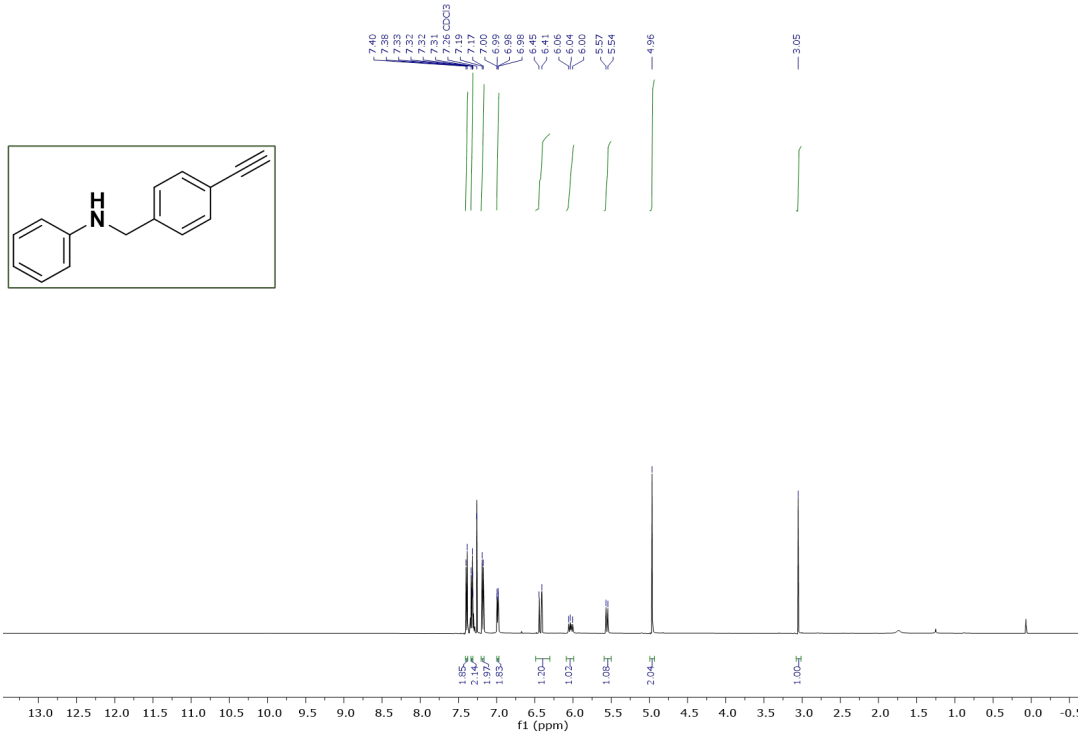

^{13}C NMR of ***N*-(4-ethynylbenzyl)aniline (S01)** in $CDCl_3$

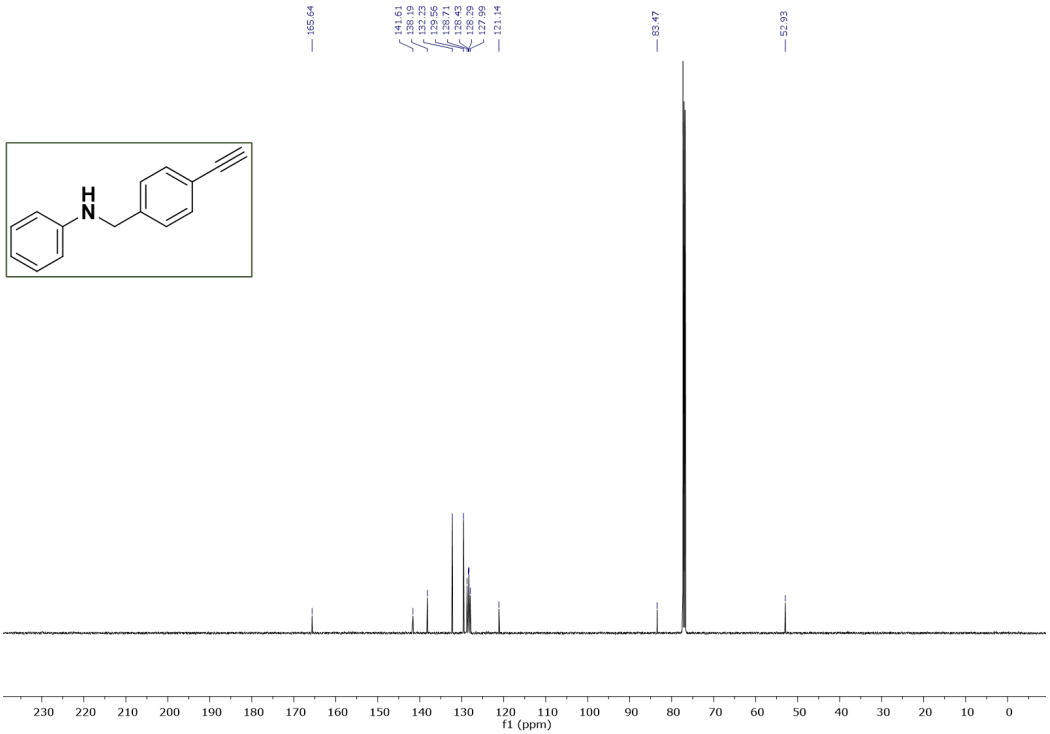

^{1}H NMR **of 2-chloro-*N*-(4-ethynylbenzyl)-*N*-phenylacetamide (1)** in $CDCl_3$

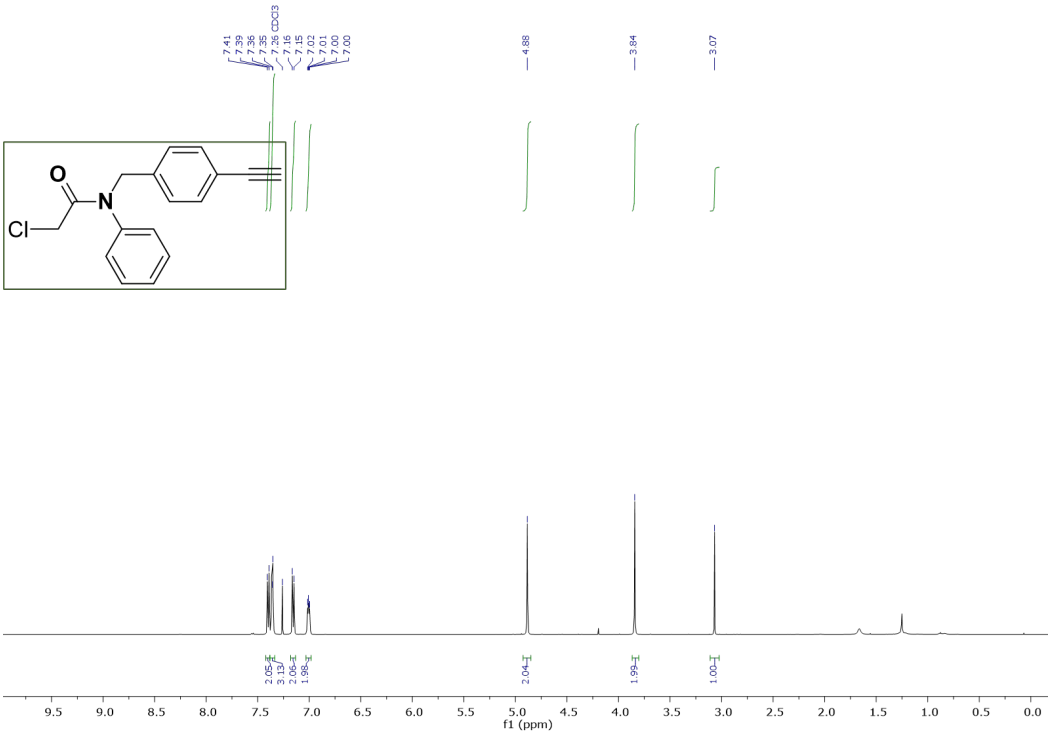

^{13}C NMR **of 2-chloro-N-(4-ethynylbenzyl)-N-phenylacrylamide (1)** in $CDCl_3$

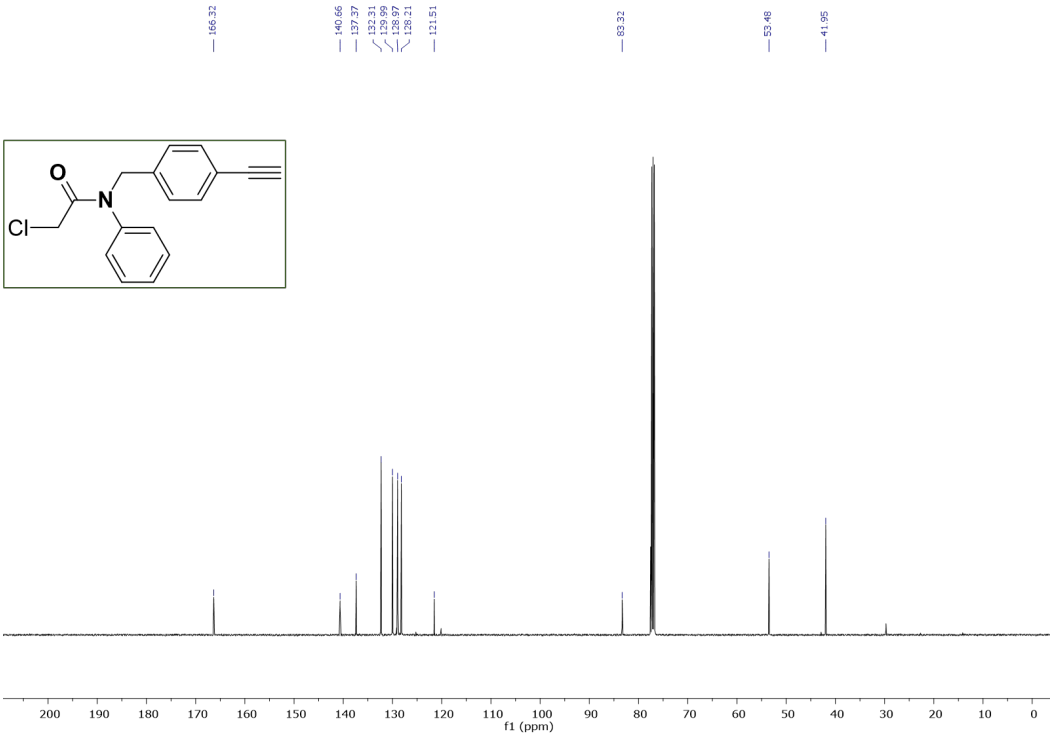

.^{1}H NMR **of 2-chloro-1-(4-((4-ethynylphenyl)sulfonyl)piperazin-1-yl)ethan-1-on (2)** in $CDCl_3$

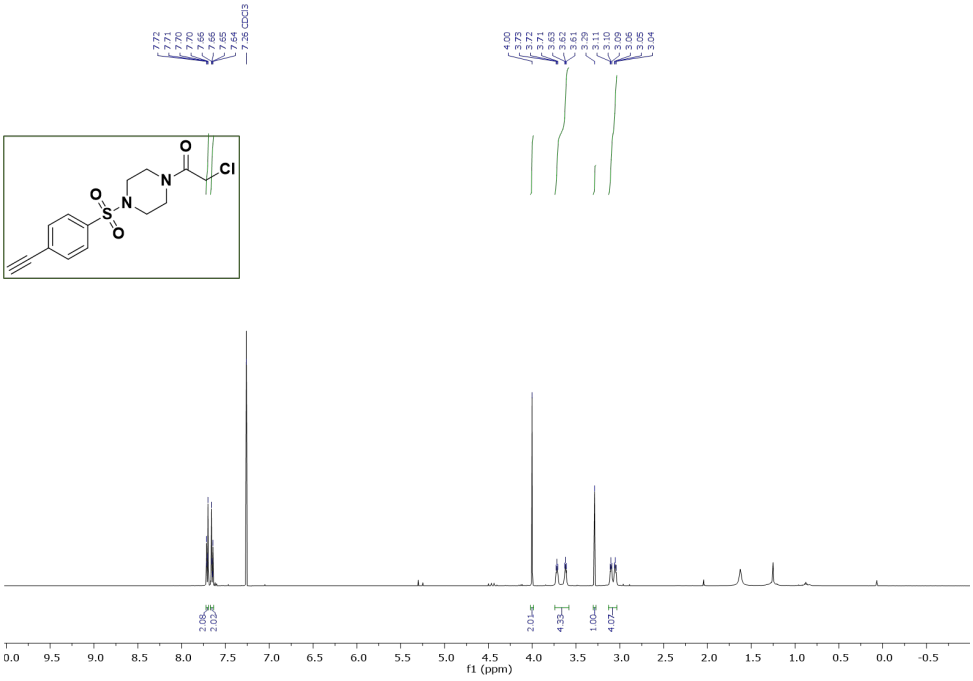

^{13}C NMR **of 2-chloro-1-(4-((4-ethynylphenyl)sulfonyl)piperazin-1-yl)ethan-1-on (2)** in $CDCl_3$

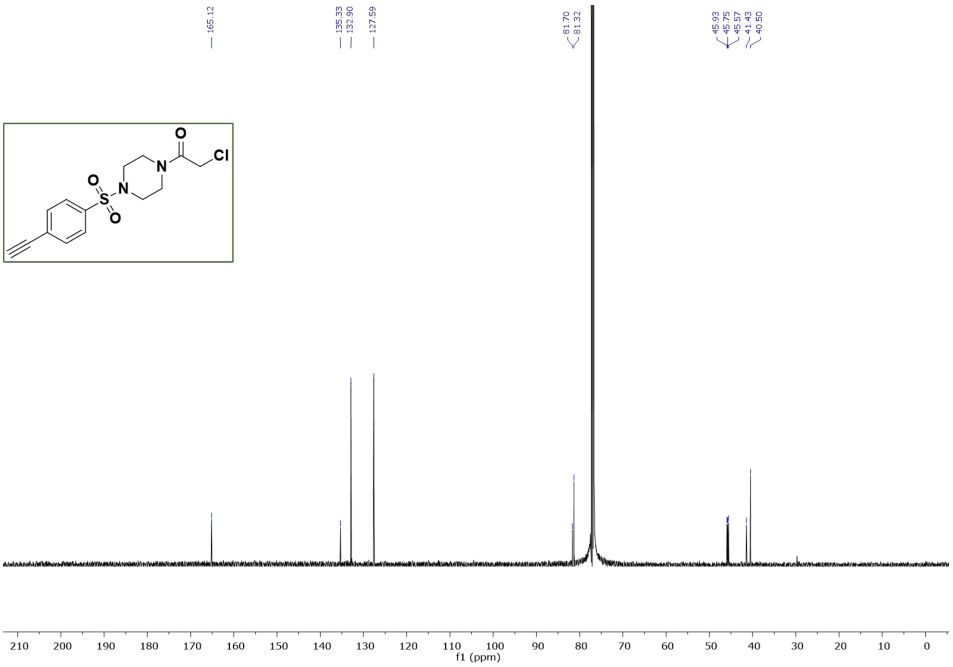

^{1}H NMR **of N-(4-ethynylbenzyl)-N-phenylacrylamide (3)** in $CDCl_3$

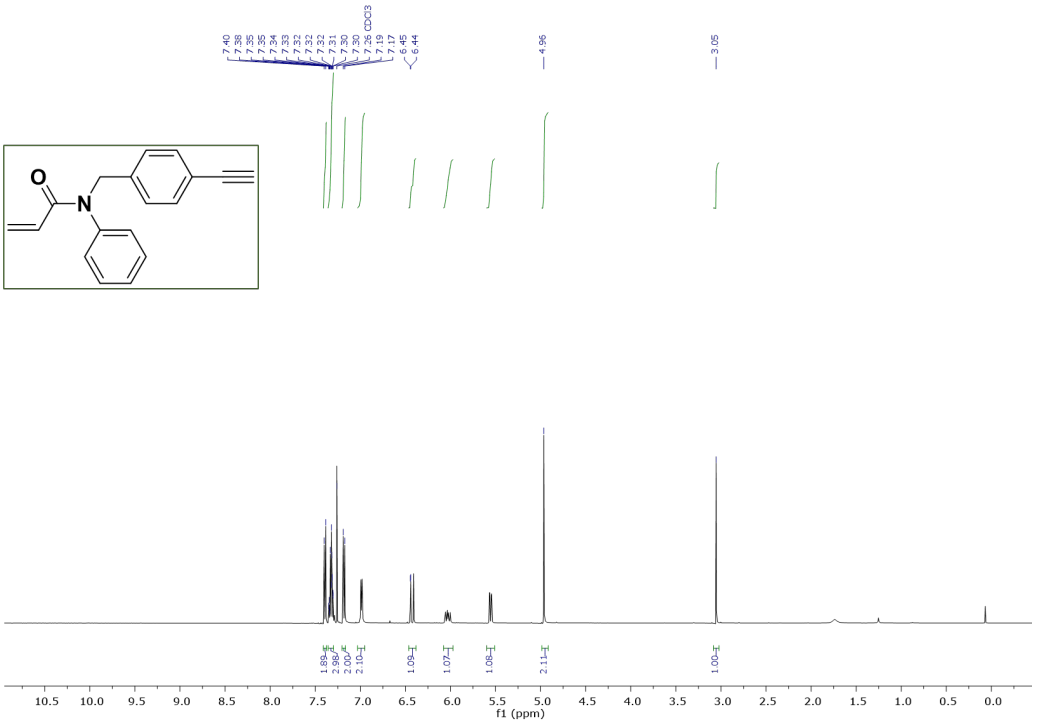

^{13}C NMR **of N2-chloro-N-(4-ethynylbenzyl)-N-phenylacetamide (3)** in $CDCl_3$

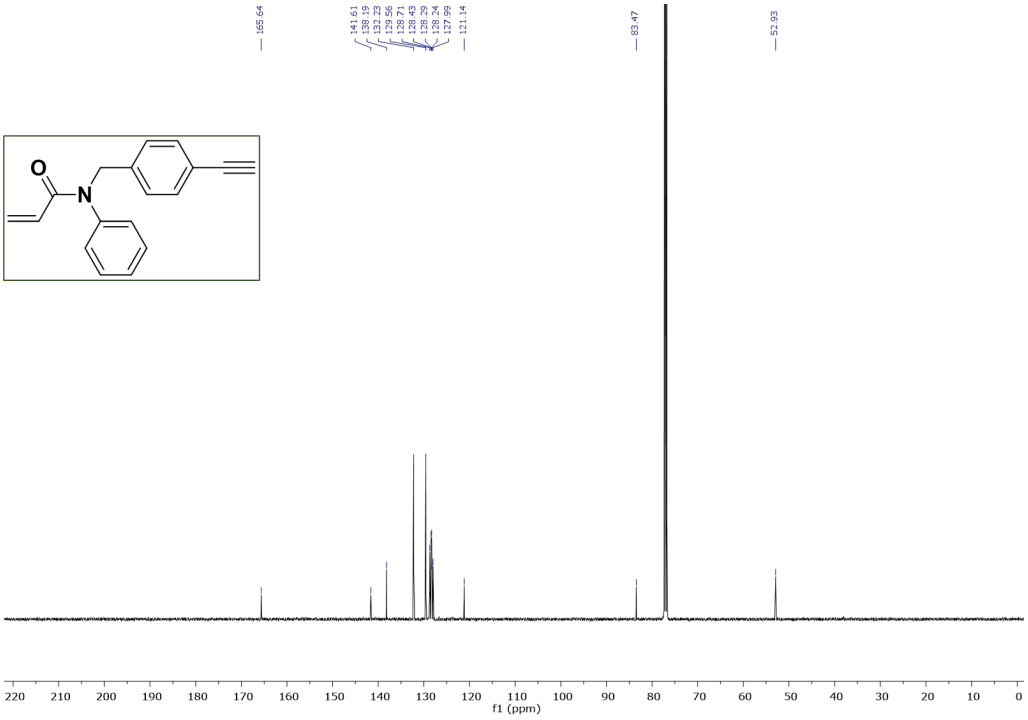

^{1}H NMR **of 1-(4-((4-ethynylphenyl)sulfonyl)piperazin-1-yl)prop-2-en-1-one (4)** in $CDCl_3$

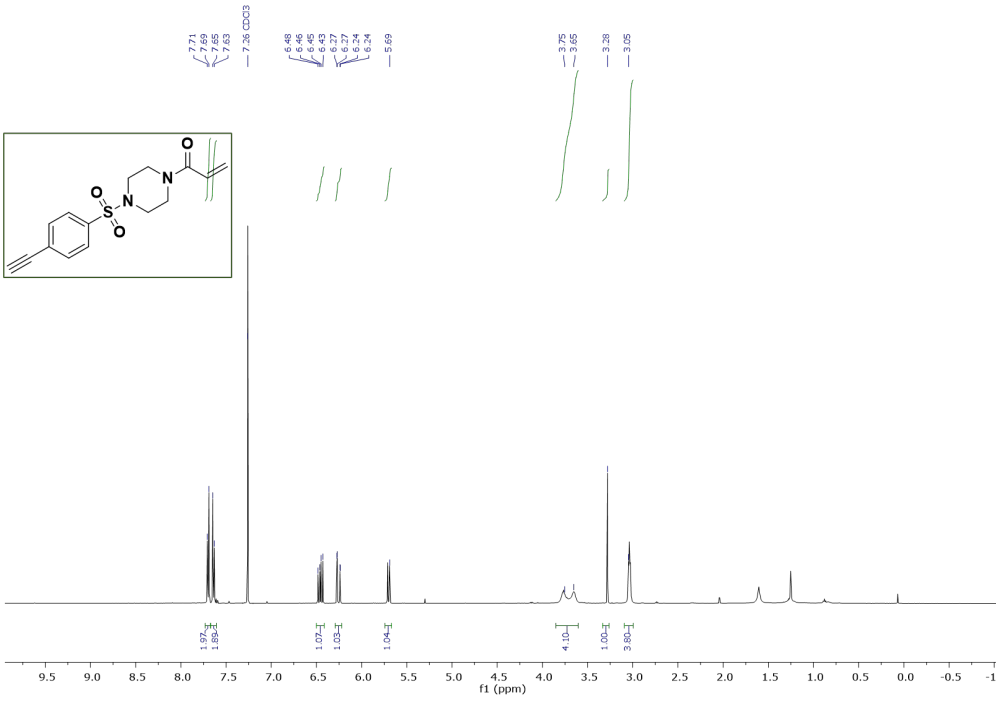

^{13}C NMR **of 1-(4-((4-ethynylphenyl)sulfonyl)piperazin-1-yl)prop-2-en-1-one (4)** in $CDCl_3$

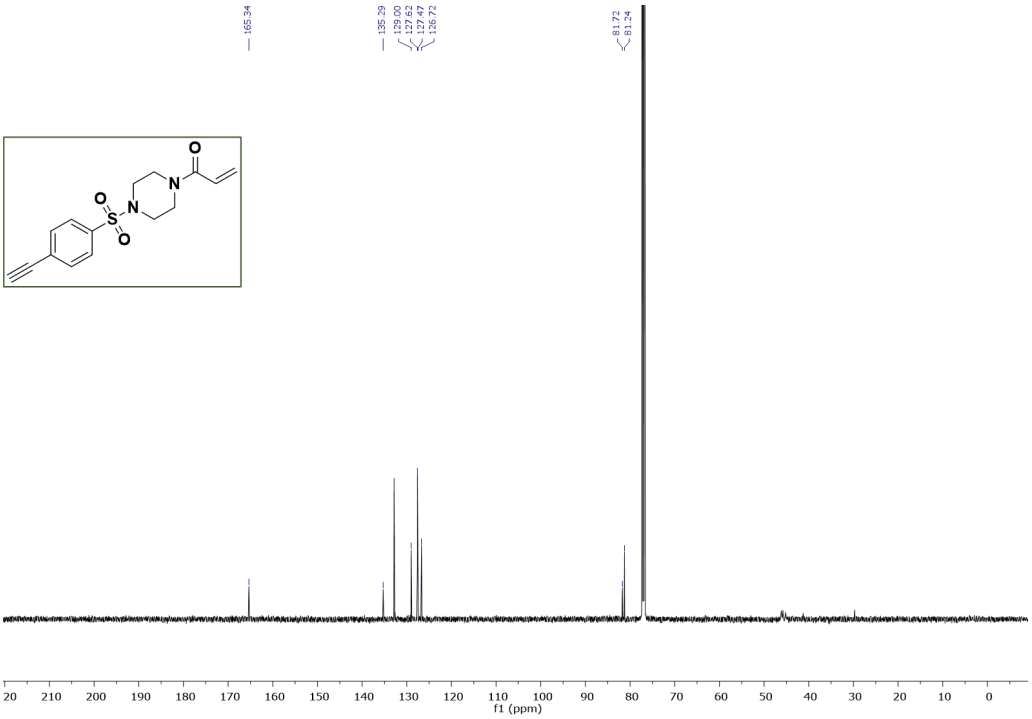

^{1}H NMR **of isopropyl 3-phenylpropiolate (5)** in $CDCl_3$

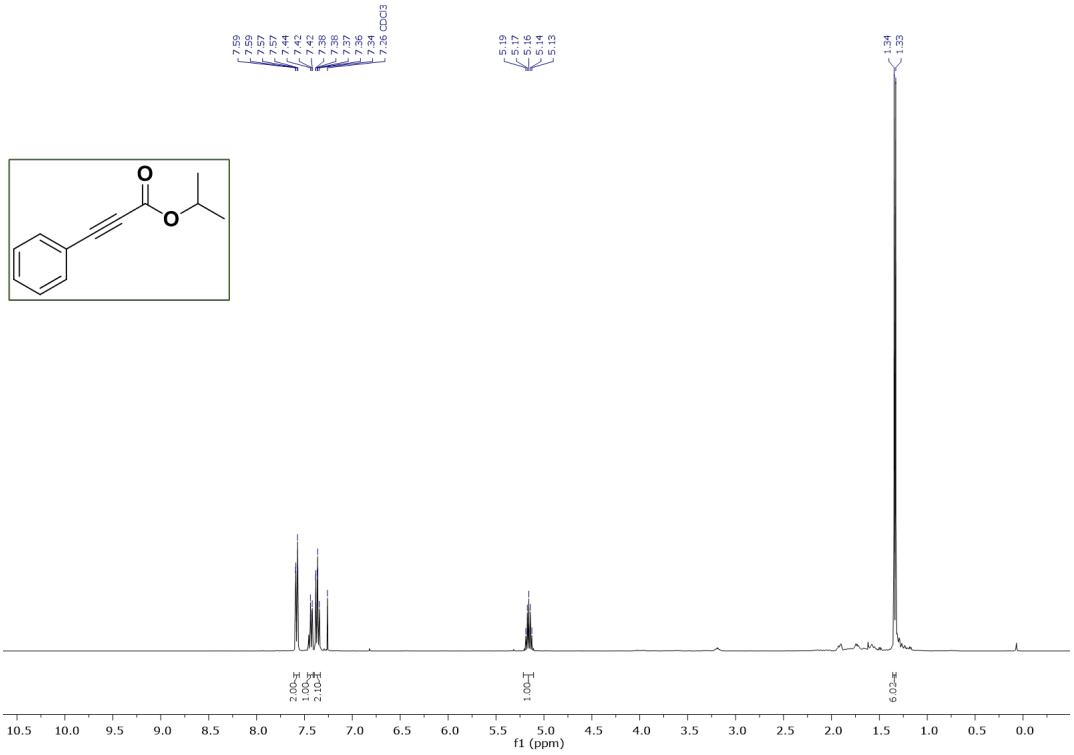

^{13}C NMR **of isopropyl 3-phenylpropiolate (5)** in $CDCl_3$

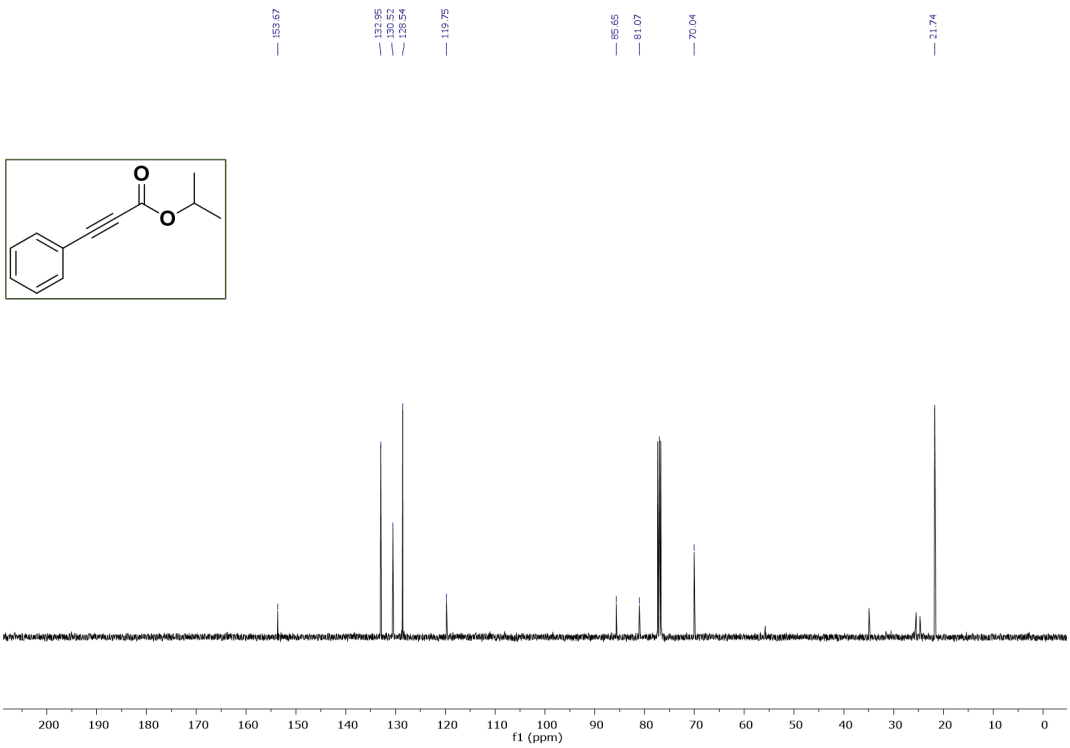

^{1}H NMR of **tert-butyl 3-(pyridin-4-yl)propiolate (6)** in $CDCl_3$

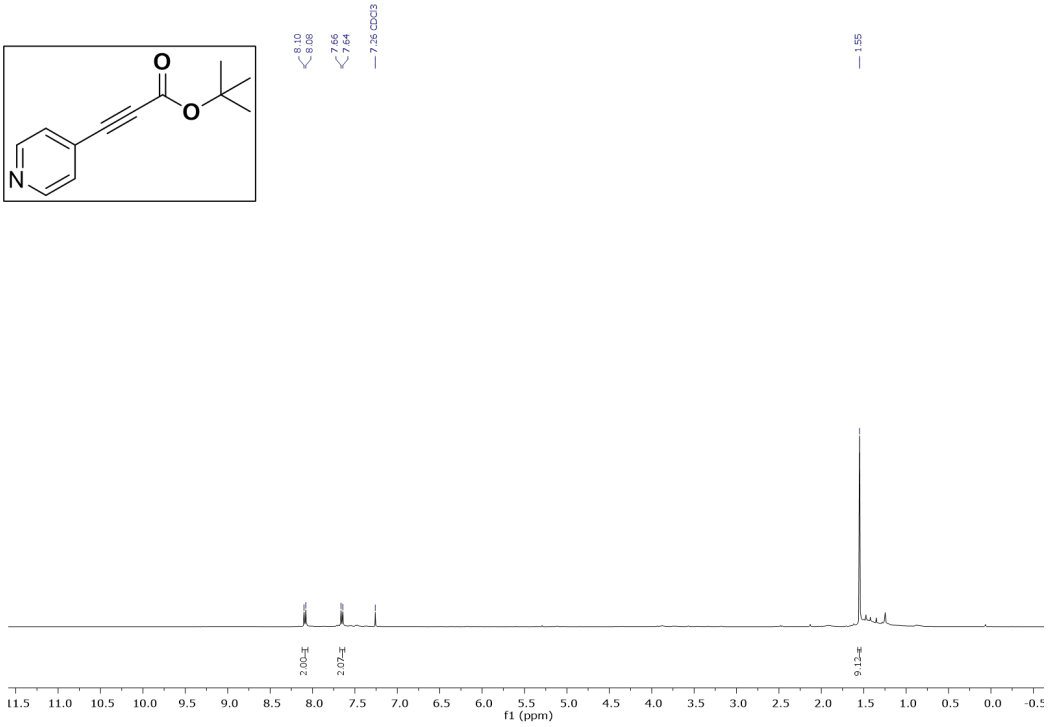

^{13}C NMR of **tert-butyl 3-(pyridin-4-yl)propiolate (6)** in DMSO-d_6

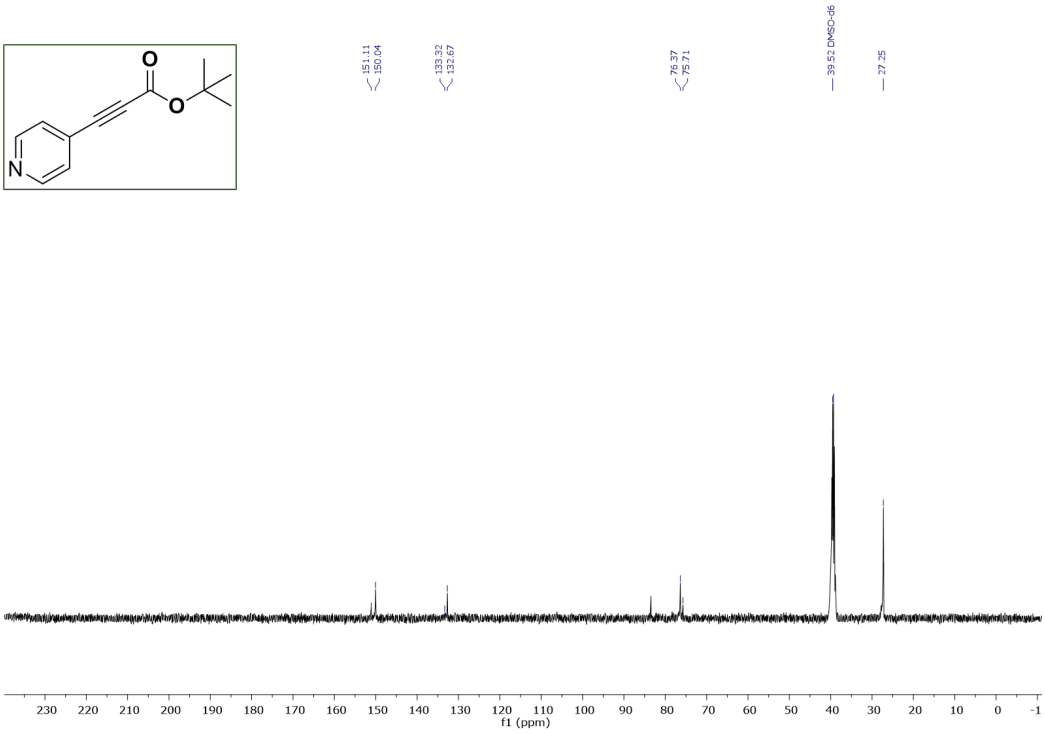

^{1}H NMR of **Methyl 3-(quinolin-6-yl)propiolate (7)** in $CDCl_3$

^{13}C NMR of **Methyl 3-(quinolin-6-yl)propiolate (7)** in $CDCl_3$

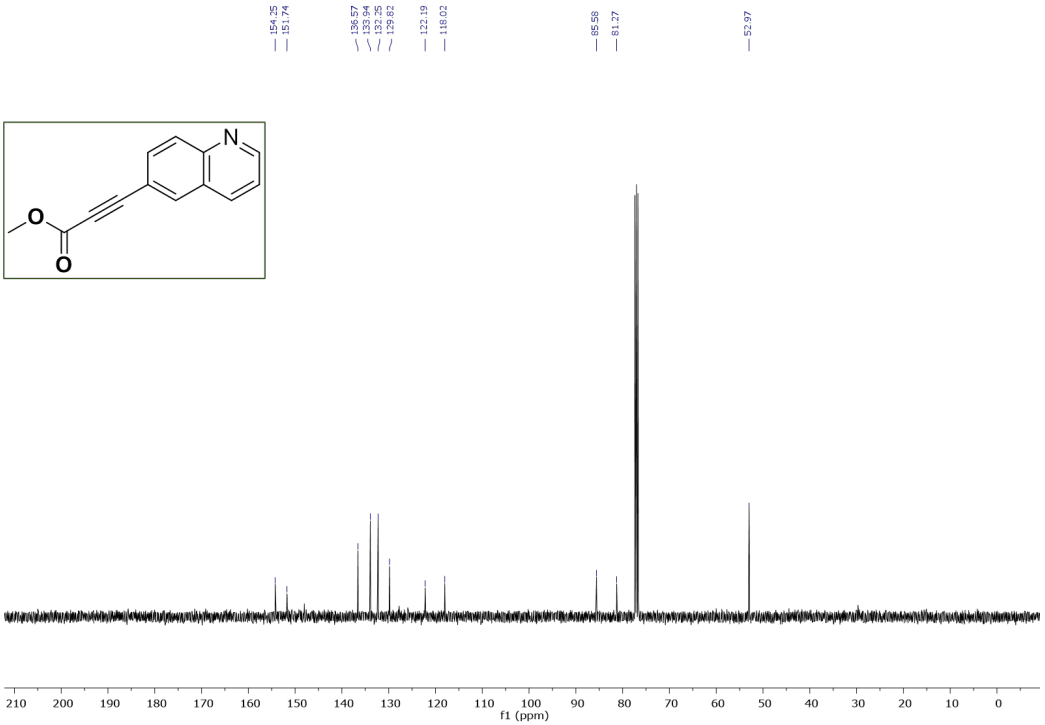

^{1}H NMR of **methyl 3-(9H-carbazol-3-yl)propiolate (8)** in $CDCl_3$

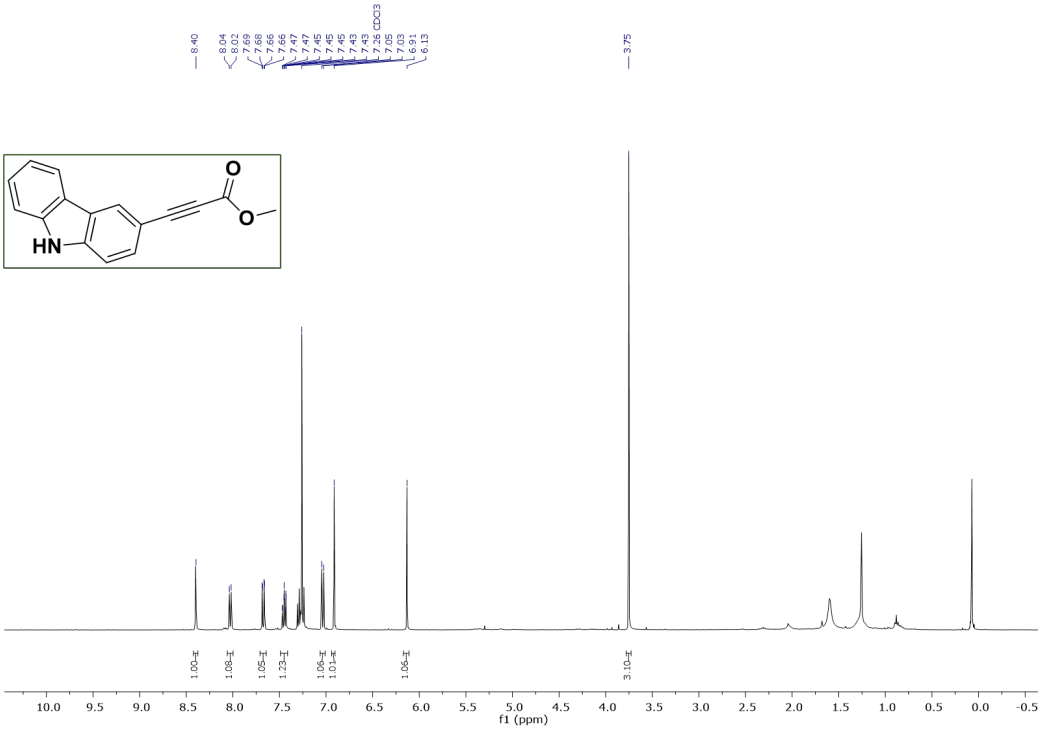

^{13}C NMR of **methyl 3-(9H-carbazol-3-yl)propiolate** (8) in $CDCl_3$

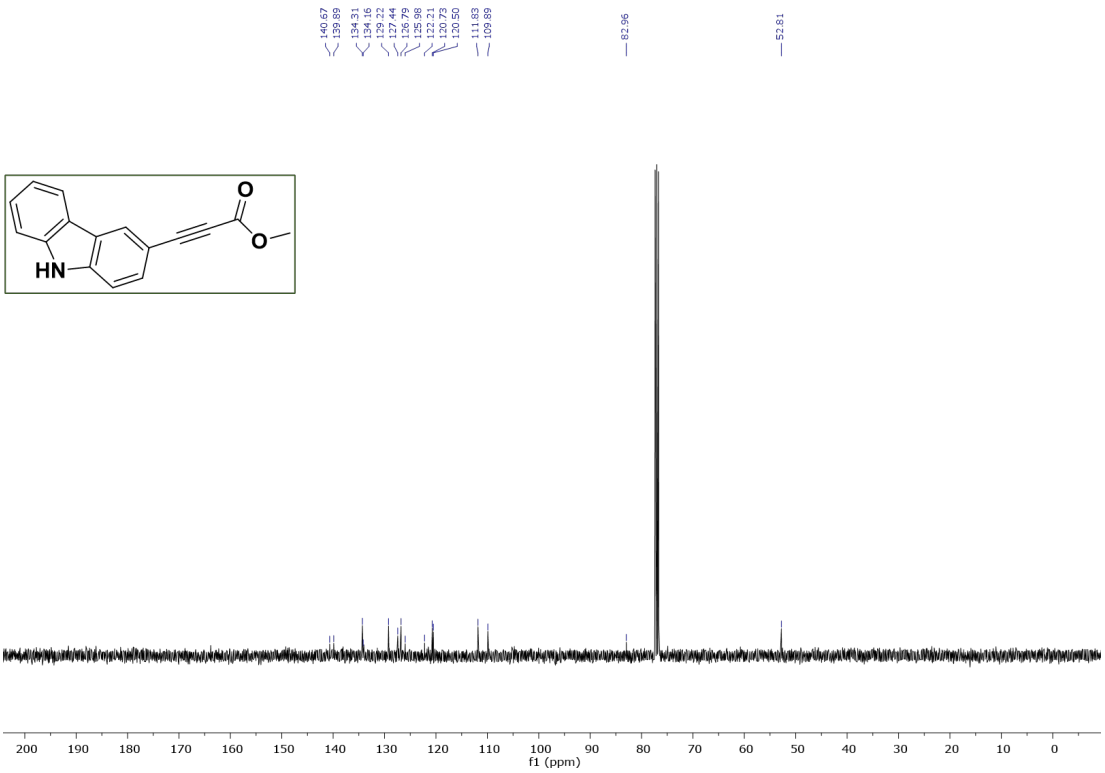

^{1}H NMR **of methyl 4-((phenylamino)methyl)benzoate (S03)** in $CDCl_3$

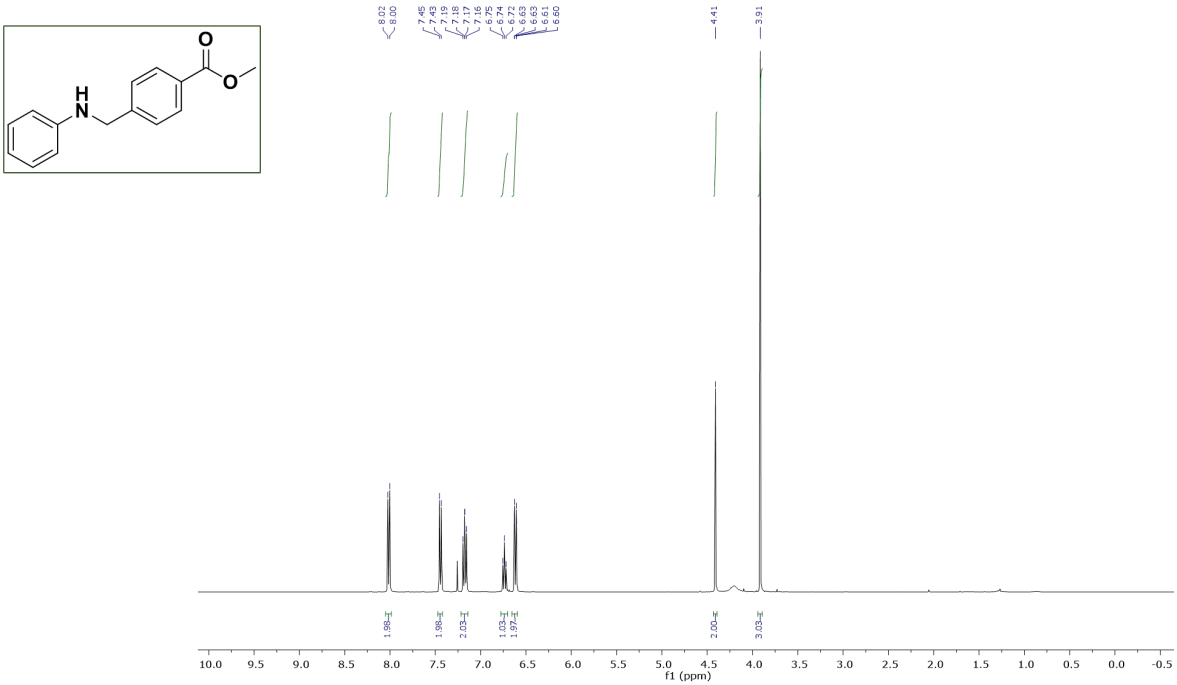

^{13}C NMR **of methyl 4-((phenylamino)methyl)benzoate (S03)** in $CDCl_3$

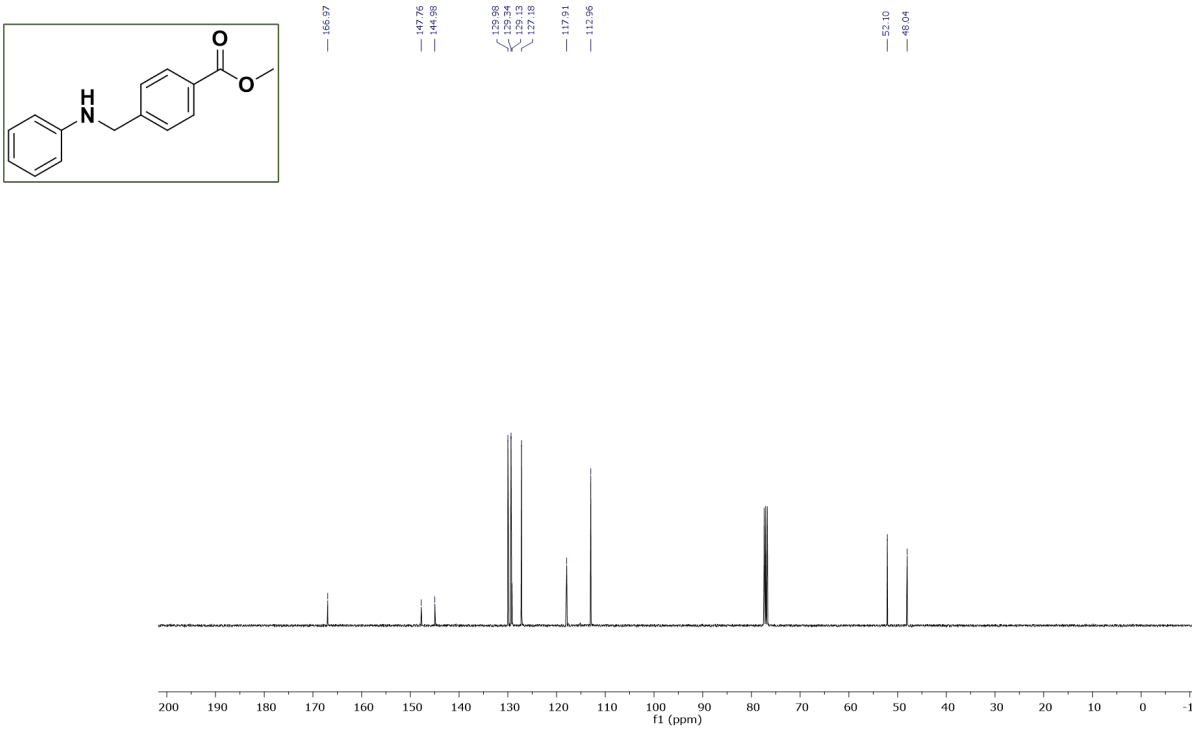

^{1}H NMR **of methyl 4-((N-phenylacrylamido)methyl)benzoate (9)** in $CDCl_3$

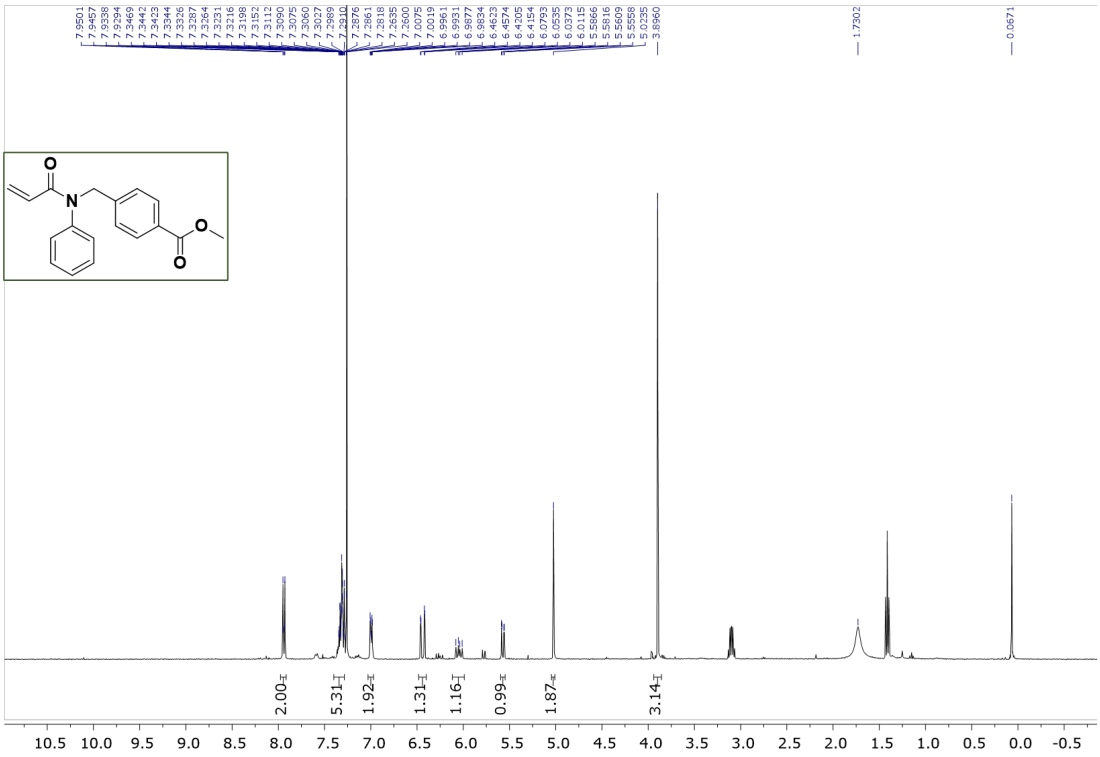

^{13}C NMR **of methyl 4-((N-phenylacrylamido)methyl)benzoate (9)** in $CDCl_3$

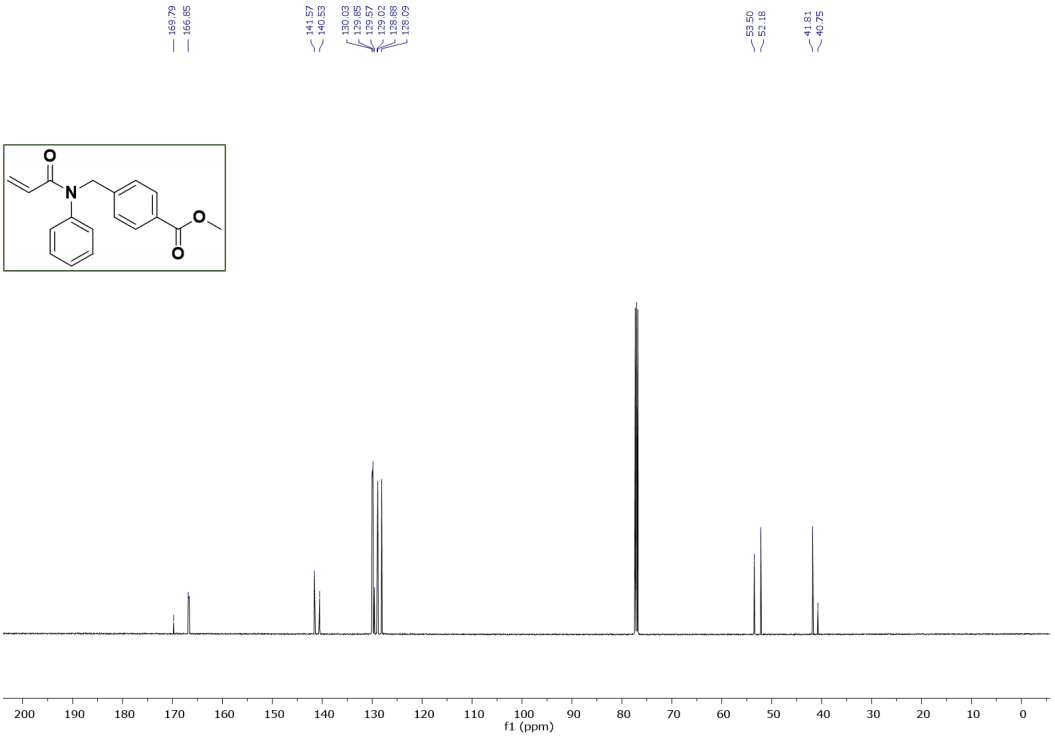

^{1}H NMR of **5-chloro-N-(pyridin-2-ylmethyl)pyrimidin-2-amine (S04)** in $CDCl_3$

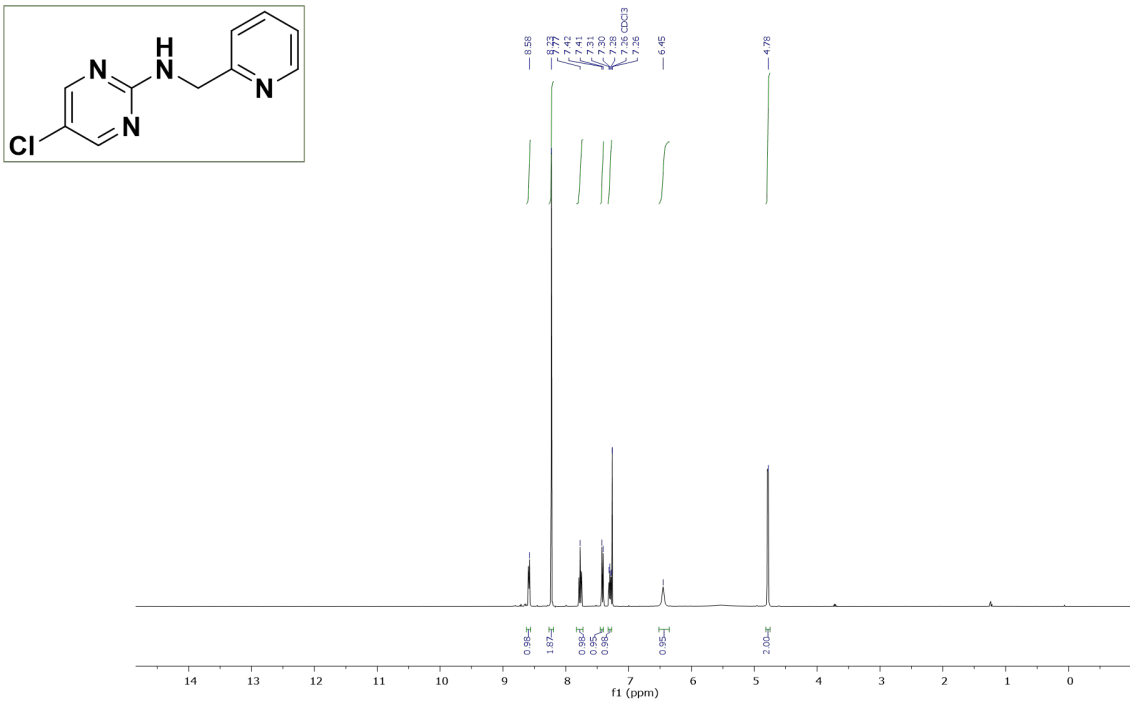

^{13}C NMR of **5-chloro-N-(pyridin-2-ylmethyl)pyrimidin-2-amine (S04)** in $CDCl_3$

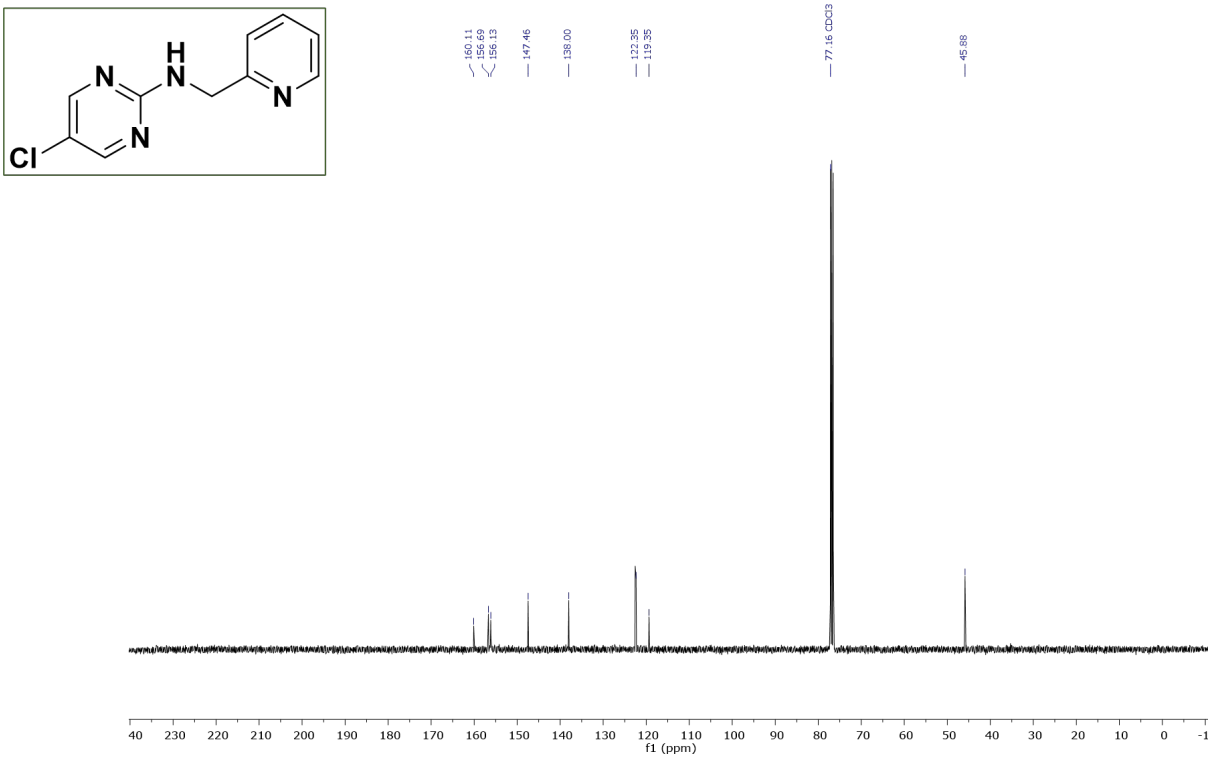

^{1}H NMR of **N-(5-chloropyrimidin-2-yl)-N-(pyridin-2-ylmethyl)acrylamide (10)** in $CDCl_3$

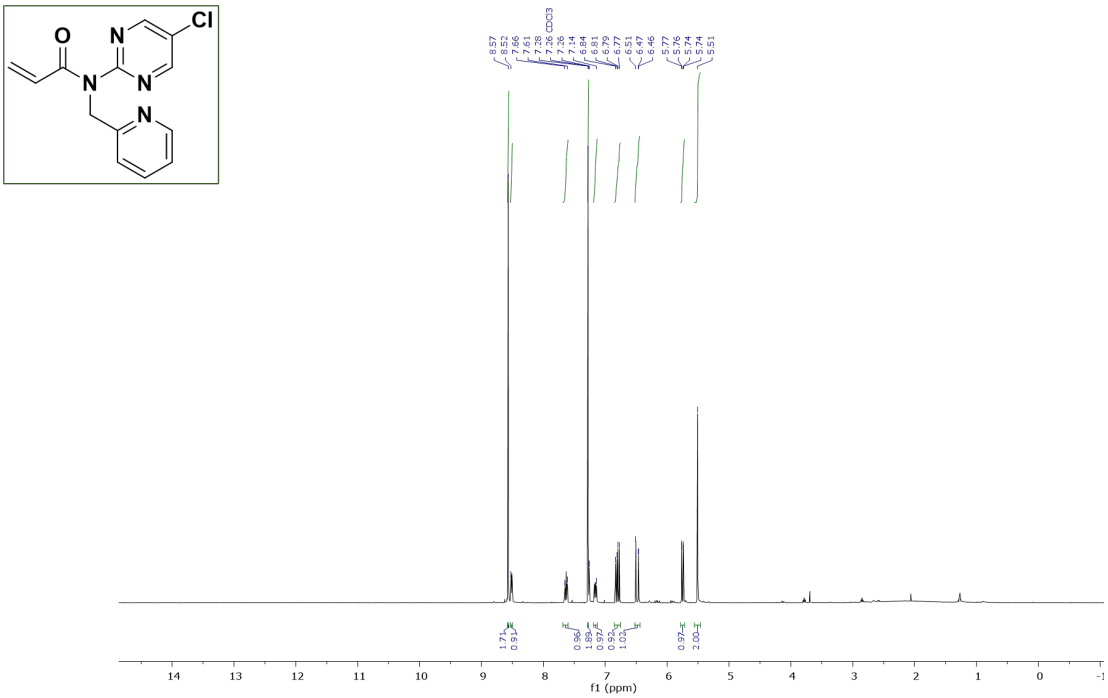

^{13}C NMR of **N-(5-chloropyrimidin-2-yl)-N-(pyridin-2-ylmethyl)acrylamide (10)** in $CDCl_3$

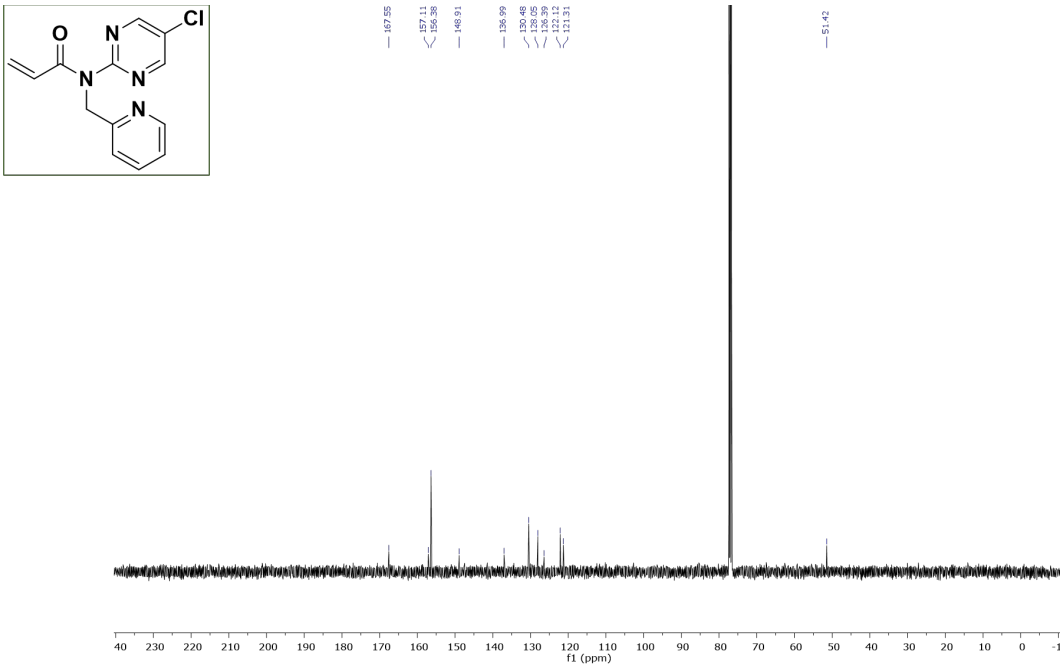

^{1}H NMR of **tert-butyl 5-formyl-1H-benzo[d]imidazole-1-carboxylate (S05)** in $CDCl_3$

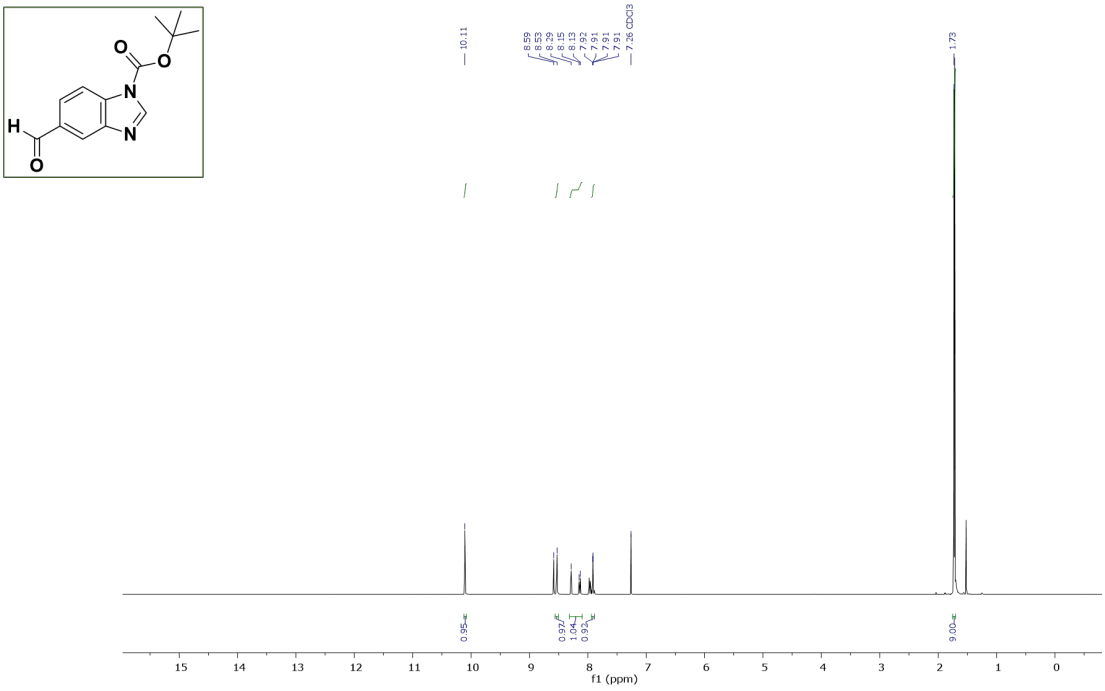

^{13}C NMR of **tert-butyl 5-formyl-1H-benzo[d]imidazole-1-carboxylate (S05)** in $CDCl_3$

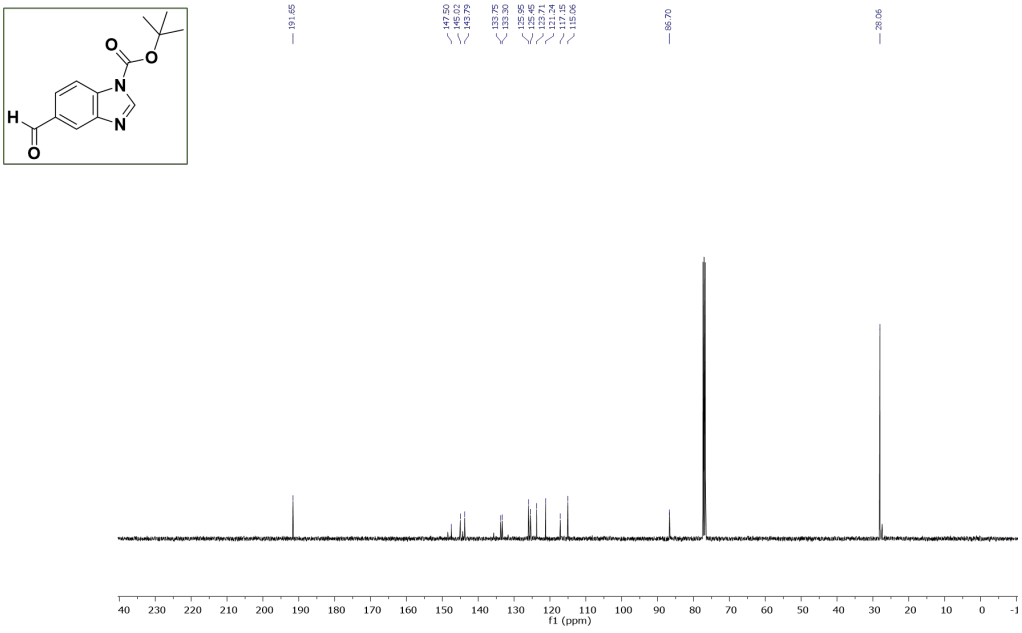

^{1}H NMR of **tert-butyl 5-((N-phenylacrylamido)methyl)-1H-benzo[d]imidazole-1-carboxylate (S06)** in $CDCl_3$

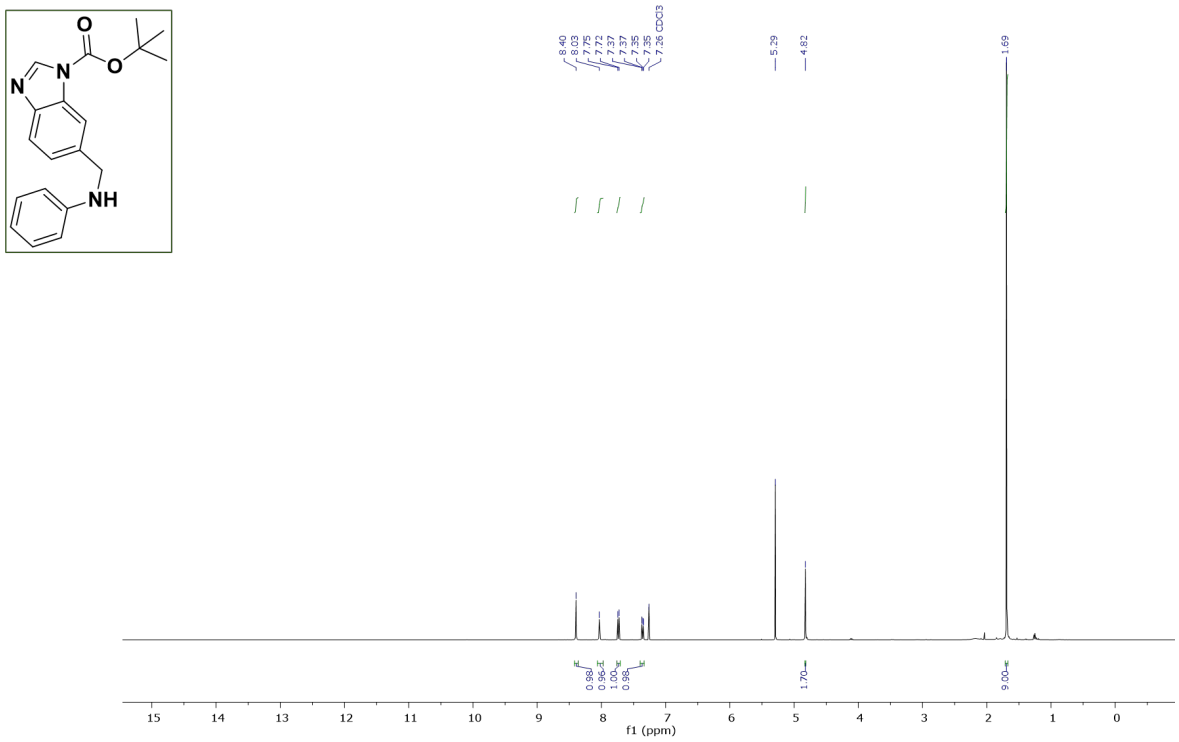

^{13}C NMR of **tert-butyl 5-((N-phenylacrylamido)methyl)-1H-benzo[d]imidazole-1-carboxylate (S06)** in $CDCl_3$

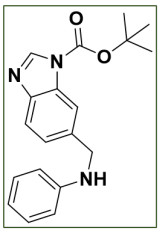

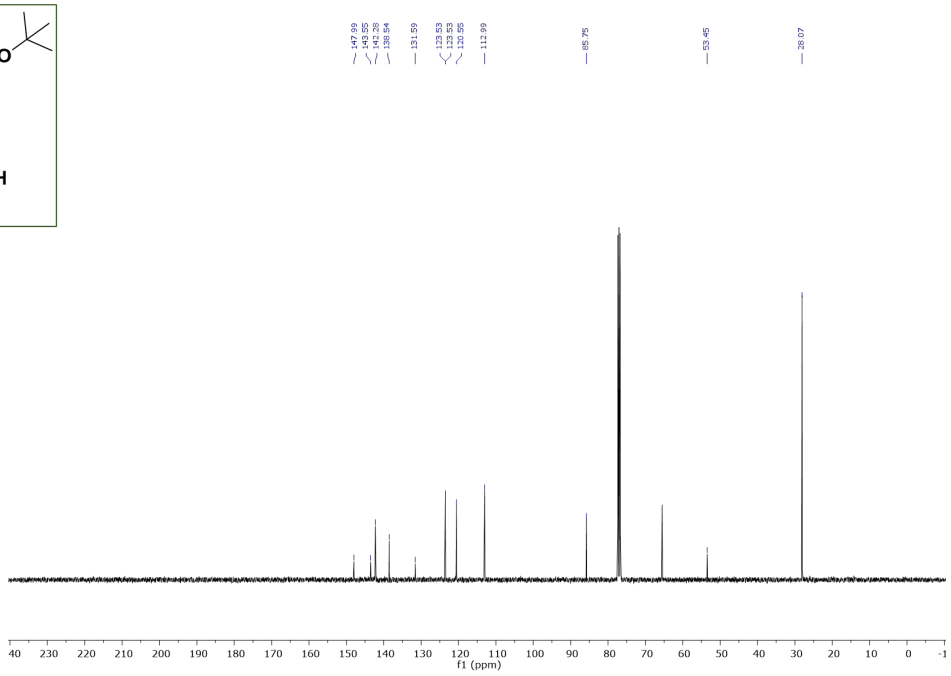

^{1}H NMR of **N-((1H-benzo[d]imidazol-5-yl)methyl)-N-phenylacrylamide (11)** in $CDCl_3$

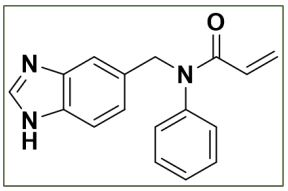

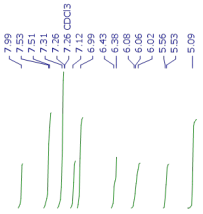

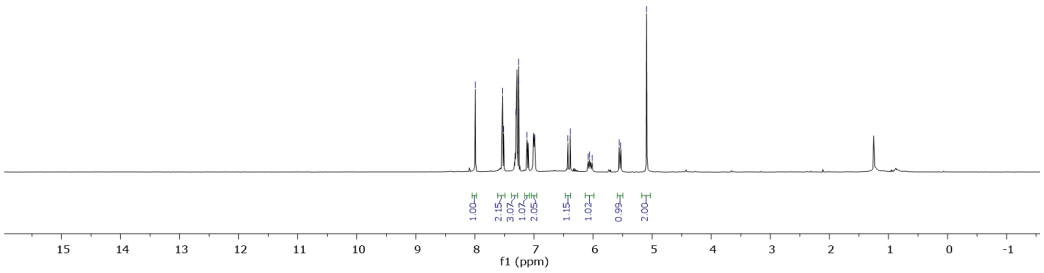

^{13}C NMR of **N-((1H-benzo[d]imidazol-5-yl)methyl)-N-phenylacrylamide (11)** in $CDCl_3$

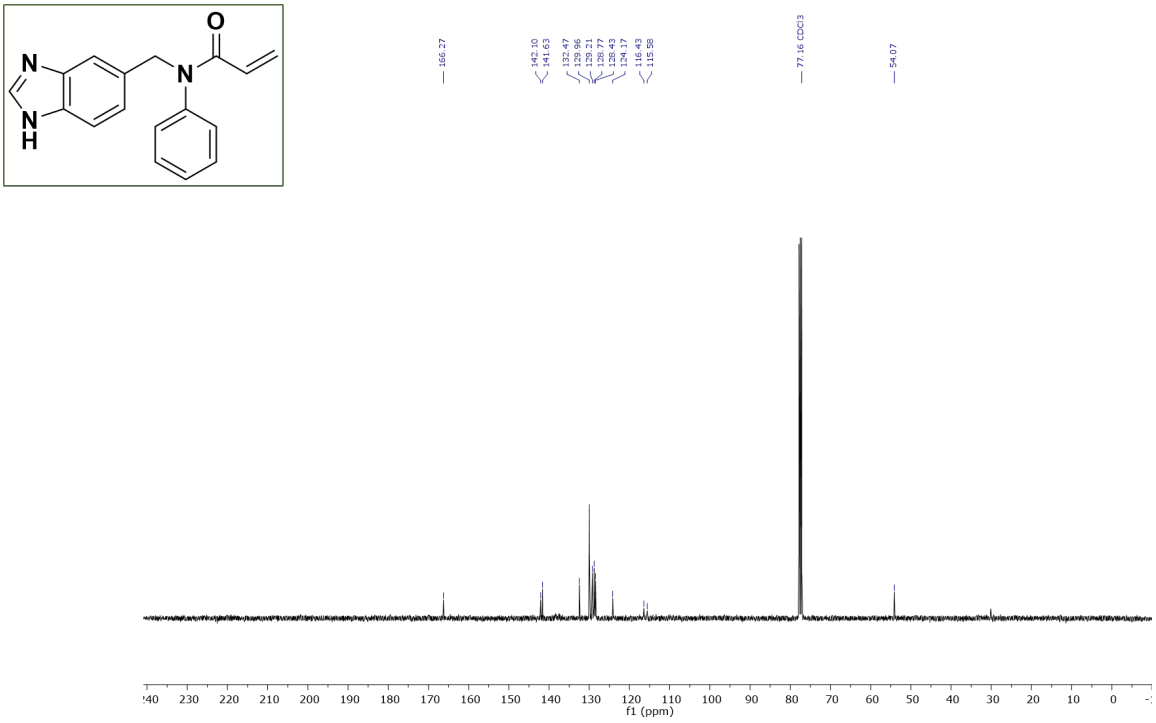

^{1}H NMR of **tert-butyl 6-((naphthalen-2-ylamino)methyl)-1H-benzo[d]imidazole-1-carboxylate (S08)** in $CDCl_3$

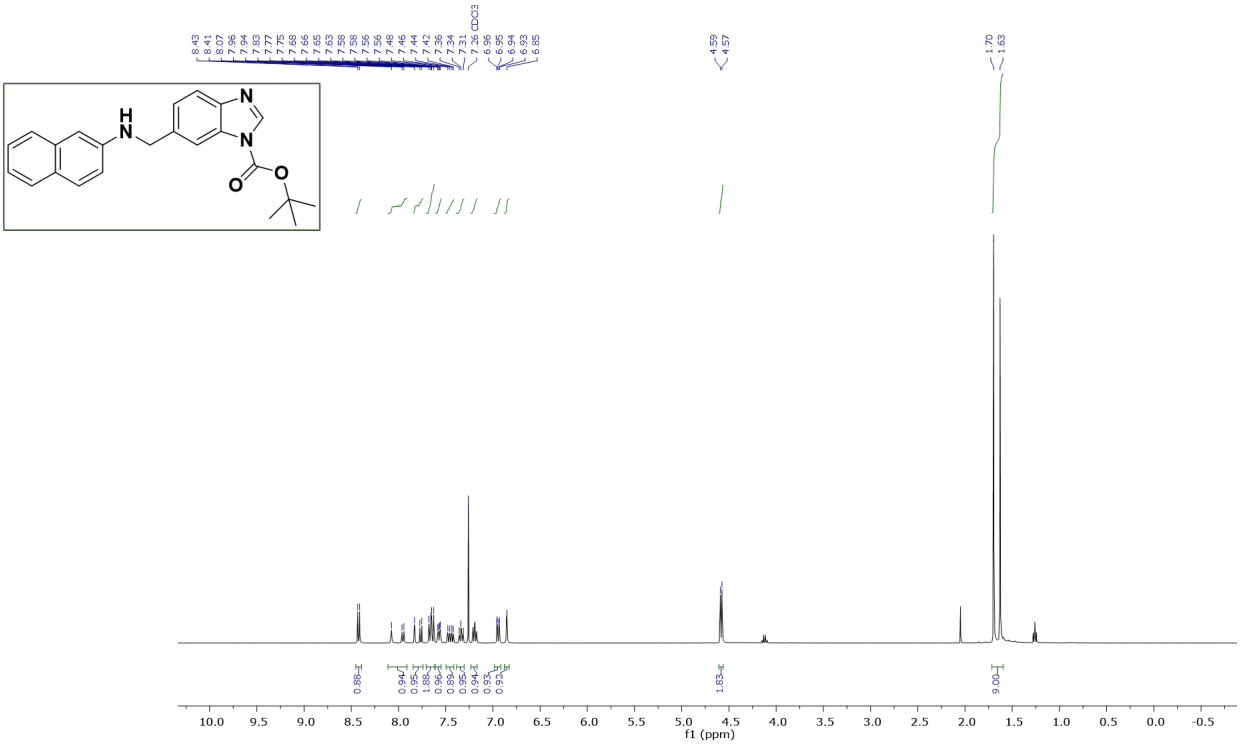

^{13}C NMR of **tert-butyl 6-((naphthalen-2-ylamino)methyl)-1H-benzo[d]imidazole-1-carboxylate (S08)** in $CDCl_3$

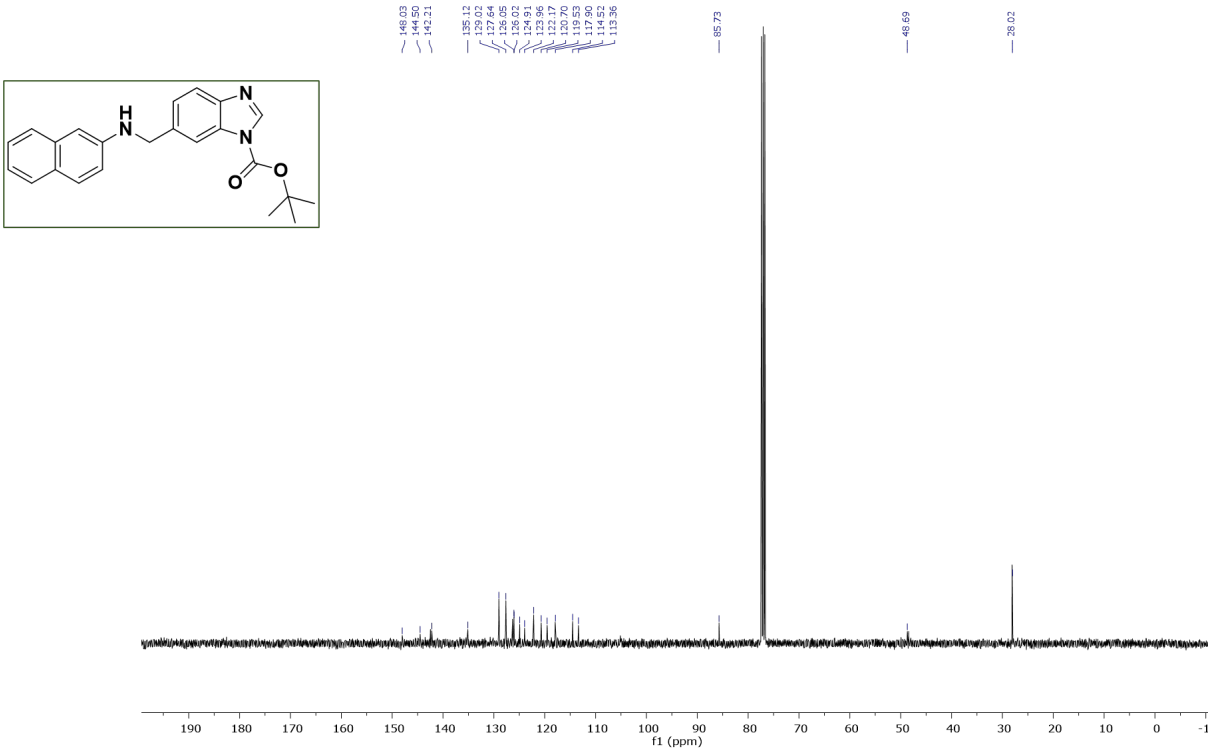

^{1}H NMR of **N-((1H-benzo[d]imidazol-6-yl)methyl)-N-(naphthalen-2-yl)acrylamide (12)** in $CDCl_3$

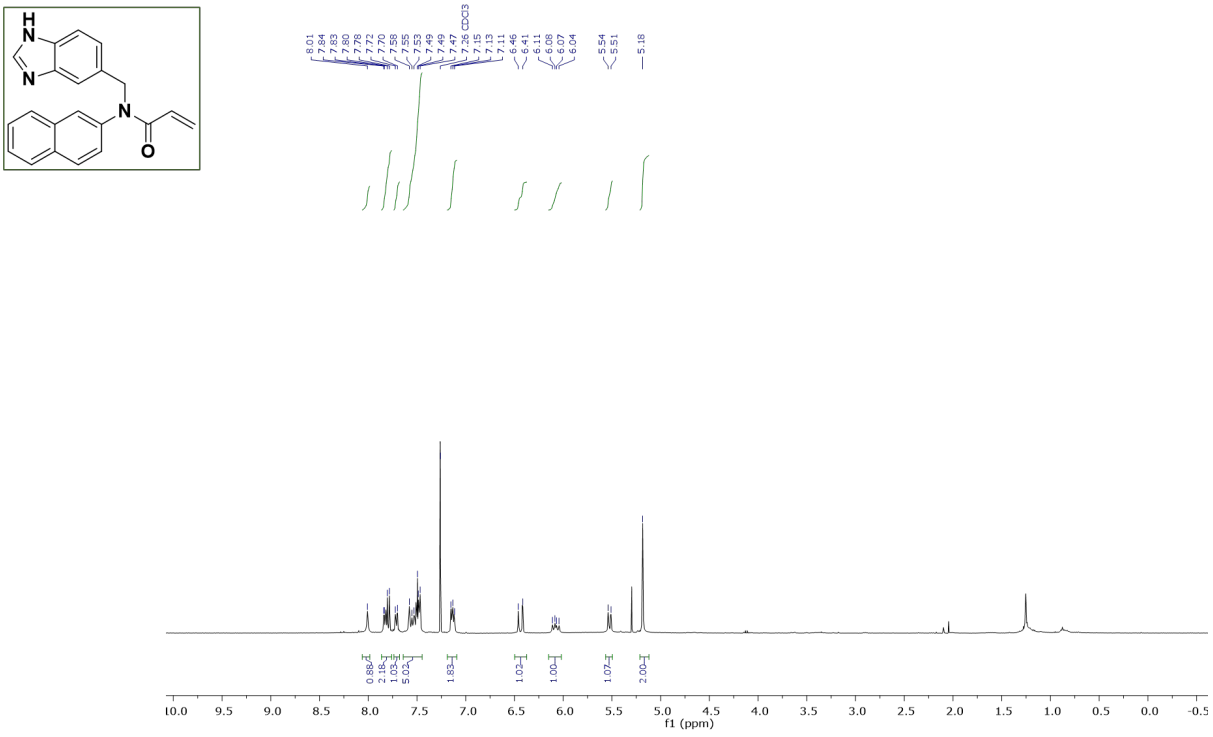

^{13}C NMR of **N-((1H-benzo[d]imidazol-6-yl)methyl)-N-(naphthalen-2-yl)acrylamide (12)** in $CDCl_3$

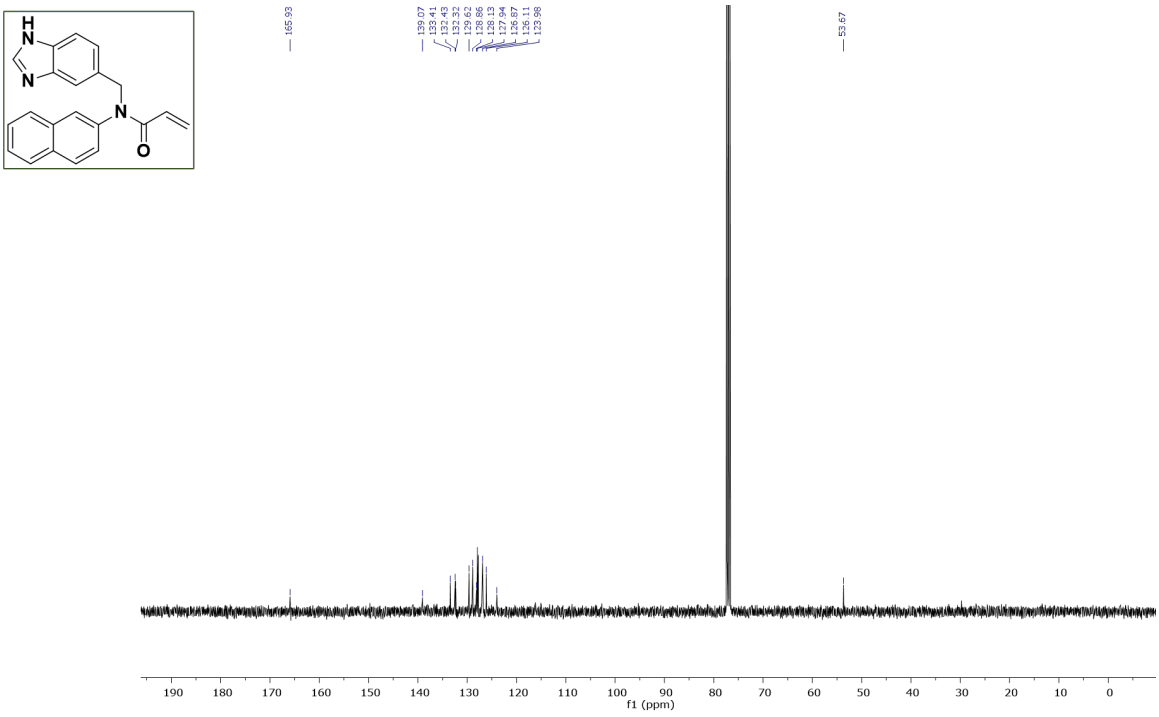

^{1}H NMR **of benzyl 3-phenylpropiolate (13)** in $CDCl_3$

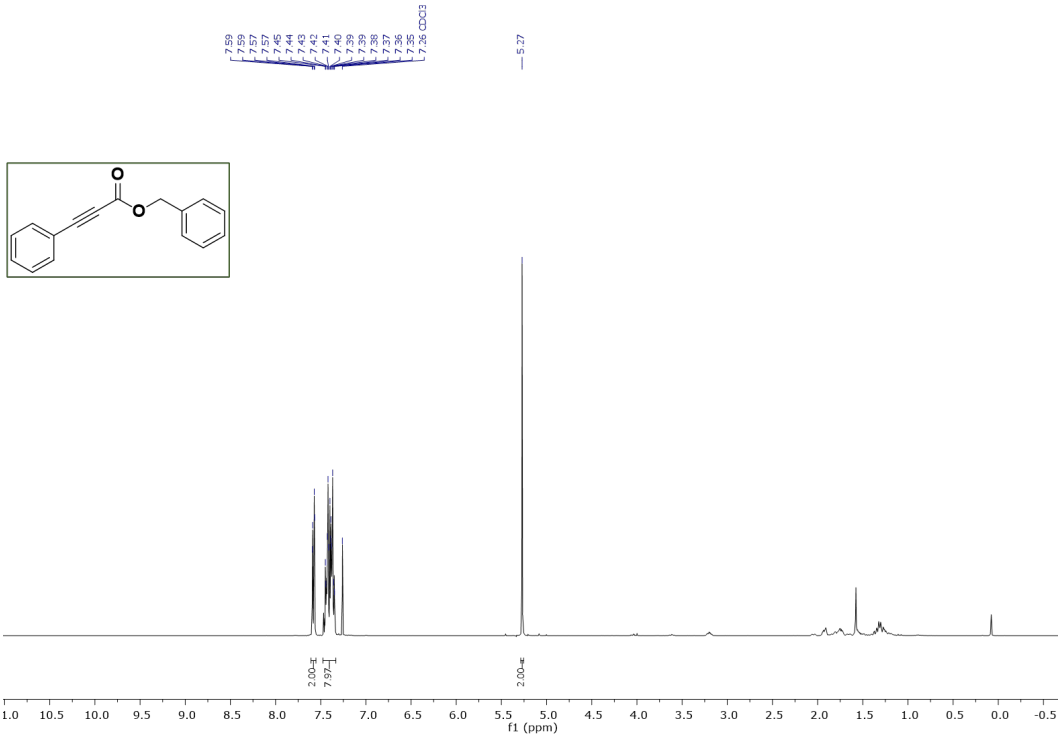

13C NMR **of benzyl 3-phenylpropiolate (13)** in CDCl3

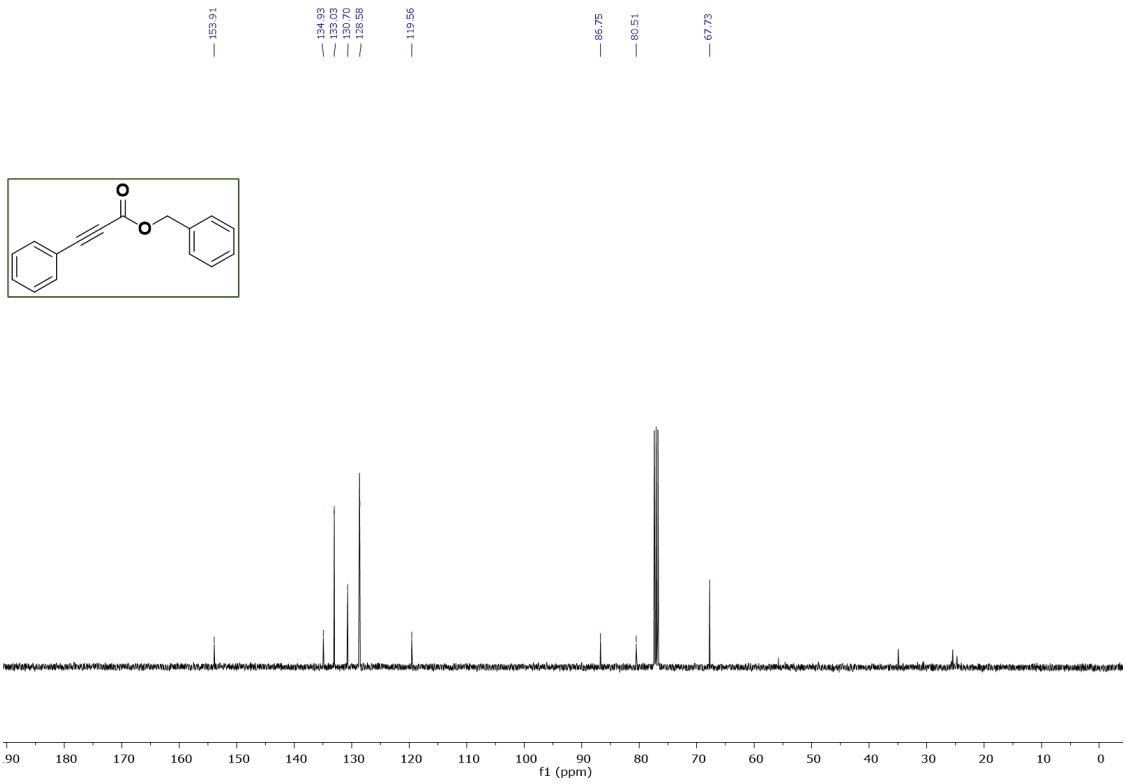

\

^{1}H NMR **of phenyl 3-phenylpropiolate (14)** in $CDCl_3$

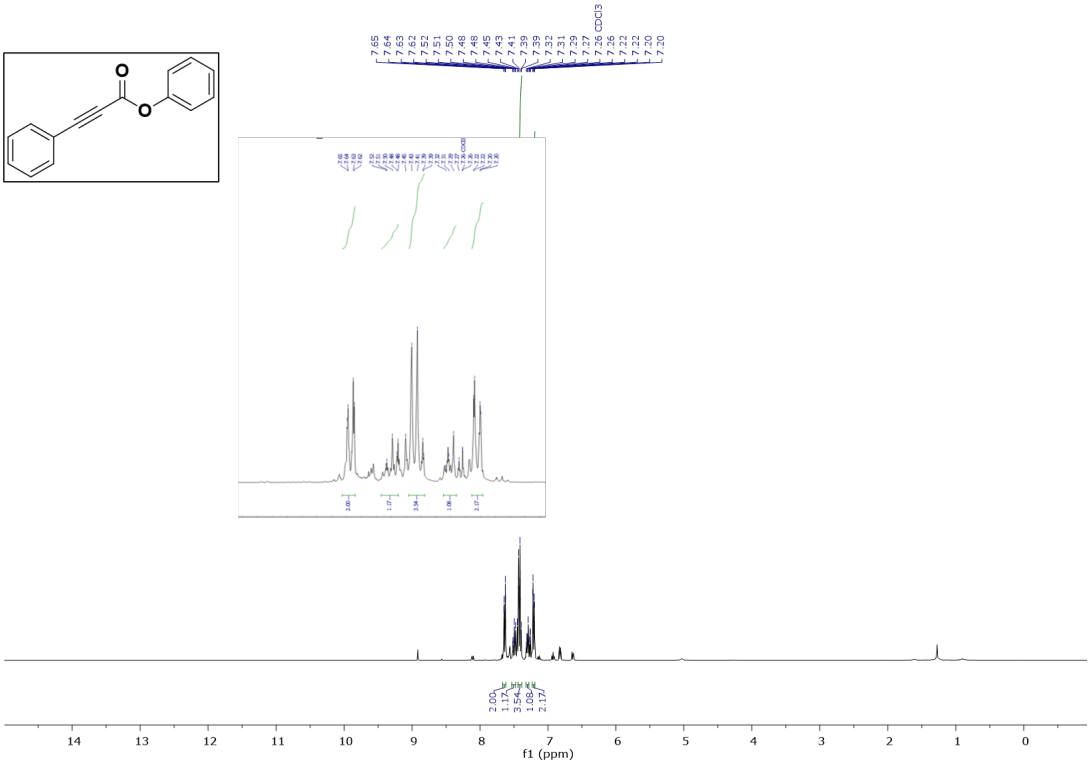

^{3}C NMR **of phenyl 3-phenylpropiolate (14)** in $CDCl_3$

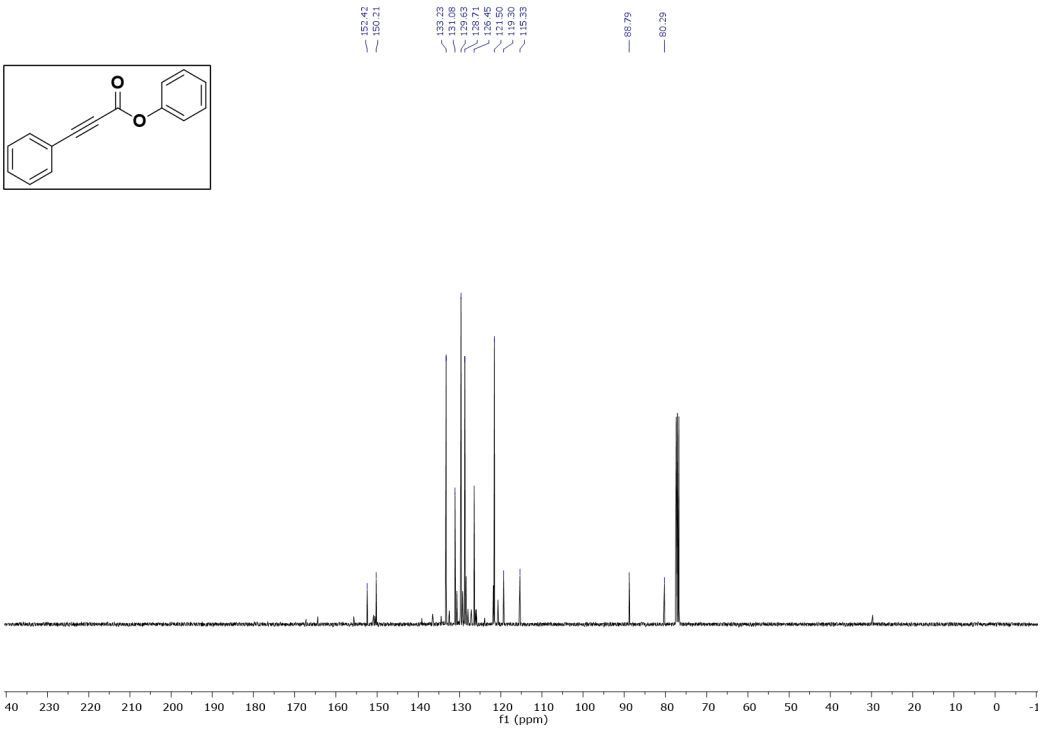

^{1}H NMR of **tert-butyl 3-phenylpropiolate (15)** in $CDCl_3$

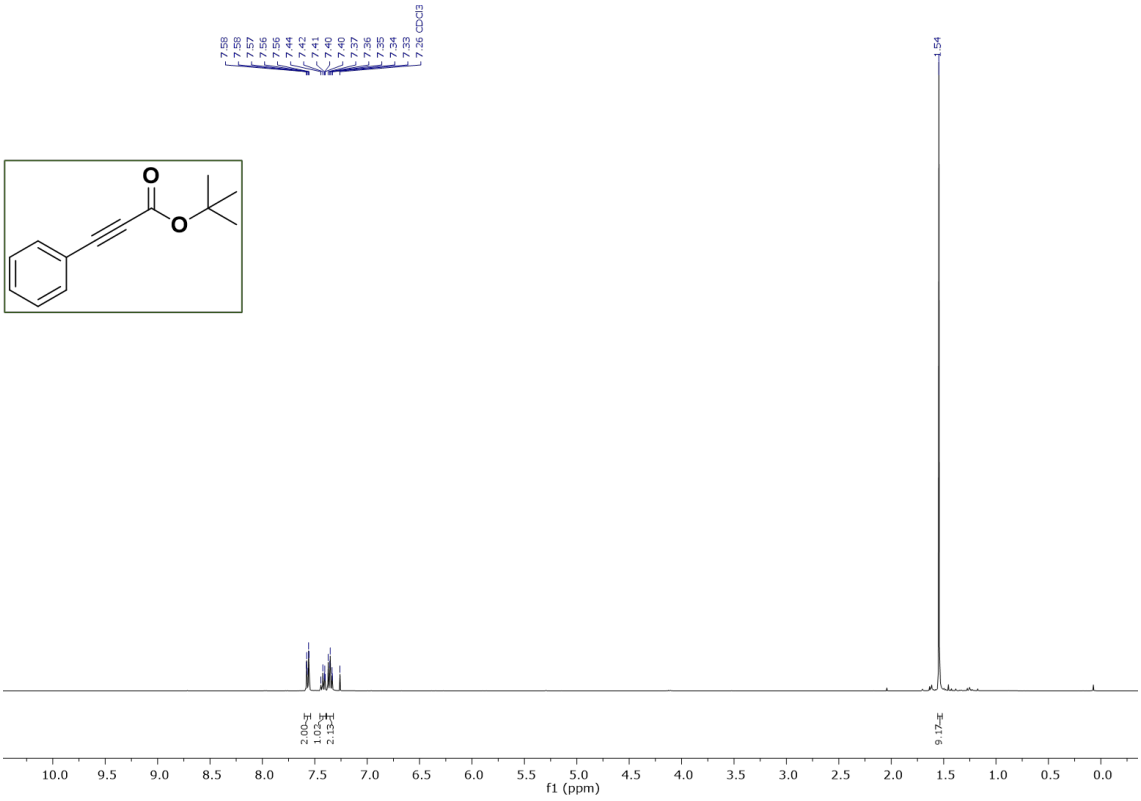

^{13}C NMR of **tert-butyl 3-phenylpropiolate (15)** in $CDCl_3$

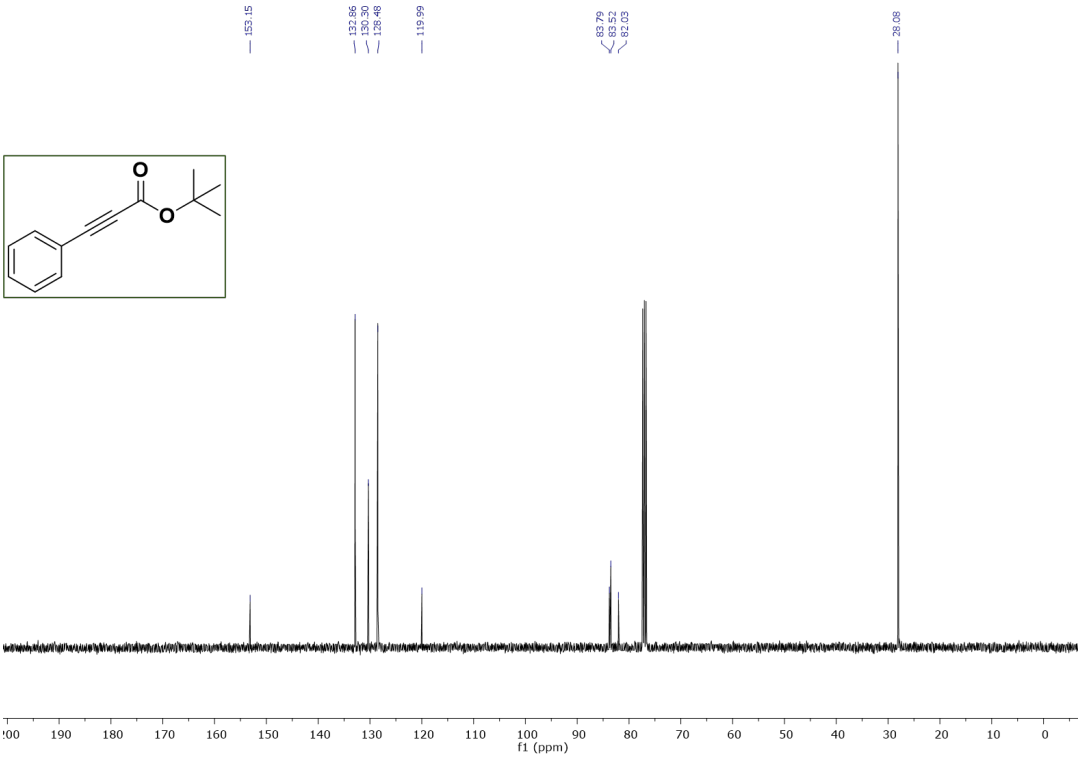

^{1}H NMR of **methyl 3-(pyridin-4-yl)propiolate (16)** in $CDCl_3$

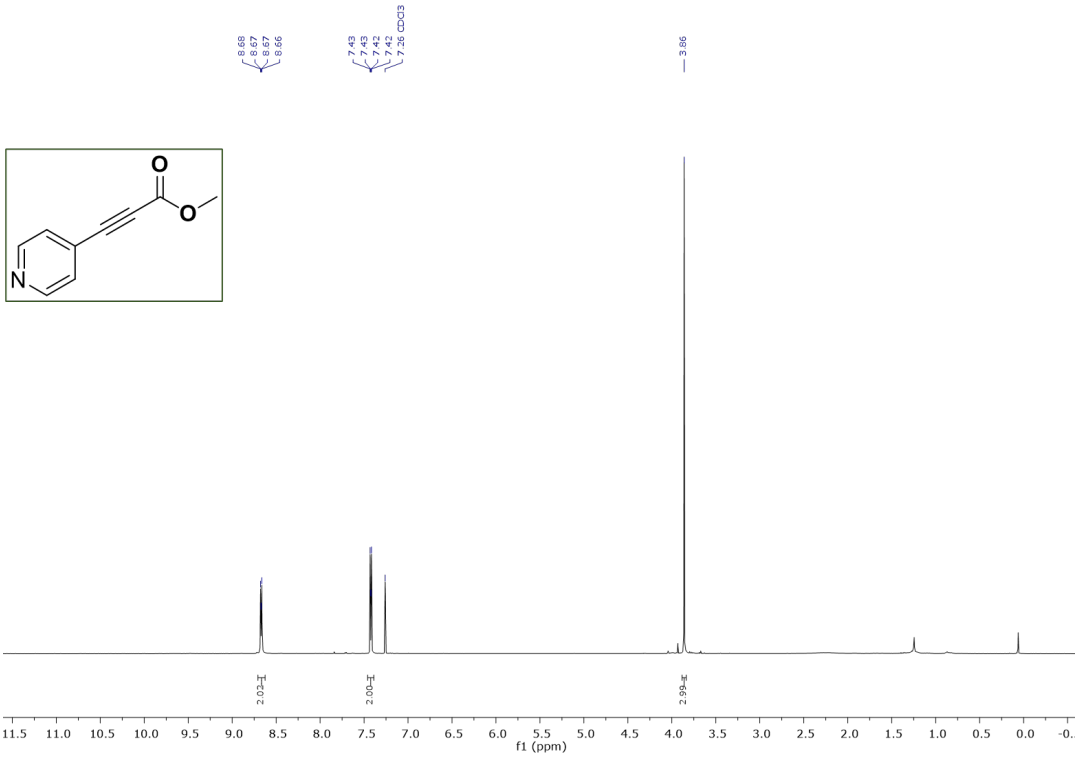

^{13}C NMR of **methyl 3-(pyridin-4-yl)propiolate (16)** in $CDCl_3$

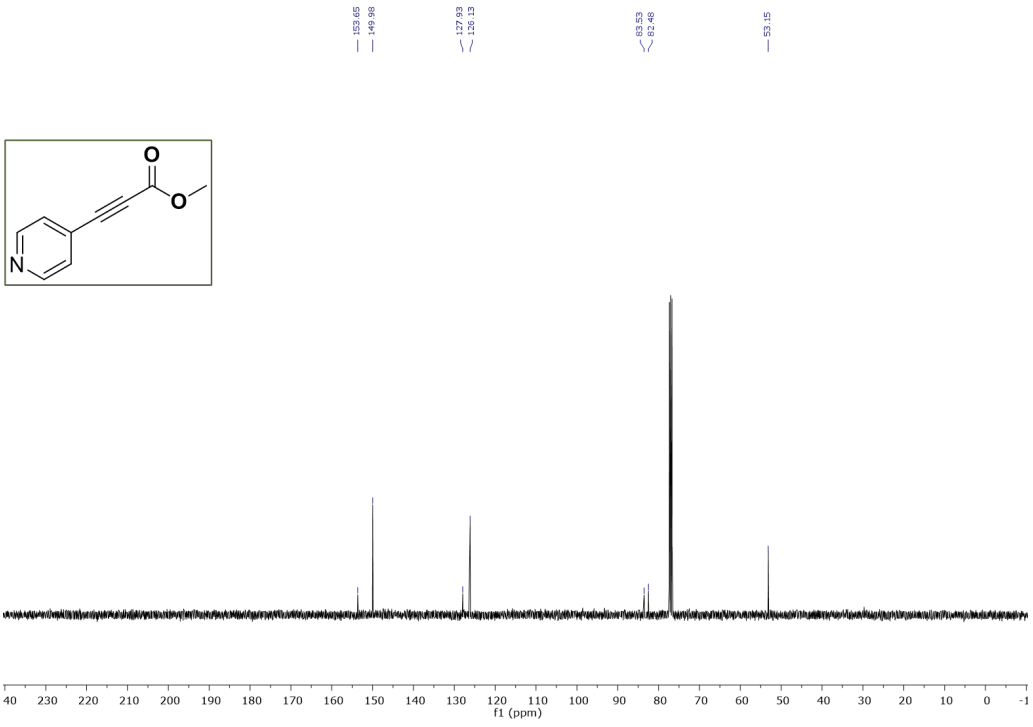

6. References

1. Vickers, C.J., G.E. González-Páez, and D.W. Wolan, *Selective detection and inhibition of active caspase-3 in cells with optimized peptides.* J Am Chem Soc, 2013. **135**(34): p. 12869-76.
2. Weerapana, E., et al., *Quantitative reactivity profiling predicts functional cysteines in proteomes.* Nature, 2010. **468**(7325): p. 790-795.
3. Weerapana, E., A.E. Speers, and B.F. Cravatt, *Tandem orthogonal proteolysis-activity-based protein profiling (TOP-ABPP)--a general method for mapping sites of probe modification in proteomes.* Nature Protocols, 2007. **2**(6): p. 1414-1425.
4. Goujon, M., et al., *A new bioinformatics analysis tools framework at EMBL-EBI.* Nucleic Acids Res, 2010. **38**(Web Server issue): p. W695-9.
5. Sievers, F., et al., *Fast, scalable generation of high-quality protein multiple sequence alignments using Clustal Omega.* Mol Syst Biol, 2011. **7**: p. 539.
6. Hughes, C.S., et al., *Single-pot, solid-phase-enhanced sample preparation for proteomics experiments.* Nature Protocols, 2019. **14**(1): p. 68-85.
7. Yan, T., et al., *SP3-FAIMS Chemoproteomics for High-Coverage Profiling of the Human Cysteinome*.* Chembiochem, 2021. **22**(10): p. 1841-1851.
8. Bekker-Jensen, S., et al., *Dynamic assembly and sustained retention of 53BP1 at the sites of DNA damage are controlled by Mdc1/NFBD1.* J Cell Biol, 2005. **170**(2): p. 201-11.
9. Vickers, C.J., G.E. González-Páez, and D.W. Wolan, *Selective detection of caspase-3 versus caspase-7 using activity-based probes with key unnatural amino acids.* ACS chemical biology, 2013. **8**(7): p. 1558-1566.
10. Backus, K.M., et al., *Proteome-wide covalent ligand discovery in native biological systems.* Nature, 2016. **534**(7608): p. 570-574.

11. Speers, A.E., G.C. Adam, and B.F. Cravatt, *Activity-based protein profiling in vivo using a copper(i)-catalyzed azide-alkyne [3 + 2] cycloaddition.* J Am Chem Soc, 2003. **125**(16): p. 4686-7.

12. Kong, A.T., et al., *MSFragger: ultrafast and comprehensive peptide identification in mass spectrometry-based proteomics.* Nat Methods, 2017. **14**(5): p. 513-520.

13. Teo, G.C., et al., *Fast Deisotoping Algorithm and Its Implementation in the MSFragger Search Engine.* J Proteome Res, 2021. **20**(1): p. 498-505.

14. Xia, J., et al., *Non-apoptotic function of caspase-8 confers prostate cancer enzalutamide resistance via NF-κB activation.* Cell Death & Disease, 2021. **12**(9): p. 833.

15. Hsiao, Y., et al., *Analysis and visualization of quantitative proteomics data using FragPipe-Analyst.* bioRxiv, 2024.

16. Schindelin, J., et al., *Fiji: an open-source platform for biological-image analysis.* Nat Methods, 2012. **9**(7): p. 676-82.

Chapter 3. An activation-based high throughput screen identifies caspase-10 inhibitors

José O. Castellón[1], Constance Yuen[3,4], Brandon Han[3], Katrina H. Andrews[1], Samuel Ofori[1], Ashley R. Julio[1,2], Lisa M. Boatner[1,2], Maria F. Palafox[1,2,5], Nithesh Perumal[1,2], Robert Damoiseaux[3,4,6,7,8], Keriann M. Backus[1, 2,3,7,8,9]

1. Biological Chemistry Department, David Geffen School of Medicine, UCLA, Los Angeles, CA,90095, USA
2. Department of Chemistry and Biochemistry, UCLA, CA 90095, USA
3. California NanoSystems Institute (CNSI), UCLA, Los Angeles, CA, 90095, United States
4. Department of Molecular and Medical Pharmacology, UCLA, Los Angeles, CA, 90095, USA
5. Department of Human Genetics, David Geffen School of Medicine, UCLA, Los Angeles, CA,90095, USA
6. Department of Bioengineering, Samueli School of Engineering, UCLA, Los Angeles, CA, 90095, USA
7. Jonsson Comprehensive Cancer Center, UCLA, Los Angeles, CA 90095, USA
8. Eli and Edythe Broad Center of Regenerative Medicine and Stem Cell Research, UCLA, Los Angeles, CA 90095 USA
9. UCLA DOE Institute for Genomics and Proteomics, UCLA, Los Angeles, CA 90095, USA

* Corresponding Author: Keriann M. Backus, Biological Chemistry Department, David Geffen School of Medicine, UCLA, Los Angeles, CA, 90095, USA, E-mail: kbackus@mednet.ucla.edu.

The UCLA Molecular Screening Shared Resource is supported by Jonsson Comprehensive Cancer Center, award number P30CA016042 by the National Cancer Institute of the National Institutes of Health.

ABSTRACT

Caspases are a family of highly homologous cysteine proteases that play critical roles in inflammation and apoptosis. Small molecule inhibitors are useful tools for studying caspase biology, complementary to genetic approaches. However, achieving inhibitor selectivity for individual members of this highly homologous enzyme family remains a major challenge in developing such tool compounds. Prior studies have revealed that one strategy to tackle this selectivity gap is to target the precursor or zymogen forms of individual caspases, which share reduced structural homology when compared to active proteases. To establish a screening assay that favors the discovery of zymogen-directed caspase-10 selective inhibitors, we engineered a low-background and high-activity tobacco etch virus (TEV)--activated caspase-10 protein. We then subjected this turn-on protease to a high-throughput screen of approximately 100,000 compounds, with an average Z' value of 0.58 across all plates analyzed. Counter screening, including against TEV protease, delineated bona fide procaspase-10 inhibitors. Confirmatory studies identified a class of low-pH activatable caspase-10 inhibitors. In parallel, mode-of-action studies revealed that pifithrin-μ (**PFTμ**), a reported TP53 inhibitor, also functions as a promiscuous caspase inhibitor. Both inhibitor classes showed preferential zymogen inhibition. Given the generalized utility of activation assays, we expect our screening platform to have widespread applications in identifying state-specific protease inhibitors.

Introduction

Human caspases are a family of 12 cysteine proteases, which are canonically associated with cell death[1-3], but have also been tied to nearly all cellular processes, spanning activation[4, 5], proliferation[6, 7], differentiation[8, 9], and cell migration[10]. Therefore, pharmacological manipulation of individual caspases represents an exciting opportunity to delineate caspase-specific functions and to intervene in human pathologies linked to dysregulated caspase activity, including metabolic[11] and immune disorders[12-15], cancers[16-20], and neurodegenerative diseases[21]. Selective inhibitors are available for caspase-1[22], caspase-2[23, 24], caspase-6[25, 26], and caspase-8[27, 28]. Despite these advances, obtaining highly selective inhibitors remains challenging, likely due in large part to the high sequence and structural homology of all caspases.

Caspase-10 is one such caspase that, while particularly intriguing from a target perspective due to its important functions in immune cell apoptosis, still lacks selective inhibitors. In fact, caspase-10 is one of the only caspases that is not labeled by many conventional peptide-based caspase inhibitors[29, 30]. Caspase-10 is absent in rodents[31] and shares high sequence homology with caspase-8. Efforts to delineate caspase-10's role in initiating apoptosis have been complicated by seemingly contradictory findings in immortalized cancer cells versus primary T cells[32, 33]. In cancer cells, caspase-8 rather than caspase-10 is the primary driver of extrinsic apoptosis[32-37]. Caspase-10 has even been implicated as a dominant negative regulator of programmed cell death in some cancer types[1, 38]. In contrast, in primary T cells, caspase-10 contributes to the initiation of apoptosis[13]; humans harboring inactivating mutations in caspase-10 experience autoimmunity and excessive T cell proliferation[39, 40] because of decreased apoptosis.

These human phenotypes indicate non-functionally redundant roles for caspase-8 and -10 and highlight the likely value of selective inhibitors targeting each caspase, both for further characterizing the unique and overlapping activities of each protease and, more broadly, towards the production of new chemical tool compounds to manipulate adaptive immune cell function.

Type II kinase inhibitors, which target the inactive form of enzymes, exemplify one strategy to improve inhibitor selectivity[41-44]. We took this approach in our prior work, which identified selective caspase-8 and caspase-2 inhibitors that function by targeting the zymogen, or uncleaved and inactive, precursor caspase proteoforms[24, 27, 45]. However, in our previous study, developing selective inhibitors for caspase-10 that did not cross-react with caspase-8 proved elusive despite our best efforts[27]. Consequently, there is an unmet need for new approaches to caspase-10 inhibitor discovery.

Here, we develop and apply a tobacco etch virus (TEV) activation-based screening platform to discover procaspase-10 inhibitors. To build this platform, we first generated an engineered caspase-10 protein (proCASP10TEV Linker) in which the caspase cleavage sites were replaced with TEV recognition sequences. This engineered protease showed low background, high stability, and robust TEV-dependent activity. After TEV activation, proCASP10TEV Linker protease showed comparable activity to recombinant active caspase-10. Enabled by this assay, we conducted a ~100,000 compound screen, which had a hit rate of ~0.22% (calculated as compounds with a z-score less than -3) and an average *Z'*-factor (a measure of how well positive and negative controls are separated)[46] of 0.58 (Table S1). Our subsequent re-screening and counter-screening efforts validated hits and delineated TEV inhibitors from those targeting proCASP10.

Resynthesis of a thiadiazine-containing hit compound (SO265) unexpectedly revealed that compound rearrangement was driving the observed caspase-10 inhibition. Additionally, mode-of-action studies revealed that the hit compound pifithrin-μ (PFTμ), a previously reported inhibitor of TP53[47], is also a broadly reactive caspase inhibitor. Taken together, we expect that our hit compounds and innovative screening platform will advance efforts to discover potent and selective procaspase-10 inhibitors.

RESULTS

Establishing TEV-protease activatable caspase-10. Guided by previous reports of TEV-activatable caspases[24, 48, 49], our first step was to engineer a TEV-activatable caspase-10 protein (**Figure 1A**). For our first attempt at engineering a TEV-cleavable construct (proCASP10TEV), we replaced the aspartate cleavage site, D415, with the TEV recognition site (**Figure S1**; D415ENLYFQG). While this protein did show substantial TEV-dependent increased activity, a high background in the absence of TEV protease was also observed (**Figure 1B**, **Figure S2**). We ascribed this background activity to the formation of activated protease in our purified protein sample (**Figure S3**). The presence of TEV-independent protease activity, and therefore, cleaved caspase, while somewhat varied between recombinant protein batches, was consistently observed in our purified protein after labeling with **Rho-DEVD-AOMK** (**Figure S3**). The background activity was also observed to increase markedly over time, even at nanomolar protein concentrations and with increasing concentration of the sodium citrate kosmotrope (**Figure S4**). Therefore, we deemed this construct incompatible with HTS, given the absolute

requirement for a highly stable and consistently performing protein for large-scale screening applications.

While caspase-10 is not known to harbor additional caspase cleavage sites, we postulated that D435 might also be recognized and cleaved, given the proximity to a likely caspase-recognition motif (PAED). Therefore, we inserted a second TEV motif to generate the proCASP2xTEV protein (**Figure S1**). Disappointingly, this enzyme showed low overall activity and negligible TEV-dependent activation, suggesting that sequence alterations at D435 are not well tolerated (**Figure 1B**).

While caspases show high selectivity for aspartyl residues, we postulated that the glutamate residue in the TEV recognition sequence could be recognized and cleaved at a low level, thereby rationalizing the observed high TEV-independent background for the proCASP10TEV protein. To test this hypothesis, we next generated a caspase-10 construct (proCASP10TEV Linker) in which a two-alanine spacer was included to reposition this glutamate further from the remainder of the caspase recognition motif. We additionally optimized our expression and purification protocol to reduce self-activation, both by decreasing the induction time and by not freezing the cell pellets prior to purification (see methods). Pleasingly, the proCASP10TEV Linker protein exhibited both higher overall activity and reduced background compared to our initial construct (**Figure 1B**). Further supporting the improved behavior of this protein, we detected no formation of cleaved caspase (~20 kDa) by gel-based analysis (**Figure S5**).

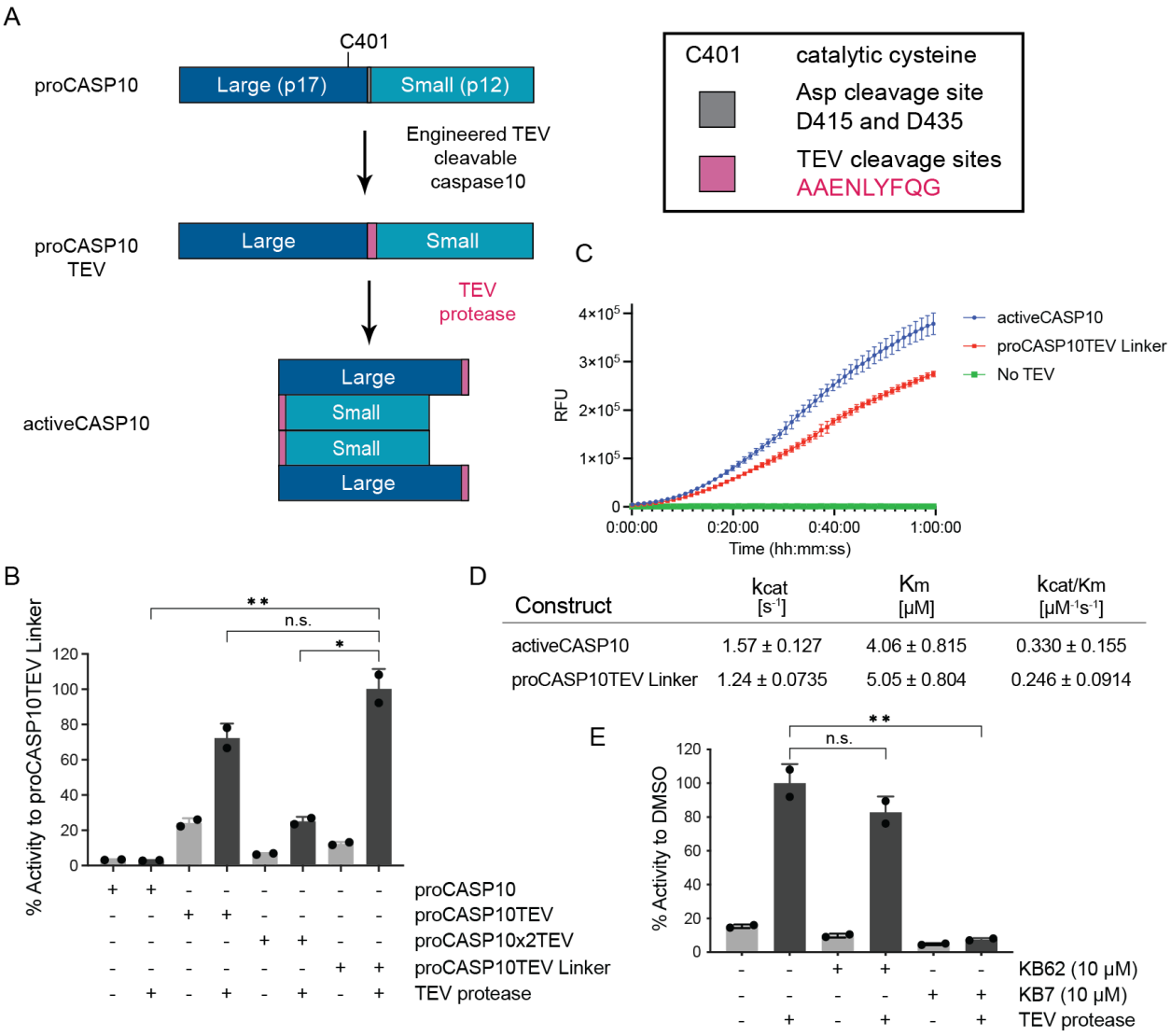

Figure 1. A robust TEV-cleavable functional caspase-10 is only cleaved in the presence of TEV protease and can be inhibited with a dual caspase-8/-10 inhibitor (KB7)[25]. (A) Design of engineered TEV cleavable caspase-10 containing TEV recognition site, ENLYFQG (pink). (B) Comparison of relative TEV-dependent and TEV-independent caspase activity for the indicated engineered proteins (333 nM) to cleave Ac-VDVAD-AFC fluorogenic substrate (10 μM) with/without TEV protease (667 nM). Sequences of engineered proteins can be found in **Figure S1**. (C) Time course comparing activeCASP10 (blue) versus proCASP10TEV Linker with (red) and without (green) TEV

protease (667 nM) in the presence of Ac-VDVAD-AFC fluorogenic substrate (10 μM). (D) Michaelis-Menten kinetics comparing proCASP10TEV Linker (333 nM) activity to activeCASP10 (333 nM) activity as measured by cleavage of the fluorogenic substrate over time. (E) Assessing the relative inhibition of proCASP10 Linker protein by dual procaspase-8/-10 inhibitor **KB7** (10 μM) and negative control compound **KB62** (10 μM)[27]. Assay conducted as in 'B.' For B and E, data represents mean value ± standard deviation for two biological replicates. For C and D, data represent mean values ± standard deviation for three biological replicates. Statistical significance was calculated with unpaired Student's t-tests, * $p<0.05$, ** $p<0.001$, ns, not significant $p>0.05$. Relative fluorescence units, RFU.

Assessing the suitability of proCASP10TEV Linker for high throughput screening (HTS). To test whether the proCASP10TEV Linker protein would faithfully recapitulate proCASP10 activity and thus prove suitable for HTS, we further assessed the activity of this protein. Gratifyingly, upon the addition of TEV protease, we observed marked TEV-dependent increased catalytic activity (**Figure 1B, C**). TEV activation occurred rapidly and required only a modest (~500 nM) concentration of TEV protease to achieve complete conversion of proCASP10TEV Linker (333 nM) to the cleaved proteoform (**Figure S6** and **Figure S7**). The proCASP10TEV Linker protein, once activated by TEV protease, showed near-comparable activity to activeCASP10 (**Figure 1C**), with only a modest decrease in kcat and Km (**Figure 1D**). We find that the protein labels robustly with our previously reported caspase-8/10 click probe **KB61** (**Figure S6**)[27], which corroborates that the proCASP10TEV Linker protein behaves similarly to proCASP10.

The TEV cleavable construct was also inhibited by the dual caspase-8 and caspase-10 inhibitor KB7 (10 μM) and was not inhibited by the structurally matched inactive control, **KB62** (10 μM) (**Figure 1E**)[27]. These findings provided further evidence that our engineered protein behaves similarly to proCASP10 and, additionally, demonstrated that the protein is well suited to assess procaspase inhibition.

We next vetted our assay conditions for HTS compatibility, with the goal of ensuring both high activity and high stability over longer assay periods. Additionally, we found that the proCASP10TEV Linker protein showed increased activity in the presence of the kosmotrope sodium citrate at increasing concentrations (37 mM, 111 mM, and 333 mM) (**Figure S8**). This added activity was restricted to the TEV-cleaved/activated protein; little TEV-independent activity was observed after chaotrope addition in the absence of TEV protease. Providing evidence of high enzyme stability, a favorable property for screening applications, proCASP10TEV Linker showed no substantial change in enzyme activity after prolonged (18h) incubations times for both 4 °C and ambient temperature (**Figure S9**). Additionally, substrate turnover was observed to progress in a linear manner for the initial ~2h period, with increasing activity observed up to 6h (**Figure S10**), which provides a wide time window for acquiring data. Thus, with high stability, low background, and high activity enzyme in hand, we turned to HTS implementation.

A small-scale screen of two pharmacologically active library compounds confirms assay compatibility with HTS. Toward large-scale library screening, our next step was to validate our TEV-mediated caspase activation assay and establish a miniaturized (384-well plate) semi-automated workflow. Following the workflow shown in **Figure 2A**, we first

screened the 'Library of Pharmacologically Active Compounds' (LOPAC@1280), which is a widely utilized library of bioactive compounds that contain known promiscuous protease inhibitors such as E-64, along with a second library consisting of structurally diverse FDA approved drugs covering a broad spectrum of therapeutic areas[50]. Key features of our screen include (1) the pre-incubation of compound library members with the proCASP10TEV Linker construct to favor the detection of procaspase inhibitors and (2) the automated dispensing of the premixed TEV protease and caspase substrate solution followed by automated plate reading. These two automation steps were designed to ensure the consistent timing of our assay to minimize both plate-to-plate and library-to-library variability. Confirming the robustness of our approach, this initial screen had a Z'-factor above 0.5 across 8 screened plates, with a total of 30 out of 2569 compounds showing less than a 50% decrease in caspase activity relative to the DMSO control (**Figure S11**). Illustrating the robust performance of our screen, the Z'-factor comparing our positive control KB7 inhibitor-treated wells to DMSO-treated wells[27] was 0.90 (**Figure S12**)—values above 0.5 are considered an acceptable range for HTS Z'-factor[46].

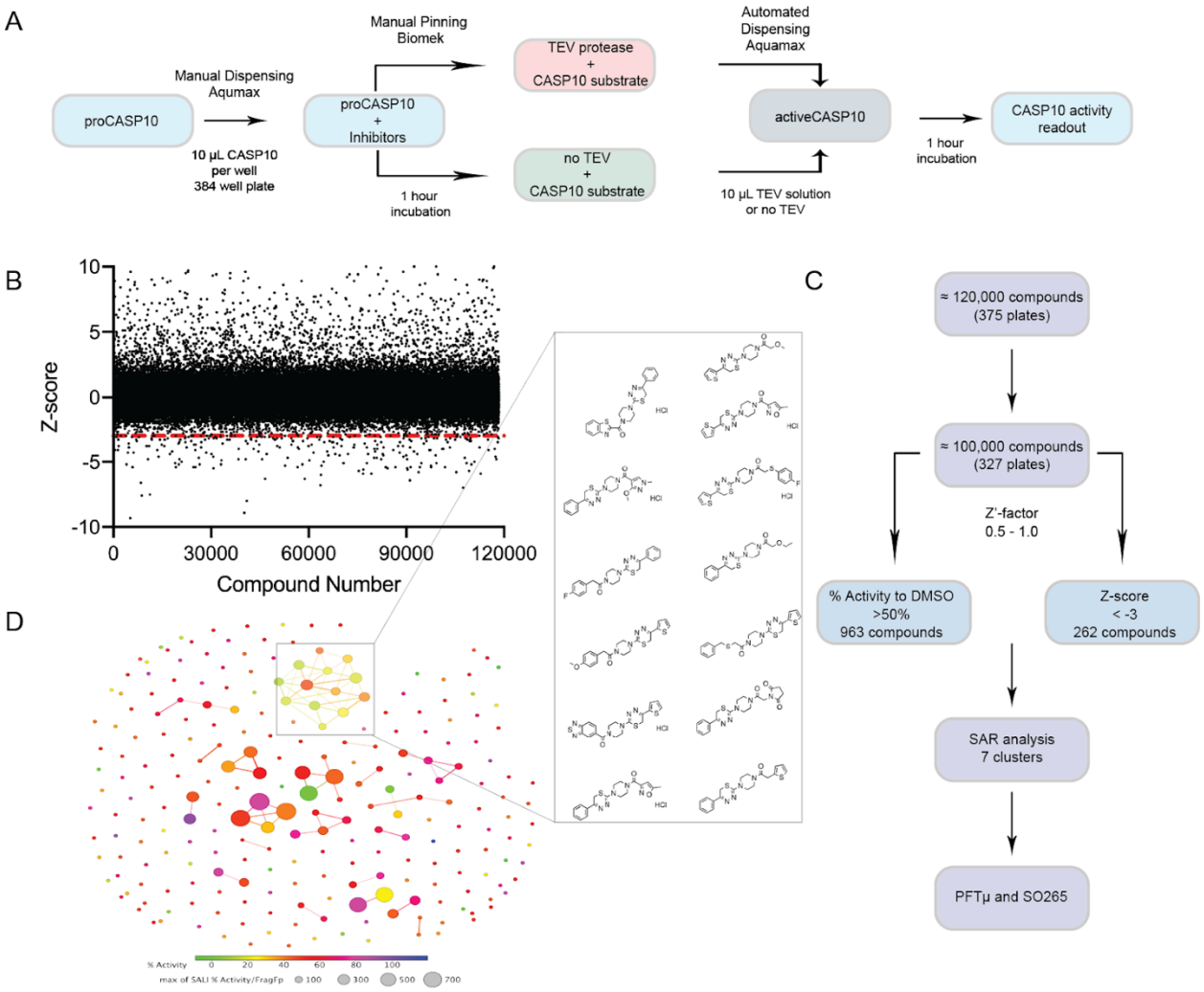

Figure 2. TEV cleavable proCASP10TEV Linker enables a >100,000 compound screen. (A) Scheme of HTS setup with proCASP10TEV Linker (333 nM concentration) incubated with screening compounds (10 µM) for 1h in a 384-well format followed by the addition of the fluorogenic substrate (Ac-VDAVAD-AFC, 10 µM). Endpoint reads were measured and collected after 1h incubation with the TEV substrate solution. (B) z-scores of >100,000 compounds (arbitrarily numbered) screened against proCASP10TEV Linker. The red line indicates hits below a z-score of -3. (C) Summary of filtering parameters for HTS screen. The first filtering step was to remove plates that were not within the desired range of Z'-values (0.5 - 1.0), followed by a second filtering step that identified a total of

237 compounds with a z-score of ≤ -3 (D) SAR analysis of 237 hit compounds identified from HTS using the structure-activity landscape index (SALI) analysis as described in the DataWarrior SAR analysis methods section. The structure of recurring hit chemotypes identified by SAR cluster analysis (DataWarrior, v06.01.04.)[51] are shown for cluster 1. All screening data is in **Table S1**.

Large-scale screen identifies hit caspase inhibitors. Guided by the successful implementation of our pilot screen, we next deployed our platform to screen 118,498 total compounds (all at 10 μM). In aggregate, this screen had Z' values ranging from 0.4 - 1.0 and a hit rate of 0.81% for a total of 963 compounds, affording a 50% decrease in proCASP10TEV Linker activity (**Figure S13**), with 237 unique hits showing a ≤ -3 (**Figure 2B**). The screen filtering steps are summarized in **Figure 2C**. Re-screen validation of the 237 compounds results in 38 compounds with < 50% activity (**Figure S14A**). z-score analysis of the follow-up screen resulted in 97 (or approximately 41%) compounds below 3 standard deviations away from the mean of DMSO control samples (**Figure S14B**). Structural similarity clustering analysis using Datawarrior[51] revealed that approximately 22% of the 237 hits (defined as z-score ≤ -3 or those values that are three standard deviations lower than the mean of the DMSO controls calculated per plate) clustered together, providing evidence of bona fide inhibitors. The 7 major hit clusters consisting of over 50 compounds are shown in **Figure 2D**. One prominent and intriguing chemotype was a class of thiadiazine-containing compounds identified in cluster 1 (**Figure 2D**). Upon closer inspection of the hits, several compounds with clear electrophilic groups stood out, including several organometallic species such as cisplatin (**Table S1**), several cyanoacryl

sulfones, such as HTS-2 and the related **HTS-6**, which is a previously reported as non-specific κB kinase (IKK) inhibitor[52], and pifithrin-μ (**PFTμ**), a previously reported TP53 inhibitor[47] (**Scheme S1**). As caspase-10 is a cysteine protease, we anticipated that some of these electrophilic compounds might react with the catalytic nucleophile.

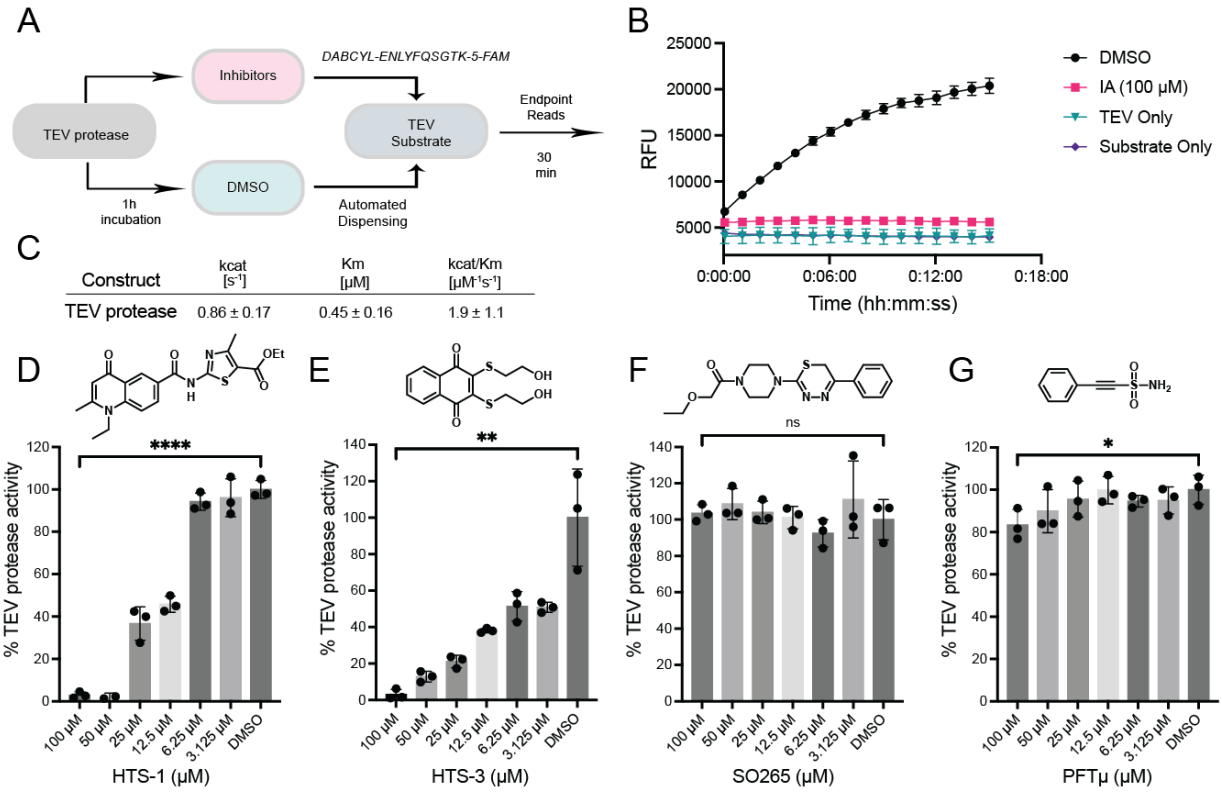

Figure 3. Pro-caspase-10 HTS identified TEV protease inhibitors. (A) General scheme of TEV protease activity assay with our in-house TEV cleavable fluorogenic substrate, DABCYL-ENLYFQSGTK-5-FAM. (B) Shows relative fluorescent units (RFUs) for time-dependent increased fluorescence (λex = 495 nm λem = 550 nm) for TEV protease (100 nM) exposed to either vehicle (DMSO) or iodoacetamide (IA). (C) Michaelis-Menten kinetics of TEV protease (667 nM) with TEV substrate. (D-G) TEV protease (50 nM) activity assay treated with the indicated screening compounds at the indicated concentrations for 1h in PBS buffer under ambient conditions. For D-G, data

represent mean values ± standard deviation for three biological replicates. Statistical significance was calculated with unpaired Student's t-tests, * $p<0.05$, ** $p<0.01$, **** $p<0.0001$, ns, not significant $p>0.05$.

Hit prioritization by re-screening and counter-screening against activeCASP10. To further interrogate our hits and confirm on-target activity against procaspase-10, our next step was determining if our hits were selective for proCASP10 over the active proteoform. Using our previously reported fluorogenic caspase assay[24], we measured the relative inhibition of recombinant active CASP10 by each of our 237 prioritized hits. This screen had a Z' value of 0.73, resulting in 9 of 237 compounds having ≤ 50% activeCASP10 activity (**Figure S15A** and **Table S1**), with 78 compounds being 3 standard deviations below the DMSO control (**Figure S15B**). Notably, several of our aforementioned hits, including **HTS-6**, **SO265**, and **PFTμ**, showed substantially reduced inhibition of activeCASP10 compared to the proCASP10TEV Linker (**Figure S14A** and **Figure S15A**). SAR clustering analysis of the counter screen showed ~20 different clustering types for activeCASP10, but overall, less reactivity towards active compared to the pro-form (**Figure S16**), consistent with more favorable inhibition of the proenzyme. Together, our prioritized compounds (**Scheme S1**) included 10 total inhibitors that showed preferential activity against proCASP10TEV when compared to activeCASP10.

TEV assay identifies likely TEV inhibitors. As our proCASP10TEV Linker screen requires the addition of TEV protease for caspase activation, we anticipated that some hits might be bona fide TEV protease inhibitors rather than caspase inhibitors. To test this

hypothesis and to filter out such compounds, we established a TEV protease activity assay using a customized fluorogenic substrate (see methods) inspired by prior TEV protease assays[53]. Following the workflow shown in **Figure 3A**, we first optimized both the substrate concentration and time points to ensure activity was within the enzyme's linear range (**Figure S17**). We find that TEV protease was highly active towards our fluorogenic substrate, with complete consumption of substrate within five minutes (**Figure 3B**). Using automated dispensing to ensure the rapid and equal delivery of substrate across assay conditions, we observed comparable Michaelis-Menten kinetic parameters to those reported previously for TEV protease[54] (**Figure 3C**).

Using this optimized assay, we used freshly sourced compound stocks to evaluate the TEV protease inhibitory activity of ten prioritized hits (**Figure 3D-G**, **Figure S18**, and **Figure S19**). Notably, while most compounds were sourced commercially, compound **SO265** required in-house synthesis (**Scheme S2** for the synthetic route for **SO265**). We observed substantial dose-dependent inhibition of TEV protease for **HTS-1** (**Figure 3D**), **HTS-2** (**Figure S18A**), and **HTS-3** (**Figure 3E**). Some inhibition was also observed for **HTS-6** (**Figure S18B**), **HTS-4** (**Figure 18C**), and **HTS-5** (**Figure S18D**). Therefore, we excluded these likely TEV inhibitors from further analysis. Encouragingly, several HTS hits stood out as having no appreciable TEV protease inhibitory activity (**Figure 3F**, **Figure S19A**, and **Figure S19B).** Notably, **PFTμ** afforded a slight, but not significant, decrease in TEV protease activity at the highest tested concentration (100 μM) (**Figure 3G**).

Caspase-10 inhibition is confirmed by activity assays. We next turned to confirm that our screening hits engage both recombinant and endogenous proCASP10 protein. We first rescreened a subset of the prioritized hits in our proCASP10TEV Linker assay. While we observed that most compounds only showed modest caspase-10 inhibition (**Figure S20**), several compounds stood out, including HTS-6 (**Figure S21**), the TEV protease inhibitor **HTS-2** (**Figure S22**), and **PFTμ** (**Figure S23**). We then turned to gel-based activity-based protein profiling (ABPP) analysis to further corroborate our inhibition data. Having previously established ABPP gel-based assays for procaspase-8 and -10 using the KB61 click probe[27] in HEK293T lysates, we first deployed this ABPP assay to assess compound engagement of recombinant procaspase-10 at the catalytic cysteine residue C401 (**Figure S24**), focusing on the compounds that contained obvious electrophilic moieties, namely **HTS-6** and **HTS-2** and **PFTμ**. We find that **PFTμ** shows similar potency when compared to established caspase-8/10 dual inhibitor **KB7**[27]. Both **HTS-6** and **HTS-2** exhibited high proteome-wide reactivity, indicating that their caspase engagement is likely driven by the high electrophilicity of the cyanoacryl sulfone moiety. Further illustrating the increased reactivity of these two compounds relative to **PFTμ**, we also observed increased competition of iodoacetamide-rhodamine (IA-Rho) (**Figure S25**), consistent with generalized cysteine reactivity rather than a caspase-10-specific effect. Due to their high reactivity, we excluded **HTS-6** and **HTS-2**, from further analyses.

Compound rearrangement drives caspase inhibition for SO265, which shows preferential inhibition of the pro-form of caspase-10. As the **SO265** thiadiazine chemotype had shown pronounced procaspase-10 inhibition in our initial screen (approximately 80% proCASP10TEV Linker inhibition; **Figure 2D** and **Figure S14**), we

were surprised by the lack of activity using our resynthesized compound (20% proCASP10TEV Linker inhibition) (**Figures S26**). Substituted thiadiazine rings can isomerize to thiol imidazole moieties, gaining aromaticity[55]. Therefore, we hypothesized that such a rearrangement of **SO265**, which could be favored by lower pH, could be driving its inhibitory activity (**Figure 4A**). To test this hypothesis, we subjected **SO265** to acidic conditions (10 mM HCl) prior to assessing caspase inhibitory activity. Consistent with our hypothesis, we observed increased inhibitory activity for stocks of SO265 pretreated with acid (**Figure S26**). This activity was generally restricted to caspase-10, with a more modest increase in inhibition observed for TEV protease (**Figure S27**).

Guided by this increased activity, we next tested the putative isomer, **SO265i** (**Figure 4A**), which we had isolated from the reaction mixture during the synthesis of **SO265**. While the masses of **SO265** and **SO265i** are identical, the two compounds can be distinguished via H-NMR analysis (**Figure S28A**) and LC-MS analysis (**Figure S28B-F**). Notably, the thiadiazine methylene signal was only present in **SO265**, with loss in the **SO265** spectra indicating that aromatization had indeed occurred. The **SO265i** spectra uniquely featured a signal for a thiol proton, consistent with the proposed isomerization. The presence of a thiol in **SO265i** was further corroborated by IR analysis (**Figure S29**). However, when tested in our activity assay, **SO265i** exhibited equivalent caspase-10 inhibition (30% inhibition) to **SO265**, indicating that the thiol imidazole was not the active species (**Figure 4B**).

Following a 2-day incubation at room temperature in DMSO, repeated NMR analysis revealed that the **SO265i** stock had converted into a second species. This species was distinguished by the loss of the thiol proton and an increase in a signal

matching the expected shift of dimethylsulfide (DMS) (**Figure S28A**). We hypothesized that DMSO-mediated oxidation of the **SO265i** thiol to a disulfide (**SO265s**) was occurring; this is a reported redox reaction that produces DMS as a byproduct and is promoted by low thiol pKa values[56, 57]. Therefore, to further assess whether **SO265s** was the active species responsible for caspase-10 inhibition, we incubated 50 mM DMSO stocks of **SO265** and **SO265i** at room temperature for one, seven, and 14 days to promote the formation of **SO265s**. We then tested the activity of each of these compound stocks alongside DMS as a control (**Figure 4C**). Consistent with **SO265s** as the active species, we observed a time-dependent increase in inhibition of proCASP10TEV Linker for both **SO265** and **SO265i**; DMS had no effects on proCASP10TEV Linker activity. Providing further evidence of the likelihood that the rearranged disulfide structure is the active compound, the addition of 5 mM DTT to the compound stock completely abolished inhibitory activity (**Figure 4D**). **SO265s** also showed increased reactivity with glutathione when compared to **SO265** and **SO265i** (**Figure S30**). Taken together, these data provide evidence that **SO265s** is a cysteine-reactive compound that blocks proCASP10TEV Linker activity with preferential inhibition of the zymogen (**Figure S31**). More broadly, we find that **SO265s** show some caspase selectivity, also inhibiting active caspase-8 (**Figure S32**), whereas only a slight decrease in activity was observed for active caspase-3 (**Figure S33**) and caspase-9 (**Figure S34**).

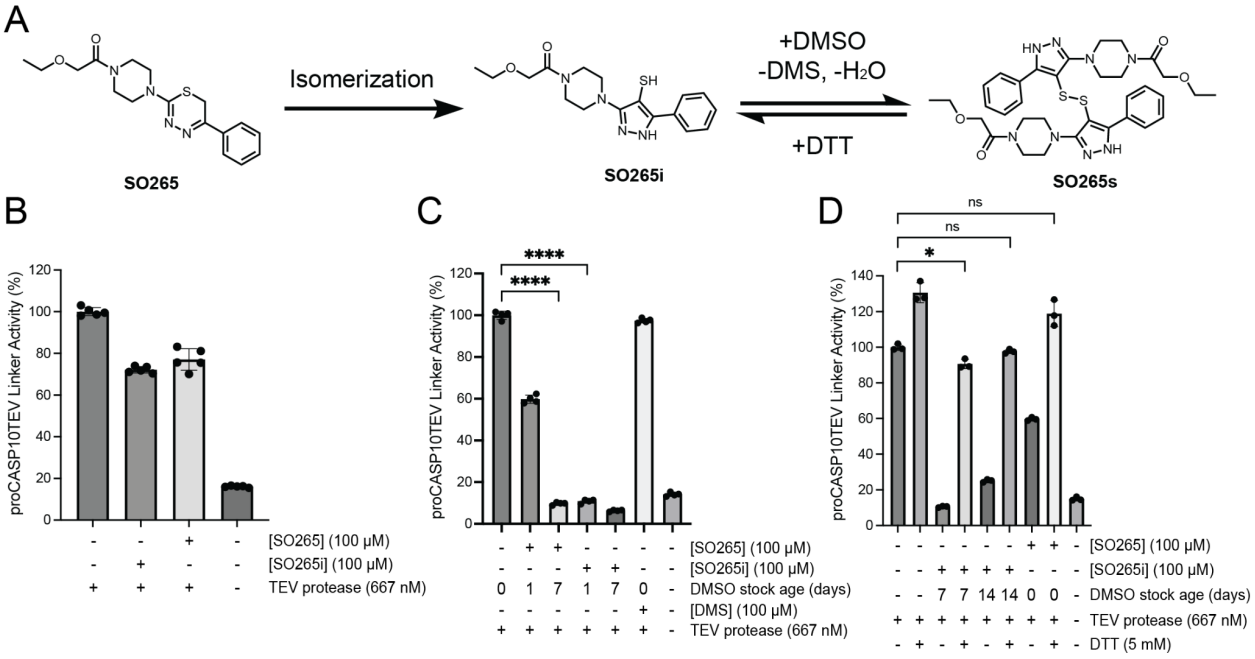

Figure 4. The rearranged product of SO265 inhibits proCASP10TEV Linker activity. (A) Proposed scheme of **SO265** isomerization and formation of the disulfide product (B) Relative activity of proCASP10 Linker protein (333 nM) treated with the indicated compounds for 1h followed by addition of TEV protease (667 nM) and fluorogenic substrate (Ac-VDAVAD-AFC, 10 µM, and 333 mM sodium citrate) in PBS buffer. (C) The indicated compound stocks were subjected to either one- or seven-day incubation in DMSO at ambient conditions. Subsequently, compound-treated proCASP10 Linker protein was assayed as in 'B' with 1h pre-exposure to either dimethyl sulfide (DMS) or the indicated compounds. (D) Compounds incubated for the indicated days in DMSO were further subjected to DTT (5 mM DTT) followed by evaluation for caspase inhibition as described in 'B.' For B-D, data represent mean values ± standard deviation for four biological replicates. Statistical significance was calculated with unpaired Student's t-tests, * $p<0.05$, **** $p<0.0001$, ns, not significant $p>0.05$.

CETSA confirms caspase-10 labeling. As all our data, thus far, had been assessed for recombinant protein, we next opted to extend our analyses to assess the compound engagement of endogenous procaspase-8 and -10. For this, we turned to Cellular Thermal Shift Assay (CETSA)[58] to measure binding-induced changes to protein thermal stability. To validate our assay, we subjected Jurkat lysates spiked with recombinant hexahistidine-tagged proCASP10 to CETSA analysis, comparing the thermal stability of the proCASP10 construct to that of the inactive catalytic cysteine mutant construct (proCASP10 C401A) with and without addition of **KB7**, as a positive control. We observe a marked decrease in thermal stability upon **KB7** treatment for both the endogenous (anti-caspase-10 signal) and recombinant (anti-His signal) caspase-10 proteins (**Figure 5A** and complete blots in **Figure S35**). The C401A mutant protein did not show a similar thermal shift (**Figure S36**), which is consistent with the covalent modification of the C401, which is the catalytic nucleophile, by **KB7**. Extension of this analysis revealed that, like **KB7**, **PFTμ** induced destabilization of the wildtype spiked proCASP10 and endogenous proCASP10 (**Figure 5B** and complete blots in **Figure S37**) but not the C401A mutant protein (**Figure 5C** and complete blots in **Figure S38**), which further confirms that **PFTμ** labels C401 Unexpectedly, the disulfide product (**SO265s**) caused some protein stabilization, suggesting an alternate mode of action compared to the two active site-directed inhibitors (**Figure 5D** and complete blots in **Figure S39**). Corroborating an alternate mode of engagement by **SO265s**, we observed no competition in gel-based ABPP analysis using the **KB61** click probe against procaspase-10 (**Figure S40A**), unlike **PFTμ** that labeled both procaspase-10 (**Figure S40A**) and procaspase-8 (**Figure S40B**). Disappointingly, we observed no similar compound-induced thermal stability shift for

endogenous procaspase-8 upon **KB7** treatment (**Figure S35**) nor **PFTμ** treatment (**Figure S37**), indicating that the CETSA assay was not suitable for evaluation of caspase-8 target engagement. Therefore, we returned to enzyme activity assays for broader target analysis.

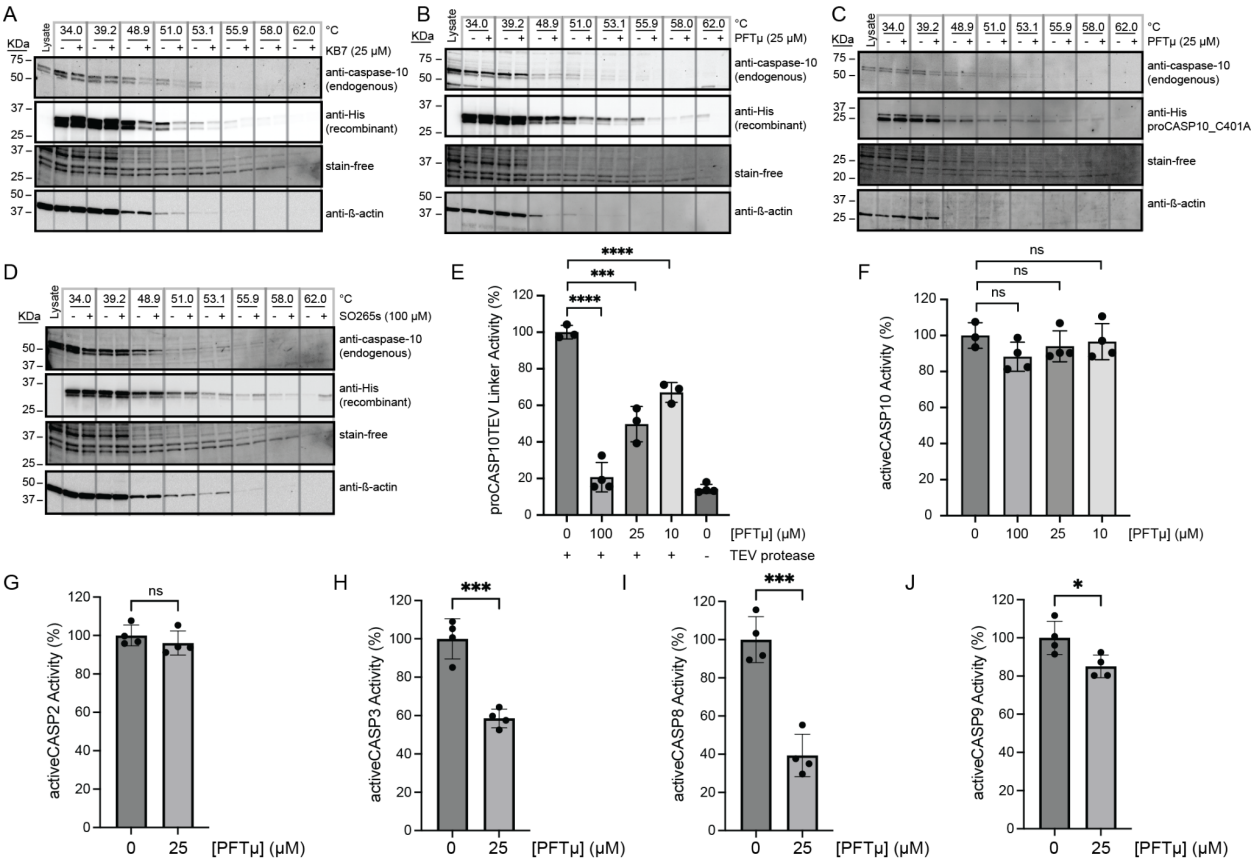

Figure 5. PFTμ and SO265s impact the stability of both recombinant and endogenous procaspase-10. (A-D) Cellular thermal shift assay (CETSA)[58] analysis blot of Jurkat cell lysates spiked with the indicated recombinant caspase-10 proteins featuring C-terminal hexahistidine tag and treated with the indicated compounds at the indicated concentrations or vehicle (DMSO) and subjected to immunoblot analysis for using both anti-His and anti-caspase-10 antibodies to visualize recombinant and endogenous protein, respectively. Loading was visualized both with the BioRad Chemidoc Stain-Free

imaging technology[59] and with anti-β-actin. For 'A, B, and D,' recombinant proCASP10 and for 'C,' recombinant proCASP10_C401A were analyzed. (E) Relative activity of proCASP10TEV Linker protein (333 nM concentration in PBS buffer) exposed to **PFTμ** at the indicated concentrations for 1h followed by TEV protease (667 nM) and analysis with Ac-VDVAD-AFC fluorogenic substrate (10 μM) in PBS supplemented with 333 mM sodium citrate. (F-J) Relative activity of recombinant active caspases in PBS buffer analyzed with Ac-VDVAD-AFC fluorogenic substrate (10 μM) after treatment with the indicated concentrations of **PFTμ** for 1h. For activeCASP10, fluorogenic substrate (10 μM) in PBS was supplemented with 333 mM citrate. Recombinant proteins used in 'F' activeCASP10 (333 nM), 'G' activeCASP-2 (0.3 μM), 'H' activeCASP-3 (0.3 μM), and 'I' activeCASP9 (1 μM). For A–D, data is representative of two biological replicates. For E–J, data represent mean values ± standard deviation for four biological replicates. Statistical significance was calculated with unpaired Student's t-tests, * $p<0.05$, *** $p<0.001$, **** $p<0.0001$, ns, not significant $p>0.05$.

Pifithrin-μ is a promiscuous caspase inhibitor that prevents FasL-mediated apoptosis. In contrast with the complex activation mechanism of **SO265s**, which likely could complicate assessing in-cell activity, we expected **PFTμ** to retain caspase inhibitory activity in complex cell environments. This expectation is further supported by **PFTμ's** well-documented anti-apoptotic activity, which has been ascribed to its function as a TP53 inhibitor[47]. Therefore, we prioritized **PFTμ** for further analysis. Activity assay analysis revealed that **PFTμ** showed some preferential inhibition across a panel of analyzed caspases; consistent with our screening data, we observed preferential inhibition of

procaspase-10 when compared to active caspase-10 (**Figure 5E**, **F**, and **Figure S14**, **S15**). Similarly, **PFTμ** also preferentially labeled procaspase-2, as analyzed using our caspase-2 directed click probe[24] and ABPP analysis (**Figure S41**). No detectable inhibition of active caspase-2 was observed, either by ABPP gel (**Figure S41**) or activity assay (**Figure 5G**). **PFTμ** also significantly inhibited active caspase-3 and active caspase-8, with slight, albeit significant, inhibition observed for active caspase-9 (**Figure 5H-J**). These data provided evidence that **PFTμ** is a promiscuous caspase inhibitor.

We next turned to chemoproteomics to more broadly assess whether PFTμ labels endogenous caspases. We deployed our established cysteine chemoproteomic platform[60] in which covalent labeling sites are identified in a competitive manner using the pan cysteine-reactive probe iodoacetamide alkyne (**IAA**) and isotopically enriched "light" and "heavy" biotin-azide capture reagents. Following the workflow shown in **Figure 6A**, out of 8925 total cysteines quantified, we find that 1070 total unique cysteines showed log2(H/L) values greater than 1.5, indicative of labeling by **PFTμ**. Included in this list were several known targets, including PARP1, HSP70 (HSPA1A), and PRDX proteins (PRDX1, PRDX2, PRDX5), which were previously identified via chemoproteomics using a clickable **PFTμ** analog[61], providing evidence of the robustness of our approach (**Table S2**). Quite strikingly, several caspases stood out as having high $\log_2$(H/L) ratios (**Figure 6B**), including caspase-8, which aligns with our aforementioned activity assay and gel-based ABPP analysis (**Figure 5I** and **Figure S40**). Aligning with our prior discovery[24] of structurally related phenylpropiolate molecules that label caspase-2 at C370, we also observe that C370 is highly sensitive to **PFTμ**, which is also consistent with our gel-based analysis (**Figure S41**). The noncatalytic cysteine residue, C264, in caspase-626, was also

observed to be labeled by **PFTμ**, as was the near-active site cysteine (C170) in caspase-3. We did not detect the catalytic cysteine nucleophile of caspase-3 (C163). Beyond these pro-apoptotic caspases, the catalytic cysteine in the pro-inflammatory caspase-4 (C258) was also labeled by **PFTμ**. The catalytic cysteine in caspase-10 was not identified, likely due to the long tryptic peptide that flanks this residue. Taken together, these data provide further evidence that **PFTμ** promiscuously labels many human caspases in addition to its previously reported targets.

Guided by these findings, we next asked whether **PFTμ** could protect cells from extrinsic apoptosis induced by Fas ligand (FasL). While **PFTμ's** anti-apoptotic activity has been reported in other contexts[47, 62-65], we selected FasL-mediated apoptosis as a model system due to the central role that caspase-8 and -10 play in this process[12, 66, 67] and the less central role of TP53[68, 69], with the goal of helping to define better the biologically active target(s) of **PFTμ's** anti-apoptotic activity. Using the CellTiter-Glo assay, we find that **PFTμ** affords near-complete protection from FasL (**Figure 6C**) without inducing cytotoxic effects (**Figure S42**). These data align with caspase inhibition as contributing to **PFTμ's** activity.

As our recent work has shown that electrophile stress can lead to the formation of stress granules[70], we also opted to rule out **PFTμ**-induced stress granules as a potential confounding variable. Using a ΔΔG3BP1/2 KO cell line that stably expresses GFP-G3BP1[71, 72], we find that **PFTμ** does not induce G3BP1 condensates using concentrations that are protective from apoptosis (**Figure 6D**) and are consistent with prior studies using **PFTμ** as a putative TP53 inhibitor[47]. Thus, we put forth a model (**Figure 6E**) that caspases are likely biological targets of **PFTμ** that contribute to the reported anti-apoptotic activity.

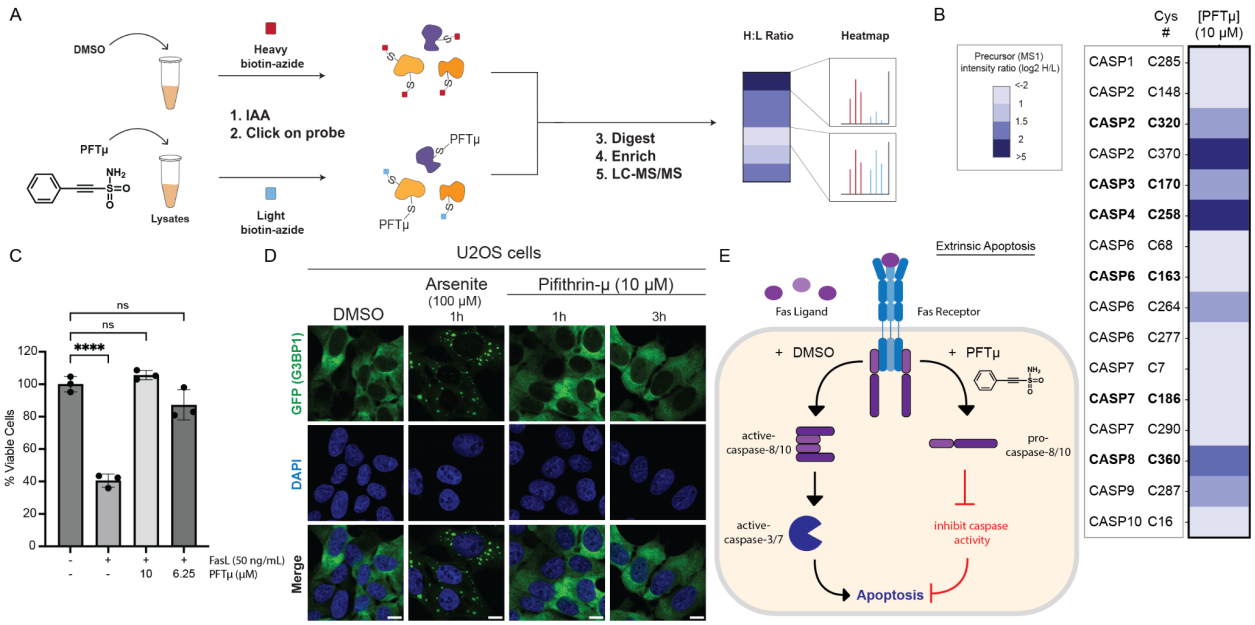

Figure 6. PFTμ labels initiator caspases and can protect Jurkat cells from FasL-mediated apoptosis. (A, B) Cysteine chemoproteomic analysis identifies protein targets of **PFTμ**. 'A' shows the general workflow in which Jurkat cell lysates were treated with either **PFTμ** (25 μM) or DMSO for 1h, followed by **IAA** (200 μM) cysteine capping, conjugated via click chemistry to isotopically differentiated biotin-azide reagents[73, 74], Single-Pot Solid-Phase-enhanced sample-preparation (SP3)[60, 75, 76] with on-resin tryptic digestion, enriched, and analyzed by LC-MS/MS. Heatmap in 'B' shows the mean quantified precursor intensity (log_2H/L) for DMSO (H, heavy) versus compound treatment (L, light) for all caspase cysteines identified. Catalytic cysteine residues are annotated in bold. (C) CellTiter-Glo® measurement of relative viability of Jurkat cells subjected to **PFTμ** at the indicated concentrations for 1h followed by FasL (50 ng/mL, 3h)-induced apoptosis. (D) Fluorescent microscopy of U2OS cells expressing GFP-G3BP1 and treated with **PFTμ** (10 μM) or positive control sodium arsenite. All scale bars = 10 μm. (E) Proposed model where **PFTμ** functions as a promiscuous initiator caspase inhibitor (labeling caspase-2, -

8, and -10) and blocks FasL-mediated extrinsic apoptosis. For B, experiments were conducted in four biological replicates, with two samples additionally analyzed as technical replicates. For C, data represent mean values ± standard deviation for three biological replicates. All MS data can be found in **Table S2**. Statistical significance was calculated with unpaired Student's t-tests, ****p<0.0001, ns, not significant p>0.05.

Discussion

To enable high throughput procaspase-10 inhibitor discovery, here we developed and applied an engineered TEV-activatable caspase-10 protein to high throughput screening. Our high quality (an average Z' of 0.58) ~100,000 compound semi-automated screen yielded 237 total hits with z-score < -3. Subsequent rescreening and counter-screening delineated bona fide procaspase-10 inhibitors from those with activity against active caspase-10 or TEV protease. Orthogonal mode of action studies confirmed target engagement for both recombinant and endogenous procaspase-10. Thus, we expect that the TEV-activatable screening platform should prove broadly useful in the discovery of inhibitors targeting precursor proteases.

Our work also highlights several intriguing opportunities for future screening efforts. As TEV protease is a cysteine protease, we found that several of our hits functioned via engaging TEV rather than procaspase-10. We expect that these newly identified TEV protease inhibitors could serve as useful tools for synthetic biology studies that rely on TEV protease activity to control engineered circuits. To favor caspase rather than TEV inhibitor discovery, future studies could also consider using alternative non-cysteine protease enzymes for activation, which we expect would prove more

substantially orthogonal to caspase cysteine protease activity. In addition to uncovering candidate TEV inhibitors, our screen also revealed that the thiadiazine chemotype is likely prone to disulfide rearrangement, as exemplified by our characterization of **SO265s**, which we found was the active species. Thus, our work both highlights the value of resynthesis in confirming screening hits and hints at the likely amenability of procaspase-10 to a disulfide trapping/tethering-style inhibitor discovery[77-79] using additional disulfide-containing compounds.

Beyond the **SO265** thiadiazine chemotype, **PFTμ**, a reported TP53 inhibitor, proved to be a key hit from our screen. Comparing active and procaspase-10 inhibitor activity, we found that **PFTμ** inhibited both proteoforms to some degree, with increased inhibition observed for the proenzyme. Looking beyond caspase-10, the in vitro, cell-based, and proteomic analysis together confirmed that **PFTμ** engages caspase-8, -3, -10, -5, and -6. These data allow us to put forth a model whereby **PFTμ's** reported activity as an anti-apoptotic agent is likely driven by caspase inhibition in addition to the previously reported TP53 inhibitory activity[47]. Therefore, we anticipate that the cysteine-reactive ethynesulfonamide chemotype will prove broadly useful as a starting point for caspase inhibitor development campaigns. We also expect our work to aid in phenotype interpretation for studies that have employed PFTμ to block p53 activity.

Acknowledgements

This study was supported by the National Institutes of Health DP2 OD030950-01 (K.M.B.), the Beckman Young Investigator Award (K.M.B.), the UCLA DOE Institute (DE-FC02-02ER63421), the NSF GRFP (1000235263), and the NIGMS System and Integrative Biology 5T32GM008185-33 (L.M.B.). We thank all members of the Backus lab for their helpful suggestions, Michael Lenardo for providing plasmids encoding caspase-10, and Dennis Wolan for providing the **Rho-DEVD-AOMK** probe.

Conflicts of Interest

The authors declare no financial or commercial conflict of interest.

DATA AVAILABILITY The MS data have been deposited to the ProteomeXchange Consortium (http://proteomecentral.proteomexchange.org) via the PRIDE partner repository with the dataset identifier PXD053315

Username: reviewer_pxd053315@ebi.ac.uk

Password: ut5UBouFBb4x

The UCLA Molecular Screening Shared Resource is supported by Jonsson Comprehensive Cancer Center, award number P30CA016042 by the National Cancer Institute of the National Institutes of Health.

References

1. Horn, S., et al., *Caspase-10 Negatively Regulates Caspase-8-Mediated Cell Death, Switching the Response to CD95L in Favor of NF-κB Activation and Cell Survival.* Cell Reports, 2017. **19**(4): p. 785-797.

2. Yang, C.Y., et al., *Deciphering DED assembly mechanisms in FADD-procaspase-8-cFLIP complexes regulating apoptosis.* Nat Commun, 2024. **15**(1): p. 3791.

3. Wang, J., et al., *Caspase-10 is an initiator caspase in death receptor signaling.* Proceedings of the National Academy of Sciences, 2001. **98**(24): p. 13884-13888.

4. Julien, O. and J.A. Wells, *Caspases and their substrates.* Cell Death & Differentiation, 2017. **24**(8): p. 1380-1389.

5. Wang, L., et al., *Biochemical Tools for Tracking Proteolysis.* J Proteome Res, 2021. **20**(12): p. 5264-5279.

6. Eskandari, E., et al., *Dependence of human cell survival and proliferation on the CASP3 prodomain.* Cell Death Discovery, 2024. **10**(1).

7. Alam, A., et al., *Early Activation of Caspases during T Lymphocyte Stimulation Results in Selective Substrate Cleavage in Nonapoptotic Cells.* The Journal of Experimental Medicine, 1999. **190**(12): p. 1879-1890.

8. Pistritto, G., et al., *Expression and transcriptional regulation of caspase-14 in simple and complex epithelia.* Cell Death & Differentiation, 2002. **9**(9): p. 995-1006.

9. Lippens, S., et al., *Epidermal differentiation does not involve the pro-apoptotic executioner caspases, but is associated with caspase-14 induction and processing.* Cell Death & Differentiation, 2000. **7**(12): p. 1218-1224.

10. Gorelick-Ashkenazi, A., et al., *Caspases maintain tissue integrity by an apoptosis-independent inhibition of cell migration and invasion.* Nature Communications, 2018. **9**(1).

11. Shao, W., et al., *The Caspase-1 Digestome Identifies the Glycolysis Pathway as a Target during Infection and Septic Shock.* Journal of Biological Chemistry, 2007. **282**(50): p. 36321-36329.

12. Consonni, F., et al., *Study of the potential role of CASPASE-10 mutations in the development of autoimmune lymphoproliferative syndrome.* Cell Death & Disease, 2024. **15**(5).

13. Krug, H.F., *Caspase-10 is the key initiator caspase involved in tributyltin-mediated apoptosis in human immune cells.* J Toxicol, 2012. **2012**: p. 395482.

14. Philip, N.H., et al., *Caspase-8 mediates caspase-1 processing and innate immune defense in response to bacterial blockade of NF-κB and MAPK signaling.* Proceedings of the National Academy of Sciences, 2014. **111**(20): p. 7385-7390.

15. Rieux-Laucat, F., F. Le Deist, and A. Fischer, *Autoimmune lymphoproliferative syndromes: genetic defects of apoptosis pathways.* Cell Death & Differentiation, 2003. **10**(1): p. 124-133.

16. Olsson, M. and B. Zhivotovsky, *Caspases and cancer.* Cell Death & Differentiation, 2011. **18**(9): p. 1441-1449.

17. Cui, Z., et al., *Caspase-8 mutations associated with head and neck cancer differentially retain functional properties related to TRAIL-induced apoptosis and cytokine induction.* Cell Death & Disease, 2021. **12**(8).

18. Jiang, M., et al., *The caspase-3/GSDME signal pathway as a switch between apoptosis and pyroptosis in cancer.* Cell Death Discovery, 2020. **6**(1).

19. Groborz, K.M., et al., *Selective chemical reagents to investigate the role of caspase 6 in apoptosis in acute leukemia T cells.* Chemical Science, 2023. **14**(9): p. 2289-2302.

20. Shaulov-Rotem, Y., et al., *A novel quenched fluorescent activity-based probe reveals caspase-3 activity in the endoplasmic reticulum during apoptosis.* Chemical Science, 2016. **7**(2): p. 1322-1337.

21. De Calignon, A., et al., *Caspase activation precedes and leads to tangles.* Nature, 2010. **464**(7292): p. 1201-1204.

22. Boxer, M.B., et al., *A Highly Potent and Selective Caspase 1 Inhibitor that Utilizes a Key 3-Cyanopropanoic Acid Moiety.* ChemMedChem, 2010. **5**(5): p. 730-738.

23. Bosc, E., et al., *Genuine selective caspase-2 inhibition with new irreversible small peptidomimetics.* Cell Death & Disease, 2022. **13**(11).

24. Castellón, J.O., et al., *Chemoproteomics Identifies State-Dependent and Proteoform-Selective Caspase-2 Inhibitors.* Journal of the American Chemical Society, 2024. **146**(22): p. 14972-14988.

25. Tubeleviciute-Aydin, A., et al., *Identification of Allosteric Inhibitors against Active Caspase-6.* Scientific Reports, 2019. **9**(1).

26. Van Horn, K.S., et al., *Engaging a Non-catalytic Cysteine Residue Drives Potent and Selective Inhibition of Caspase-6.* Journal of the American Chemical Society, 2023. **145**(18): p. 10015-10021.

27. Backus, K.M., et al., *Proteome-wide covalent ligand discovery in native biological systems.* Nature, 2016. **534**(7608): p. 570-574.

28. Bucur, O., et al., *A novel caspase 8 selective small molecule potentiates TRAIL-induced cell death.* Scientific Reports, 2015. **5**(1): p. 9893.

29. Dhani, S., Y. Zhao, and B. Zhivotovsky, *A long way to go: caspase inhibitors in clinical use.* Cell Death & Disease, 2021. **12**(10).

30. Lopez-Hernandez, F.J., et al., *Z-FA-fmk inhibits effector caspases but not initiator caspases 8 and 10, and demonstrates that novel anticancer retinoid-related molecules induce apoptosis via the intrinsic pathway.* Mol Cancer Ther, 2003. **2**(3): p. 255-63.

31. Jänicke, R.U., et al., *Caspase-10 in mouse or not?* Science, 2006. **312**(5782): p. 1874.

32. Sprick, M.R., et al., *FADD/MORT1 and Caspase-8 Are Recruited to TRAIL Receptors 1 and 2 and Are Essential for Apoptosis Mediated by TRAIL Receptor 2.* Immunity, 2000. **12**(6): p. 599-609.

33. Bodmer, J.-L., et al., *TRAIL receptor-2 signals apoptosis through FADD and caspase-8.* Nature Cell Biology, 2000. **2**(4): p. 241-243.

34. Juo, P., et al., *Essential requirement for caspase-8/FLICE in the initiation of the Fas-induced apoptotic cascade.* Current Biology, 1998. **8**(18): p. 1001-1008.

35. Kawahara, A., et al., *Caspase-independent Cell Killing by Fas-associated Protein with Death Domain.* The Journal of Cell Biology, 1998. **143**(5): p. 1353-1360.

36. Grotzer, M.A., et al., *Resistance to TRAIL-induced apoptosis in primitive neuroectodermal brain tumor cells correlates with a loss of caspase-8 expression.* Oncogene, 2000. **19**(40): p. 4604-4610.

37. Teitz, T., et al., *Caspase 8 is deleted or silenced preferentially in childhood neuroblastomas with amplification of MYCN.* Nature Medicine, 2000. **6**(5): p. 529-535.

38. Mühlethaler-Mottet, A., et al., *Individual caspase-10 isoforms play distinct and opposing roles in the initiation of death receptor-mediated tumour cell apoptosis.* Cell Death & Disease, 2011. **2**(3): p. e125-e125.

39. Chun, H.J., et al., *Pleiotropic defects in lymphocyte activation caused by caspase-8 mutations lead to human immunodeficiency.* Nature, 2002. **419**(6905): p. 395-399.

40. Grønbaek, K., et al., *The V410I (G1228A) variant of the caspase-10 gene is a common polymorphism of the Danish population.* Blood, 2000. **95**(6): p. 2184-5.

41. Nagar, B., et al., *Crystal Structures of the Kinase Domain of c-Abl in Complex with the Small Molecule Inhibitors PD173955 and Imatinib (STI-571)1.* Cancer Research, 2002. **62**(15): p. 4236-4243.

42. Capdeville, R., et al., *Glivec (STI571, imatinib), a rationally developed, targeted anticancer drug.* Nature Reviews Drug Discovery, 2002. **1**(7): p. 493-502.

43. van Montfort, R.L.M. and P. Workman, *Structure-based design of molecular cancer therapeutics.* Trends in Biotechnology, 2009. **27**(5): p. 315-328.

44. Lin, Y.-L., et al., *Explaining why Gleevec is a specific and potent inhibitor of Abl kinase.* Proceedings of the National Academy of Sciences, 2013. **110**(5): p. 1664-1669.

45. Xu, J.H., et al., *Integrative X-ray Structure and Molecular Modeling for the Rationalization of Procaspase-8 Inhibitor Potency and Selectivity.* ACS Chemical Biology, 2020. **15**(2): p. 575-586.

46. Zhang, J.H., T.D. Chung, and K.R. Oldenburg, *A Simple Statistical Parameter for Use in Evaluation and Validation of High Throughput Screening Assays.* J Biomol Screen, 1999. **4**(2): p. 67-73.

47. Strom, E., et al., *Small-molecule inhibitor of p53 binding to mitochondria protects mice from gamma radiation.* Nat Chem Biol, 2006. **2**(9): p. 474-9.

48. Gray, D.C., S. Mahrus, and J.A. Wells, *Activation of Specific Apoptotic Caspases with an Engineered Small-Molecule-Activated Protease.* Cell, 2010. **142**(4): p. 637-646.

49. Oberst, A., et al., *Inducible Dimerization and Inducible Cleavage Reveal a Requirement for Both Processes in Caspase-8 Activation.* Journal of Biological Chemistry, 2010. **285**(22): p. 16632-16642.

50. Kim, K., et al., *High throughput screening of small molecule libraries for modifiers of radiation responses.* International Journal of Radiation Biology, 2011. **87**(8): p. 839-845.

51. Sander, T., et al., *DataWarrior: an open-source program for chemistry aware data visualization and analysis.* J Chem Inf Model, 2015. **55**(2): p. 460-73.

52. Pierce, J.W., et al., *Novel Inhibitors of Cytokine-induced IκBα Phosphorylation and Endothelial Cell Adhesion Molecule Expression Show Anti-inflammatory Effects in Vivo.* Journal of Biological Chemistry, 1997. **272**(34): p. 21096-21103.

53. Kraft, M., et al., *A fluorogenic substrate as quantitative in vivo reporter to determine protein expression and folding of tobacco etch virus protease in Escherichia coli.* Protein Expression and Purification, 2007. **52**(2): p. 478-484.

54. Nam, H., et al., *Tobacco etch virus (TEV) protease with multiple mutations to improve solubility and reduce self-cleavage exhibits enhanced enzymatic activity.* FEBS Open Bio, 2020. **10**(4): p. 619-626.

55. Gerasimova, E.L., et al., *Antioxidant properties of 2,5-substituted 6H-1,3,4-thiadiazines promising for experimental therapy of diabetes mellitus.* Russian Chemical Bulletin, 2022. **71**(12): p. 2730-2739.

56. Yiannios, C.N. and J.V. Karabinos, *Oxidation of Thiols by Dimethyl Sulfoxide.* The Journal of Organic Chemistry, 1963. **28**(11): p. 3246-3248.

57. Wallace, T.J. and J.J. Mahon, *Reactions of Thiols with Sulfoxides. II. Kinetics and Mechanistic Implications.* Journal of the American Chemical Society, 1964. **86**(19): p. 4099-4103.

58. Jafari, R., et al., *The cellular thermal shift assay for evaluating drug target interactions in cells.* Nature Protocols, 2014. **9**(9): p. 2100-2122.

59. Ghosh, R., J.E. Gilda, and A.V. Gomes, *The necessity of and strategies for improving confidence in the accuracy of western blots.* Expert Review of Proteomics, 2014. **11**(5): p. 549-560.

60. Yan, T., et al., *SP3-FAIMS Chemoproteomics for High-Coverage Profiling of the Human Cysteinome**.* ChemBioChem, 2021. **22**(10): p. 1841-1851.

61. Yang, J., et al., *PES derivative PESA is a potent tool to globally profile cellular targets of PES.* Bioorg Med Chem Lett, 2022. **60**: p. 128553.

62. Maj, M.A., et al., *Inhibition of Mitochondrial p53 Accumulation by PFT-mu Prevents Cisplatin-Induced Peripheral Neuropathy.* Front Mol Neurosci, 2017. **10**: p. 108.

63. Sekihara, K., et al., *Pifithrin-mu, an inhibitor of heat-shock protein 70, can increase the antitumor effects of hyperthermia against human prostate cancer cells.* PLoS One, 2013. **8**(11): p. e78772.

64. Yang, L.Y., et al., *The p53 inactivators pifithrin-mu and pifithrin-alpha mitigate TBI-induced neuronal damage through regulation of oxidative stress, neuroinflammation, autophagy and mitophagy.* Exp Neurol, 2020. **324**: p. 113135.

65. Zhu, J., et al., *Pifithrin-alpha alters p53 post-translational modifications pattern and differentially inhibits p53 target genes.* Sci Rep, 2020. **10**(1): p. 1049.

66. Coe, G.L., et al., *Ceramide mediates FasL-induced caspase 8 activation in colon carcinoma cells to enhance FasL-induced cytotoxicity by tumor-specific cytotoxic T lymphocytes.* Scientific Reports, 2016. **6**(1): p. 30816.

67. Milhas, D., et al., *Caspase-10 Triggers Bid Cleavage and Caspase Cascade Activation in FasL-induced Apoptosis.* Journal of Biological Chemistry, 2005. **280**(20): p. 19836-19842.

68. Uriarte, S.M., et al., *Akt inhibition upregulates FasL, downregulates c-FLIPs and induces caspase-8-dependent cell death in Jurkat T lymphocytes.* Cell Death & Differentiation, 2005. **12**(3): p. 233-242.

69. Mohr, A., et al., *Caspase-10: a molecular switch from cell-autonomous apoptosis to communal cell death in response to chemotherapeutic drug treatment.* Cell Death & Differentiation, 2018. **25**(2): p. 340-352.

70. Julio, A.R., et al., *Delineating cysteine-reactive compound modulation of cellular proteostasis processes.* Nature Chemical Biology, 2024.

71. Kedersha, N., et al., *G3BP–Caprin1–USP10 complexes mediate stress granule condensation and associate with 40S subunits.* Journal of Cell Biology, 2016. **212**(7): p. 845-860.

72. Götte, B., et al., *Separate domains of G3BP promote efficient clustering of alphavirus replication complexes and recruitment of the translation initiation machinery.* PLOS Pathogens, 2019. **15**(6): p. e1007842.

73. Shikwana, F., et al., *CySP3-96 enables scalable, streamlined, and low-cost sample preparation for cysteine chemoproteomic applications*. 2024, American Chemical Society (ACS).

74. Yan, T., et al., *Enhancing Cysteine Chemoproteomic Coverage through Systematic Assessment of Click Chemistry Product Fragmentation.* Analytical Chemistry, 2022. **94**(9): p. 3800-3810.

75. Hughes, C.S., et al., *Ultrasensitive proteome analysis using paramagnetic bead technology.* Molecular Systems Biology, 2014. **10**(10): p. 757.

76. Hughes, C.S., et al., *Single-pot, solid-phase-enhanced sample preparation for proteomics experiments.* Nature Protocols, 2019. **14**(1): p. 68-85.

77. Hallenbeck, K.K., et al., *A Liquid Chromatography/Mass Spectrometry Method for Screening Disulfide Tethering Fragments.* SLAS Discovery, 2018. **23**(2): p. 183-192.

78. Sadowsky, J.D., et al., *Turning a protein kinase on or off from a single allosteric site via disulfide trapping.* Proceedings of the National Academy of Sciences, 2011. **108**(15): p. 6056-6061.

79. Erlanson, D.A., et al., *Site-directed ligand discovery.* Proceedings of the National Academy of Sciences, 2000. **97**(17): p. 9367-9372.

SUPPORTING INFORMATION

An activation-based high throughput screen identifies caspase-10 inhibitors

José O. Castellón[1], Connie Yuen[6], Brandon Han[6], Katrina H. Andrews[1,2], Samuel Ofori[1,2], Ashley Julio[1,2], Lisa M. Boatner[1, 2], Maria F. Palafox[1], Nitesh Perumal[1,2], Robert Damoiseaux[4,5,6,7,8], Keriann M. Backus[1, 2,3,4,5*]

1. Biological Chemistry Department, David Geffen School of Medicine, UCLA, Los Angeles, CA,90095, USA
2. Department of Chemistry and Biochemistry, UCLA, CA 90095, USA
3. DOE Institute for Genomics and Proteomics, UCLA, Los Angeles, CA 90095, USA
4. Jonsson Comprehensive Cancer Center, UCLA, Los Angeles, CA 90095, USA
5. Eli and Edythe Broad Center of Regenerative Medicine and Stem Cell Research, UCLA, Los Angeles, CA 90095 USA
6. California NanoSystems Institute (CNSI), UCLA, Los Angeles, CA, 90095, United States
7. Department of Molecular and Medical Pharmacology, UCLA, Los Angeles, CA, 90095, USA
8. Department of Bioengineering, Samueli School of Engineering, UCLA, Los Angeles, CA, 90095, USA

The UCLA Molecular Screening Shared Resource is supported by Jonsson Comprehensive Cancer Center, award number P30CA016042 by the National Cancer Institute of the National Institutes of Health.

* Corresponding Author: Keriann M. Backus, Biological Chemistry Department, David Geffen School of Medicine, UCLA, Los Angeles, CA, 90095, USA, E-mail: kbackus@mednet.ucla.edu.

Table of Contents

(A) Supplementary Schemes

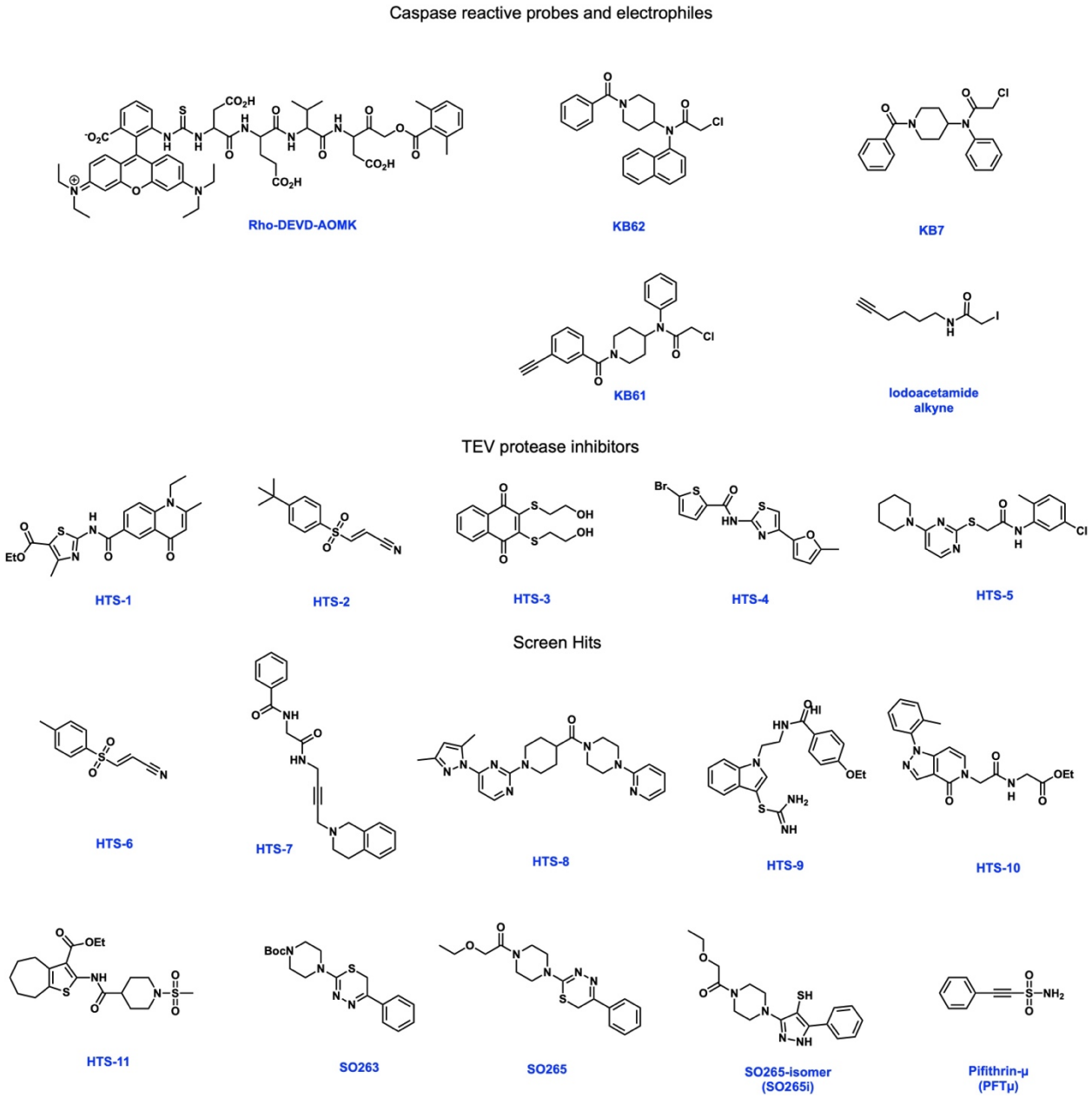

Scheme S1. Structure of compounds used in this study, including previously reported compounds **KB7**, **KB61**, and **KB62**[1].

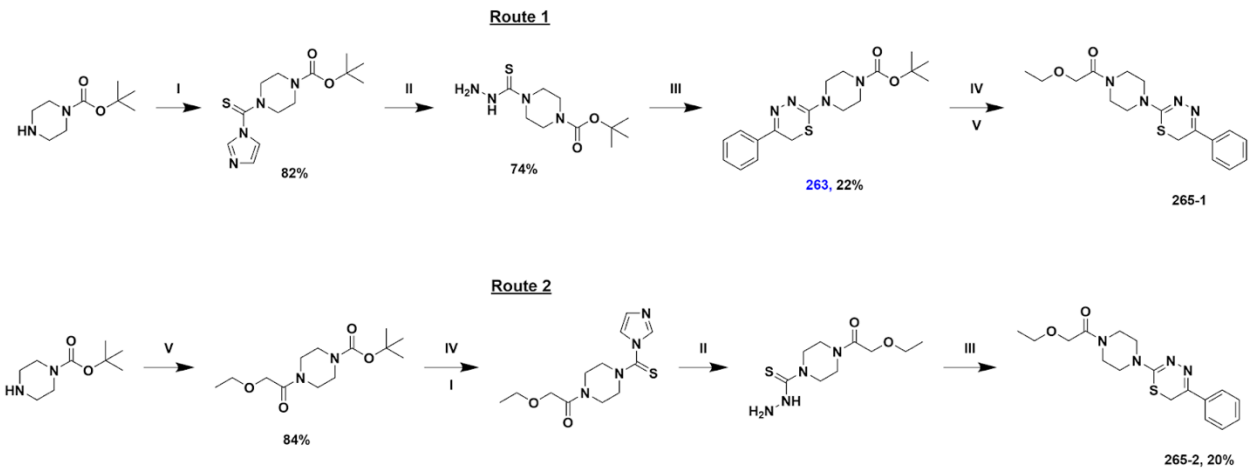

Scheme S2: Synthesis of 263, 265-1, 265-2 : (I)1,1′-Thiocarbonyldiimidazole, CH_2Cl_2, rt, 24 h (II) Hydrazine monohydrate, EtOH, 80 ^oC, 3 h (III) 2-Bromoacetophenone, EtOH, 80 ^oC, 0.5 h (IV) TFA, CH_2Cl_2, rt, 1-2 h., (V) 2-Ethoxyacetyl chloride, Et_3N, CH_2Cl_2, 0 ^oC - rt, 18h.

(B) Supplementary Figures

```
Wildtype                  FGAVYSSDEALIPIREIMSHFTALQCPRLAEKPKLFFIQACQGEEIQPSVSIEAD-----   415
procASP10TEVx2            FGAVYSSDEALIPIREIMSHFTALQCPRLAEKPKLFFIQACQGEEIQPSVSIE--AENLY   418
proCAPS10 C401A           FGAVYSSDEALIPIREIMSHFTALQCPRLAEKPKLFFIQAAQGEEIQPSVSIEAD-----   415
proCASP10TEV              FGAVYSSDEALIPIREIMSHFTALQCPRLAEKPKLFFIQACQGEEIQPSVSIE--AENLY   418
proCASP10TEV Linker       FGAVYSSDEALIPIREIMSHFTALQCPRLAEKPKLFFIQACQGEEIQPSVSIEAAAENLY   420
proCASP10TEV D435A        FGAVYSSDEALIPIREIMSHFTALQCPRLAEKPKLFFIQACQGEEIQPSVSIE--AENLY   418
                          ************************************.************

Wildtype                  ---ALNPEQAPTSLQDSIPAEA------DFLLGLATVPGYVSFRHVEEGSWYIQSLCNHL   466
procASP10TEVx2            FQGALNPEQAPTSLQDSIPAEAENLYFQGFLLGLATVPGYVSFRHVEEGSWYIQSLCNHL   478
proCAPS10 C401A           ---ALNPEQAPTSLQDSIPAEA------DFLLGLATVPGYVSFRHVEEGSWYIQSLCNHL   466
proCASP10TEV              FQGALNPEQAPTSLQDSIPAEA------DFLLGLATVPGYVSFRHVEEGSWYIQSLCNHL   472
proCASP10TEV Linker       FQGALNPEQAPTSLQDSIPAEA------DFLLGLATVPGYVSFRHVEEGSWYIQSLCNHL   474
proCASP10TEV D435A        FQGALNPEQAPTSLQDSIPAE-------AFLLGLATVPGYVSFRHVEEGSWYIQSLCNHL   471
                             ******************      .******************************
```

Figure S1. Sequences modified to generate the indicated engineered caspase-10 proteins. Shows sequence alignments for the amino acid region of caspase-10 (Q92851-4, 10-L isoform**)** engineered to insert the indicated mutations and TEV cleavage motifs. Catalytic cysteine (C401) is highlighted in yellow. residue highlighted in green indicates proteolytic target aspartate residue, pink residues correspond to TEV protease proteolytic recognition sequence. Suspected additional cleavage site, D435 was replaced with an additional TEV cleavage motif (proCASP10TEVx2).

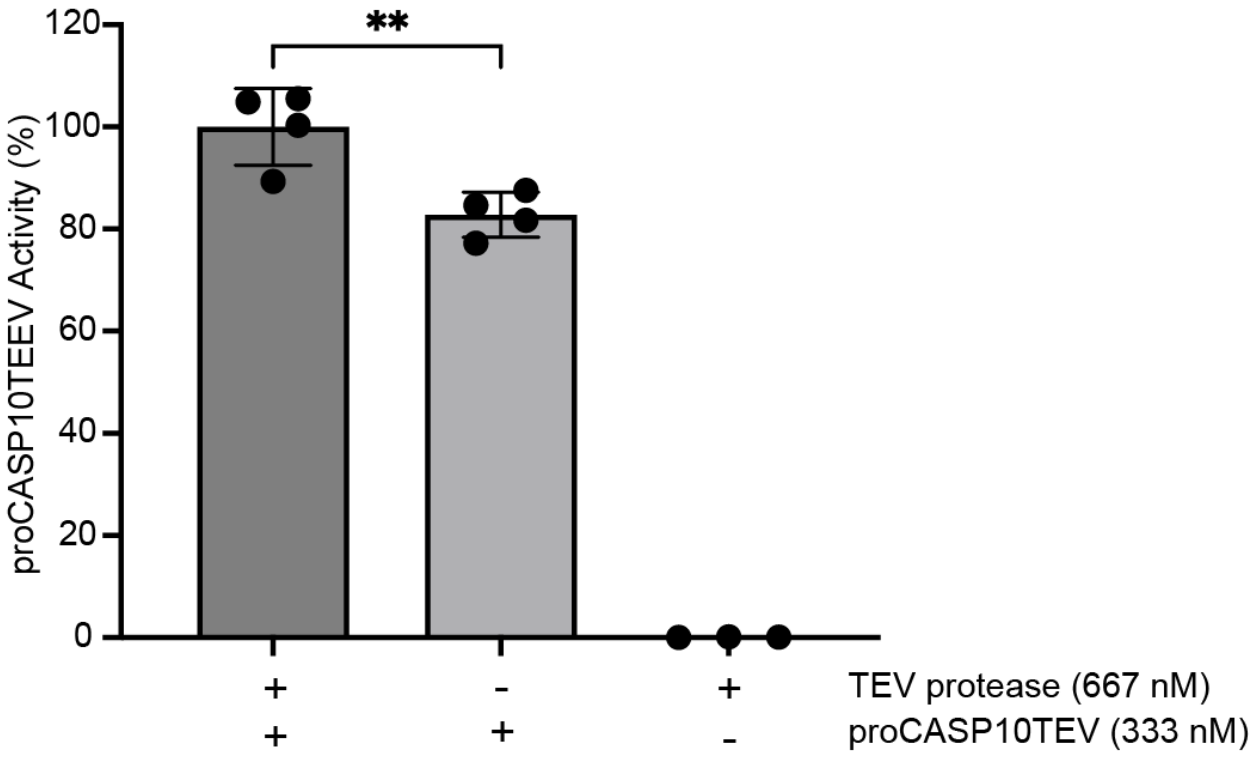

Figure S2. **proCASP10TEV has higher background activity in the absence of TEV protease**. Activity of a proCASP10TEV (333 nM final concentration) stored in the -80 ºC after treatment with TEV protease (667 nM) solution containing 333 mM citrate, 5 mM DTT, and 10 μM **Ac-VDVAC-AFC** substrate in PBS. Data represents mean values and standard deviation (n = 4 biological replicates). Statistical significance was calculated with unpaired Student's t-tests, **p<0.001.

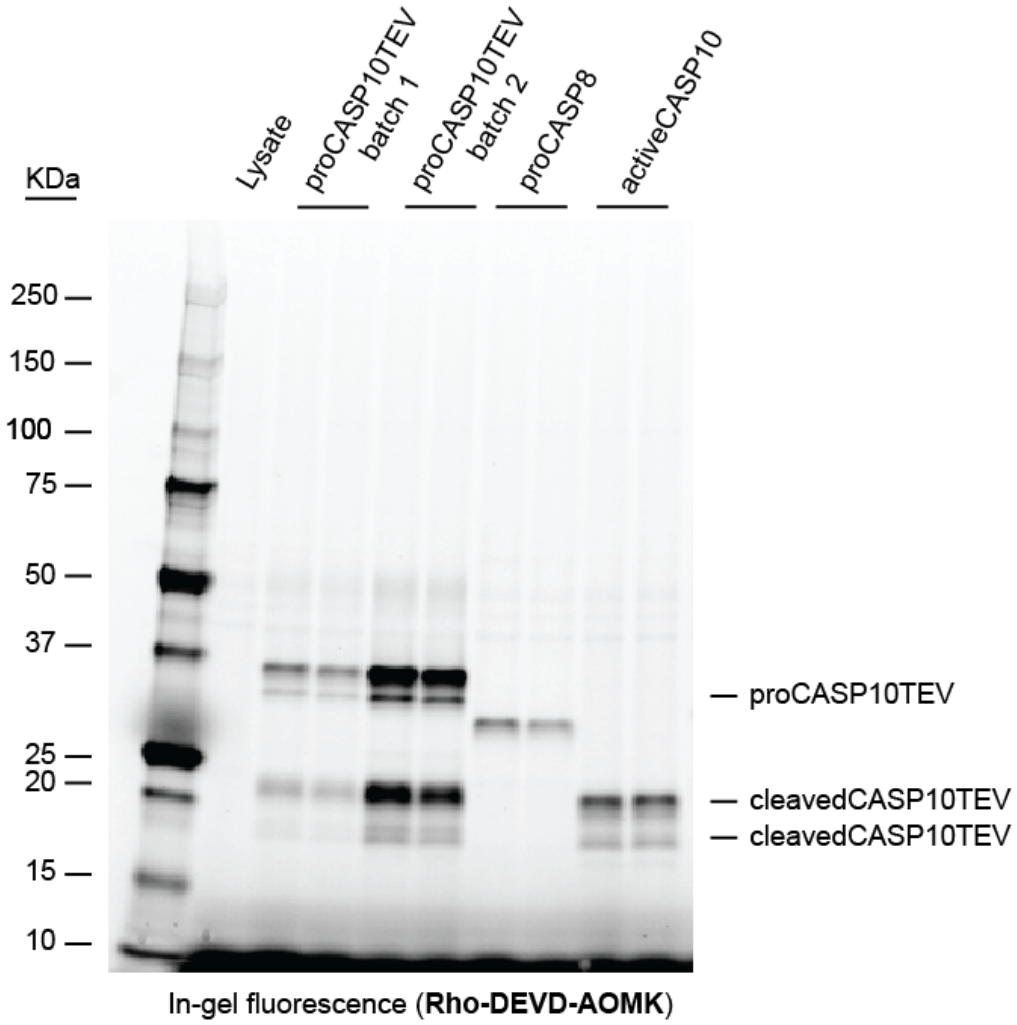

Figure S3. **proCASP10TEV self-activates in the absence of TEV protease**. **Rho-DEVD-AOMK** (1 μM) was used to visualize proCASP10TEV by gel-based ABPP. Both batches of recombinant protein show cleaved protein (~20 kDa band), consistent with the molecular weight of activeCASP10. ProCAP10, proCASP8 and activeCASP10 were prepared in PBS buffer at a final concentration of 1 μM in duplicates and treated with **Rho-DEVD-AOMK** for 1h at ambient conditions.

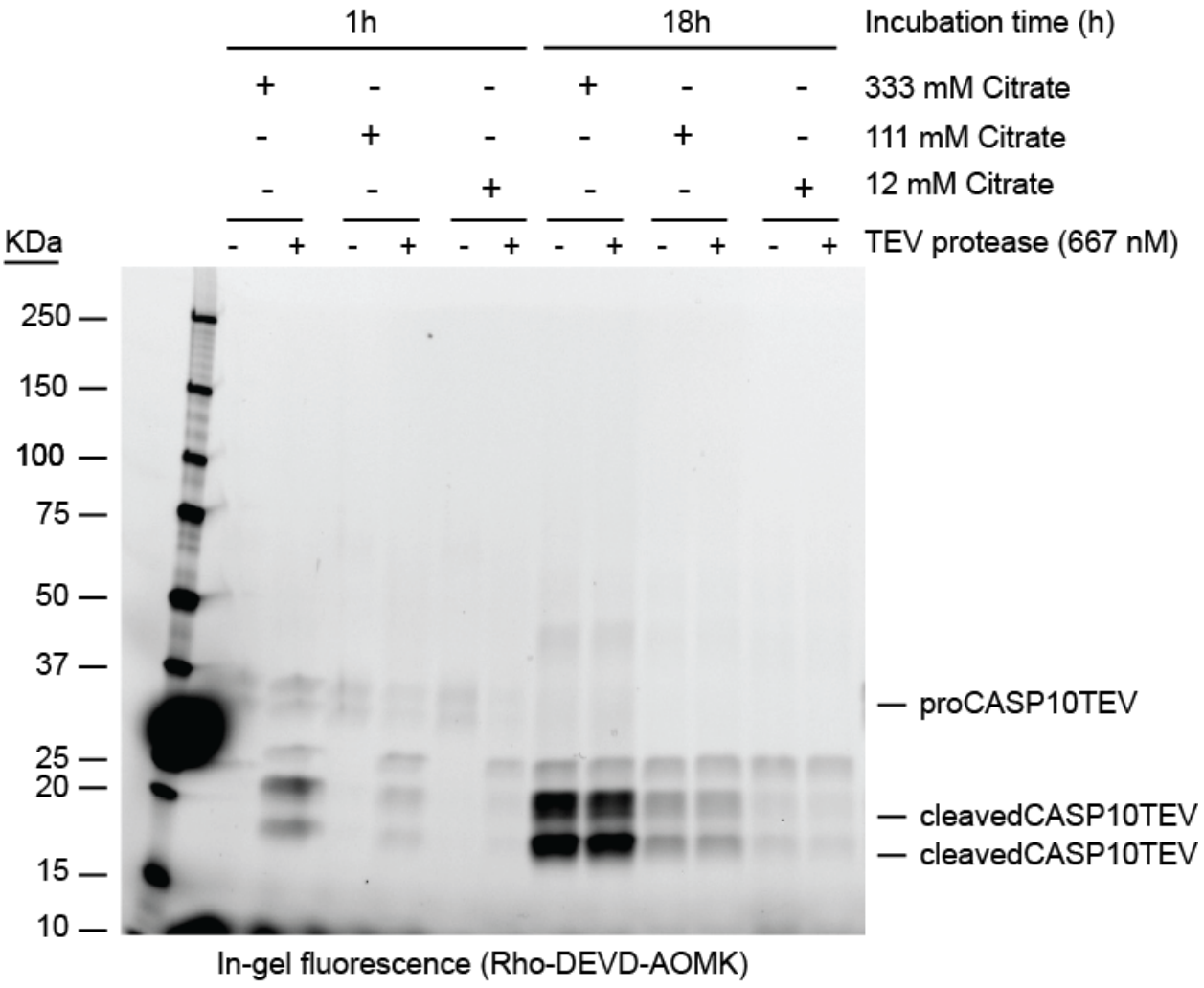

Figure S4. **proCASP10TEV self-activation increases over time and is enhanced by the addition of sodium citrate kosmotrope.** Recombinant proCASP10TEV (300 nM) was subjected to incubation in storage buffer (20 mM Tris-HCl pH 7.2, 50 mM NaCl, 1 mM DTT) for the indicated times with or without addition of TEV protease (667 nM) and sodium citrate (pH 7.4) at the indicated concentrations (333 mM, 111 mM, and 12 mM). Protein activity was then visualized by gel-based ABPP after labeling with **Rho-DEVD-AOMK** (1 μM).

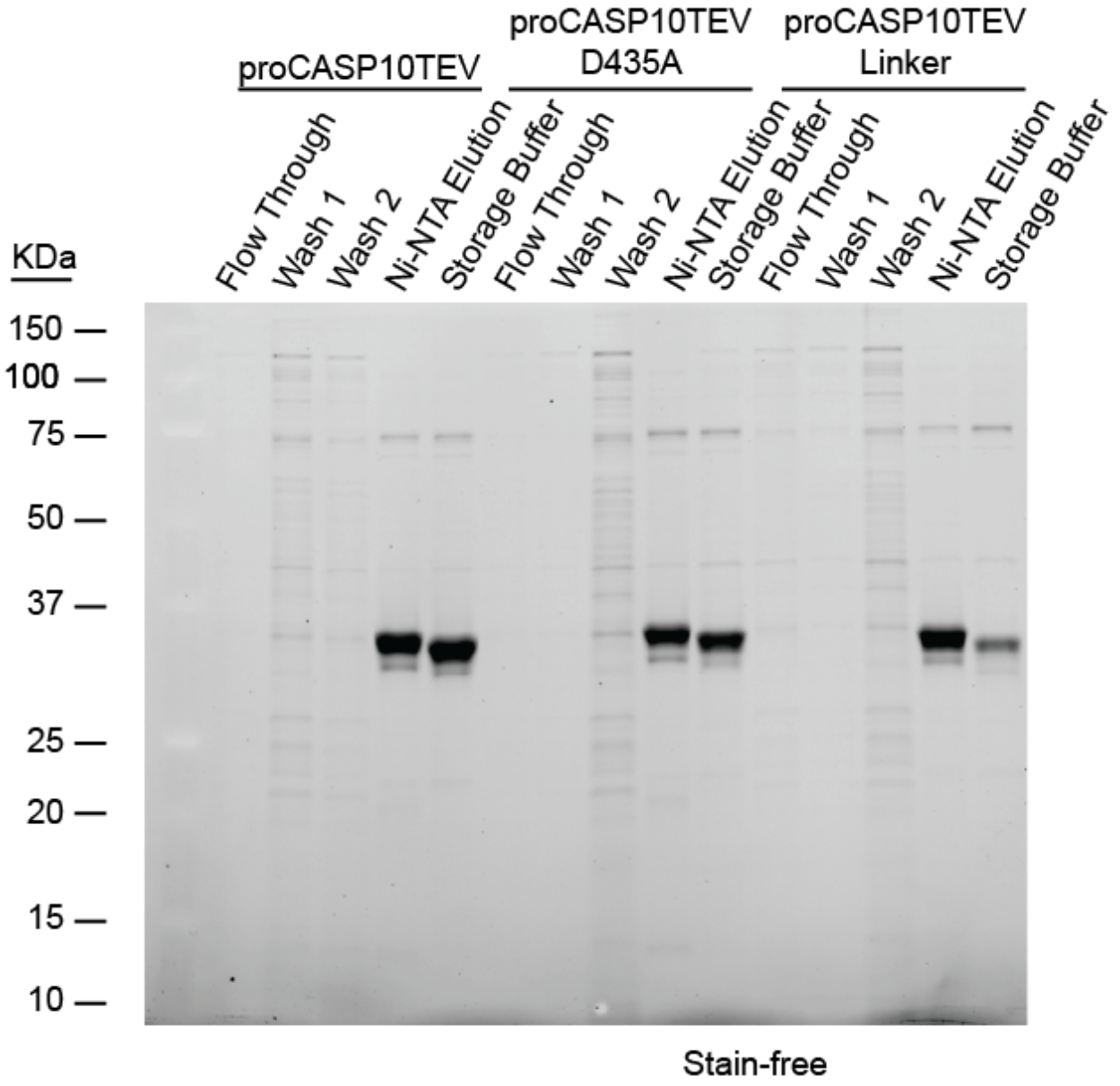

Figure S5. **Enhanced protein production conditions reduce caspase self-activation.** Recombinant proCASP10 construct purification stain-free gel for proCASP10TEV, proCASP10TEV D435A, proCASP10TEV linker, and proCASP10TEV delD435. Caspase storage buffer consists of 20 mM Tris pH 7.4, 50 mM NaCl, 1 mM DTT.

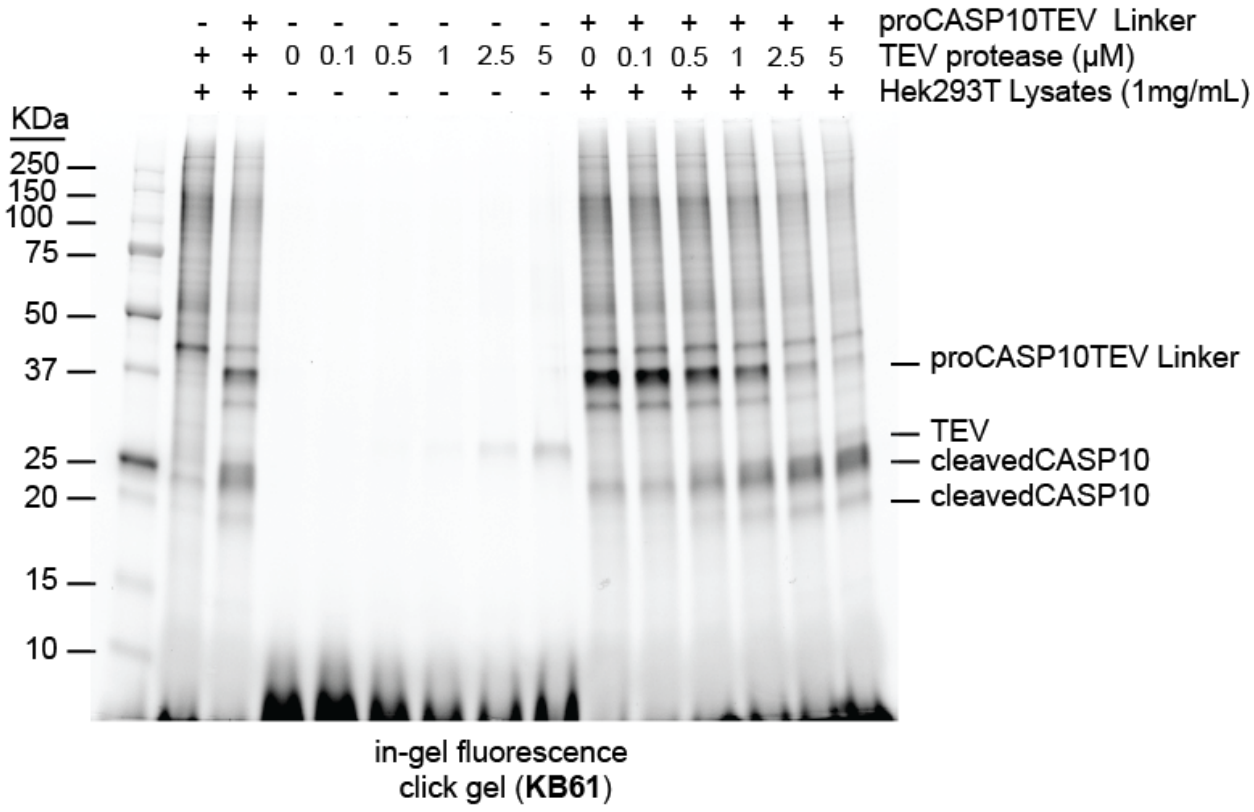

in-gel fluorescence
click gel (**KB61**)

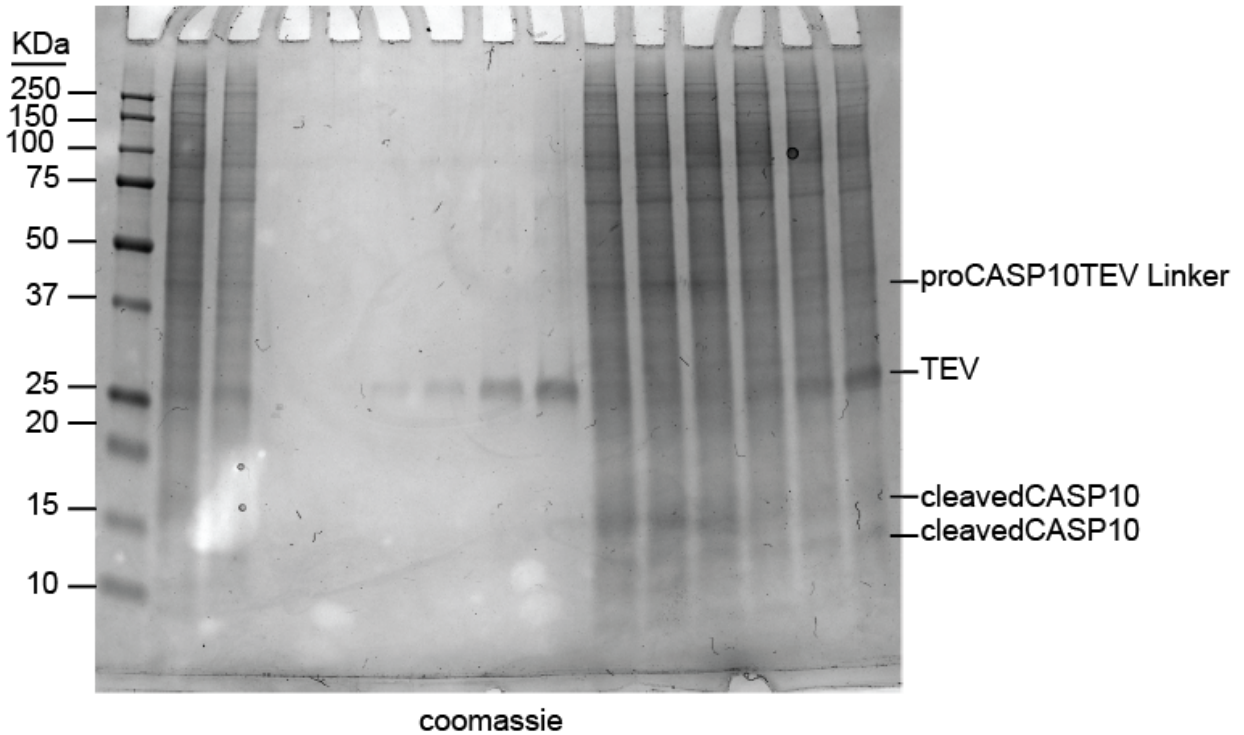

coomassie

Figure S6. **proCASP10TEV Linker is cleaved with addition of TEV protease in a dose-dependent manner**. 1 mg/mL HEK293T cell lysates were spiked with proCASP10TEV Linker (1 μM) followed by treatment with increasing TEV protease concentrations (0 nM, 100 nM, 500 nM, 1 μM, 2.5 μM, and 5 μM) for 1h at ambient conditions. All samples were then treated with KB61 (10 μM final concentration) for 1h. Each sample was clicked with rhodamine azide click mix for 1 additional hour and visualized by in-gel fluorescence.

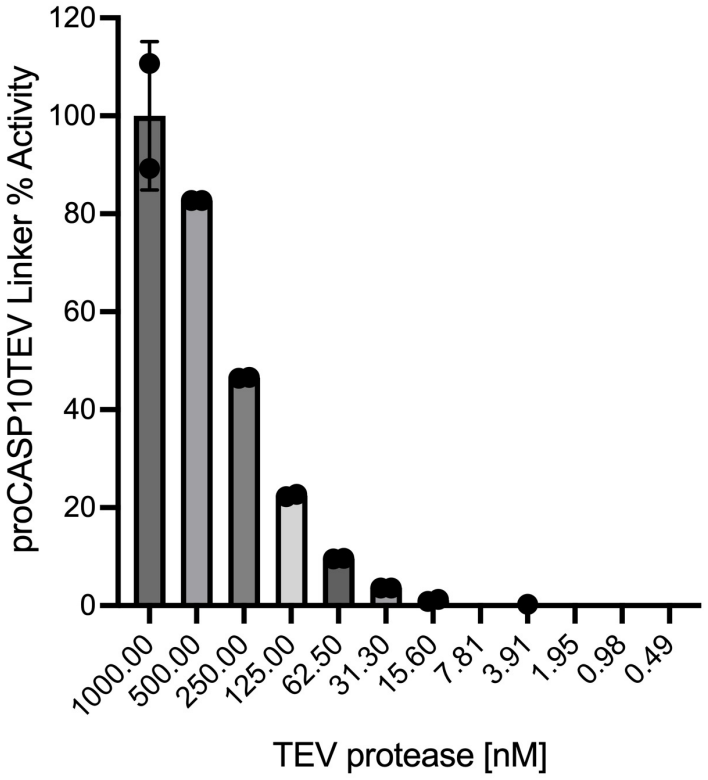

Figure S7. **Defining the minimal concentration of TEV protease required for screening.** Caspase substrate (Ac-VDVAD-AFC 10 μM) in citrate buffer (333 mM citrate, 5 mM DTT in PBS) was dispensed into 96-well plates containing TEV protease in PBS. TEV protease dilutions were prepared at the final concentrations: 1000 μM, 500 μM, 250 μM, 125 μM 62.5 μM, 31.3 μM, 15.6 μM 7.81 μM, 3.91 μM, 1.95 μM, 0.98 μM and 0.49

μM. Activity of proCASP10TEV Linker was read immediately after mixing proCASP10TEV Linker (333 μM in PBS) with TEV protease samples. (400 nm excitation, 505 nm emission). Data represents mean values and standard deviations (n = 2 biological replicates).

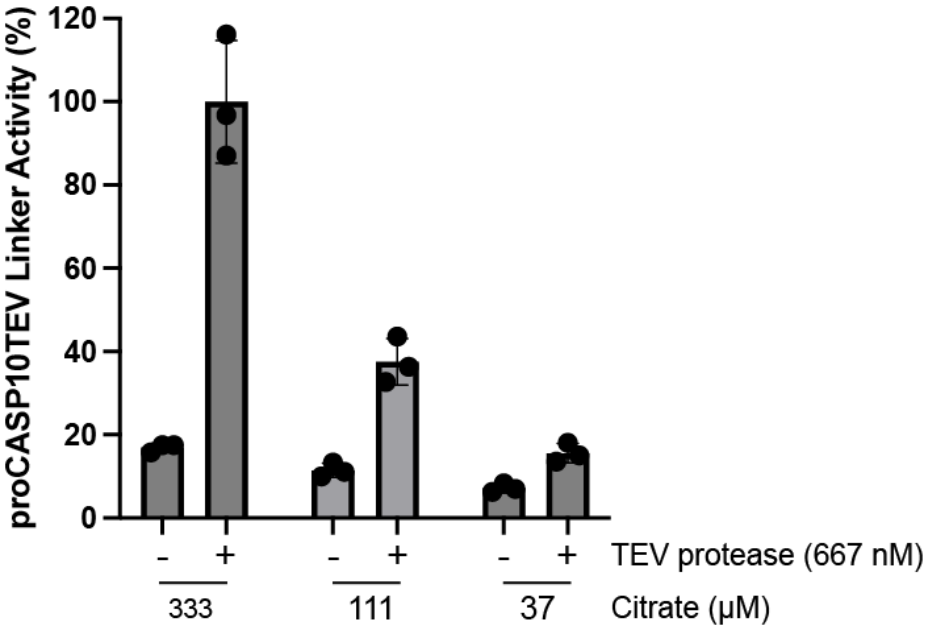

Figure S8. **Increasing sodium citrate concentration enhances proCASP10TEV Linker activity in a TEV-dependent manner**. proCASP10TEV Linker (333 nM) was diluted in PBS buffer and mixed with substrate solution containing 5 mM DTT, 10 μM substrate (Ac-VDVAD-AFC), and the indicated final concentrations (333 nM, 111 nM, and 37 nM) of sodium citrate (pH 7.4) in the absence or presence of TEV protease. Data represent mean values and standard deviations (n = 2 biological replicates).

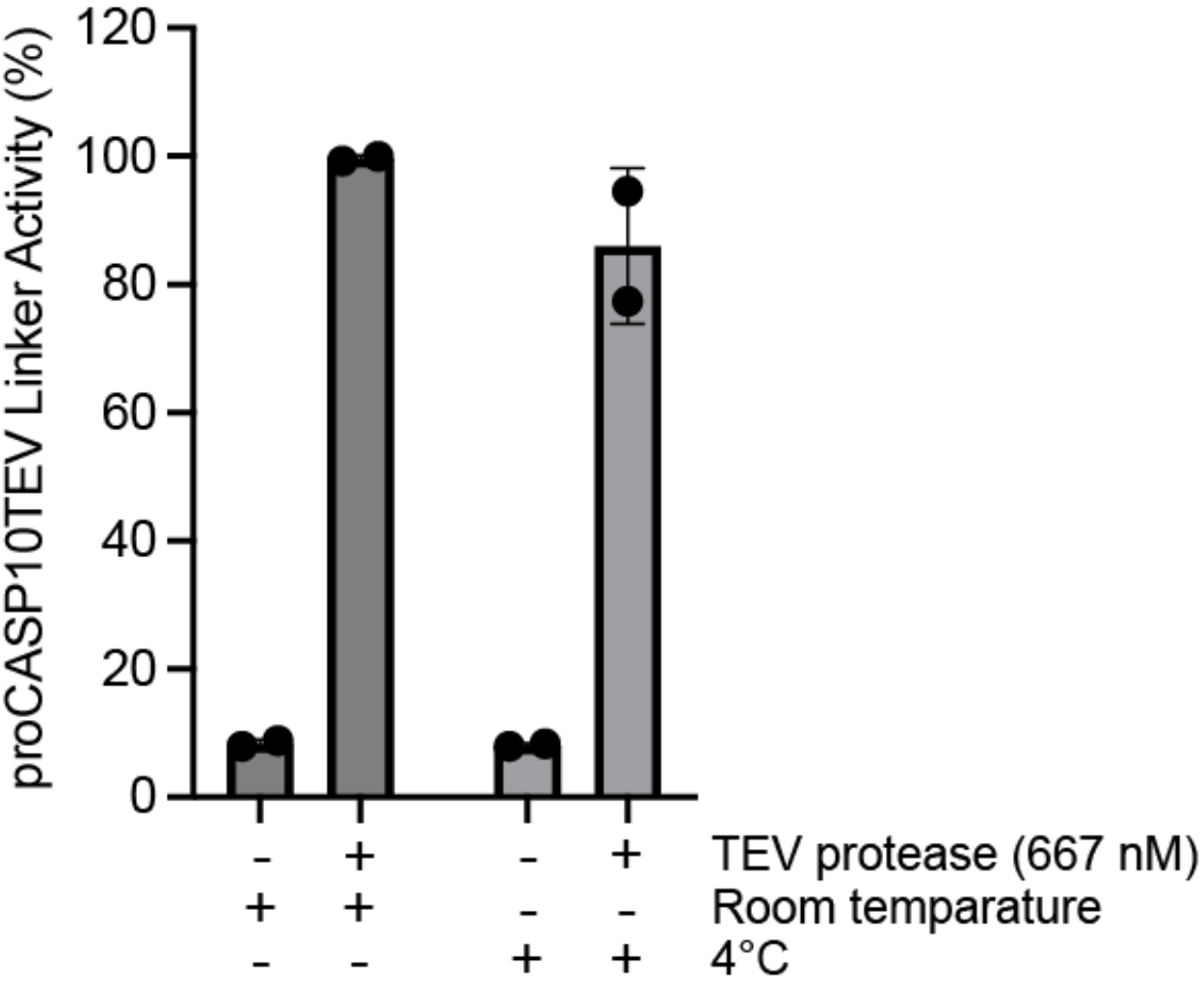

Figure S9. **ProCASP10TEV Linker is stable after 18h incubation in two different storage conditions (ambient, 4 ºC, and -80 ºC)**. proCASP10TEV Linker was diluted in PBS buffer at a final concentration of 333 mM and mixed with substrate solution containing 5 mM DTT, 10 μM of the caspase fluorogenic substrate, Ac-VDVAD-AFC, and 333 mM citrate pH 7.4. TEV-treated and non-TEV-treated samples were also treated with the same substrate solutions containing citrate and DTT in PBS. Data represent mean values and standard deviations (n = 2 biological replicates).

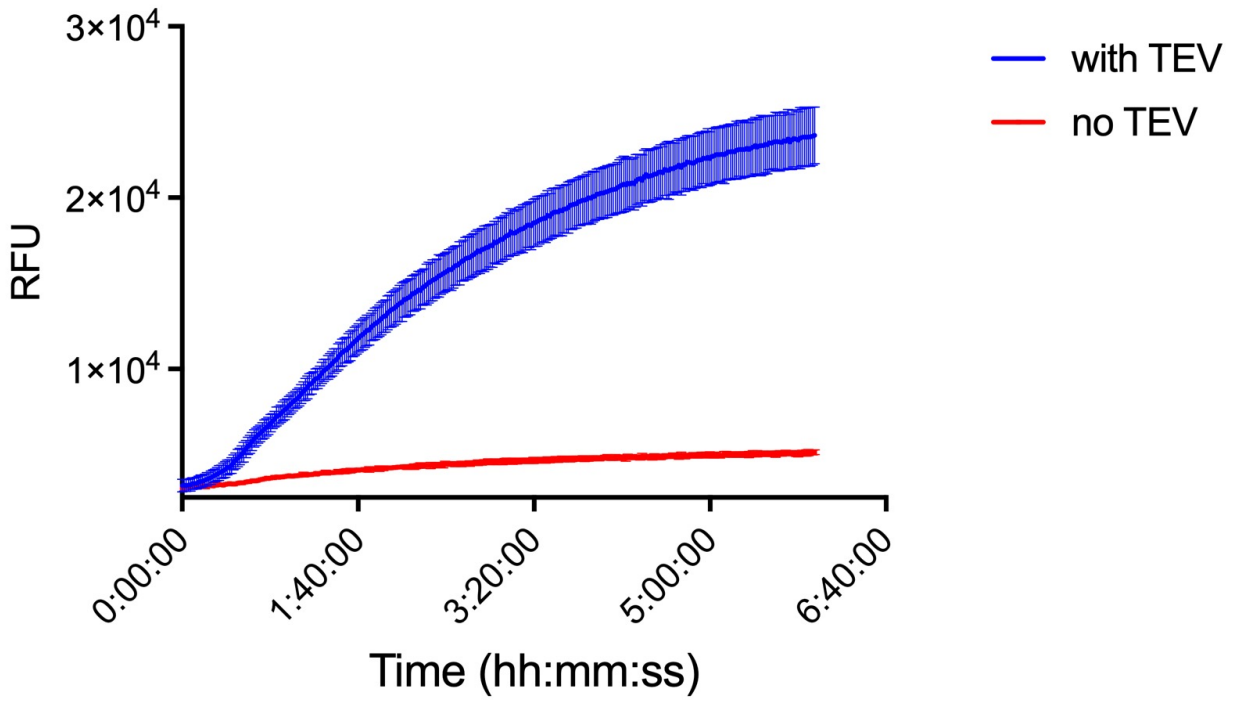

Figure S10. **Assaying the time-dependence of the proCASP10TEV Linker assay**. Caspase Fluorogenic substrate, **Ac-VDVAD-AFC**, can be cleaved by proCASP10TEV Linker and maintains activity after 6h at ambient conditions. 10 µL of proCASP10TEV Linker at 333 nM final concentration in PBS was dispensed using the Mantis liquid handler followed by the addition of 10 µL of citrate buffer with and without TEV (333 mM citrate, 5 mM DTT, 10 µM substrate, and 667 nM TEV protease in PBS). Data represent mean values and standard deviations (n = 5 biological replicates).

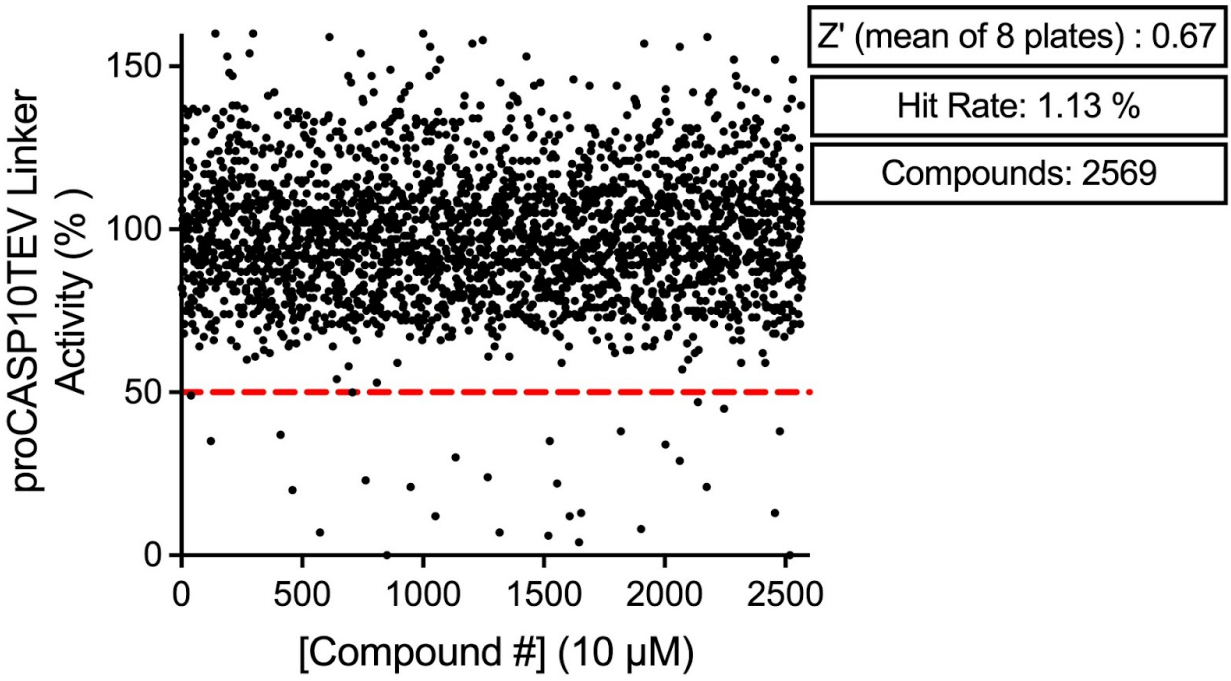

Figure S11. Initial manual screening of proCASP10TEV Linker with LOPAC and NPW library identified 29 compounds (1.13% hit rate) with less than 50% proCASP10TEV Linker activity. A total of eight low volume 384-well plates were prepared by dispensing 10 µL of proCASP10TEV Linker (333 nM) in PBS using the Mantis Liquid Dispenser (Formulatrix). Plates were manually pinned with compounds (Beckman Coulter Biomek FX system) from two different FDA approved libraries and left to incubate for 1h at ambient conditions. 10 µL of TEV solution was dispensed onto each plate containing 667 nM TEV protease, 333 mM citrate pH 7.2, 5 mM DTT and 10 µM substrate (Ac-VDVAD-AFC) in PBS. Plates were left to incubate for 1h. Endpoint reads were obtained for each well and percent activity was calculated to the average of DMSO positive controls (n = 16).

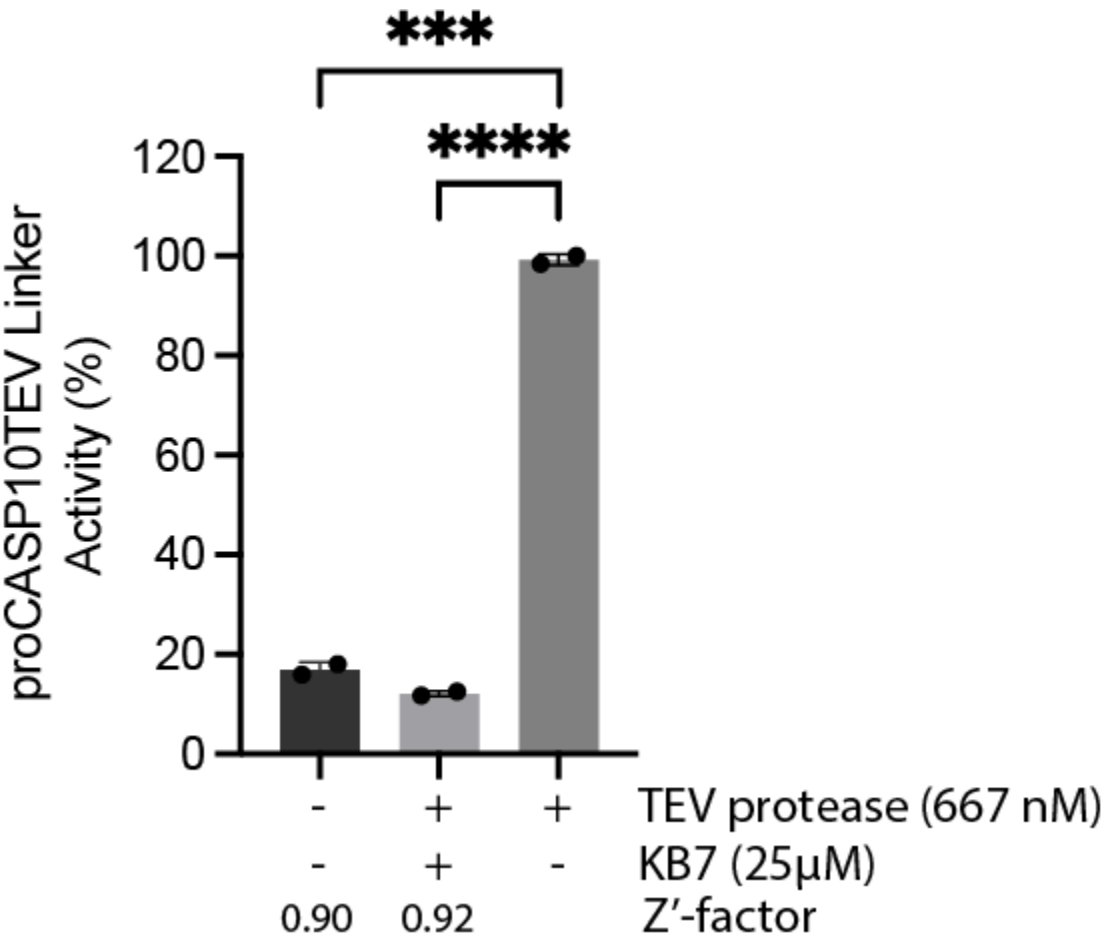

Figure S12. **Control plate confirms compatibility of proCASP10TEV Linker with HTS**. Z' for the no TEV protease control of 0.90 and the positive control, **KB7** (25 μM), of 0.92 supports compatibility of the proCASP10TEV Linker with high throughput screening. proCAPS10TEV Linker at 333 nM with citrate buffer in the absence of TEV protease was treated with KB7 for 1h followed by the addition of citrate buffer containing TEV protease at 667 nM final concentration. Data represent mean values and standard deviations (n =

2 biological replicates). Statistical significance was calculated with unpaired Student's t-tests, ****p<0.0001.

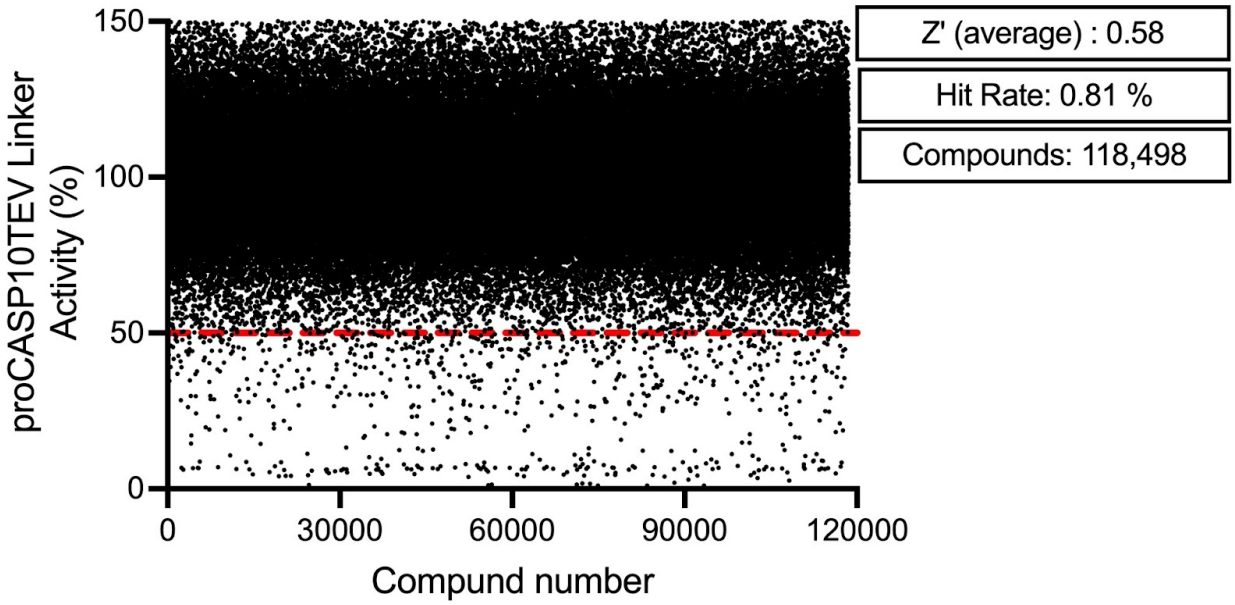

Figure S13. **A total of 963 initial hit compounds were found to have less than 50% proCASP10TEV Linker activity**. A total of 118,498 were analyzed to determine if they were hits based on proCASP10TEV Linker activity (0.81% hit rate). Endpoint values from each well of the 384-well plates (375 plates) were used to calculate percent activity against the average of DMSO.

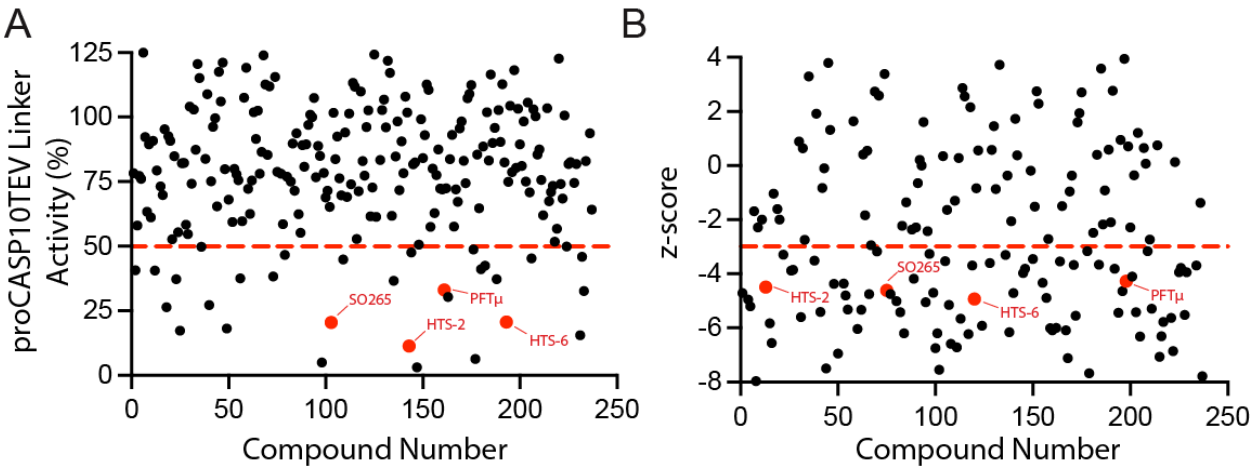

Figure S14. **Re-screen of proCASP10TEV Linker validated hit compounds**. A) Percent activity of proCASP10TEV Linker re-screen results showing approximately 32 of 237 compounds having ≤ 50% activity (red horizontal line). Percent activity of LOPAC hit compounds are represented as red dots (compound number 143 for **HTS-2**, compound number 193 for **HTS-6,** and compound number 163 for **PFTμ**) B) z-score of proCASP10TEV Linker re-screen results showing 38 compounds with a z-score ≤ -3 (red horizontal line) calculated using the mean of the control lanes. The z-score of LOPAC hit compounds are represented as red dots (compound number 13 for **HTS-2**, compound number 120 for **HTS-6,** and compound 198 for **PFTμ**).

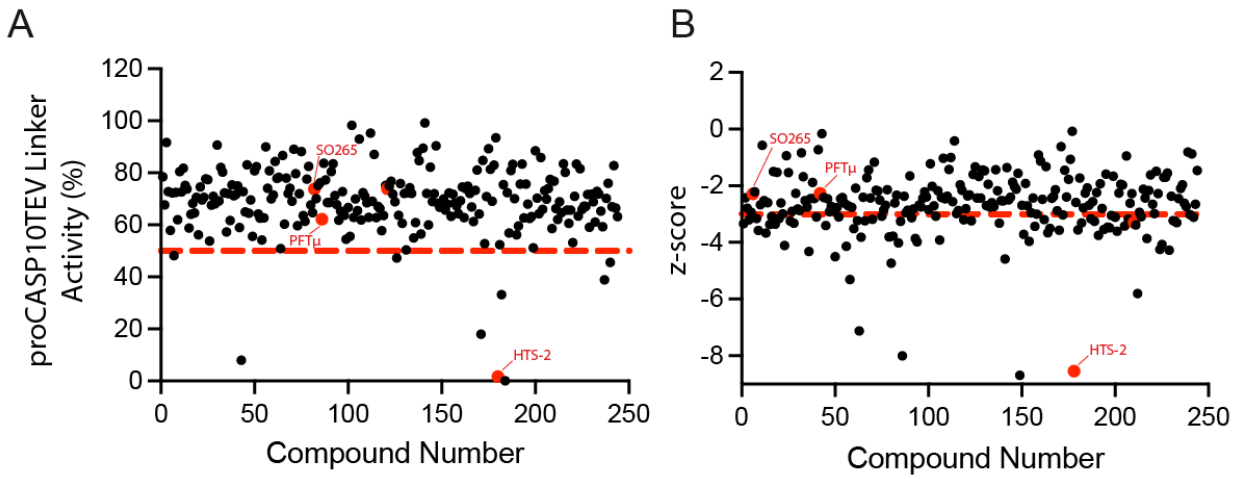

Figure S15. **Caspase-10 counter screen identified inhibitors for the active form (activeCASP10)**. A) Percent activity of activeCAP10 counter screen results showing 40 of 237 compounds having ≤ 60% activity (red horizontal line). B) z-score of activeCASP10 counter screen results showing 78 compounds with a z-score of ≤ -3 (red horizontal line) calculated using the mean and standard deviation of the DMSO wells (n = 12). The z-score of LOPAC hit compounds is represented as red dots.

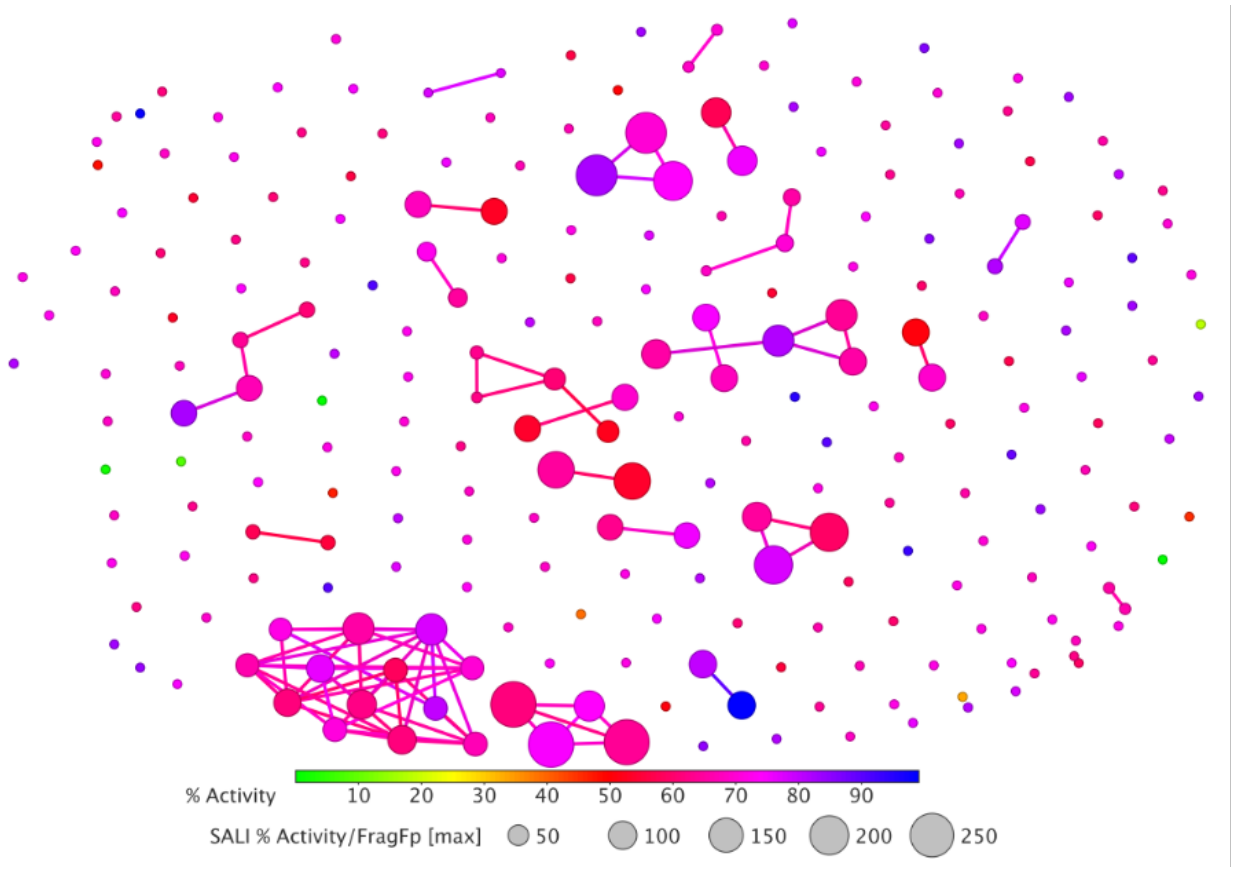

Figure S16. SAR analysis of activeCASP10 counter screen results showed 19 clusters. Analysis was performed as described in the DataWarrior SAR analysis methods section. The structure-activity landscape index (SALI) was first calculated using the percent activities based on the DMSO controls (n = 16)[2].

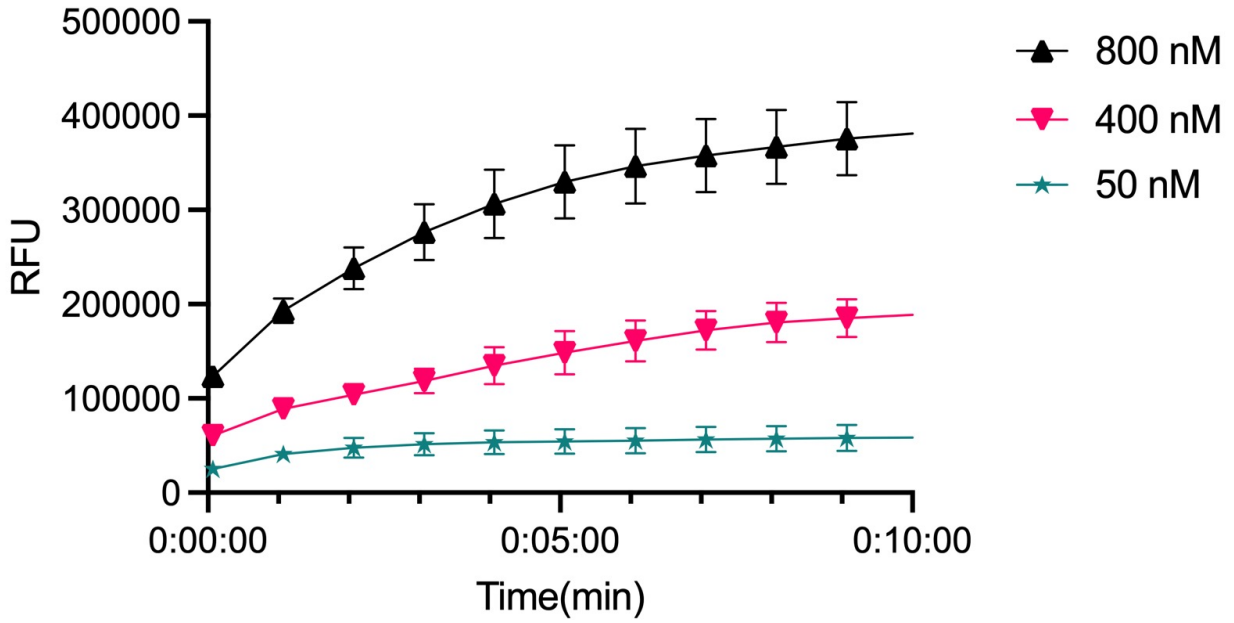

Figure S17. **Determining optimal concentration of TEV protease substrate to validate screen hits**. ABCYL-ENLYFQSGTK-5-FAM substrate was added to citrate buffer containing 333 mM citrate and 5 mM DTT in PBS. TEV protease (100 nM) in PBS was then mixed with the citrate buffer at a 1:1 mixture (100 µL of TEV protease with 100 µL of citrate buffer) and immediately ran on a plate reader for analysis. Data represents mean values and standard deviations (n = 4 biological replicates).

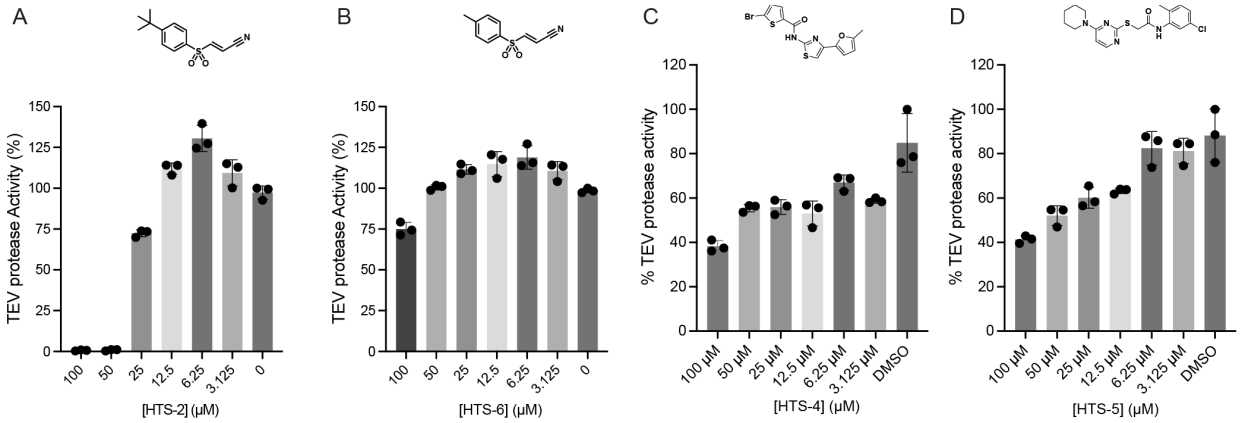

Figure S18. **proCASP10TEV Linker hit compounds have little to no effect on TEV protease activity at increasing concentration of compounds**. TEV protease at 100 nM was treated with (A) **HTS-2**, (B) **HTS-6**, (C) **HTS-4**, and (D) **HTS-5** at indicated concentrations for 1h followed by the addition of TEV substrate solution. Data represents mean values and standard deviations (n = 3 biological replicates).

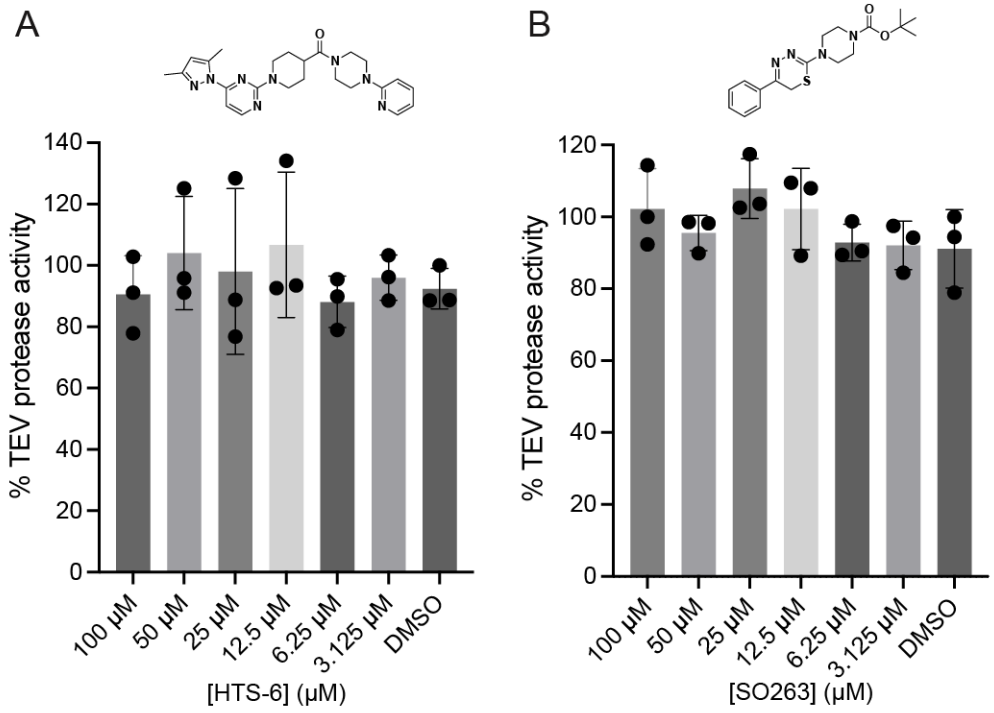

Figure S19. **Initial screen compounds can inhibit TEV protease at higher concentrations**. TEV protease (100 nM) was treated with (A) **HTS-8** and (B) **SO263** in DMSO at indicated final concentrations for 1h followed by the addition of TEV substrate solution. Data represents mean values and standard deviations (n = 3 biological replicates).

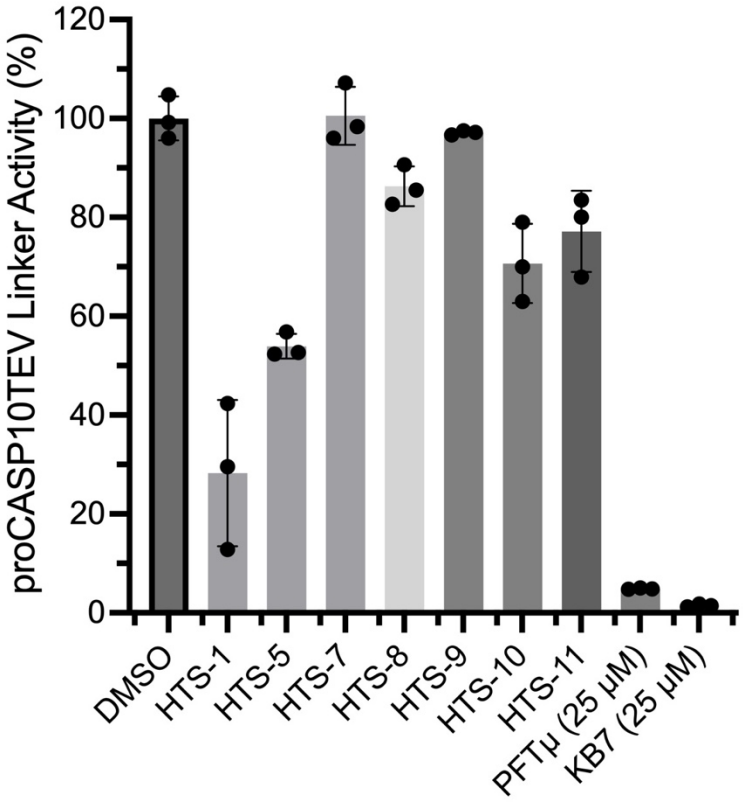

Figure S20. **Validation of proCASP10TEV Linker re-screen results**. proCASP10TEV Linker at 333 nM final concentration was treated with screen electrophiles at 100 μM or 10 μM for **KB7** and **PFTμ** for 1h at ambient conditions. Data represents mean values and standard deviations (n = 3 biological replicates).

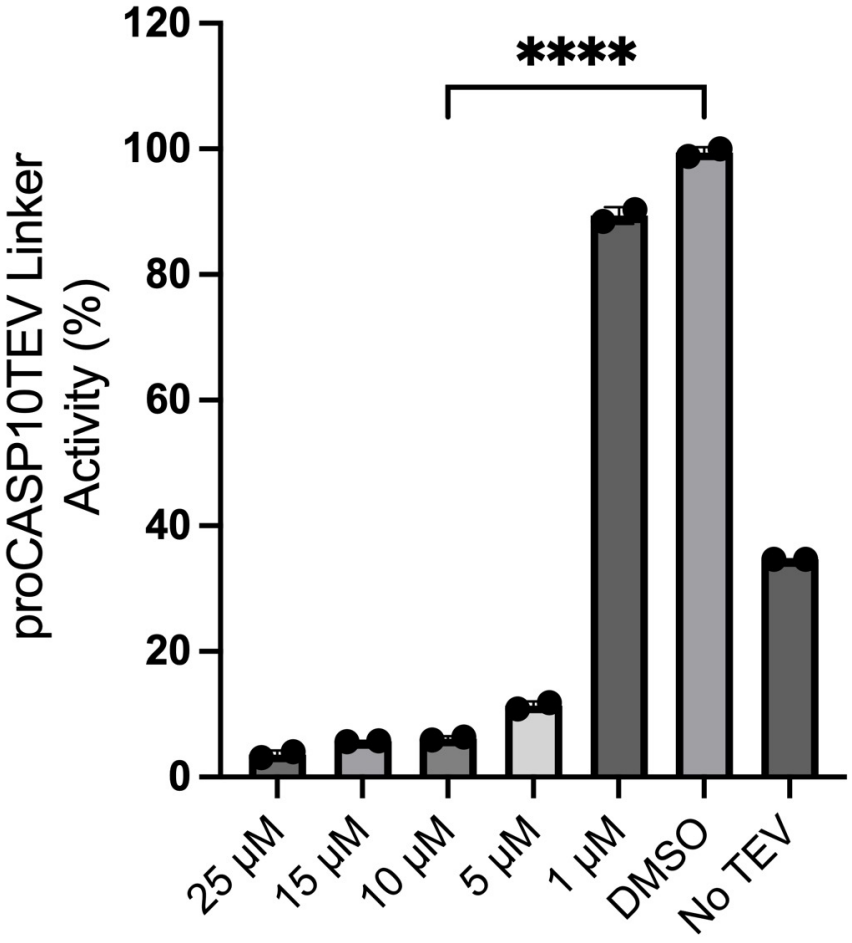

Figure S21. pro-caspase-10 TEV Linker is inhibited by the highly reactive screen hit HTS-6 in buffer. proCASP10TEV Linker in PBS (333 nM) was treated with **HTS-6** for 1h at decreasing concentrations (25 µM, 15 µM, 10 µM, 5 µM and 1 µM). Data represents mean values and standard deviations (n = 2 biological replicates). Statistical significance was calculated with unpaired Student's t-tests, ****p<0.0001.

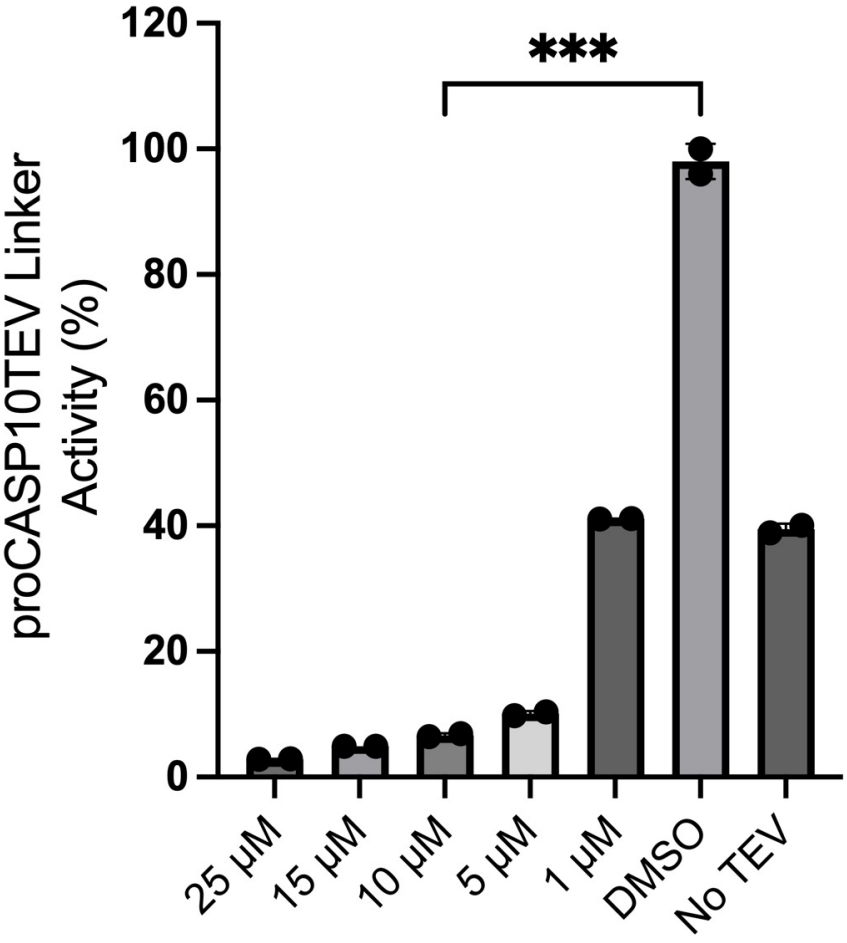

Figure S22. **pro-caspase-10 TEV Linker is inhibited by the highly reactive screen hit HTS-2 in buffer**. Data represents mean values and standard deviations (n = 2 biological replicates). Statistical significance was calculated with unpaired Student's t-tests, ***p<0.001.

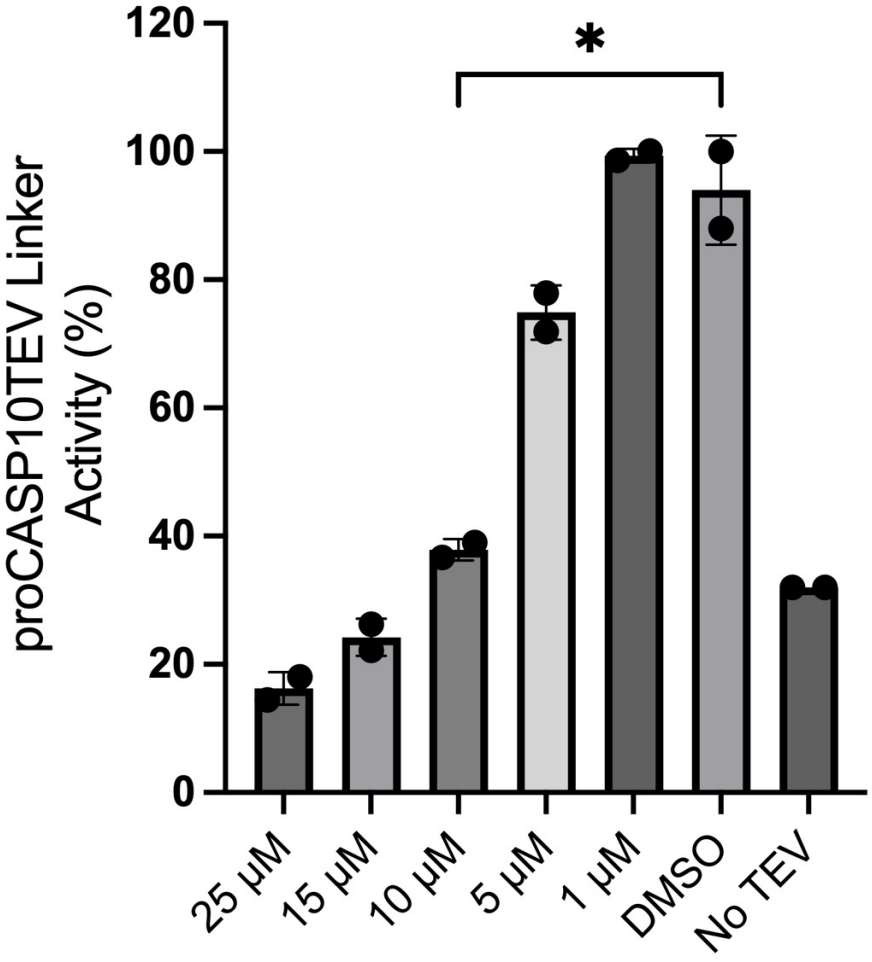

Figure S23. pro-caspase-10 TEV Linker is inhibited by the highly reactive screen hit PFTµ in phosphate buffer. proCASP10TEV Linker (333 nM) spiked in PBS was treated with compound at varying concentrations (25, 15, 10, 5 and 1 µM) for 1h. Data represents mean values and standard deviations (n = 2 biological replicates). Statistical significance was calculated with unpaired Student's t-tests, *p<0.05.

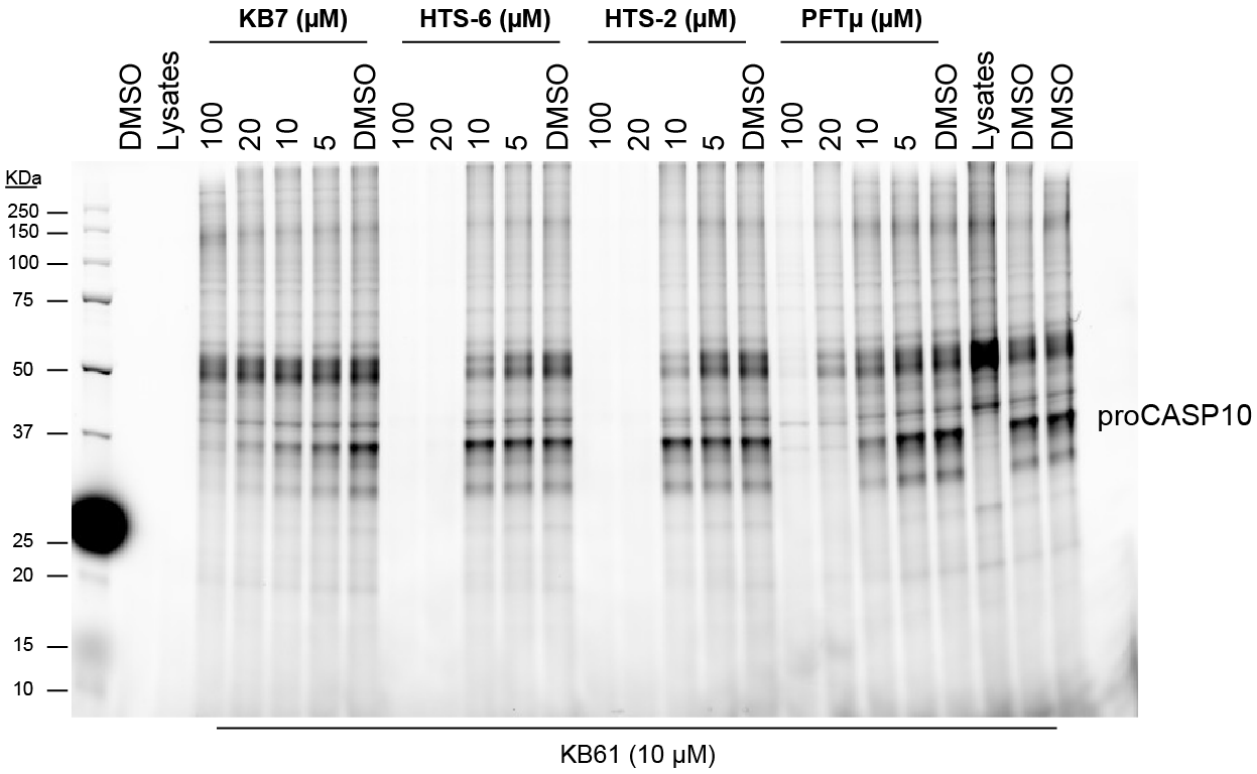

Figures S24. **Initial screen compounds can compete for pro-caspase-10 labeling against KB61**. 1 mg/mL HEK293T cell lysates were spiked with 1 μM proCASP10 and treated with LOPAC compounds at decreasing final concentrations (100 μM, 20 μM, 10 μM, and 5μM) for 1h. Samples were then treated with 10 μM **KB61** for 1h followed by clicking onto rhodamine azide for 1h. Protein labeling was then visualized by competitive gel-based ABPP and visualized with rhodamine.

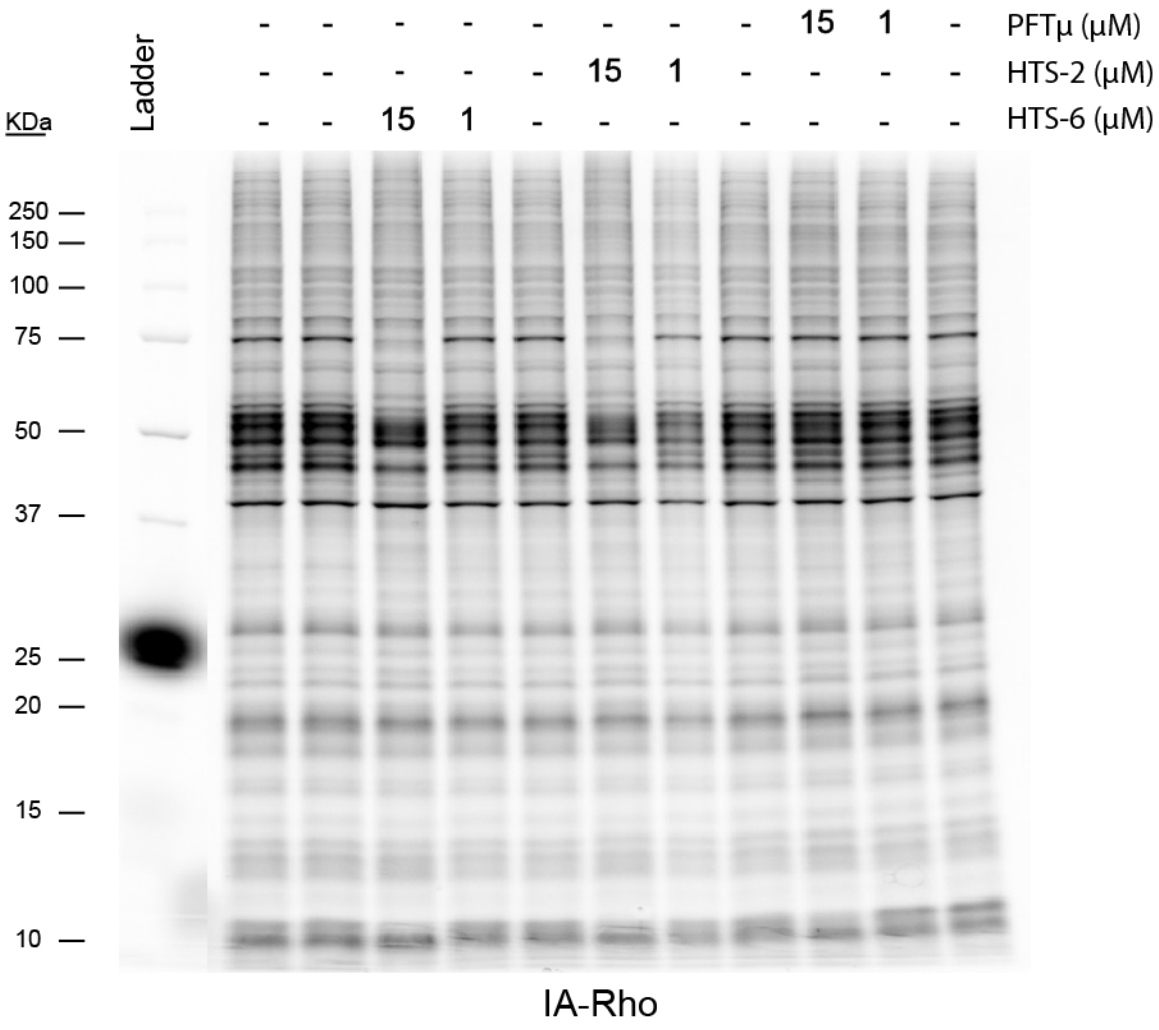

Figure S25. Initial hit screen compounds are promiscuous. 1 mg/mL HEK293T lysates were treated with LOPAC compounds at 15 μM and 1 μM concentrations for 1h followed by treatment with IA-Rho (1 μM) for 1h at ambient conditions.

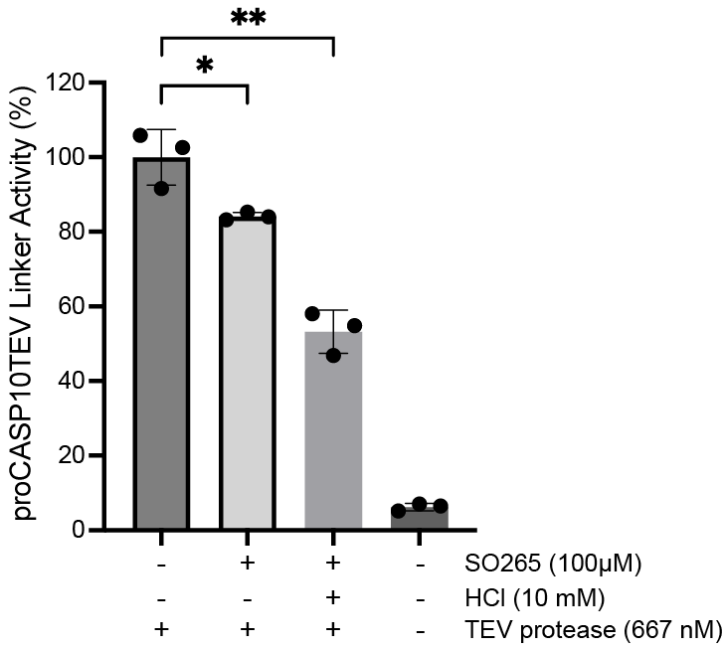

Figure S26. Compound SO265 activates under acidic conditions, decreasing proCASP2TEV Linker activity. Compound **SO265** was prepared as a 10 mM stock in DMSO, 333 mM sodium citrate, or 10 mM HCl and left to incubate at 37 °C for 15 min. proCASP10TEV Linker (333 nM in PBS) was treated with 10 mM stocks (concentration of 100 μM) for 1 h. Samples were then treated with TEV protease and substrate solution (10 μM substrate, 667 nM TEV protease in PBS). Data represents mean values and standard deviations (n = 4 biological replicates). Statistical significance was calculated with unpaired Student's t-tests, **p<0.001, *p<0.05.

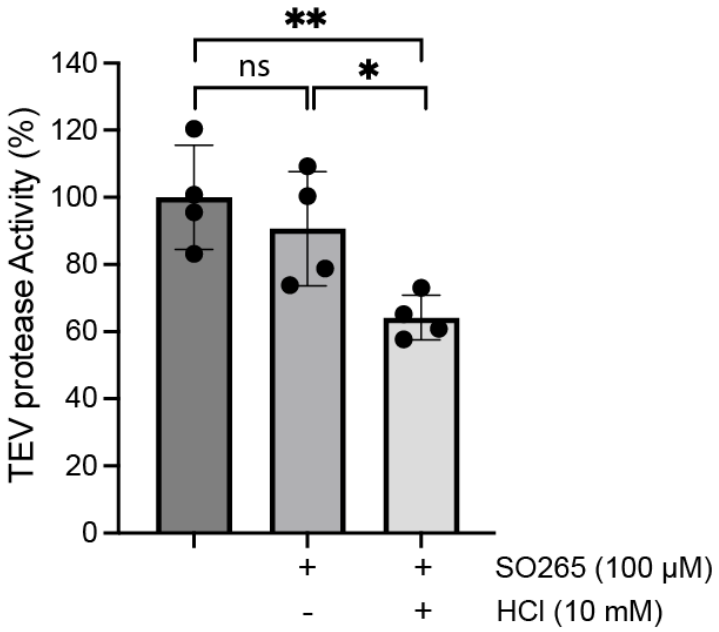

Figure S27. SO265 becomes active under acidic conditions and slightly reduces TEV protease activity. TEV protease treated with **SO265** stocks (100 uM) prepared under acidic conditions (stocks prepared in 10 mM HCl at 37°C for 15 min). Data represents mean values and standard deviations (n = 4 biological replicates). Statistical significance was calculated with unpaired Student's t-tests, *p<0.05, ns = not significant.

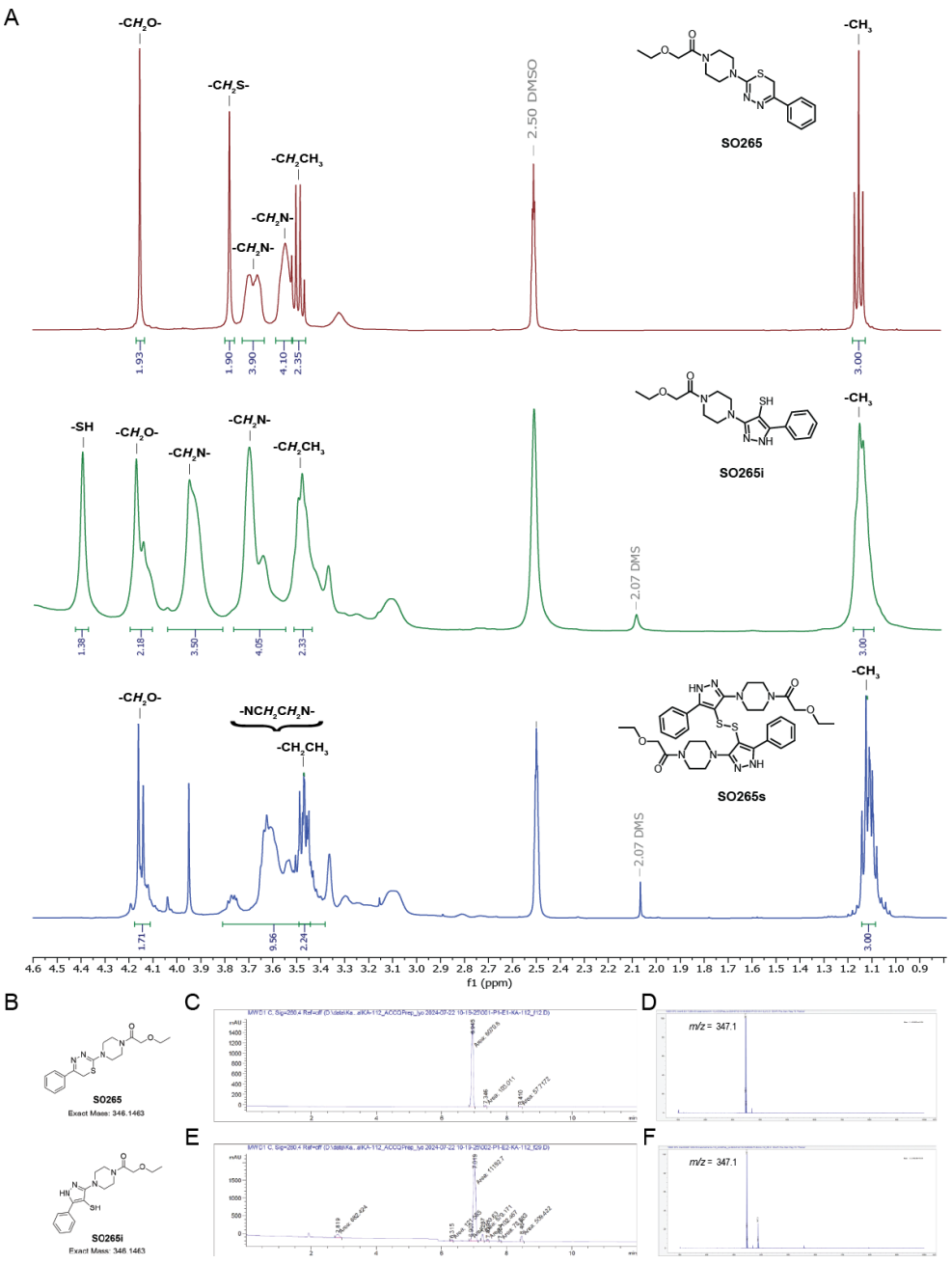

Figure S28. Isomer SO265 shows a slight retention time shift in LC-MS compared to SO265. (A) H NMR comparison of purified **SO265** compounds including **SO265** (red), the isomer **SO265i** (green), and the disulfide rearrange product **SO265s** (blue) (B) Structures of **SO265** and structural isomer **SO265i**. (C) LC trace of **SO265** (λ = 280 nm) with compound retention time = 6.945 min. (D) Mass spectrum (ESI+) for the **SO265** peak

at 6.945 min showing *m/z* = 347.1 (**SO265** monoisotopic mass = 346.1). (E) LC trace of **SO265i** (λ = 280 nm) with compound retention time = 7.019 min. (F) Mass spectrum (ESI+) for the SO265i peak at 7.019 min showing m/z = 347.1 (SO265i monoisotopic mass = 346.1).

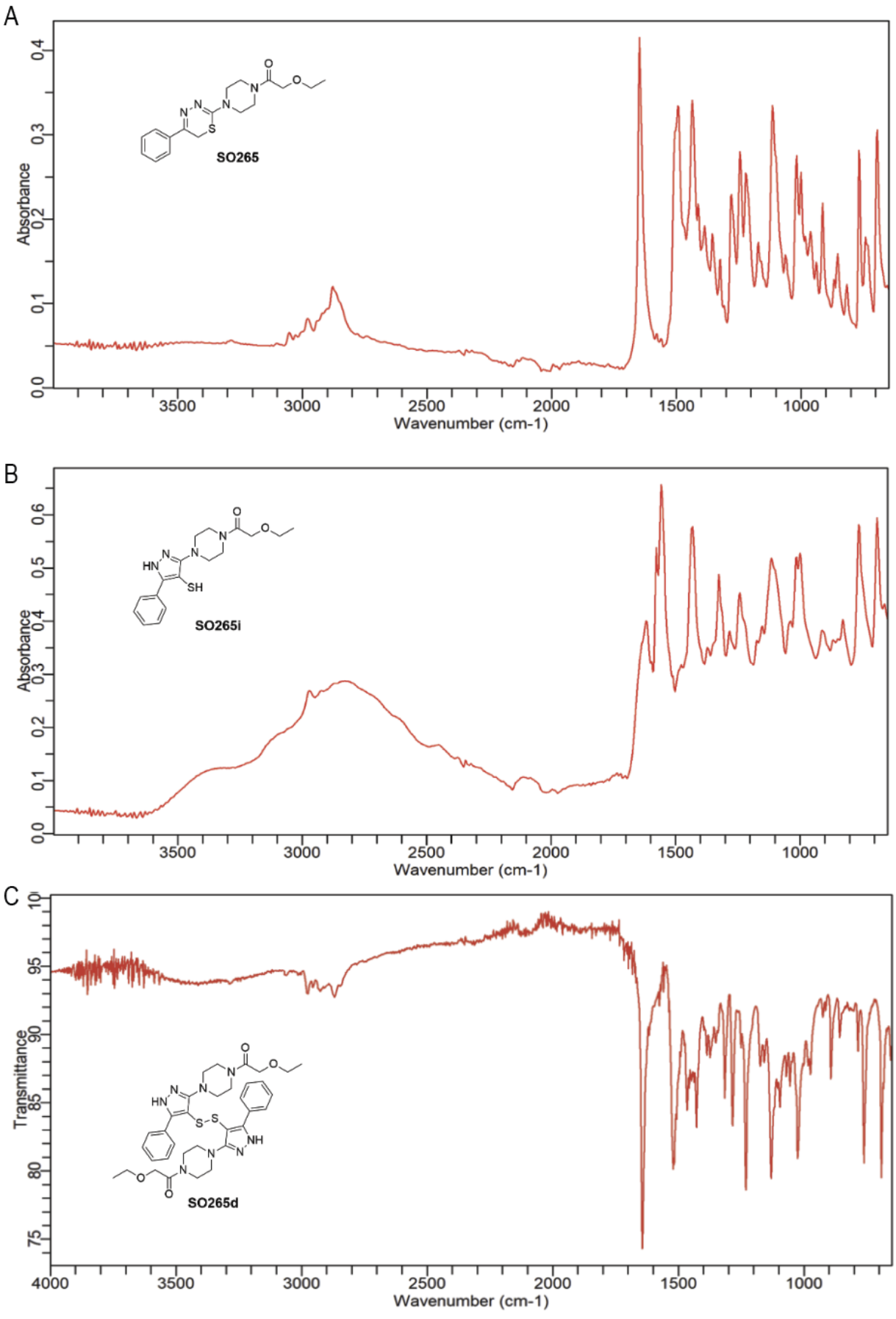
A
Absorbance
0,0
0,1
0,2
0,3
0,4
SO265
3500
3000
2500
2000
1500
1000
Wavenumber (cm-1)
B
Absorbance
0,0
0,1
0,2
0,3
0,4
0,5
0,6
SO265i
3500
3000
2500
2000
1500
1000
Wavenumber (cm-1)
C
Transmittance
75
80
85
90
95
100
SO265d
4000
3500
3000
2500
2000
1500
1000
Wavenumber (cm-1)

Figure S29. Purified SO265, purified isomer SO265i, and proposed disulfide SO265s exhibit different banding in IR spectroscopy. (A) IR spectrum of **SO265**. (B) IR spectrum of **SO265i**. (C) IR spectrum of the SO265i NMR sample which had been left at room temperature for 3 days resulting in the formation of **SO265s**.

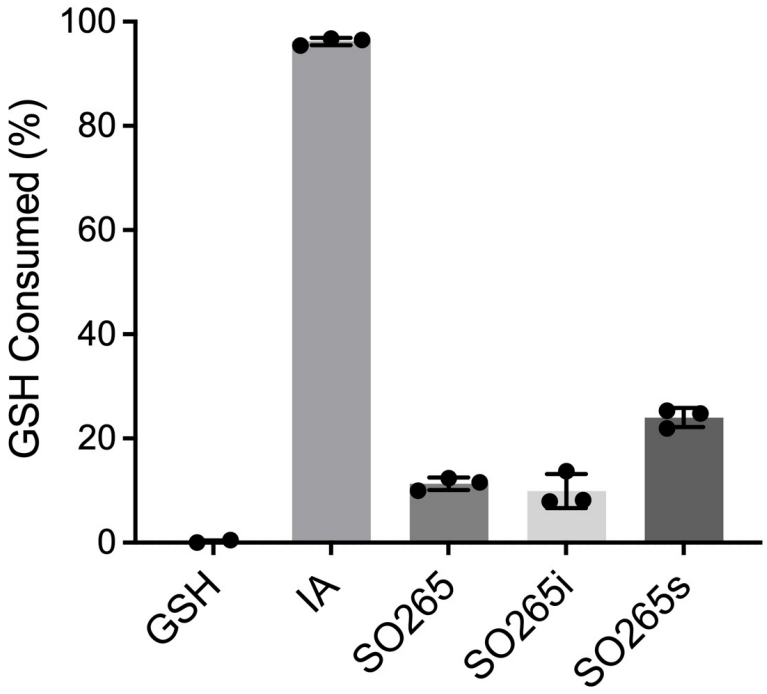

Figure S30. The rearranged disulfide compound (SO265s) has higher activity with glutathione. Consumed glutathione (GSH) was measured using Ellman's reagent and tested against **SO265** compounds, and iodoacetamide (IA). Data represents mean values and standard deviations (n = 3 biological replicates).

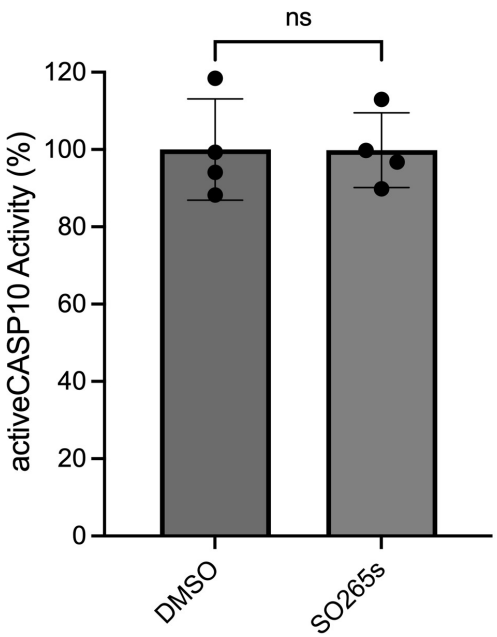

Figure S31. ActiveCASP10 is not inhibited by SO265s. ActiveCASP10 at 1 μM in PBS was treated with **SO265s** at final concentration of 100 μM for 1h at ambient conditions. Data represents mean values and standard deviations (n = 4 biological replicates). Statistical significance was calculated with unpaired Student's t-tests, ns = not significant.

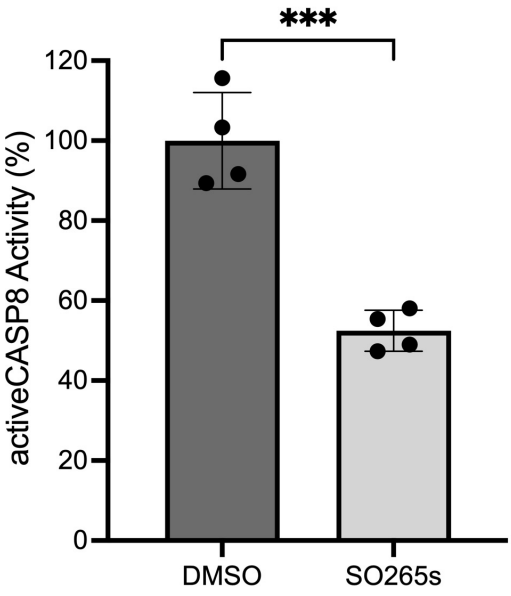

Figure S32. ActiveCASP8 is partially inhibited by SO265s. ActiveCASP8 at 1μM in PBS was treated with 100 μM **SO265s** for 1h at ambient conditions. Data represents mean values and standard deviations (n = 4 biological replicates). Statistical significance was calculated with unpaired Student's t-tests, ***p<0.001.

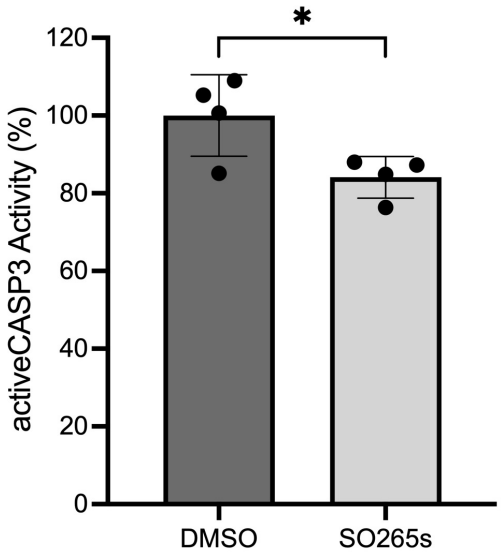

Figure S33. ActiveCASP3 is partially inhibited by SO265s. Active enzyme (0.1 μM) in PBS was treated with 100 μM of **SO265s** for 1h at ambient conditions. Data represents mean values and standard deviations (n = 4 biological replicates). Statistical significance was calculated with unpaired Student's t-tests, *p<0.05.

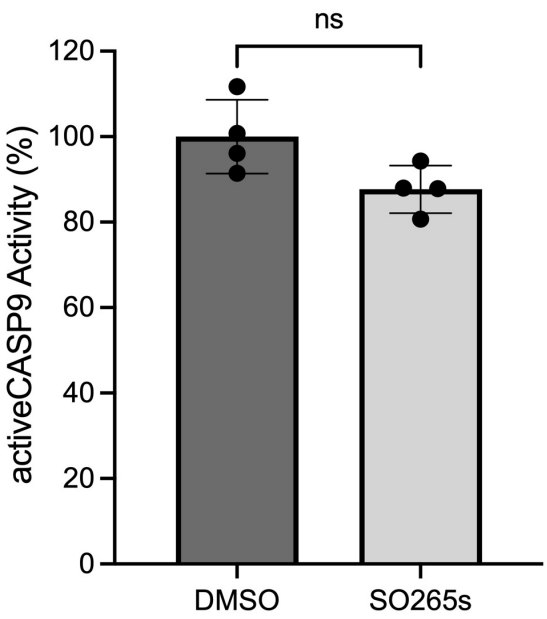

Figure S34. SO265s modestly inhibit activeCASP9. Active enzyme (1 μM) in PBS was treated with 100 μM of SO265s for 1h at ambient conditions. Data represents mean values and standard deviations (n = 4 biological replicates). Statistical significance was calculated with unpaired Student's t-tests, ns = not significant.

c

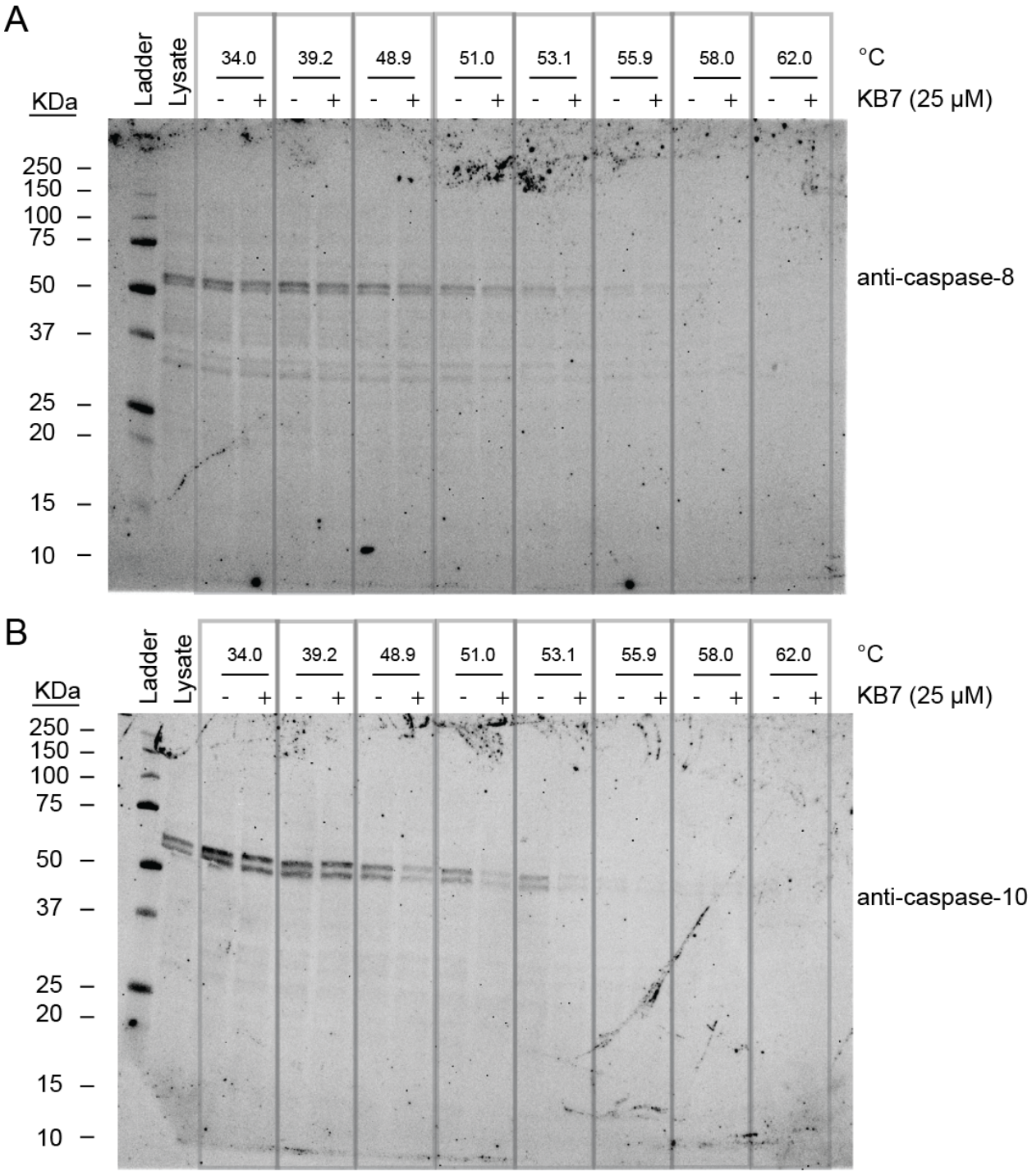
A
Ladder
Lysate
34.0
39.2
48.9
51.0
53.1
55.9
58.0
62.0
°C
- + - + - + - + - + - + - + - +
KB7 (25 μM)
KDa
250
150
100
75
50
37
25
20
15
10
anti-caspase-8
B
Ladder
Lysate
34.0
39.2
48.9
51.0
53.1
55.9
58.0
62.0
°C
- + - + - + - + - + - + - + - +
KB7 (25 μM)
KDa
250
150
100
75
50
37
25
20
15
10
anti-caspase-10

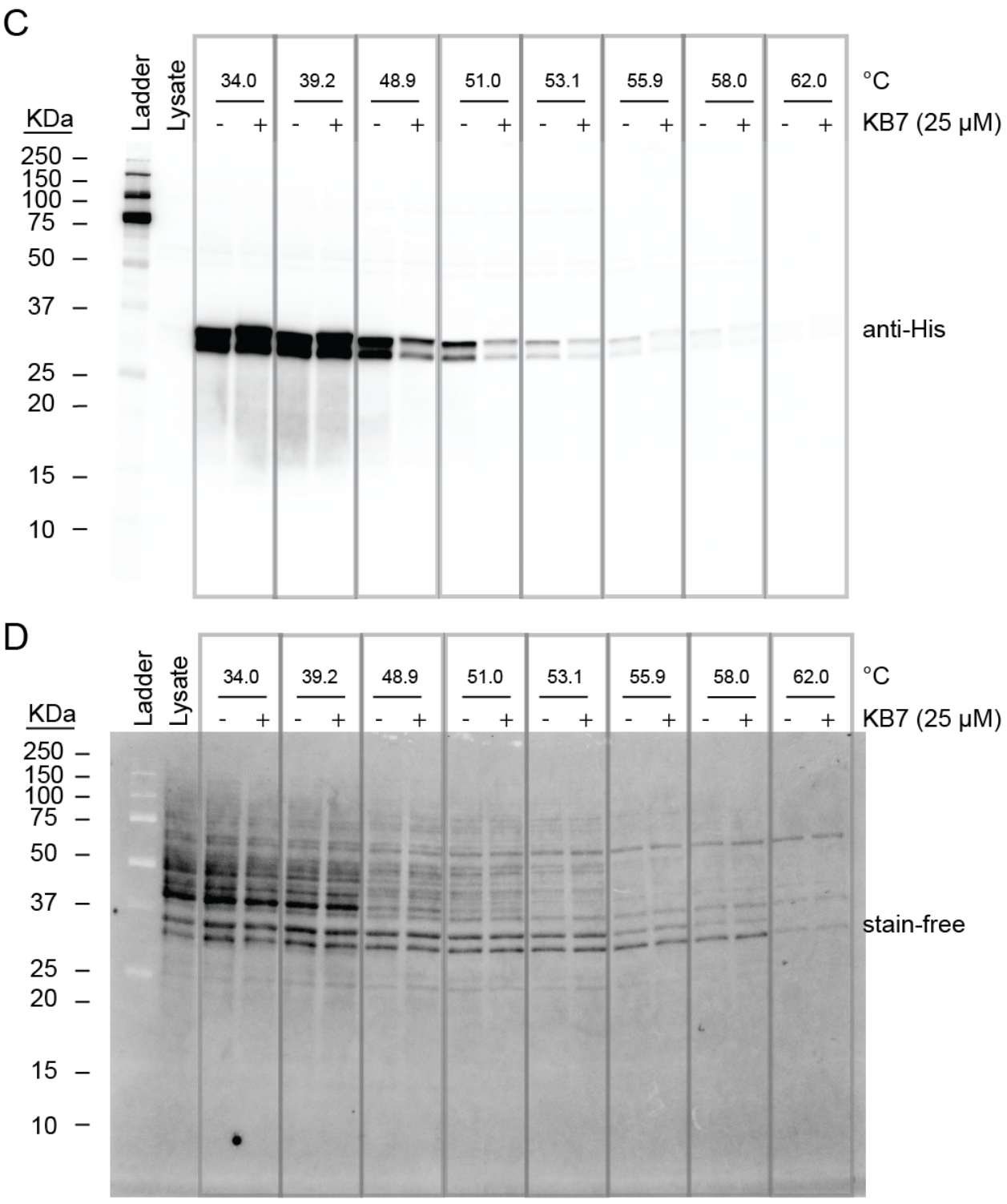
C
KDa
Ladder
Lysate
34.0
39.2
48.9
51.0
53.1
55.9
58.0
62.0
°C
- + - + - + - + - + - + - + - +
KB7 (25 µM)
250
150
100
75
50
37
25
20
15
10
anti-His
D
KDa
Ladder
Lysate
34.0
39.2
48.9
51.0
53.1
55.9
58.0
62.0
°C
- + - + - + - + - + - + - + - +
KB7 (25 µM)
250
150
100
75
50
37
25
20
15
10
stain-free

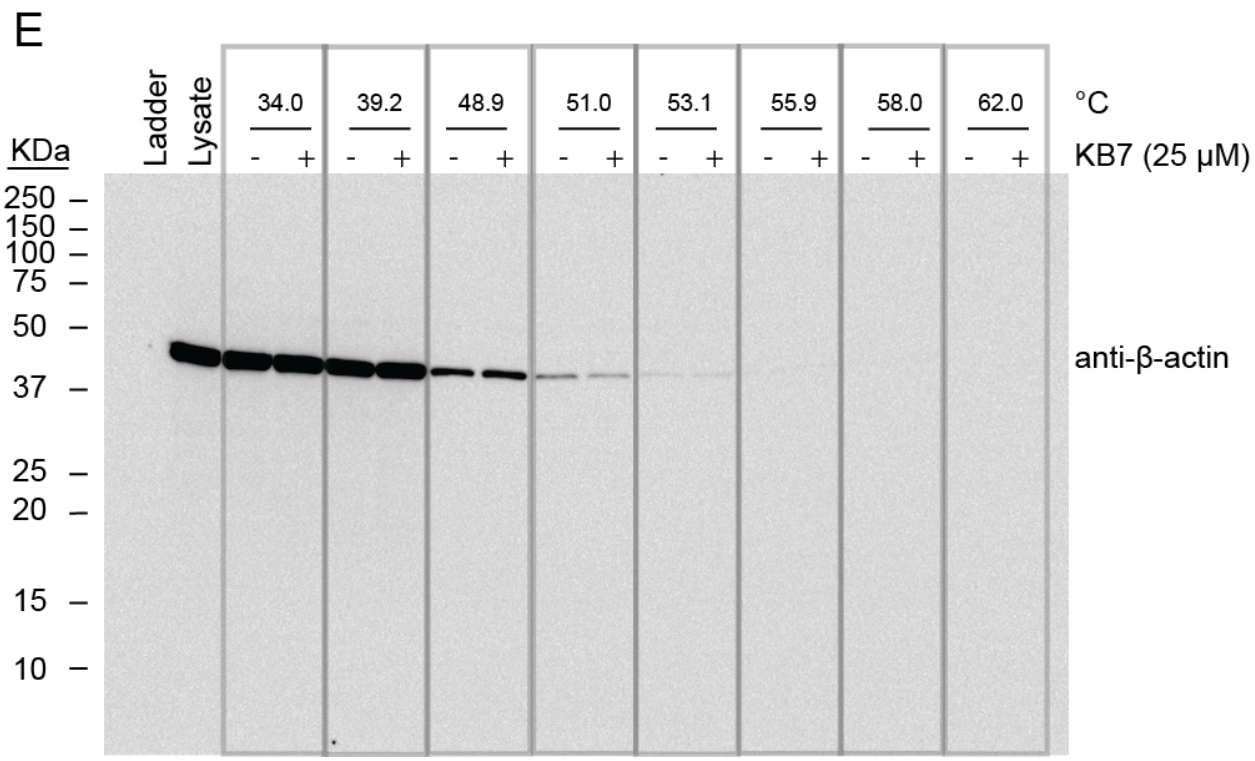

Figure S35. Establishing CETSA assay using positive control KB7. Recombinant caspase-10 (proCASP10) was spiked into 3.1 mg/mL Jurkat lysates and treated with KB7 (25 µM) for 1h at ambient conditions. Samples were treated at indicated temperatures for 5 min in a Thermal Cycler. Samples were blotted onto a nitrocellulose membrane followed by imaging for pro-caspase-8 using an (A) anti-caspase-8 primary antibody, (B) blotted for pro-caspase-10 using an anti-caspase-10 primary antibody, (C) blotted for His tag using an anti-His primary antibody. Loading was imaged using (D) stain-free and (E) by blotting for ß-actin using an anti-ß-actin primary antibody.

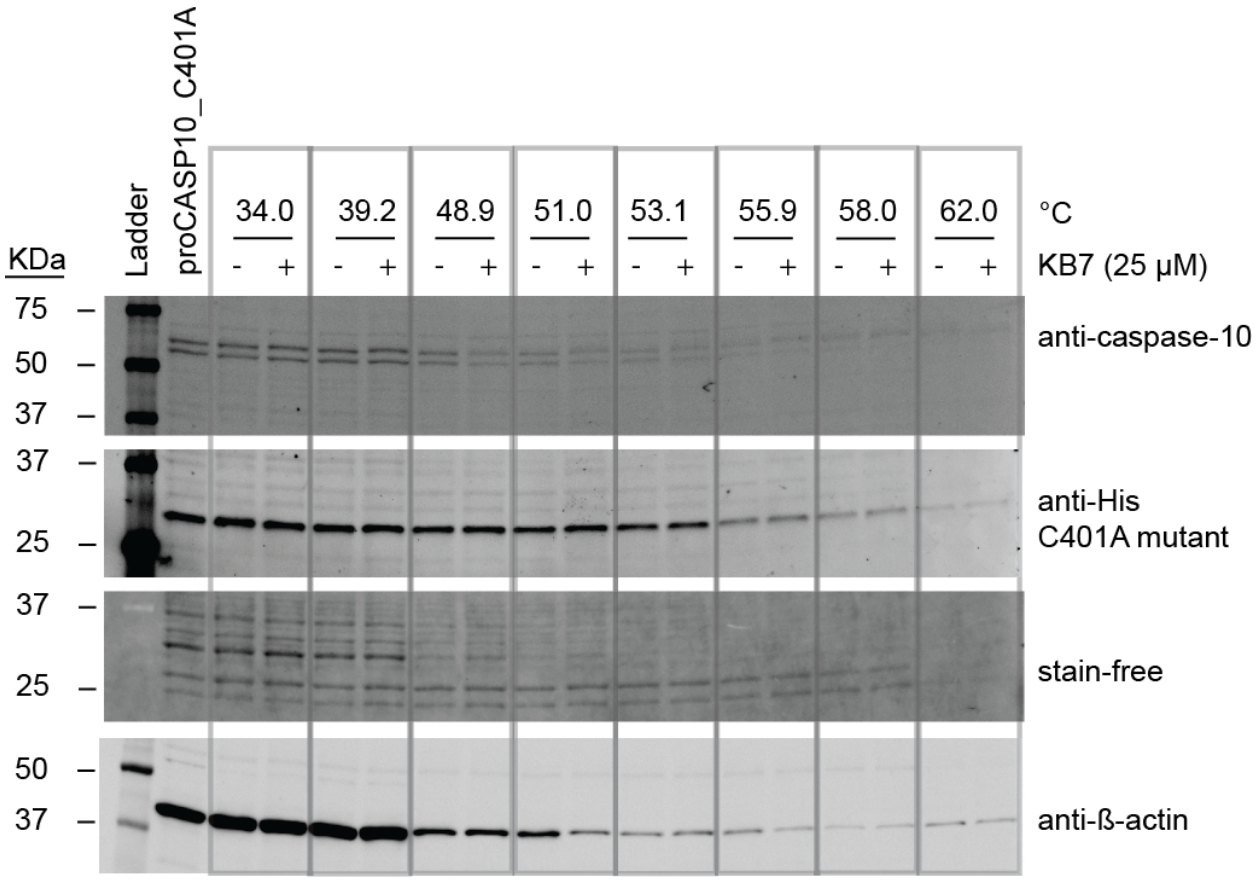

Figure S36. KB7 treatment has little effect on thermal stability of recombinant proCASP10_C401A. Recombinant caspase-10 catalytic mutant (proCASP10_C401A) was spiked into 2.4 mg/mL Jurkat lysates and treated with KB7 (25 µM) for 1h at ambient conditions. Samples were treated at indicated temperatures for 5 min in a Thermal Cycler. Samples were blotted onto a nitrocellulose membrane followed by imaging for the indicating antibodies.

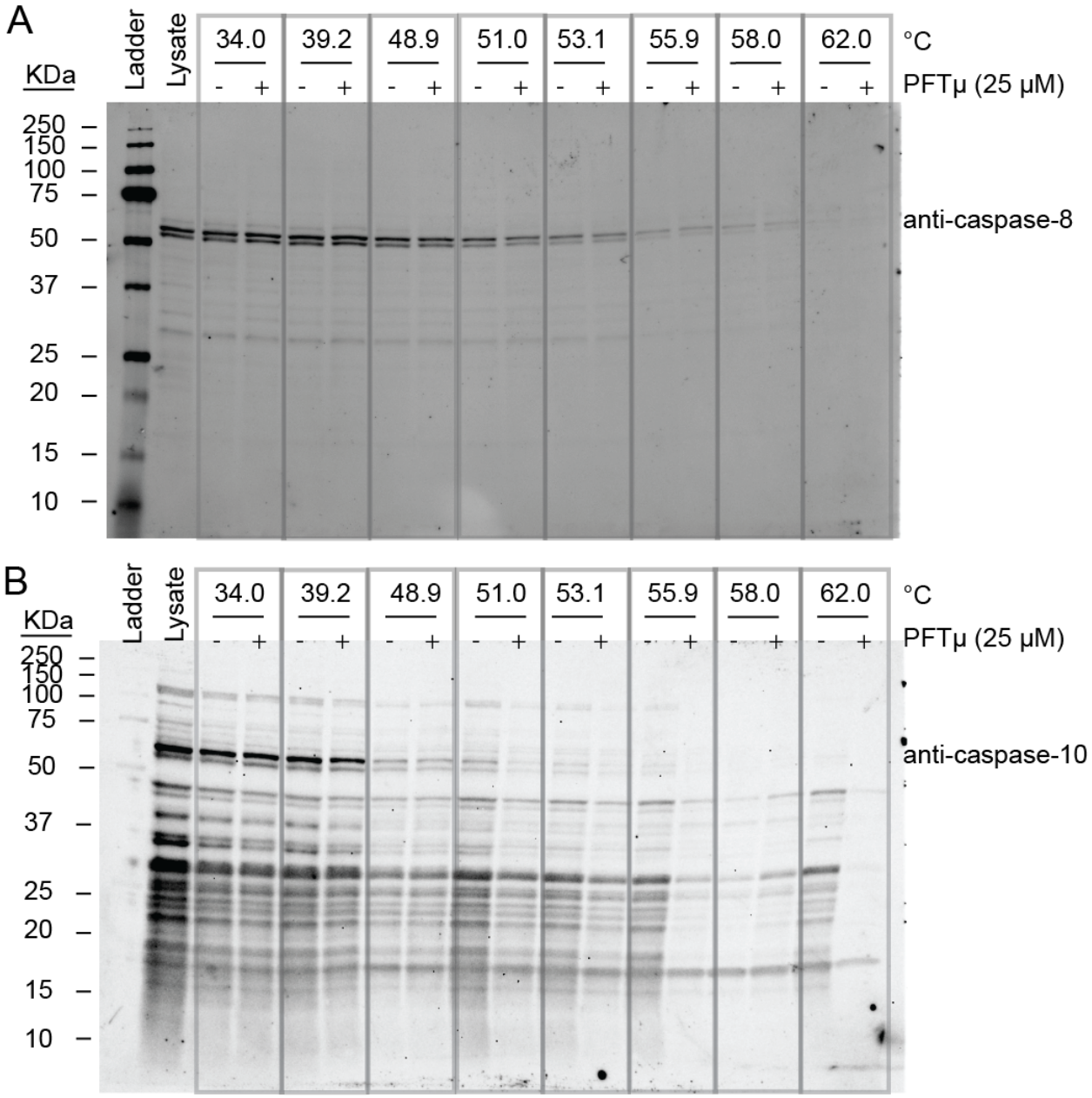
A
Ladder
Lysate
34.0
39.2
48.9
51.0
53.1
55.9
58.0
62.0
°C
- + - + - + - + - + - + - + - +
PFTμ (25 μM)
KDa
250
150
100
75
50
37
25
20
15
10
anti-caspase-8
B
Ladder
Lysate
34.0
39.2
48.9
51.0
53.1
55.9
58.0
62.0
°C
- + - + - + - + - + - + - + - +
PFTμ (25 μM)
KDa
250
150
100
75
50
37
25
20
15
10
anti-caspase-10

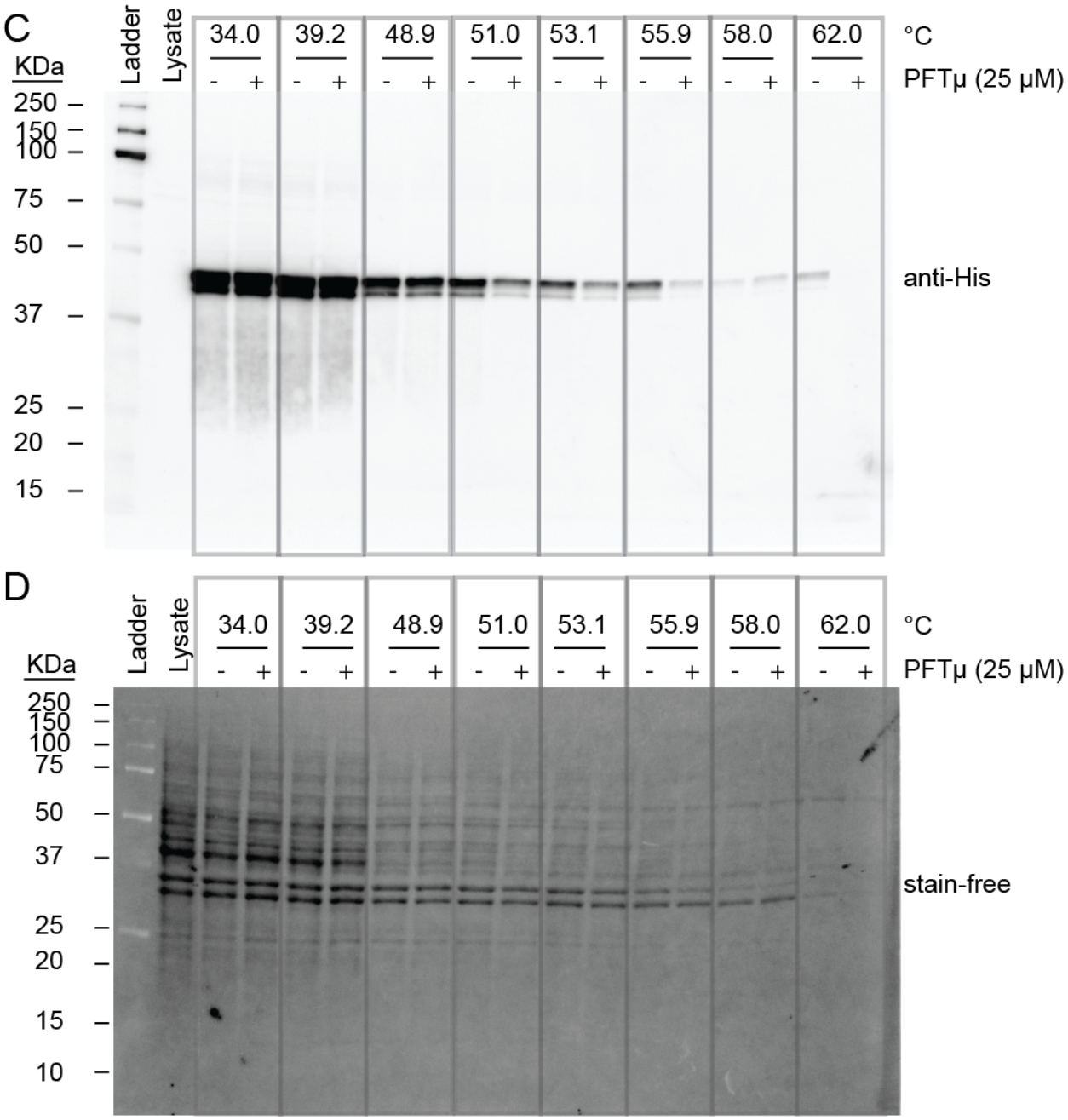
C
KDa
Ladder
Lysate
34.0
39.2
48.9
51.0
53.1
55.9
58.0
62.0
°C
- + - + - + - + - + - + - + - +
PFTμ (25 μM)
250
150
100
75
50
37
25
20
15
anti-His
D
KDa
Ladder
Lysate
34.0
39.2
48.9
51.0
53.1
55.9
58.0
62.0
°C
- + - + - + - + - + - + - + - +
PFTμ (25 μM)
250
150
100
75
50
37
25
20
15
10
stain-free

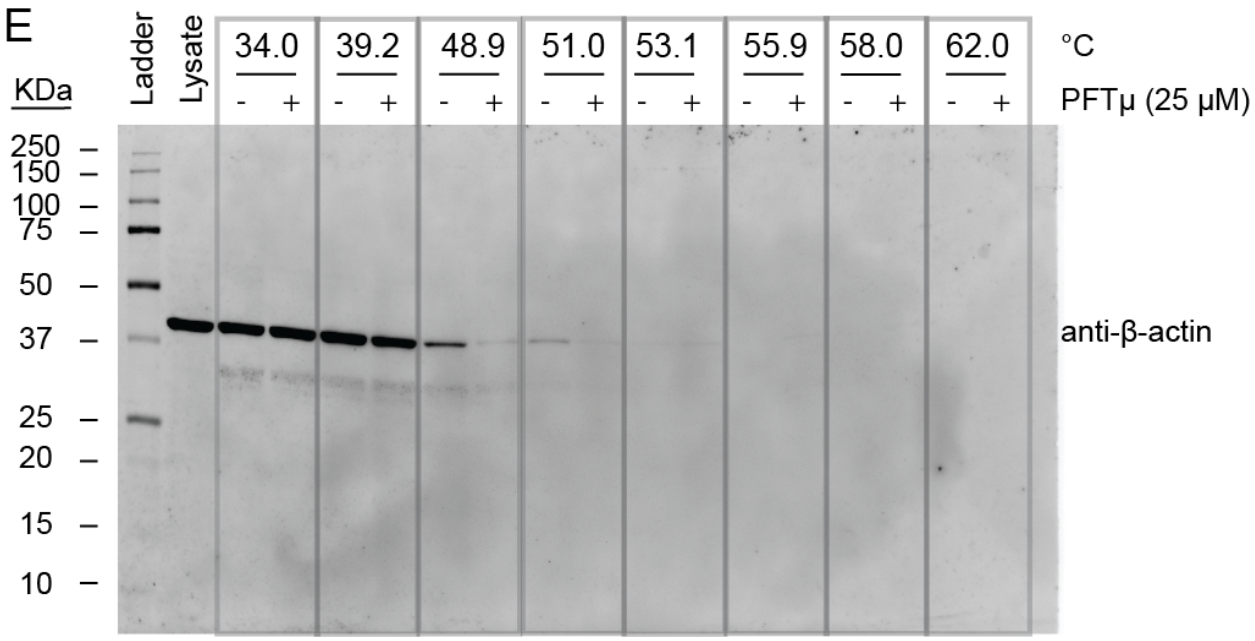

Figure S37. CETSA analysis reveals that PFTμ destabilizes caspase-10. Recombinant caspase-10 (proCASP10) was spiked into 2.8 mg/mL Jurkat lysates and treated with **PFTμ** (25 μM) for 1h under ambient conditions. Samples were treated at the indicated temperatures for 5 min in a Thermal Cycler. Samples were blotted onto a nitrocellulose membrane followed by imaging for procaspase-8 using an (A) anti-caspase-8 primary antibody, (B) blotted for pro-caspase-10 using the anti-caspase-10 primary antibody, (C) blotted for His tag using the anti-His primary antibody. (D) Loading was imaged using stain-free and (E) by blotting for ß-actin using the anti-ß-actin primary antibody.

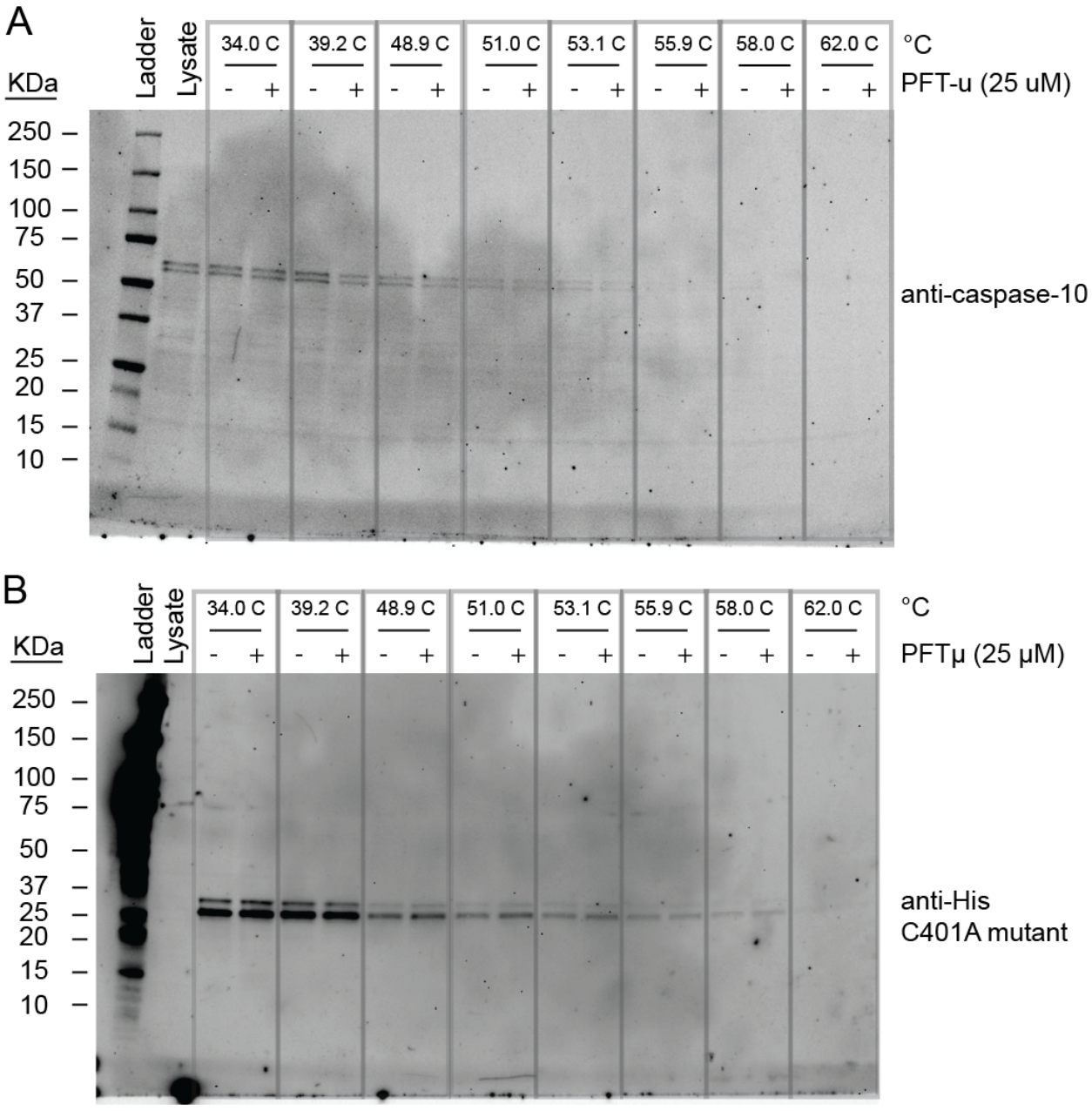
A
Ladder
Lysate
34.0 C
39.2 C
48.9 C
51.0 C
53.1 C
55.9 C
58.0 C
62.0 C
°C
KDa
- + - + - + - + - + - + - + - +
PFT-u (25 uM)
250
150
100
75
50
37
25
20
15
10
anti-caspase-10
B
Ladder
Lysate
34.0 C
39.2 C
48.9 C
51.0 C
53.1 C
55.9 C
58.0 C
62.0 C
°C
KDa
- + - + - + - + - + - + - + - +
PFTμ (25 μM)
250
150
100
75
50
37
25
20
15
10
anti-His
C401A mutant

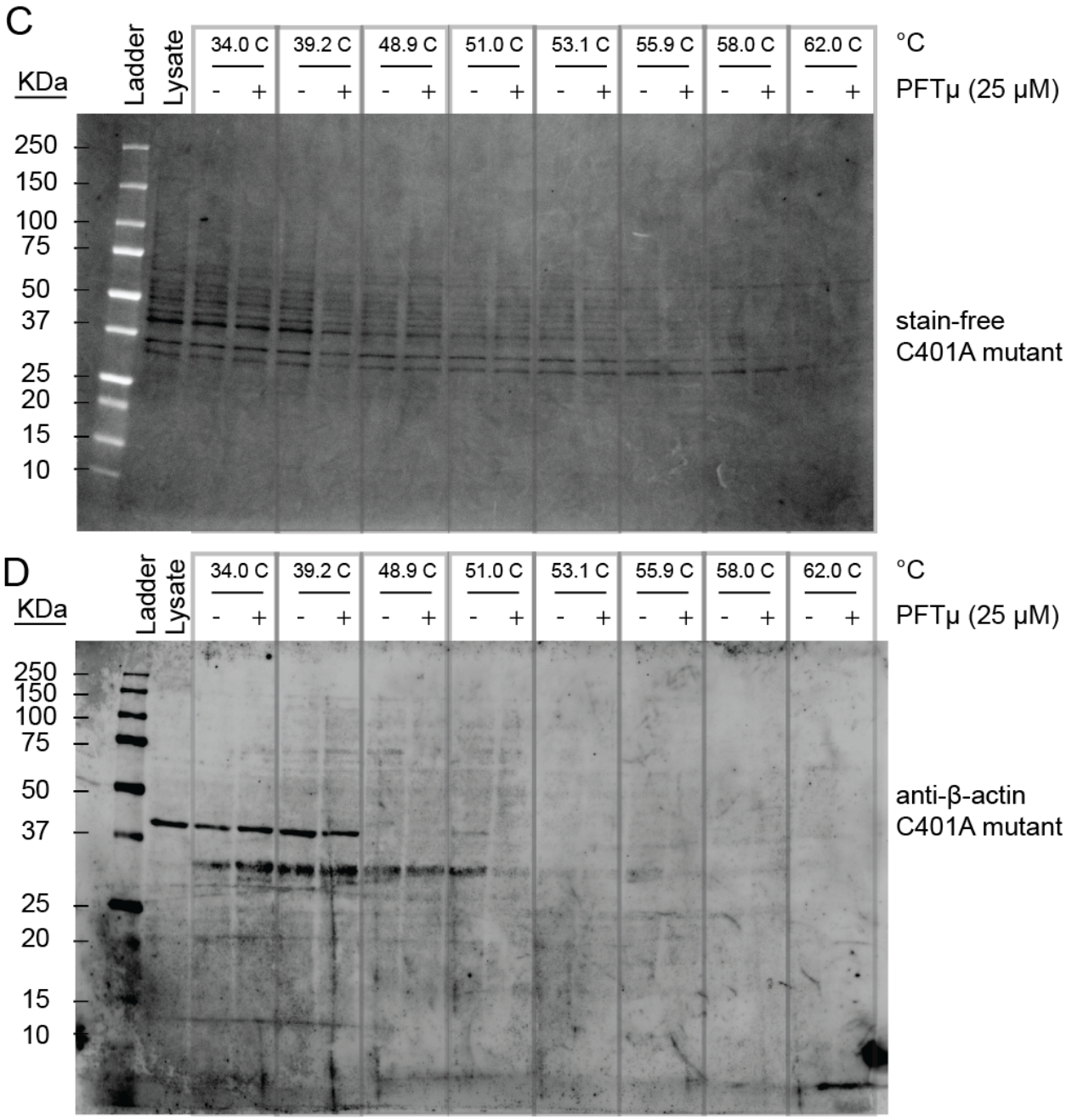

Figure S38. CETSA analysis reveals that PFTμ does not destabilize recombinant pro-caspase-10_C401A. Recombinant procaspase-10 C401A mutant (1 μM) spiked into 3.3 mg/mL Jurkat lysates treated with **PFTμ** (25 μM) for 1h at ambient conditions. Samples were treated at the indicated temperatures for 5 min in a Thermal Cycler. Samples were blotted onto a nitrocellulose membrane followed by (A) imaging for pro-

caspase-10 using the procaspase-10 using the anti-caspase-10 primary antibody, (B) blotted for His tag using the anti-His primary antibody. (C) Loading was imaged using stain-free and (D) by blotting for ß-actin using the anti-ß-actin primary antibody.

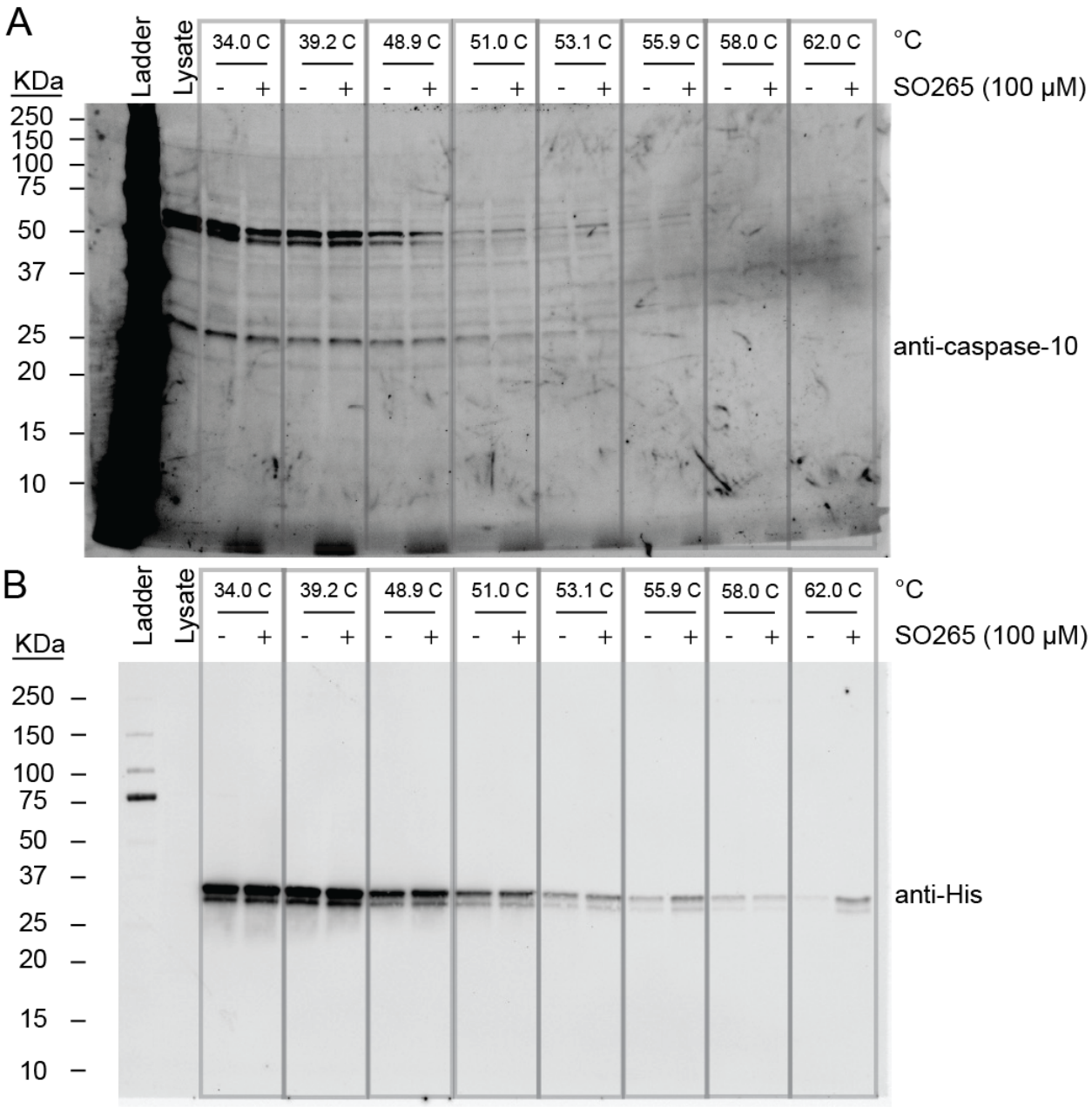

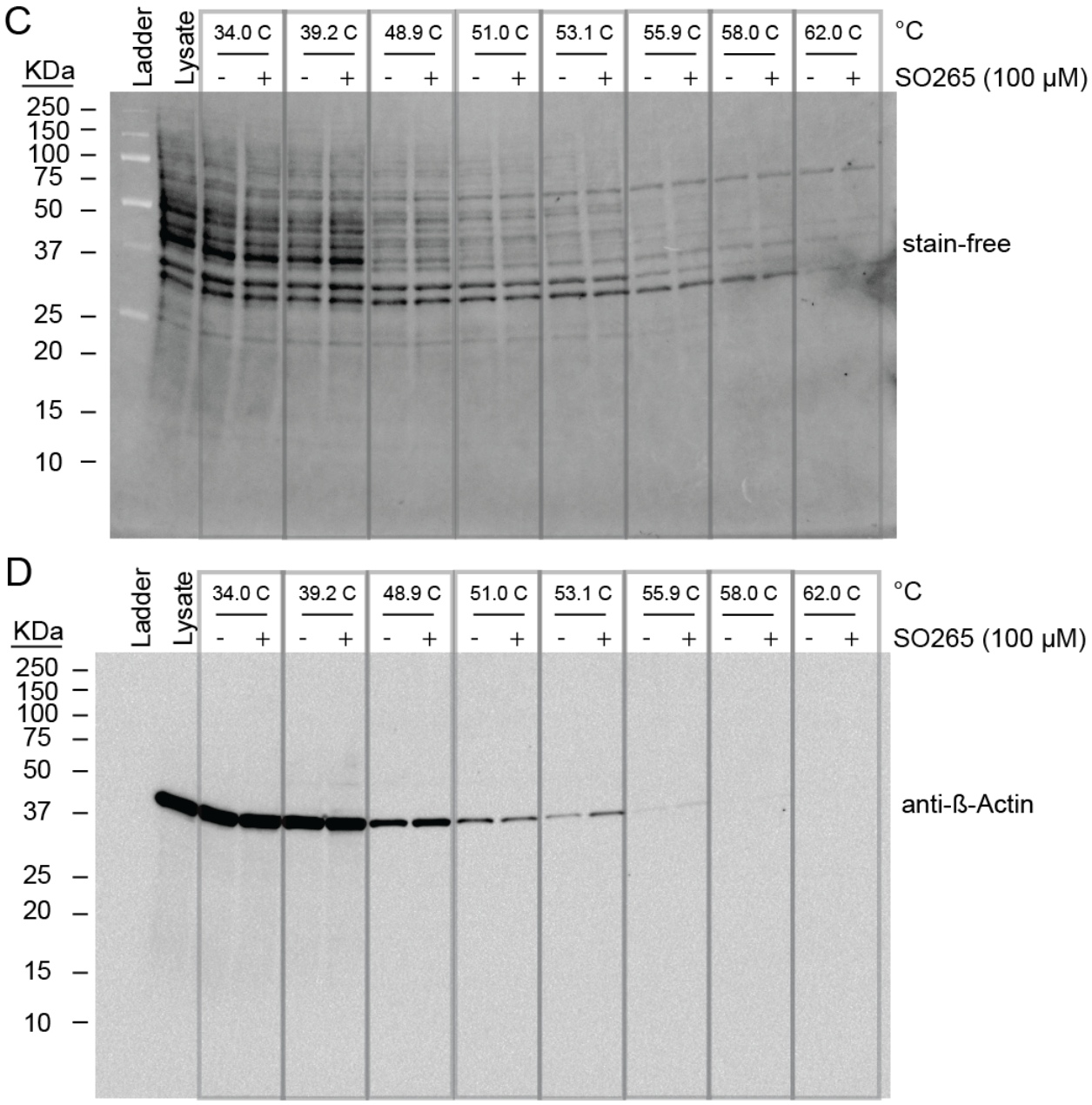

Figure S39. CETSA analysis reveals slight stabilization of endogenous caspase-10 and recombinant caspase-10 by SO265s. Recombinant procaspase-10 (proCASP10) (1 µM) was spiked into 3.0 mg/mL Jurkat lysates followed by treatment with **SO265s** (100 µM) for 1h at ambient conditions. Samples were treated at indicated temperatures for 5 min in a Thermal Cycler. Samples were blotted onto a nitrocellulose membrane followed

(A) by imaging for pro-caspase-10 using the anti-caspase-10 primary antibody, (B)blotted for His tag using the anti-His primary antibody. (C) Loading was imaged using stain-free and (D) by blotting for ß-actin using the anti-ß-actin primary antibody.

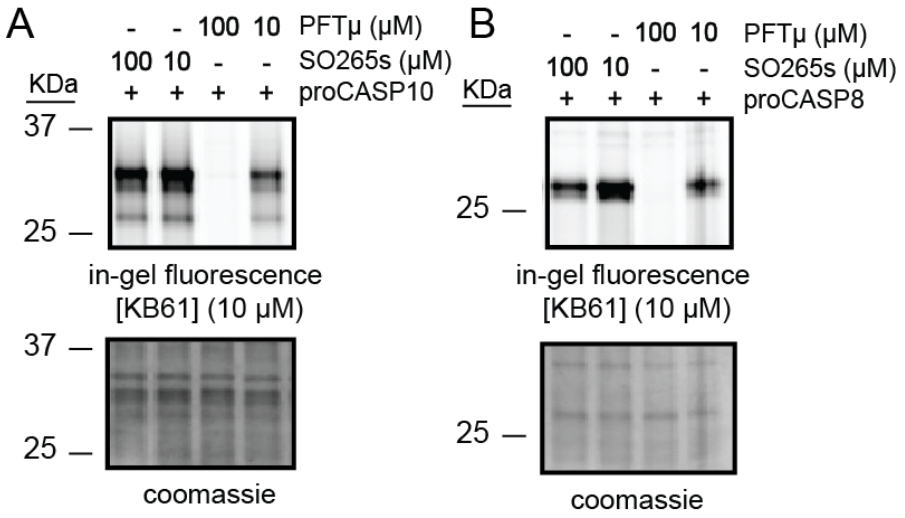

Figure S40. PFTµ competes for labeling of caspase-10 and caspase-8 against KB7 but SO265s only modestly competes for labeling of caspase-8. Competitive ABPP gel of Jurkat lysates (1 mg/ mL) spiked with (A) proCASP10 at 1 µM or (B) proCASP8 at 1 µM followed by treatment with **PFTµ** or **SO265** at the indicated final concentrations (100 µM and 10 µM) for 1h followed by treatment with **KB61** (10 µM) for 1h. Samples were then clicked to rhodamine azide (25 M) for 1h and visualized using in-gel fluorescence.

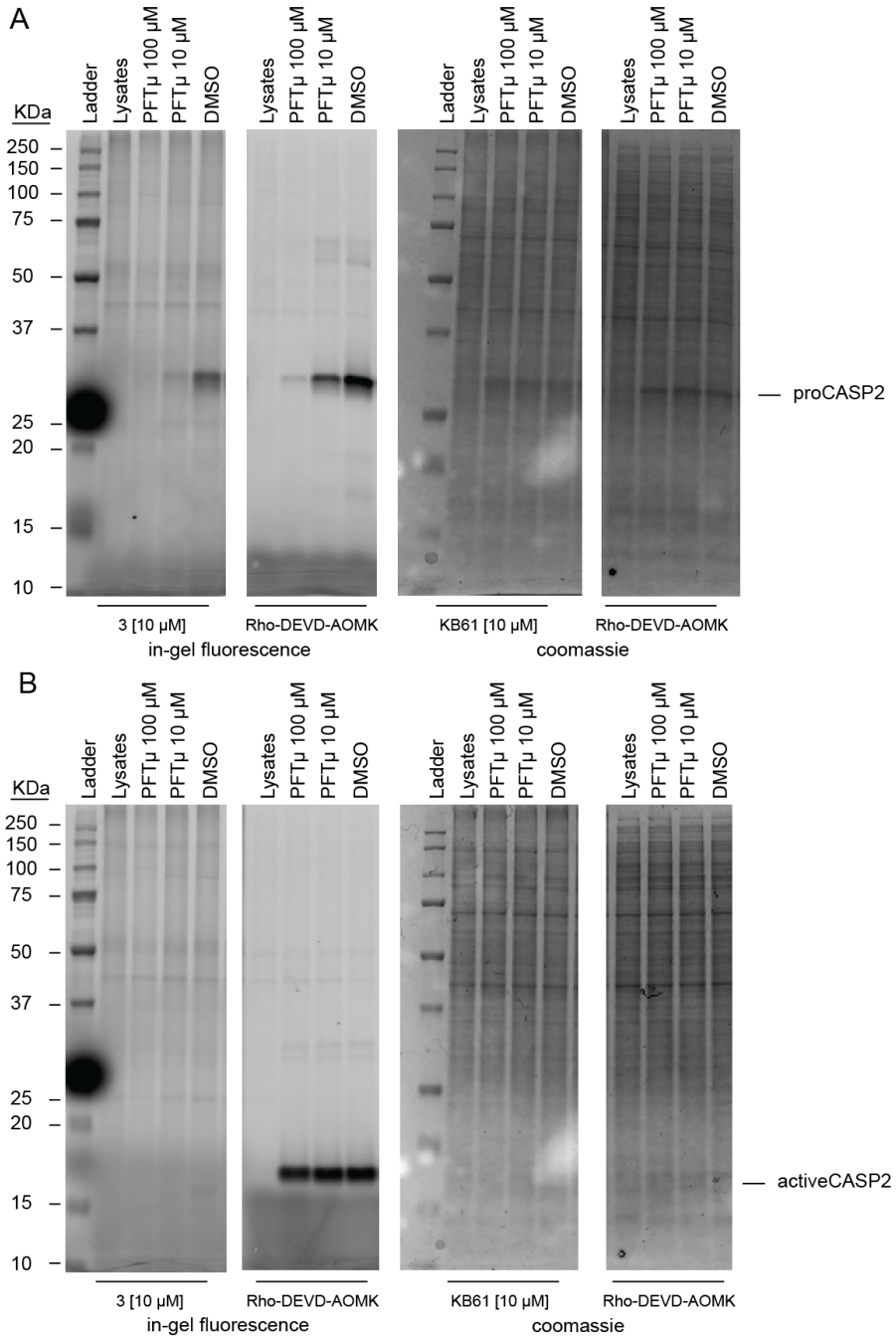

Figure S41. PFTμ competes for labeling of proCASP2 but not activeCASP2. Recombinant procaspase-2 (proCASP2) and active caspase-2 (activeCASP2) were spiked into 1 mg/mL HEK293T lysates at a final concentration of 1 μM. Samples were treated first with **PFTμ** at 100 μM and 10 μM or vehicle control DMSO for 1h followed by

treatment with the click probe **3**[3] for an additional hour at ambient conditions. Samples were then clicked onto rhodamine-azide and visualized by gel-fluorescence. Gels were stained with Coomassie.

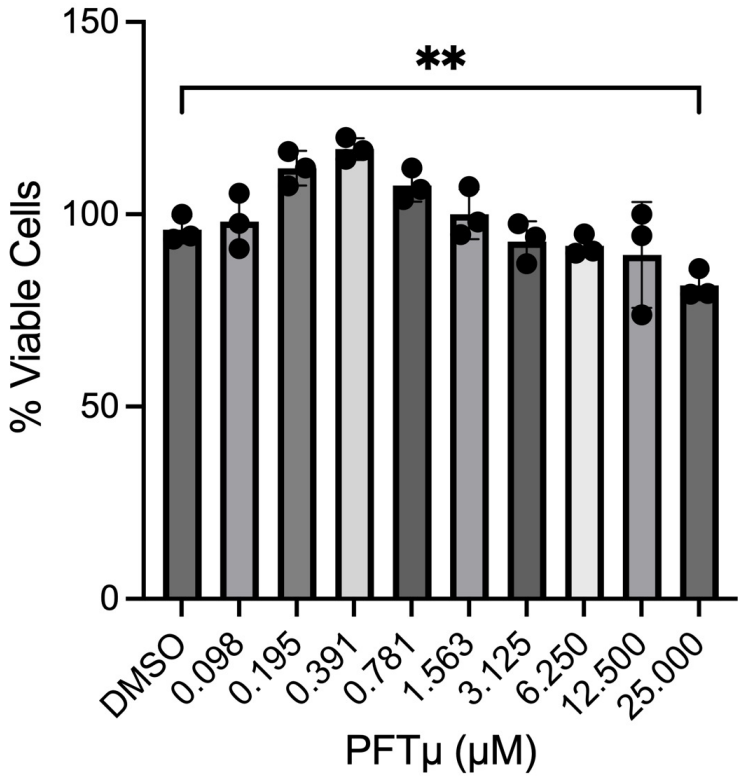

Figure S42. PFTμ treatment results in minimal cytotoxicity in Jurkat cells. Cell viability assay with PFTμ serial dilutions in Jurkat cells treated with compound for 1h followed by CellTiter Glo. Data represents mean values and standard deviations (n = 3 biological replicates). Statistical significance was calculated with unpaired Student's t-tests, **p<0.001.

(C) Supplementary Tables

Table S1 and **Table S2.** Datasets corresponding to each figure, provided in the attached supplementary files (.xlsx).

Table S3. Summary list of recombinant caspase-8 and caspase-10 constructs used in this study.

Construct	Mutation	Source
activeCASP8	n/a	[1]
proCASP8	D347A, D384A, C409S, C433S	[1]
activeCASP3	n/a	Abcam (ab52101)
activeCASP2	n/a	[3]
activeCASP9	n/a	Sigma-Aldrich (218807)
proCASP10	D415A	[1]
activeCASP10	n/a	[1]
proCASP10_C401A	C401A	This study
proCASP10TEV	D415 → ENLYFQG	This study
proCASP2xTEV	D415 and D428 → ENLYFQG	This study
proCASP10TEV Linker	D415 → AAENLYFQG	This study

Table S4. List of caspase-10 primer sequences used in this study.

Purpose	**Primer Sequence**	
TEV insertion 1 D415 to AAENLYFQG	GAAAATCTCTACTTCCAGGGCGGTAAAGAAAAGTTGCCG	Forward
	CAGGTTTTCTGCTGCTTCGATGGATACGGAAGGCTGTATCTC	Reverse
TEV insertion 2 D428 to AAENLYFQG	GGCACCCACTTCCCTGCAGGCAGCAGAAAACCTGTATTTTCAGGGCAG	Forward
	CGGCAGGAATACTGCCCTGAAAATACAGGTTTTCTGCTGCCTGCAGGG	Reverse

TEV insertion No Linker D415 to ENLYFQG	GCCTTCCGTATCCATCGAAAACCTGTATTTTCAGGGCGCTCTGAA	Forward
	CAGAGCGCCCTGAAAATACAGGTTTTCTGCTTCGATGGATACGGAAGG	Reverse
pET23B subcloning (NdeI)	CAGATCATATGGTTAAGACATTCTTGGAAGCCTTACC	forward
pET23B subcloning (XhoI)	CGGCCTCGAGTAATGAAAGTGCATCCAGGGGC	reverse
D428A	CCCACTTCCCTGCAGGCCAGTATTCCTGCCGAGGCTGACTTCC	Forward
	GCAGGAATACTGGCCTGCAGGGAAGTGGGTGCCTGCTCAGGG	Reverse

D415A	CCTTCCGTATCCATCGAAGCAGCTGCTCTGAACCCTGAGCAGG	Forward
	CCTGCTCAGGGTTCAGAGCAGCTGCTTCGATGGATACGGAAGG	Reverse
C401A	CCTAAACTCTTTTTCATCCAGGCCGCCCAAGGTGAAGAGATACAGC	forward
	GCTGTATCTCTTCACCTTGGGCGGCCTGGATGAAAAAGAGTTTAGGT	Reverse

Table S5. Files in Proteomics Identification Database (PRIDE) datasets. PRIDE IDENTIFIER: PXD053315.

Figure	File name	Compound	Experiment
Figure 5B	2023_05_09_KB_noFAIMS_KB_JOC_chymo_tryp_double_5	PFTμ	HL biotin azide
	2023_05_09_KB_noFAIMS_KB_JOC_chymo_tryp_double_6	PFTμ	HL biotin azide

	2024_06_03_KB_NoFAIMS_JOC_biotinazide_PFT_T1_rerun_0523	PFTμ	HL biotin azide
	2024_06_03_KB_NoFAIMS_JOC_biotinazide_PFT_T2_rerun_0523	PFTμ	HL biotin azide
	2024_06_11_KB_FAIMS_JOC1_biotinazide_T1_rerun1_0523	PFTμ	HL biotin azide
	2024_06_11_KB_FAIMS_JOC2_biotinazide_T2_rerun2_0523	PFTμ	HL biotin azide

(D) Biology Methods

Cell lines, culture conditions

Jurkat cells were cultured in Roswell Park Memorial Institute (RPMI) media (Fisher Scientific, 11875119) with 10% fetal bovine serum (Avantor Seradigm Lot # 214B17) and 100U/mL penicillin and 100U/mL streptomycin at 37oC and 5% CO_2. Jurkat cells were obtained from ATCC (TIB-152). ΔΔG3BP1/2 KO U2OS cells stably expressing GFP-G3BP1 were a generous gift from the lab of Dr. Melody Li and were originally generated in the lab of Dr. Paul Anderson[4]. U2OS cells were cultured in Dulbecco's Modified Eagle Medium (DMEM) media (Fisher Scientific, 11995073) supplemented with 10 % fetal bovine serum (Avantor Seradigm Lot # 214B17) and 1 % antibiotics (Pen/Strep, 100 U/mL). Cell culture reagents including RPMI 1640 and DMEM media, trypsin-EDTA and penicillin/streptomycin (Pen/Strep) were purchased from Fisher Scientific.

Mycoplasma testing

Mycoplasma testing was conducted monthly using the MycoAlert® kit (LT07-703, Lonza Rockland, Rockland, ME) following the manufacturer's instructions.

Cell Harvesting

Suspension cells were centrifuged at 1,400 x *g* for 5 minutes and the supernatant was aspirated. The pellets were then washed in 10 mL PBS and centrifuged at 1,400 *g* for 5 minutes. PBS wash was repeated, and the subsequent pellet was then resuspended in 1 mL PBS in a microcentrifuge tube and centrifuged at 1,400 *g* for 5 minutes. The supernatant was aspirated, and the cell pellets were stored at -80 oC.

Cell Lysis

Jurkat lysates used for competitive ABPP gel analysis were lysed using an Ultrasonic Probe Sonicator at Power 2 for 10 pulses, 1-second pulse, and 1 second off on the ice. For western blotting samples, cells were reconstituted and lysed using 100 uL of cold 0.3% 3-[(3-Cholamidopropyl) dimethylammonio]-1-propanesulfonate (CHAPS) buffer in PBS. The reconstituted cell pellet was left to incubate with the CHAPS buffer on ice for 15 min. The samples were then harvested by centrifugation (1,400 x *g*, 10 min), and the clarified supernatant was then transferred to a new tube.

Subcloning of caspase-10

Caspase-10 (Q92851-4, 10-L isoform) expression vector was obtained as a kind gift from Dr. Michael Lenardo. The sequence encoding caspase-10, lacking the prodomain (residue numbers 220-521) was then subcloned into the pET23b(+) at ndeI and xhoI fused to a C-terminal hexahistidine-tag. Plasmids were propagated in chemically competent TOP10 cells.

Mutagenesis

Point mutations (C401A, D415A, D428, and insertions of TEV cleavage motifs at D415) were created by PCR-based site-directed mutagenesis using the primers in **Table S2**. Plasmids were propagated in TOP10 chemically competent cells and isolated by Zyppy Plasmid Miniprep following the manufacturer's protocol (Zymo Research, D4037).

Protein expression and purification

The sequence encoding caspase-10, lacking the prodomain (truncated at D219 and earlier residues) was subcloned into the pET23b(+) with a C-terminal hexaHis-tag. Point mutations (C401A, D415A, D428A) were created by PCR-based site-directed mutagenesis. TEV insertion mutations (ENLYFQG and AAENLYFQG) were created by PCR-based site-directed mutagenesis. Plasmids were propagated in TOP10 chemically competent cells. Single colonies from TOP10 grown cells were collected in 5 mL of LB supplemented with 100 µg/ml ampicillin and grown overnight (16h). Cells were harvested the following day and subjected to Zyppy Plasmid Miniprep following the manufacturer's protocol (Zymo Research, D4037). Following sequencing of plasmids, validated plasmids were transformed to BL21(DE3) *E. coli* cells. Single colonies were picked from an LB agar plate and grown in 10 mL of LB media supplemented with 100 µg/mL ampicillin at 37 oC for 18h. The cell culture was then transferred and grown in 1 L of Miller LB medium at 37°C to an optical density (OD600) of 0.5. The TEV cleavable construct cultures were then cooled to 18°C, induced with 1 mM isopropyl-β-D-galactopyranoside (IPTG), and incubated for an additional 4 h at 18°C. he other active- and pro-constructs were cooled to 18°C, induced with 1 mM IPTG, and incubated overnight (16-18 h) at 18°C. The cells were centrifuged at 8,000 x *rpm* for 45 min. All cell pellets were stored at -80°C except for the TEV cleavable constructs (i.e. proCASP10TEV Linker) which was lysed and processed immediately after induction. The cells were resuspended in 10 mL lysis buffer (100 mM Tris pH 7.5, 100 mM NaCl, 25 mM Imidazole) per 1 g of cells. The resuspended cells were passed through a microfluidizer (Avestin Emulsiflex C3 Homogenizer; 8,000 psi x2 rounds) to ensure lysis. The cell debris was removed by centrifugation (20,000 x

g, 45 min, at 4 oC) and the supernatant was resuspended with 1 mL of Hispur Ni-NTA agarose resin (Thermo Scientific™, PI88222). The sample was washed with lysis buffer (2 x 50 mL). His-tagged caspase-2 was eluted from the resin using an elution buffer with high imidazole concentration (100 mM Tris pH 7.5, 100 mM NaCl, 250 mM imidazole). The eluted sample was concentrated (Amicon Ultra Centrifugal Filter Unit, 4 mL 10 kDa, Fisher Scientific, UFC801024) and buffer exchanged via PD10 desalting column (Cytiva, GE17-0851-01) into storage buffer (20 mM Tris pH 7.5, 50 mM NaCl, 5 mM DTT). Recombinant TEV protease was purchased from the Berkeley MacroLab QB3, where it was was expressed as a double mutant (L56V / S135G) pRK793 plasmid in Rosetta2(DE3) pLysS cells (TEV-DM-Prk793 L56V/ S135G) and stored in 25 mM HEPES pH 7.5, 400 mM NaCl, 10% glycerol, 1 mM DTT. Recombinant proCASP8 and proCASP10 were purified , as reported previously[1].

Recombinant TEV protease

Recombinant TEV protease was purchased from the Berkeley MacroLab QB3, where it was was expressed as a double mutant (L56V / S135G) pRK793 plasmid in Rosetta2(DE3)pLysS cells (TEV-DM-Prk793 L56V/ S135G) and stored in 25 mM HEPES pH 7.5, 400 mM NaCl, 10% glycerol, 1 mM DTT.

Recombinant Caspases

Recombinant active, proCASP8, proCASP10, proCASP10TEV, and proCASP2TEV were purified as reported previously[1]. In brief, plasmids were transformed to BL21(DE3) *E. coli* cells (New England Biolabs). Starter cultures were grown from single colonies in 10 mL

of LB media under ampicillin selection (100 µg/mL) at 37°C for 18 hours. 1 L of Miller LB medium was inoculated with each starter culture (10 mL) and grown with shaking (200 rpm) at 37°C to an optical density (OD600) of 0.5. The culture was then cooled (18°C) and induced for 4h at 18°C with 1 mM IPTG. The cells were centrifuged at 8,000 x *rpm* for 45 min, and the cell pellet mass was measured. The cells were resuspended in 10 mL lysis buffer (100 mM Tris pH 7.5, 100 mM NaCl, 25 mM imidazole) per 1 g of cells. The resuspended cells were passed through a microfluidizer (Avestin Emulsiflex C3 Homogenizer; 8,000 psi x2 rounds) to ensure lysis. The cell debris was removed by centrifugation (20,000 x *g*, 45 min*),* and the supernatant was resuspended with 1 mL of Hispur Ni-NTA agarose resin (Thermo Scientific™, PI88222). The sample was washed with lysis buffer (2 x 50 mL). His-tagged recombinant caspase was eluted from the resin using an elution buffer with a high imidazole concentration (100 mM Tris pH 7.5, 100 mM NaCl, 250 mM imidazole). The eluted sample was concentrated (Amicon Ultra Centrifugal Filter Unit, 4 mL 10 kDa, Fisher Scientific, UFC801024), and buffer was exchanged via PD10 desalting column (Cytiva, GE17-0851-01) into storage buffer (20 mM Tris pH 7.5, 50 mM NaCl, 5 mM DTT).

High throughput screening

proCASP10TEV Linker activity was analyzed per well in a low-volume 384-well plate (Fisher Scientific, 784900). First, 10 µL of proCASP10TEV Linker (in PBS) was added to all wells using the Aquamax liquid handler. Each plate was then pinned with compounds (10 µM) or DMSO using a 250 nL pin (Beckman Coulter Biomek FX system) followed by a 1 h incubation (95% humidity, 25 oC). Substrate solution (5 mM DTT, 10 µM Ac-VDVAD-

AFC substrate, 333 mM citrate in PBS with either 667 nM TEV protease or no TEV protease) was then dispensed into each well using an Aquamax liquid handler (Aquamax DW4, Surplus Solutions, 324757). A total of 16 wells were treated with DMSO, and sodium citrate solution containing TEV protease was used as the negative control. A total of 16 wells were treated with DMSO and substrate solution without adding TEV protease and used as the positive controls. The first and last columns of the plates were not used. Z'-factor was calculated per well using the mean and standard deviation of the negative and positive controls (endpoint data) as the first filtering step. From a total of 375 plates, the average Z'-factor calculated was 0.58. Each 384-well plate had a total of 320 wells that were pinned and treated with compounds. The total number of compounds was approximately 120,000 (320 wells x 375 plates). After filtering out plates outside the Z'-factor range (0.5 - 1.0), the resulting number of plates was 327. The average Z'-factor for these plates was 0.72 (from a total of 104,640 compounds) (**Table S1**). The next filtering step was determined with the help of z-scores (refer to *Z'-factor and z-score calculations* methods section). In our study, values with z-scores lower than -3 or those with 3 significant figures lower than the average of the DMSO controls per plate. A total of 237 hit compounds were obtained with a z-score of -3 or lower and used for re-screen, counter-screen, and validation assays.

Re-screening and counter screening (proCASP10TEV and activeCASP10)

proCASP10TEV Linker and activeCASP10 were analyzed per well in a low-volume 384-well plate each. First, 10 µL of proCASP10TEV Linker or activeCASP10 (in PBS) were added to all wells using the Mantis Precise Liquid Dispenser (Formulatrix). Each plate

was then pinned with compounds (10 μM) or DMSO using a 250 nL pin (Beckman Coulter Biomek FX system) followed by a 1h incubation in ambient conditions. Substrate solution was then dispensed using the Mantis Liquid Dispenser. The substrate solution consisted of 5 mM DTT, 10 μM Ac-VDVAD-AFC substrate, 333 mM citrate in PBS for the counterscreen plate (activeCASP10), and the same substrate solution with the addition of TEV protease at 667 nM was used for the re-screen plate (proCASP10TEV Linker). A total of 16 wells were treated with DMSO and used as the positive control wells. For the re-screen plate, 16 wells were treated with a substrate solution in the absence of TEV protease (no TEV, negative controls). The first and last columns of the 384-well plate were not used. z-score was calculated per well using the mean and standard deviation of the positive controls (DMSO wells, n = 16) as shown in the *Z'-factor and z-score calculations* methods section.

Gel-based ABPP

Recombinant proteins were added to 1 mg/mL Jurkat cell lysates to a final concentration of 2 μM recombinant protein. 25 μL of the cell lysate-recombinant protein mixture was then treated with compounds (100 μM) or vehicle (DMSO) for 1h at ambient conditions. The samples were then incubated for 1h with 1 μL of 250 μM click probes (**IAA or KB61yne**) at a final concentration of 10 μM. Samples were then subjected to either click conjugation to rhodamine azide in 3 uL of click mix containing TBTA (1.5 μL of 1.7 mM for a final concentration of 100 μM), $CuSO_4$ (0.5 μL of 50 mM for a final concentration of 1 mM), Rhodamine-azide (0.5 μL of 1.25 mM for a final concentration of 25 μM), and TCEP (0.5 of μL 50 mM for a final concentration of 1 mM) or activity-based probe **Rho-**

DEVD-AOMK (2 μM)**.** Next, 10 μL of 4x Laemmle loading dye (BioRad, 1610747) was added, and the samples were denatured at 95°C for 5 minutes. Samples were resolved by SDS-PAGE and imaged using a BioRad ChemiDoc Imaging System with visualization of protein loading with Coomassie InstantBlue (Fisher Scientific, ISB1L).

TEV activation Gel-based ABPP

Purified recombinant caspase-10-TEV cleavable construct at 2 μM final concentration in 1 mg/mL Jurkat lysates were first treated with either compound **KB61** or **Rho-DEVD-AOMK** at 10 μM final concentration for 1h at ambient conditions. proCASPTEV constructs were then activated with TEV protease (2 mg/mL stock) at increasing final concentrations (0 μM, 0.1 μM, 0.5 μM, 1.0 μM, 2.5 μM, 5.0 μM) for 1h at ambient conditions. Samples treated with compound **KB61** were then subjected to 'click' conjugation to rhodamine azide as prepared in the "Gel-based ABPP" section and visualized by SDS-PAGE in-gel fluorescence using a BioRad ChemiDoc Imaging System. Coomassie InstantBlue was used for the visualization of protein loading.

Caspase activity assay

Enzymatic activity of purchased active-caspase constructs (1 μM recombinant protein, 5 mM DTT, and 333 mM citrate in PBS) [caspase-3, Abcam, product number: ab52101; caspase-7, Abcam, product number: ab52173; caspase-9, Abcam, product number: ab52203] recombinant constructs (activeCASP10, proCASP2, proCASP8 and proCASP10), and TEV cleavable recombinant constructs (333 nM recombinant protein, 5 mM DTT, 333 mM citrate in PBS) were all determined using the fluorescent caspase-2

substrate Ac-VDVAD-AFC (Cayman Chemicals, item number 37351) at 10 μM final concentration. Activity assay is read on a BioTek Plate reader immediately after mixing active- or TEV-cleavable constructs with the substrate solution containing 5 mM DTT, 333 mM citrate pH 7.4, and 10 μM substrate. 7-amino-4-trifluoromethylcoumarin (AFC) released by substrate cleavage was detected at λ_{ex} = 400 nm and λ_{em} = 505 nm using a multimodal Synergy H1 microplate reader (BioTek). Reads were collected every minute after substrate addition. For the HCl acidic acid treatment, compound SO265 was prepared as a 10 mM stock in DMSO, 1 M citrate, 333 mM citrate, or 10 mM HCl and left to incubate at 37°C for 15 min. 10 mM stocks were directly used to treat proCASP10TEV Linker (333 nM in PBS) or TEV protease (667 nM in PBS) at a final concentration of 100 μM for 1h. Samples were then treated with substrate solution (10 μM substrate, 667 nM TEV protease, and 5 mM DTT in PBS). Percent activities were calculated from the slope of the linear range determined from the reaction progress curves. GraphPad Prism (Version Prism 10.2.3) was used to obtain K_m and k_{cat} values by fitting reaction velocities into the Michaelis-Menten equation using varied fluorogenic substrate Ac-VDVAD-AFC concentrations of 100 μM, 75 μM, 50 μM, 20 μM, 10 μM, 5 μM, 2.5 μM, and 1.0 μM.

TEV protease activity assay

TEV protease (100 nM final concentration) in PBS buffer was treated with a custom-ordered TEV protease substrate, **DABCYL-ENLYFQSGTK-5-FAM**, from GenScript. TEV substrate was prepared as 1 μM aliquot in DMSO, added to TEV protease samples at 50 nM final concentration, and detected at λ_{ex} = 495 nm and λe_m = 550 nm. Activity assay is read on a BioTek Plate reader immediately after mixing TEV protease samples (first

treated with DMSO or compounds at indicated concentrations for 1h) with the substrate in PBS buffer supplemented with 333 mM citrate and 5 mM DTT.

DataWarrior SAR analysis (SALI Plots)

Rescreen and counter-screen results were analyzed to determine the structure-activity relationship (SAR) using DataWarrior[2]. The linear region of progress curves from re-screen and counter-screen were used to calculate slopes for each treatment. The percent activity of caspase-10 was calculated to the DMSO control slopes. A list of generated percent activity values and SMILES corresponding to each compound were saved in a .csv file (**Table S1**). The generated file was opened with DataWarrior (v6.1.0). Data was decomposed to R-groups before running SAR analysis. The R-group decomposition chosen for our analysis was the “Most central ring system” to generate a new column of similar R-groups for our hit list. Similarity analysis using the structure-activity landscape index (SALI) was then used to generate the clustering SAR analysis based on the most central ring system.

Cellular thermal shift assay (CETSA)

Freshly lysed Jurkat cell lysates were spun down at 12,000 x *g* and 4°C for 10 min to remove any insoluble cell debris, then diluted to a final concentration of 3.0 mg/mL. These lysates were then labeled with either DMSO or compound (100 µM) for 1h at ambient temperature. Next, in 8 PCR tubes, DMSO treated lysates were added (50 µL each). In a different set of 8 tubes, compound-treated lysates (50 µL) were added to each. These lysates were then heated using a PCR block at the specified temperature for 3 min,

immediately followed by an indefinite hold at 4°C. After heating, the lysates were transferred back to 1.5 mL microcentrifuge tubes and centrifuged at 21,100 x *g* and 4°C for 45 min. After centrifugation, 30 µL of the soluble portion of each sample was carefully pipetted into fresh microcentrifuge tubes, and 10 µL of 4x loading dye (Bio-Rad) was added. Samples were resolved by SDS-PAGE (Bio-Rad 4 - 20% Criterion Stain-Free™), and the gel was imaged using Bio-Rad Chemidoc Stain-Free setting for protein loading. The gel was then transferred to a nitrocellulose membrane (Bio-Rad) and blocked in 5% (w/v) milk in TBS (Tris-buffered saline) for 60 min at ambient conditions. Membranes were incubated with primary antibodies in 5% (w/v) milk in TBS overnight (16 - 18 hrs) at 4°C. Blots were then washed 3 times with TBS for 5 min. Membranes were then incubated with secondary antibodies (Goat anti-Rabbit IgG, DyLight 647 and DyLight 800; VWR, 102673-328 and 102673-412) in 5% (w/v) milk in TBST (Tris-buffered saline with 0.1% Tween20) for 1h at room temperature and washed 3 times with TBS. The membrane was then imaged using a Bio-Rad ChemiDoc imager. The primary antibodies and dilutions used are as follows: anti-CASP3 (Cell Signaling, 9662, 1:1,000), anti-caspase-8 (cleaved form, Cell Signaling, 9746, 1:1,000), anti-caspase-8 (pro-form, Cell Signaling, 4970, 1:1,000), anti-actin (Cell Signaling, 3700, 1:5,000), anti-caspase-2 (ProteinTech, 10436-1-AP, 1:1,000), and anti-caspase-9 (Cell Signaling, 9502, 1:1,000), anti-caspase-10 (MBL Life Science, M059-3, 1:1000).

Confocal Microscopy.

Sterilized coverslips were placed in each well of a 24-well plate and coated with poly-d-lysine for 30 minutes at 37°C, then washed 3 times with sterile water and allowed to dry.

ΔΔG3BP1/2 KO U2OS cells stably expressing GFP-G3BP1 were seeded on coverslips overnight (80,000 cells/well) and then treated with the indicated compounds. Following treatment, media was aspirated, and each well was washed 1 time with 500 µL DPBS, followed by fixation with 3.7% formaldehyde in DPBS for 15 minutes at room temperature. Each well was then washed 2 times with 500 µL DPBS and permeabilized with 500 µL 0.1% TritonX in DPBS for 6 minutes at room temperature. Cells were then washed 2x with 500 µL of DPBS and blocked in 1% FBS in DPBS for 30 min at ambient conditions. Cells were then incubated with 500 µL 1 µg/mL DAPI stain in PBS for 5 minutes. Cells were then washed 2 times with 500 µL PBS and mounted onto glass slides using Aqua-Poly/Mount mounting media (Polysciences, Inc., 18606-20). Samples were left to sit in the dark for 24h. Slides were then imaged on a Zeiss LSM880 confocal microscope at 63X oil objective with 2X manual zoom.

Compound treatment and biotinylation

Competitive chemoproteomic analysis was performed as reported previously[5]. In brief, Jurkat lysates were prepared by Ultrasonic Probe Sonicator lysis (Power 2, 10x pulses; 1-second pulse, 1 second off) on ice. Lysate concentrations were then adjusted to 2 mg/mL) and 200 µL lysates (2 mg/mL) were treated with the pifithrin-µ (10 µM) or vehicle (DMSO) for 1h at ambient temperature. Samples were then labeled with 200 µM iodoacetamide alkyne (IAA) for 1h at ambient temperature. Samples were subjected to bioorthogonal copper(I)-catalyzed azide-alkyne cycloaddition (CuAAC)[11] or “click" conjugation to isotopically differentiated “light-” and “heavy-” biotin-azide. The samples were treated with a premixed cocktail of click reagents consisting of biotin-azide tags (4

µl of 5 mM stock), TCEP (4 µL of fresh 50 mM stock in water), TBTA (12 µl of 1.7 mM stock in DMSO/t-butanol 1:4), and $CuSO_4$ (4 µl of 50 mM stock in water). After 1h, the samples were then combined pairwise (400 µL total) and treated with 40 µL of 10% SDS (1% SDS final) followed by 0.5 µL of benzonase (Fisher Scientific, 707464). Samples were left to incubate for 30 min at 37°C. Following benzonase treatment, samples were subjected to Single-Pot Solid-Phase-enhanced sample preparation (SP3), as reported previously[6-9].

Single-Pot Solid-Phase-enhanced Sample-Preparation (SP3)

Following the previously reported protocol, for each 400 µL sample (400 µg protein), 40 µL Sera-Mag SpeedBeadsTM Carboxyl Magnetic Beads, hydrophobic (Thermo ScientificTM, 09-981-123) and 40 µL Sera-Mag SpeedBeadsTM Carboxyl Magnetic Beads, hydrophilic (Thermo ScientificTM, 09-981-121) were gently mixed and washed with 1 mL distilled water. Beads were combined using a magnetic rack (Sergi Lab Supplies, 1005a), and water was carefully aspirated. Washes were repeated 3x. Mixed beads were resuspended in 80 µL of double distilled water and then added to the 400 µL of combined samples. The bead-sample mixture was then incubated for 5 min at ambient conditions with shaking (1000 rpm). 200 proof ethanol was added to each sample such that each sample contained ≥55% ethanol by volume (for 480 µL of combined sample/SP3 beads, 600 µL of ethanol was added). The samples were incubated for 5 min at ambient conditions with shaking (1000 rpm). The beads were then washed three times with 600 µL 80 % ethanol in water. After washes, ethanol was removed using the magnetic rack, and beads were then resuspended in 200 µL 0.5 % SDS in PBS containing

2 M urea. 10 µL of 200 mM DTT (10 µM final concentration) was then added to each sample, and the samples were incubated at 65°C for 15 min. Following reduction, 10 µL of 400 mM iodoacetamide (20 µM final concentration) was added to each sample, and the samples were incubated for 30 min at 37°C with shaking at 300 rpm. Subsequently, 600 µL of 200-proof ethanol was added to each sample, and the samples were incubated for 5 min at ambient conditions with shaking (500 rpm). Beads were then washed three times with 80 % ethanol in water. Samples were then diluted with 150 µL 2 M urea in PBS, followed by the addition of reconstituted MS-grade trypsin (2 µg, Promega, V5111) and chymotrypsin (1 µg, ThermoFisher, PI90056). The samples were subjected to water bath sonication for 1 min and subsequently left to digest overnight (16 - 18hr) at 37oC and shaking at 200 rpm. The digested peptide solution and SP3 beads were then transferred into 15 mL falcon tubes. Peptides were then re-bound to SP3 beads by adding 3.8 mL of 100% acetonitrile for a final percentage of ≥95% acetonitrile by volume. The peptides were then shaken at 1000 rpm for 10 min at ambient temperature. Beads were collected using a magnet, and the solution was discarded. Samples were washed with 1 mL of 100% acetonitrile three times. Digested peptides were then eluted with 100 µL of 2% DMSO in water, shaking at 1000 rpm for 30 min at 37°C. The supernatant was collected on ice in a 1.5 mL centrifuge tube after separating SP3 beads with a magnetic rack. SP3 beads were resuspended with an additional 100 µL of 2% DMSO in water, shaking at 1000 rpm for 45 min at 37°C. The supernatant was collected after separating SP3 beads with a magnetic rack and combined with the previous elution volume (200 µL total).

Streptavidin Enrichment

PierceTM Streptavidin Agarose resin (Thermo ScientificTM, PI20353) (100 µL of resin) was first washed for a total of 3 times in 10 mL of PBS followed by centrifugation at 1,800 x g, 3 min each wash. Following the final wash with PBS, the buffer was carefully aspirated, ensuring it did not disturb spun-down agarose resin. The samples were then resuspended in 1 mL PBS in a 1.5 mL microcentrifuge tube. The 200 µL peptide elution from previously prepared SP3 clean-up and digestion method was added directly to the 1 mL of streptavidin resin in PBS. The samples were left rotating for 2h at ambient conditions. Following enrichment, the samples were spun down by centrifugation at 1,400 x *g* for 5 min, and the supernatant was aspirated and discarded. The streptavidin agarose was then subjected to washes, 2x with 1 mL of PBS and 2x with 1 mL of water. After each wash, the samples were spun down by centrifugation at 1,400 x g for 5 min.

MS Sample Clean-up

Following the manufacturer's protocol, the eluted peptides were subjected to buffer exchange using protein desalting columns, PierceTM C18 100 µL Tips (Thermo ScientificTM, 87784). First, 10 mL of the following four solutions were prepared: A) 100% acetonitrile (MeCN), B) 50:50 MeCN: ultra-pure water mixture, C) Ultrapure water with 0.1% trifluoroacetic acid, and D) 60% MeCN with 0.1% trifluoroacetic acid prepared in ultrapure water. MS sample clean-up was started by equilibrating one Pierce^{TM} C18 100 µL Tip with 100 µL of solution A. This was repeated a total of two times while not allowing the tips to dry between washes. After equilibration, the tips were washed with 100 µL of solution B 2x. The final washing step was using 100 µL of solution C and repeating this wash step three times. Once the tips were washed with solution C, 100 µL of samples

were loaded into the tips, making sure to pipette up/down at least 10x for higher peptide binding efficiency. Once peptides were bound, the tips were washed for a total of 2x with solution C. Finally, elution of peptides proceeded with 100 µL of solution D. Following MS sample clean-up, the 100 µL samples were completely dried by speedvac and the resulting dried peptides were then reconstituted in 20 µL of a solvent composed of 5% acetonitrile and 1% formic acid in ultrapure water.

Proteomics acquisition

The prepared mass spectrometry samples were analyzed using liquid chromatography-tandem mass spectrometry (LC-MS/MS) with a Thermo Scientific™ Orbitrap Eclipse™ Tribrid™ mass spectrometer (Thermo Scientific™) coupled to an Easy-nLC™ 1200 pump and to a High Field Asymmetric Waveform Ion Mobility Spectrometry (FAIMS) Interface, stated when used. The peptides were fractionated using a C18 reversed phase resin packed in-house and prepared using a 16 cm long, 100 µM inner diameter (ID) fused silica capillary (particle size, 1.9 µm; pore size, 100 Å; Dr. Maisch GmbH). An 80-minute water-acetonitrile gradient was delivered using the EASY-nLCTM 1200 system at varying flow rates (Buffer A: water with 3% DMSO and 0.1% formic acid and Buffer B: 80% acetonitrile with 3% DMSO and 0.1% formic acid). The detailed 80-minute gradient includes 0 – 5 min from 1 % to 15 % at 220 nL/min, 3 – 63 min from 15 % to 45 % at 220 nL/min, 63 – 73 min at 45% to 55% at 220nL/min, 73-74 min from 55 % to 95 % at 250 nL/min, and 74 to 80 min at 95% buffer B in buffer A. Data was collected with charge exclusion (1≥8). The data was acquired using a Data-Dependent Acquisition (DDA) method consisting of a full orbitrap MS1 scan (Resolution = 120,000) followed by

sequential MS2 scans (Resolution = 15,000) to utilize the remainder of the 1-second cycle time. The precursor isolation window was set to 1 m/z and high energy c-trap dissociation (HCD) normalized collision energy was set to 30%. The run time was 80 minutes, and the injection volume was 5 µL. Data acquired with the FAIMS device utilized 3 compensation voltages (CV; -35, -45, -55V) as used in our previous study[6].

Data analysis

The proteomic workflow for the experiments was analyzed using FragPipe with initial tool parameters set as default. FragPipe output data was compiled using in-house Python scripts. Custom python scripts compiled modified_peptide_label_quant.tsv (quantification) outputs from FragPipe (v21.0). As a preprocessing step, the logged ratios from singleton peptides (ratios that come from peptides that are unpaired) were removed before further analysis. Unpaired heavy- or light-identified peptides remained by setting ratios to $\log_2(20)$ or $\log_2(1/20)$. Median heavy-over-light ratios were computed for the same cysteine residue from cysteine peptides of different charges and missed cleavages in the same replicate. The average of medians was calculated to obtain a final "average_of_medians" metric. This "average_of_medians" value was utilized to compare the isotopical quantification of the same identified peptides, modified cysteine residues and proteins across replicates within the same experiment.

Protein, peptide, and cysteine identification:

The MS RAW files were searched with MSFragger (v4.0) and FragPipe (v21.0). Precursor and fragment mass tolerance was set as 20 ppm. Missed cleavages were allowed up to

1. Peptide length was set to 7 – 50, and peptide mass range was set to 500 - 5000. For identification, cysteine residues were searched with differential modification C+. For ligandability quantification, MS1 labeling quant was enabled with Light set as C+463.2366 and Heavy set as C+469.2742. MS1 intensity ratio of heavy and light labeled cysteine peptides were reported with Ionquant (v1.8.10). Calibrated and deisotoped spectrum files produced by FragPipe were reused for further analysis. The MS search data have been deposited to the ProteomeXchange Consortium via the PRIDE partner repository with the dataset identifiers PXD053315. File details can be found in **Table S2**. Custom python scripts were implemented to compile labeled peptide datasets. Unique proteins, unique cysteines, and unique peptides were quantified for each dataset. Unique proteins were established based on UniProt protein IDs. Unique peptides were found based on sequences containing a modified cysteine residue. Unique cysteines were classified by an identifier consisting of a UniProt protein ID and the amino acid number of the modified cysteine (ProteinID_C#); residue numbers were found by aligning the peptide sequence to the corresponding UniProt protein sequences found in protein.fas FragPipe output files. A new identifier for each modified cysteine residue number was created for cases where multiple cysteines were labeled on the same peptide. Multiplexed peptide identifiers were reported as ProteinID_C#1 and ProteinID_C#2, instead of ProteinID_C#1_C#2.

Cell Titer Glo ® Cell viability analysis

Using a multichannel pipette, jurkat cells in complete RPMI media (100 µL of 1.0 x 10^6 cells/mL) were added to a 96-well white/clear bottom tissue culture-treated plate. To each well, samples were treated with the indicated compounds at the indicated concentrations or vehicle (DMSO). Following 1h incubation, mega FasL (AdipoGen; AG-40B-0130-C010) was Cell viability assay (Promega, G9242) was added to each well, and the relative luminescence (RLU) was measured. Percent cell viability was calculated as reactive to the DMSO-treated Jurkat cells. Samples were analyzed in three biological replicates.

Ellman's Assay

10mM stock Ellman's Reagent solution was prepared by dissolving 4 mg of 5,5′-dithiobis-(2-nitrobenzoic acid) (DTNB) in 1 mL of Reaction Buffer (0.1M sodium phosphate, pH 8.0, containing 1mM EDTA). Reduced GSH standards (0, 31.25, 62.5, 125, 250 µM) were prepared using the same Reaction Buffer. In a 96-well plate, 2.5 µL of the 10mM Ellman's reagent was added to each 200 uL of the GSH standards, and the plates were incubated for 15 mins at room temperature in the dark. Next, the absorbance of the resultant yellow-colored 5-thio-2-nitrobenzoic acid (TNB) product was measured at 412 nm using a Tecan Infinite F500 microplate reader. The data was used to generate a standard curve. For the samples, the indicated compounds were added to 200uL of 125 µM GSH (to the specified final concentrations) and incubated at room temperature for 1 h. Next, 2.5 µL of the 10mM Ellman's reagent was added to this mix and incubated for 15 mins at room temperature. Next, the absorbance of the resultant yellow-colored TNB product was measured at 412 nm using a Tecan Infinite F500 microplate reader. The GSH consumption for each of the indicated compounds was determined from the standard curve.

Statistics

Statistical significance was calculated with an unpaired two-tailed Student's t-test using GraphPad Prism 10(version 10.3.0. GraphPad Software Inc., La Jolla). Data are shown as mean values and standard deviations for replicates ranging from n = 2 to 16, as stated for each experiment. P values of < 0.05 were considered significant.

Z'-factor and z-score calculations

Z-prime (Z'-factor) statistic was used to measure assay quality, showing the separation between the distribution of the positive control (DMSO) and the negative controls (noTEV treatment and **KB7** treatment). Z'-factor was calculated per plate as follows:

$$Z'\ factor\ =\ 1\ -\ \frac{3\ x\ (\sigma p - \sigma n)}{|\mu p - \mu n|}$$

σ = standard deviation

μ = mean

p = positive controls (DMSO)

n = negative controls

Standard score or Z-score is a measure of standard deviations from the mean for each readout value. Z-scores were calculated to the positive controls of each plate (DMSO) for each readout. Z-score was calculated as follows:

$$Z\ -\ score\ =\ \frac{sample - DMSO\ control\ mean}{standard\ deviation\ of\ DMSO\ control}$$

(E) Chemistry Methods

General Methods. All reactions were performed in dried, clean glassware. Silica gel P60 (SiliCycle) was used for column chromatography. Plates were visualized by fluorescence quenching under UV light or by staining with iodine, $KMnO_4$, or bromocresol green. Other reagents were purchased from Sigma-Aldrich (St. Louis, MO), Alfa Aesar (Ward Hill, MA), EMD Millipore (Billerica, MA), Fisher Scientific (Hampton, NH), Oakwood Chemical (West Columbia, SC), Combi-blocks (San Diego, CA) and Cayman Chemical (Ann Arbor, MI) and used without further purification. Additionally, all isotopically enriched reagents were purchased from Sigma-Aldrich (St. Louis, MO) or Cambridge Isotope Laboratories (Cambridge, MA) and used without further purification. ^{1}H NMR and ^{13}C NMR spectra for characterization of new compounds and monitoring reactions were collected in $CDCl_3$, CD_3OD, D_2O, or DMSO-d_6 (Cambridge Isotope Laboratories, Cambridge, MA) on a Bruker AV 400 MHz spectrometer in the Department of Chemistry & Biochemistry at The University of California, Los Angeles. All chemical shifts are reported in the standard notation of parts per million using the peak of residual proton signals of the deuterated solvent as an internal reference. Coupling constant units are in Hertz (Hz). Splitting patterns are indicated as follows: br, broad; s, singlet; d, doublet; t, triplet; q, quartet; m, multiplet; dd, doublet of doublets; dt, doublet of triplets. Low-resolution mass spectrometry was performed on an Agilent Technologies InfinitiyLab LC/MSD single quadrupole LC/MS (ESI source). High-resolution mass spectrometry was performed on a Waters LCT Premier with ACQUITY LC and autosampler (ESI source).

Synthesis of *tert*-butyl 4-(1*H*-imidazole-1-carbonothioyl)piperazine-1-carboxylate (1)

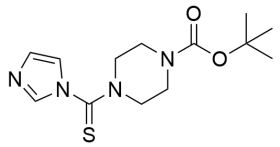

To a stirred solution of 1,1'-thiocarbonyldiimidazole (1.30 g, 7.50 mmol, 1.0 eq.) in CH_2Cl_2 (200 mL) was added *N*-Boc-piperazine (1.40 g, 7.50 mmol, 1.0 equiv.) and the reaction mixture was stirred overnight at room temperature (RT). The reaction mixture was quenched with water, dried (Na_2SO_4), filtered, and concentrated *in vacuo* to afford *tert*-butyl 4-(1*H*-imidazole-1-carbonothioyl)piperazine-1-carboxylate (**1**) (1.83 g, 6.17 mmol, 82 %) as a white solid : ^{1}H NMR (400 MHz, $CDCl_3$) δ_H 7.86 (1 H, s), 7.18 (1 H, s), 7.08 (1 H, s), 3.95 – 3.78 (4 H, m), 3.63 – 3.41 (4 H, m), 1.46 (9 H, s); ^{13}C NMR (101 MHz, $CDCl_3$) δ_C 179.3, 154.3, 137.4, 130.2, 119.2, 81.0, 51.4, 28.3; LRMS *m/z* (ESI^+) 297.1 $[M+H]^+$.

Synthesis of *tert*-butyl 4-(2-hydrazineylethanethioyl)piperazine-1-carboxylate (2)

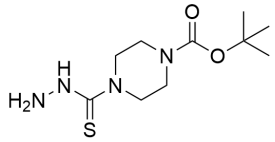

To a stirred solution of *tert*-butyl 4-(1*H*-imidazole-1-carbonothioyl)piperazine-1-carboxylate (**1**) (1.60 g, 5.40 mmol, 1.0 eq.) in EtOH (30 mL) was slowly added hydrazine monohydrate (307 µL, 5.94 mmol, 1.1 eq.). The reaction mixture was stirred at RT for 5 min then heated under reflux for 3 h. The resultant off-white precipitate was filtered, washed with *tert*-butyl methyl ether, and dried by suction to afford *tert*-butyl 4-(2-hydrazineylethanethioyl)piperazine-1-carboxylate (**2**) (670 mg, 2.57 mmol, 47%) as an off-white solid : ^{1}H NMR (400 MHz, DMSO-d_6) δ 3.71 (4 H, dd, *J* 6.2, 4.3), 3.32 (4 H, d, *J*

10.5), 1.40 (9 H, s); ^{13}C NMR (101 MHz, DMSO-d_6) δ 183.0, 154.3, 79.6, 47.4, 28.5; LRMS *m/z* (ESI$^-$) 259.1 [M-H]$^-$.

Synthesis of *tert*-butyl 4-(5-phenyl-6H-1,3,4-thiadiazin-2-yl)piperazine-1-carboxylate (SO263)

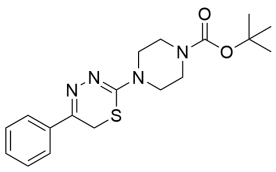

A solution of the 4-(2-hydrazineylethanethioyl)piperazine-1-carboxylate (**2**) (600 mg, 2.30 mmol, 1.0 eq.) and 2-bromoacetophenone (459 mg, 2.30 mmol, 1.0 eq.) in EtOH (10 mL) was stirred under reflux for 30 min. The hot reaction mixture was filtered, and dilute aq. NH_3 was added to the filtrate to achieve pH 8. The resulting precipitate was filtered and recrystallized in EtOH to afford *tert*-butyl 4-(5-phenyl-6*H*-1,3,4-thiadiazin-2-yl)piperazine-1-carboxylate (**SO263**) (180 mg, 499 mmol, 22%) as an off-white solid: ^{1}H NMR (400 MHz, $CDCl_3$) δ_H 7.89 (2 H, s), 7.41 (4 H, d, *J* 7.1), 3.77 – 3.68 (4 H, m), 3.58 – 3.46 (6 H, m), 1.47 (9 H, s); ^{13}C NMR (101 MHz, $CDCl_3$) δ_C 154.7, 151.7, 147.6, 135.5, 129.8, 128.7, 126.7, 80.3, 47.4, 28.4, 28.4, 22.7; LRMS *m/z* (ESI$^+$) 361.1 [M+H]$^+$.

Synthesis of *tert*-butyl 4-(2-ethoxyacetyl)piperazine-1-carboxylate (3)

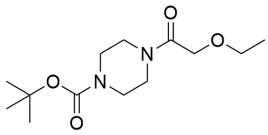

To a solution of *tert*-butyl piperazine-1-carboxylate (2.00 g, 10.7 mmol, 1.0 eq.) and DIPEA (4.50 mL, 26.0 mmol, 2.4 eq.) in CH_2Cl_2 (40 mL) was added 2-ethoxyacetyl chloride (1.41 mL, 12.9 mmol, 1.2 eq.) dropwise. The reaction mixture was stirred at RT

for 2 h before being washed with 10% aq. $(NH_4)_2CO_3$ (2 × 40 mL) then sat. NH_4Cl (2 × 40 mL). The organic component was dried (Na_2SO_4), filtered, concentrated *in vacuo* to afford *tert*-butyl 4-(2-ethoxyacetyl)piperazine-1-carboxylate (2.90 g, 10.7 mmol, 99%) as a yellow oil: ^{1}H NMR (400 MHz, $CDCl_3$) δ_H 4.11 (2 H, s), 3.53 (4 H, t, *J* 7.0), 3.48 (2 H, d, *J* 12.8), 3.40 (4 H, s), 1.43 (9 H, s), 1.19 (3 H, t, *J* 7.0); ^{13}C NMR (101 MHz, $CDCl_3$) δ_C 168.1, 154.6, 80.3, 70.4, 66.8, 45.1, 41.7, 28.4, 15.1; LRMS *m/z* (ESI^+) 186.1 $[M+H]^+$.

Synthesis of 4-(2-ethoxyacetyl)piperazine-1-carbothiohydrazide (X)

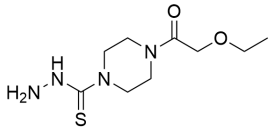

To *tert*-butyl 4-(2-ethoxyacetyl)piperazine-1-carboxylate (2.80 g, 10.3 mmol, 1.0 eq.) in CH_2Cl_2 (40 mL) was added 4 M HCl in dioxane (7.71 mL, 30.8 mmol, 3.0 eq.) dropwise. The reaction mixture was stirred at RT for 2 h before being concentrated *in vacuo* to afford the *tert*-butyl piperazine-1-carboxylate hydrochloride intermediate as an off-white solid. The residue was redissolved in CH_2Cl_2 (40 mL) and DIPEA (3.00 mL, 17.2 mmol, 1.7 eq.) was added followed by di(1*H*-imidazol-1-yl)methanethione (1.83 g, 10.3 mmol, 1.0 eq.). The reaction mixture stirred at RT for 18 h before being concentrated *in vacuo* to afford the 1*H*-imidazol intermediate as a yellow oil. The residue was redissolved in EtOH (40 mL) and hydrazine monohydrate (549 µL, 11.3 mmol, 1.1 eq.) was added and the reaction mixture was stirred under reflux for 3 h. The reaction mixture was cooled to rt and the volume concentrated to ca. 5 mL *in vacuo*. *tert*-Butyl methyl ether (40 mL) was added and the resultant precipitate was collected by centrifugation. The solid was washed with *tert*-butyl methyl ether (2 × 10 mL), collected by centrifugation, and dried *in vacuo* to afford 4-

(2-ethoxyacetyl)piperazine-1-carbothiohydrazide (**X**) (686 mg, 2.78 mmol, 27%) as an off-white solid: ^{1}H NMR (400 MHz, $CDCl_3$) δ_H 4.15 (2 H, d, *J* 2.08), 3.99 – 3.93 (2 H, m), 3.81 – 3.76 (2 H, m), 3.76 – 3.65 (4 H, m), 3.56 (2 H, q, *J* 7.03), 1.23 (3 H, t, *J* 7.03); ^{13}C NMR; LRMS *m/z* (ESI^+) 247.1 $[M+H]^+$.

Synthesis of 2-ethoxy-1-(4-(5-phenyl-6H-1,3,4-thiadiazin-2-yl)piperazin-1-yl)ethan-1-one (SO265) and 2-ethoxy-1-(4-(4-mercapto-5-phenyl-1*H*-pyrazol-3-yl)piperazin-1-yl)ethan-1-one (SO265i)

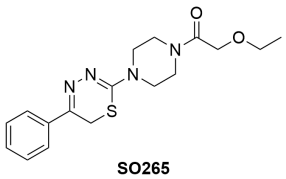

SO265

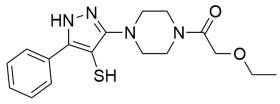

SO265i

A solution of 4-(2-ethoxyacetyl)piperazine-1-carbothiohydrazide (**X**) (300 mg, 1.22 mmol, 1.0 eq.) and 2-bromo-1-phenylethan-1-one (242 mg, 1.22 mmol, 1.0 eq.) in EtOH (10 mL) was stirred under reflux for 30 min. The reaction mixture was concentrated *in vacuo*, and H-NMR indicated an incomplete reaction. The residue was redissolved in EtOH (10 mL), further 2-bromo-1-phenylethan-1-one (121 mg, 0.61 mmol, 0.5 eq.) was added, and the reaction mixture was stirred under reflux for 30 min. The reaction mixture was concentrated *in vacuo* then redissolved in a ca. 1:1 MeOH and water (6 mL) solution before being purified by reverse phase column chromatography (elution with a gradient of 20 – 80% MeCN in water). Relevant fractions were dried by lyophilization to afford the

isomer products. 2-Ethoxy-1-(4-(5-phenyl-6*H*-1,3,4-thiadiazin-2-yl)piperazin-1-yl)ethan-1-one (**SO265**) (49 mg, 0.14 mmol, 12%) was obtained as a pale yellow solid: R*f* 0.44 (EtOAc); ^{1}H -NMR (400 MHz, DMSO-d_6) δ 7.93 (2 H, dd, *J* 8.13, 7.67), 7.50 – 7.43 (3 H, m), 4.15 (2 H, s), 3.77 (2 H, s), 3.72 – 3.63 (4 H, m), 3.57 – 3.52 (4 H, m), 3.49 (2 H, q, *J* 7.01), 1.14 (3 H, t, *J* 7.01); C-NMR (101 MHz, DMSO-d_6) δ 167.6, 153.6, 148.6,135.4, 130.1, 129.1, 127.1, 69.5, 66.3, 47.5, 44.4, 22.0, 15.5; LRMS *m/z* (ESI+) 347.1. 2-Ethoxy-1-(4-(4-mercapto-3-phenyl-1*H*-pyrazol-5-yl)piperazin-1-yl)ethan-1-one (**SO265i**) (131 mg, 378 μmol, 31%) was obtained as an orange oil: R*f* 0.00 (EtOAc); H-NMR (400 MHz, DMSO-d_6) δ_H 14.28 (1 H, br s), 9.34 – 8.75 (2 H, m), 7.63 – 7.48 (3 H, m), 4.40 (1 H, s), 4.17 (2 H, s), 4.03 – 3.82 (4 H, m), 3.78 – 3.59 (4 H, m), 3.51 – 3.41 (2 H, m), 1.17 – 1.07 (3 H, m); ^{13}C -NMR (101 MHz, DMSO-d_6) δ_C 168.4, 162.8, 153.2, 132.8, 132.2, 129.6, 127.7, 69.4, 68.0, 66.3, 49.5, 40.4, 15.5; LRMS (ESI+) 347.1.

Synthesis of 1,1'-((disulfanediylbis(5-phenyl-1*H*-pyrazole-4,3-diyl))bis(piperazine-4,1-diyl))bis(2-ethoxyethan-1-one) (SO265d)

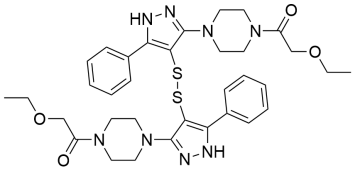

SO265d

A solution of 2-ethoxy-1-(4-(4-mercapto-3-phenyl-1*H*-pyrazol-5-yl)piperazin-1-yl)ethan-1-one (**SO265i**) in DMSO-d_6 (0.5 mL) was left at RT for 2 days. After which time, H-NMR analysis indicated that DMSO-mediated thiol oxidation had occurred, forming 1,1'-((disulfanediylbis(5-phenyl-1*H*-pyrazole-4,3-diyl))bis(piperazine-4,1-diyl))bis(2-ethoxyethan-1-one) **(SO265d)**: ^{1}H-NMR (400 MHz, DMSO-d_6) δ_H (400 MHz, DMSO-d_6)

14.29 (2 H, br s), 7.82 – 7.75 (2 H, m), 7.73 – 7.67 (2 H, m), 7.56 – 7.42 (6 H, m), 4.20 – 4.10 (4 H, m), 3.81 – 3.49 (14 H, m), 3.49 – 3.45 (4 H, m), 3.45 – 3.39 (2 H, m), 1.14 – 1.08 (6 H, m); ^{13}C -NMR (101 MHz, DMSO-d_6) δ_C 167.7, 157.5, 134.3, 129.7, 128.9, 126.0, 118.8, 68.7, 65.4, 49.0, 42.1, 14.6.

General procedures

General procedure I

A round bottom flask was charged with 1,1 '-thiocarbonyldiimidazole (1 equiv.) and dichloromethane (200mL) and stirred at room temperature (RT). And to this solution was added the amine (1 equiv.) Stirring continued overnight at RT. The reaction was stopped after LC-MS showed complete consumption of the starting materials. Next, the reaction mixture was quenched with water, dried over sodium sulfate, filtered, and concentrated to yield the target compound.

General procedure II

To a flask charged with the 1H-imidazole-1-carbonothioyl-based substrate (1 equiv.). 30 ml of ethanol was added and stirred at RT. To this resultant solution was added hydrazine monohydrate (1.1 equiv.). The reaction mixture was continuously stirred for 5 minutes and next refluxed for 3 h. to form off-white precipitates. These precipitates were filtered off, rinsed severally with t-butylmethylether, and dried to yield the target compound.

General procedures III

To a round bottom flask charged with the hydrazineylethanethioyl-based intermediate, (1 equiv.) and 2-bromoacetophenone (1eq.) was added to ethanol solution (10 mL) and stirred under reflux for 30 min. Next, the resultant hot solution was filtered, and to this filtrate was added, dropwise, a dilute aqueous solution of ammonia until the pH= 8 was reached. Next, the precipitate that formed was filtered off and recrystallized from ethanol to yield the target compound.

General procedures IV

To a solution of the starting material in dichloromethane (3.5 mL) at 0oC was added trifluoroacetic acid (1.5 mL) and the mixture was stirred at RT for 1 - 2h. After LC-MS showed complete deprotection, the reaction mixture was concentrated in vacuo to remove the volatiles. The crude was diluted with ethylacetate, washed with sat'd aq Na_2CO_3, then brine. The combined organic extract was dried with anhydrous sodium sulphate and concentrated in vacuo to provide the crude product and used as is without further purification

General procedures V

The amine (1 equiv.) was added to a round bottom flask with a stir bar and dissolved in DCM with stirring. Triethylamine (2 equiv.) was added and the reaction was cooled to 0^{o}C. Chloroacetyl chloride (1.5 equiv.) was added dropwise to the flask, and the reaction was allowed to warm to room temperature as it stirred for 18 h. The reaction was washed with water, extracted with ethyl acetate, dried over anhycrous sodium sulphate. The

combined extracts were concentrated under reduced pressure, then redissolved in DCM and precipitated with hexanes to yield the desired product.

Synthesis of tert-butyl 4-(1H-imidazole-1-carbonothioyl)piperazine-1-carboxylate (1)

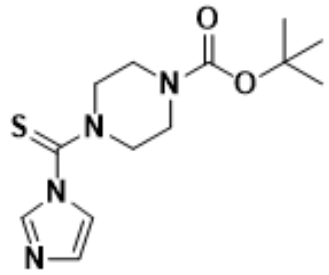

Tert-butyl 4-(1H-imidazole-1-carbonothioyl)piperazine-1-carboxylate was synthesized according to general procedure **I,** using 1,1 '-thiocarbonyldiimidazole (1.3 g, 7.5 mmol, 1 equiv.) and N-Boc-piperazine (1.4g, 7.5 mmol, 1 equiv.) as the amine. Yield: 1.83g (82 %)

^{1}H NMR (400 MHz, $CDCl_3$) : δ 7.86 (s, 1H), 7.18 (s, 1H), 7.08 (s, 1H), 3.95 – 3.78 (m, 3H), 3.63 – 3.41 (m, 5H), 1.46 (s, 9H).

^{13}C NMR (101 MHz, $CDCl_3$) : δ 179.27, 154.25, 137.36, 130.20, 119.21, 80.97, 51.42, 28.33.

LRMS $[M+H]^+$ = $C_{13}H_{21}N_4O_2S^+$: calculated for 297.13; Found 297.1

Synthesis of tert-butyl 4-(2-hydrazineylethanethioyl)piperazine-1-carboxylate (2)

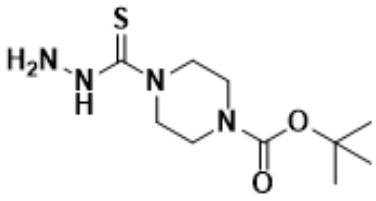

Tert-butyl 4-(2-hydrazineylethanethioyl)piperazine-1-carboxylate was synthesized according to general procedure II, using tert-butyl 4-(1H-imidazole-1-carbonothioyl)piperazine-1-carboxylate (**1**) (1.60 g, 5.4 mmol, 1 equiv.)as the 1H-imidazole-1-carbonothioyl-based substrate.Product: Off-white solid 670 mg (74 %).

^{1}H NMR (400 MHz, DMSO-d_6) δ 3.71 (dd, J = 6.2, 4.3 Hz, 4H), 3.32 (d, J = 10.5 Hz, 4H), 1.40 (s, 9H).

^{13}C NMR (101 MHz, DMSO-d_6) δ 183.04, 154.30, 79.61, 47.36, 28.49.

LRMS $[M-H]^-$ = $C_{11}H_{21}N_4O_2S^-$: calculated for 259.13; Found 259.1

Synthesis of tert-butyl 4-(5-phenyl-6H-1,3,4-thiadiazin-2-yl)piperazine-1-carboxylate (263)

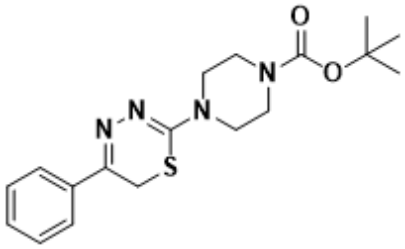

Tert-butyl4-(5-phenyl-6H-1,3,4-thiadiazin-2-yl)piperazine-1-carboxylate was synthesized according to general procedure III using 4-(2-hydrazineylethanethioyl)piperazine-1-carboxylate as the intermediate source and reacted with 2-bromoacetophenone (459 mg, 2.30 mmol, 1 equiv.). Product: 180 mg (22 %)

^{1}H NMR (400 MHz, $CDCl_3$): δ 7.89 (s, 2H), 7.41 (d, J = 7.1 Hz, 4H), 3.77 – 3.68 (m, 4H), 3.58 – 3.46 (m, 6H), 1.47 (s, 9H).

^{13}C NMR (101 MHz, $CDCl_3$): δ 154.65, 151.73, 147.56, 135.51, 129.81, 128.70, 126.71, 80.27, 47.42, 28.42, 28.42, 22.65.

LRMS $[M+H]^+$ = $C_{18}H_{25}N_4O_2S^+$: calculated for 361.16; Found 361.1

Synthesis of tert-butyl 4-(2-ethoxyacetyl)piperazine-1-carboxylate

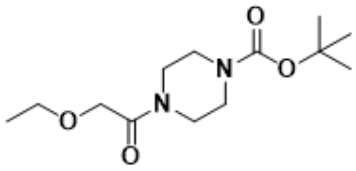

Tert-butyl 4-(2-ethoxyacetyl)piperazine-1-carboxylate was synthesized according to general procedure V using tert-butyl piperazine-1-carboxylate (60 mg, 1 eq, 0.23 mmol) as the amine.

^{1}H NMR (400 MHz, $CDCl_3$): δ 4.11 (s, 2H), 3.53 (t, J = 7.0 Hz, 4H), 3.48 (d, J = 12.8 Hz, 2H), 3.40 (s, 4H), 1.43 (s, 9H), 1.19 (t, J = 7.0 Hz, 3H).

^{13}C NMR (101 MHz, $CDCl_3$): δ 168.13, 154.55, 80.30, 70.42, 66.82, 45.05, 41.68, 28.35, 15.05.

LRMS $[M+H]^+ = C_9H_{19}N_2O_2^+$: calculated for 186.14; Found 186.1

Synthesis of 2-ethoxy-1-(4-(5-phenyl-6H-1,3,4-thiadiazin-2-yl)piperazin-1-yl)ethan-1-one (265)

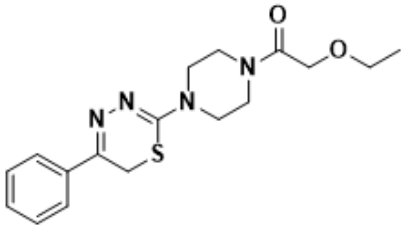

2-ethoxy-1-(4-(5-phenyl-6H-1,3,4-thiadiazin-2-yl)piperazin-1-yl) ethan-1-one (**265-2**) was synthesized according to general procedure III using 4-(2-ethoxyacetyl)piperazine-1-carbothiohydrazide ().

^{1}H NMR (400 MHz, $CDCl_3$) : δ 7.86 (d, J = 7.3 Hz, 2H), 7.39 (s, 3H), 4.14 (s, 2H), 3.78 (s, 2H), 3.74 – 3.64 (m, 4H), 3.63 – 3.51 (m, 6H), 1.21 (t, J = 7.0 Hz, 3H).

^{13}C NMR (101 MHz, $CDCl_3$) : δ 168.19, 151.74, 147.80, 135.36, 129.94, 128.74, 126.74, 70.37, 66.91, 44.84, 41.63, 22.66, 15.11.

HRMS $[M+H]^+$ = $C_{17}H_{23}N_4O_2S^+$: calculated for; Found 347.1571

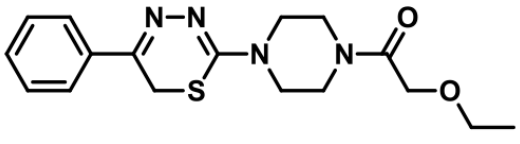

SO265

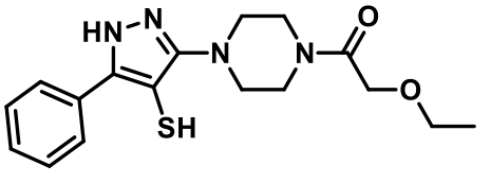

SO265i

A solution of 4-(2-ethoxyacetyl)piperazine-1-carbothiohydrazide (300 mg, 1.22 mmol, 1.0 eq.) and 2-bromo-1-phenylethan-1-one (242 mg, 1.22 mmol, 1.0 eq.) in EtOH (10 mL) was stirred at reflux for 30 min. The reaction mixture was concentrated in vacuo, and H-NMR indicated an incomplete reaction. The residue was redissolved in EtOH (10 mL), further 2-bromo-1-phenylethan-1-one (121 mg, 0.61 mmol, 0.5 eq.) was added, and the reaction mixture was stirred at reflux for 30 min. The reaction mixture was concentrated in vacuo, then redissolved in a ca. 1:1 MeOH and water (6 mL) solution and purified by reverse phase column chromatography (elution with a gradient of 20 – 80% MeCN in H2O). Relevant reactions were dried by lyophilization. 2-Ethoxy-1-(4-(5-phenyl-6H-1,3,4-thiadiazin-2-yl)piperazin-1-yl)ethan-1-one (SO265) (49 mg, 0.14 mmol, 12 %) was obtained as a yellow solid: Rf 0.44 (EtOAc); LRMS (ESI+) 347.1; H-NMR (400 MHz, DMSO-d6) δH 7.93 (2 H, dd, J 8.13, 7.67), 7.50 – 7.43 (3 H, m), 4.15 (2 H, s), 3.77 (2 H, s), 3.72 – 3.63 (4 H, m), 3.57 – 3.52 (4 H, m), 3.49 (2 H, q, J 7.01), 1.14 (3 H, t, J 7.01); C-NMR (101 MHz, DMSO-d6) δC 167.6, 153.6, 148.6,135.4, 130.1, 129.1, 127.1, 69.5, 66.3, 47.5, 44.4, 22.0, 15.5. 2-Ethoxy-1-(4-(4-mercapto-3-phenyl-1H-pyrazol-5-yl)piperazin-1-yl)ethan-1-one (SO265i) (131 mg, 378 µmol, 31.0 %) was obtained as an orange oil: Rf 0.00 (EtOAc); LRMS (ESI+) 347.1; H-NMR (400 MHz, DMSO-d6) δH 14.28

(1 H, br s), 9.34 – 8.75 (2 H, m), 7.63 – 7.48 (3 H, m), 4.40 (1 H, s), 4.17 (2 H, s), 4.03 – 3.82 (4 H, m), 3.78 – 3.59 (4 H, m), 3.51 – 3.41 (2 H, m), 1.17 – 1.07 (3 H, m); C-NMR (101 MHz, DMSO-d6) δC 168.7, 162.8, 153.2, 132.8, 132.2, 129.6, 127.7, 69.4, 66.3, 49.5, 40.4, 15.5

(F) NMR Spectra

^{1}H NMR of **tert-butyl 4-(1H-imidazole-1-carbonothioyl)piperazine-1-carboxylate (1)** in $CDCl_3$

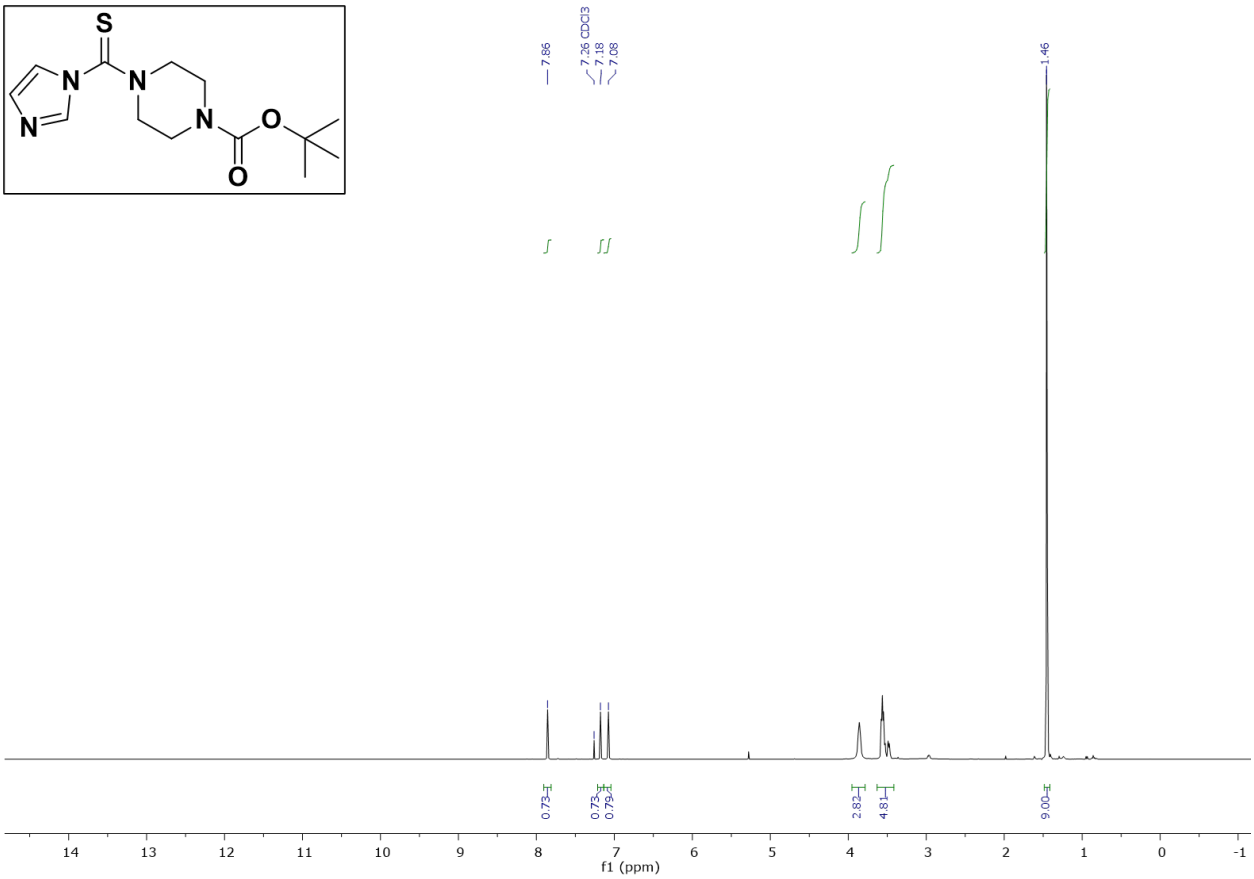

^{13}C NMR of **tert-butyl 4-(1H-imidazole-1-carbonothioyl)piperazine-1-carboxylate (1)** in $CDCl_3$

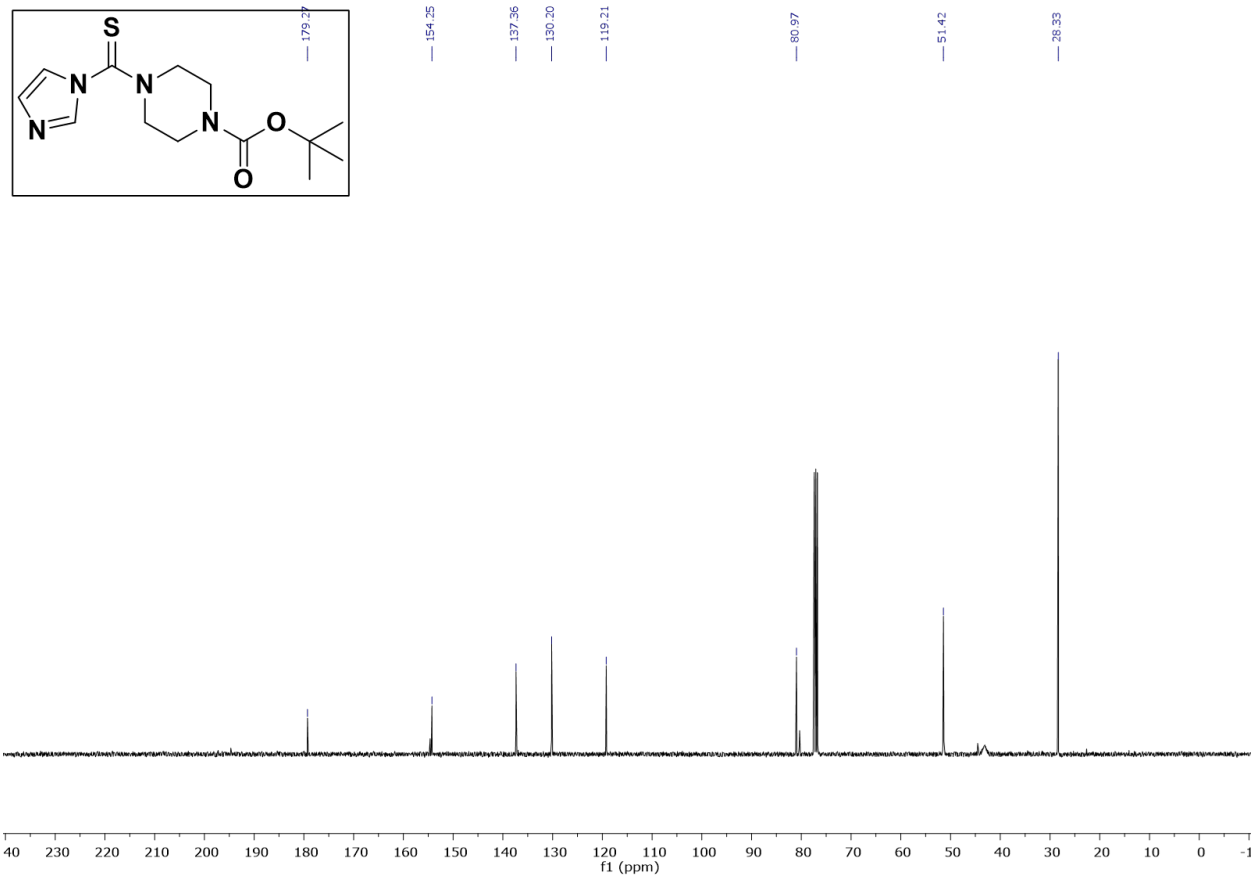

^{1}H NMR of ***tert*-butyl 4-(2-hydrazineylethanethioyl)piperazine-1-carboxylate (2)** in DMSO-d_6

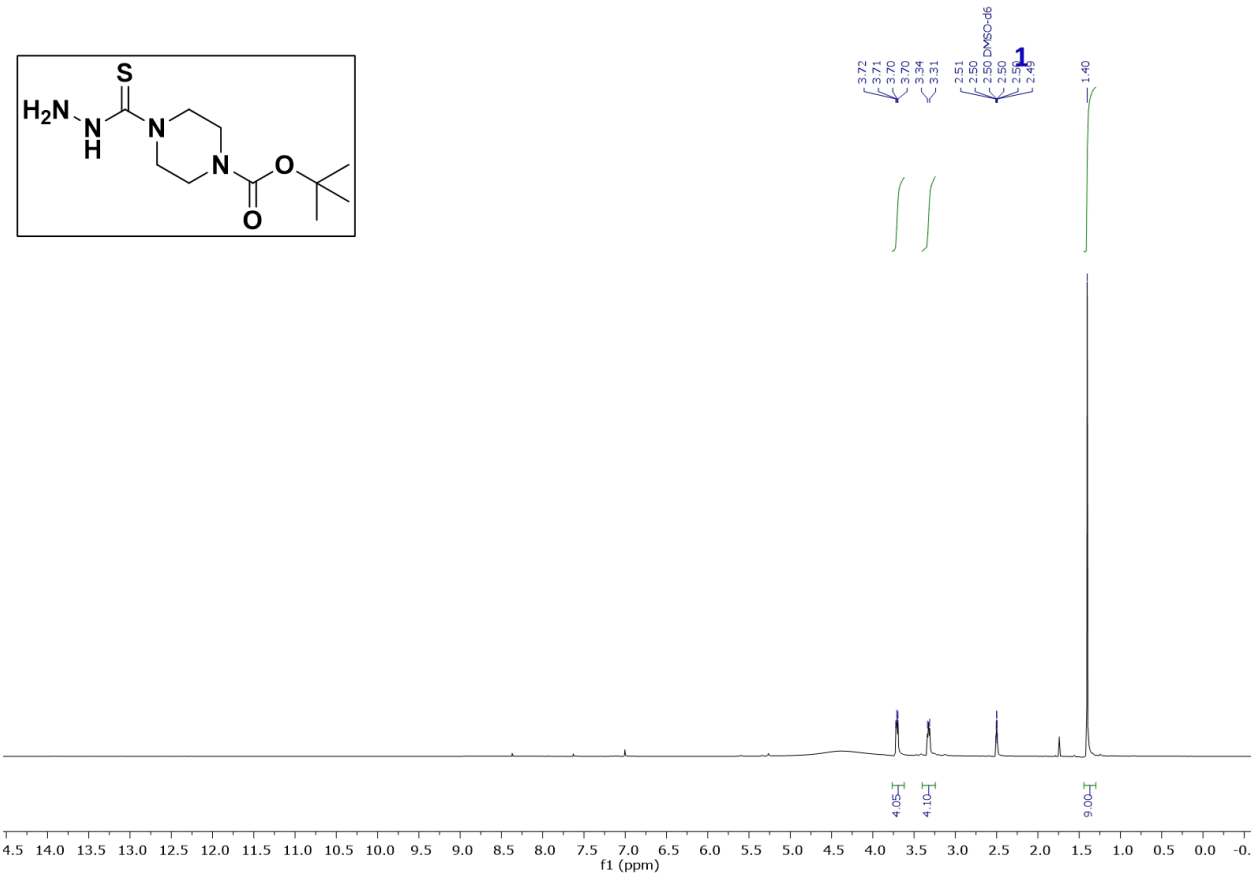

^{13}C NMR of ***tert*-butyl 4-(2-hydrazineylethanethioyl)piperazine-1-carboxylate (2)** in DMSO-d_6

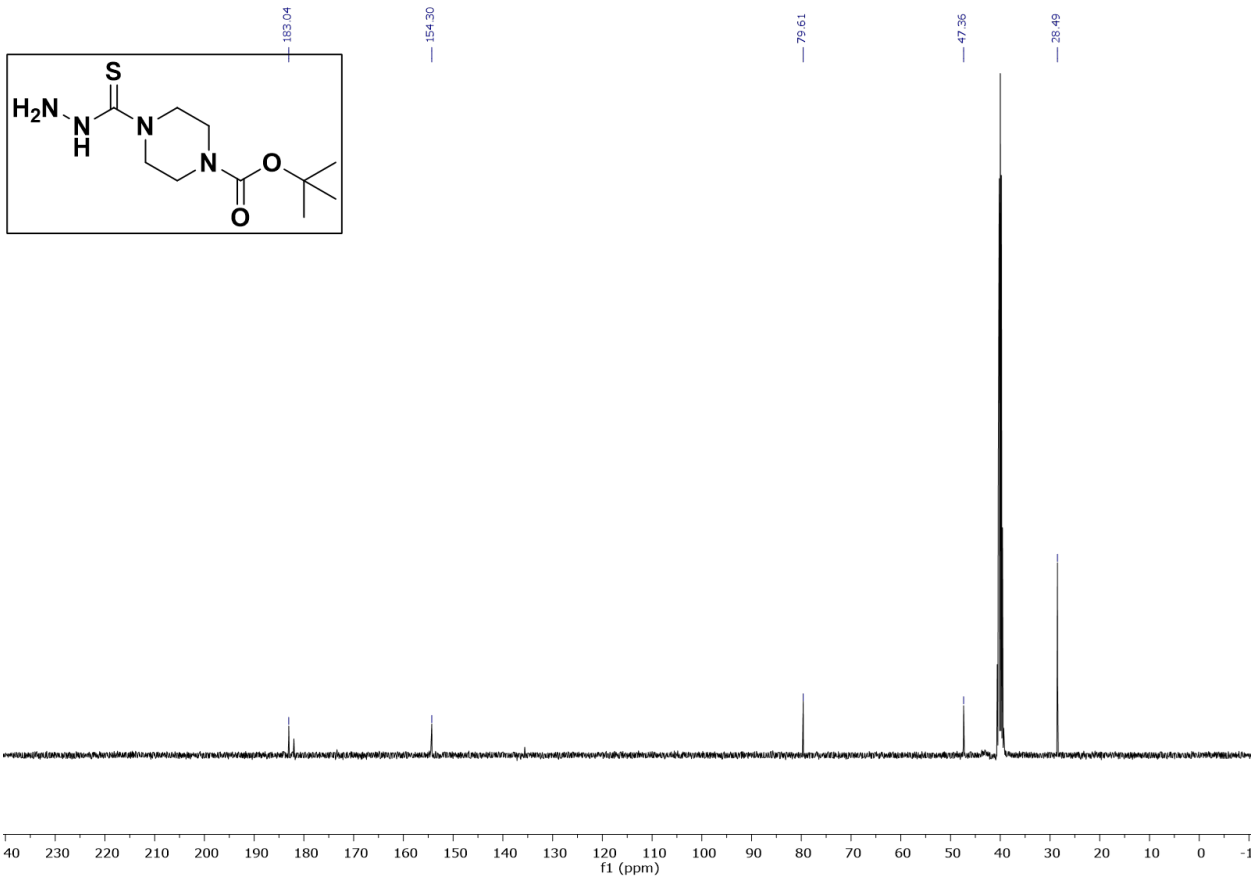

^{1}H NMR of ***tert*-butyl 4-(5-phenyl-6H-1,3,4-thiadiazin-2-yl)piperazine-1-carboxylate (263)** in $CDCl_3$

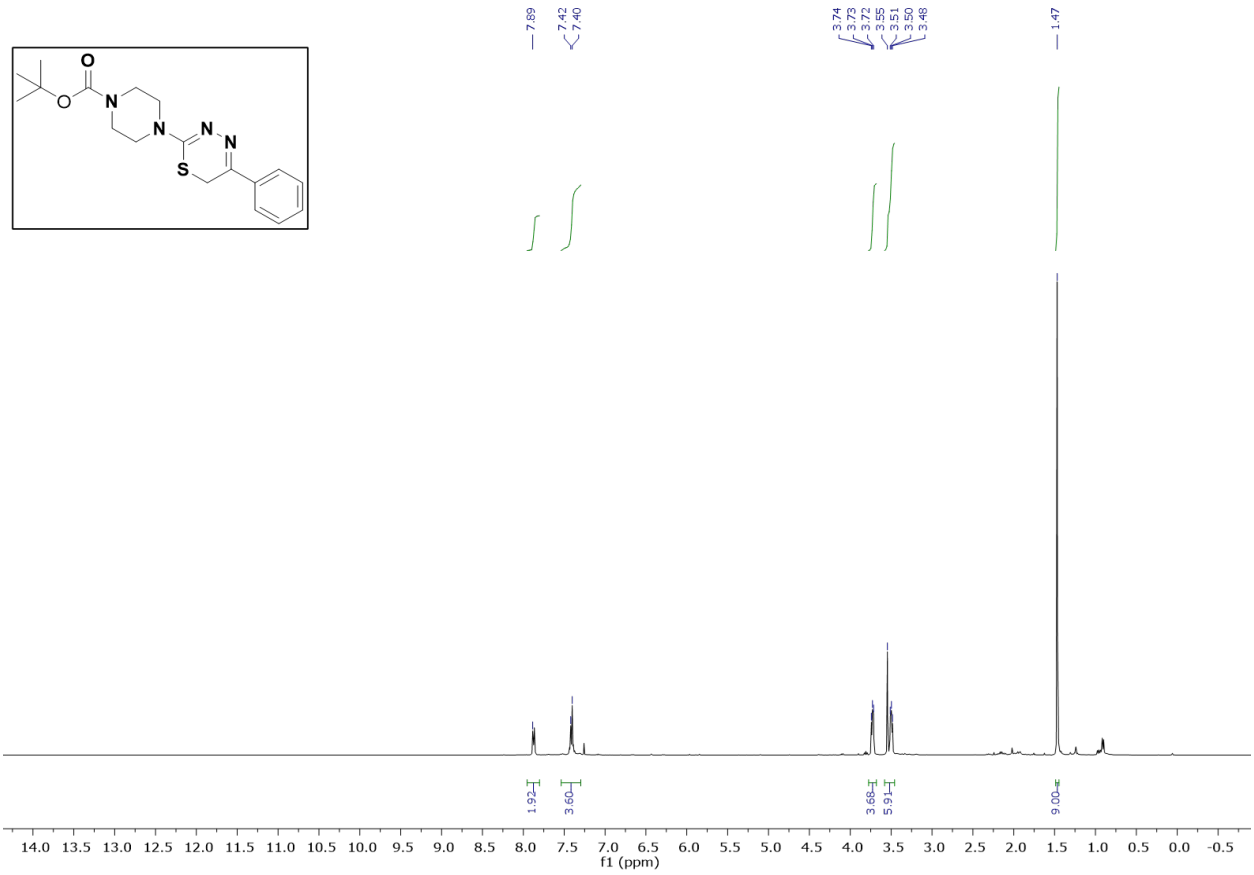

^{13}C NMR of ***tert*-butyl 4-(5-phenyl-6H-1,3,4-thiadiazin-2-yl)piperazine-1-carboxylate (263)** in $CDCl_3$

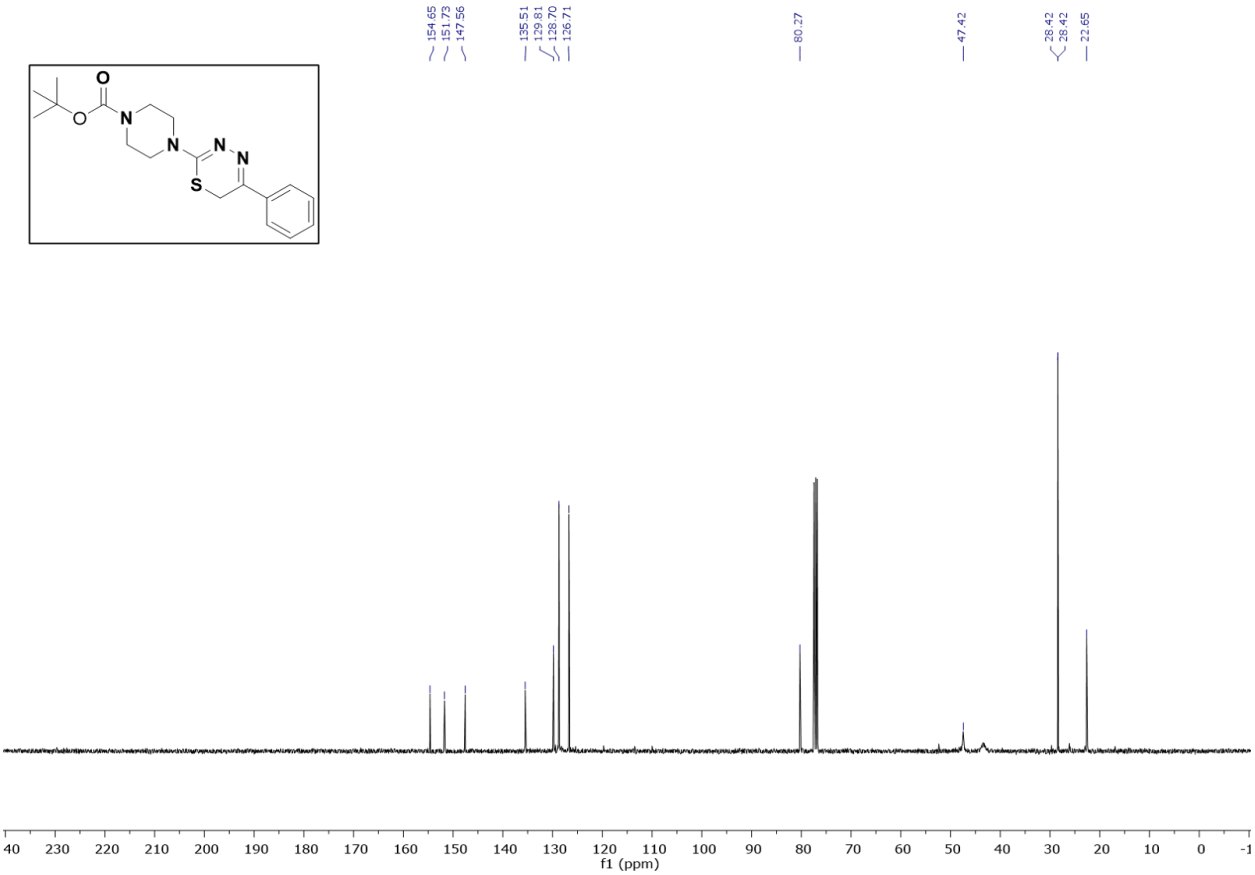

^{1}H NMR of ***tert*-butyl 4-(2-ethoxyacetyl)piperazine-1-carboxylate** in $CDCl_3$

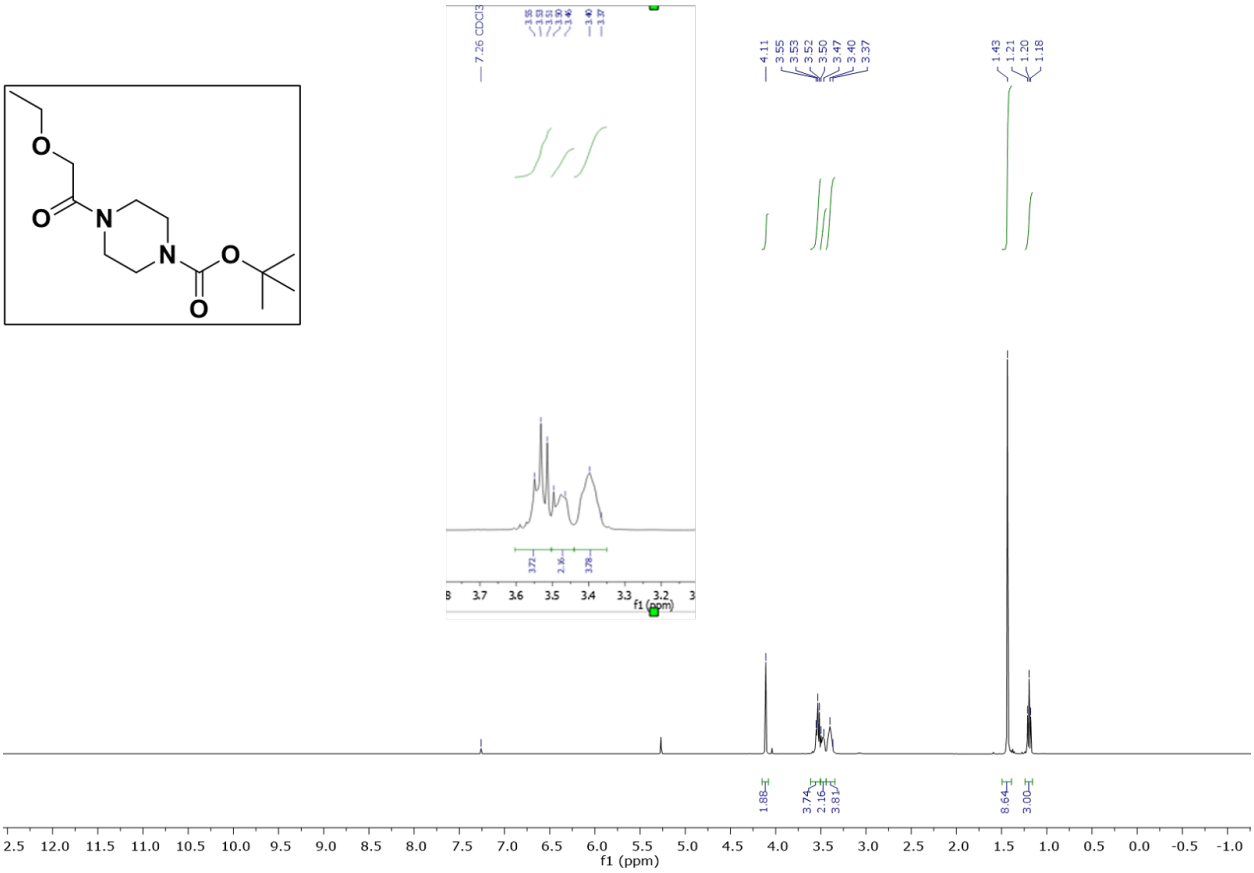

^{12}C NMR of ***tert*-butyl 4-(2-ethoxyacetyl)piperazine-1-carboxylate** in $CDCl_3$

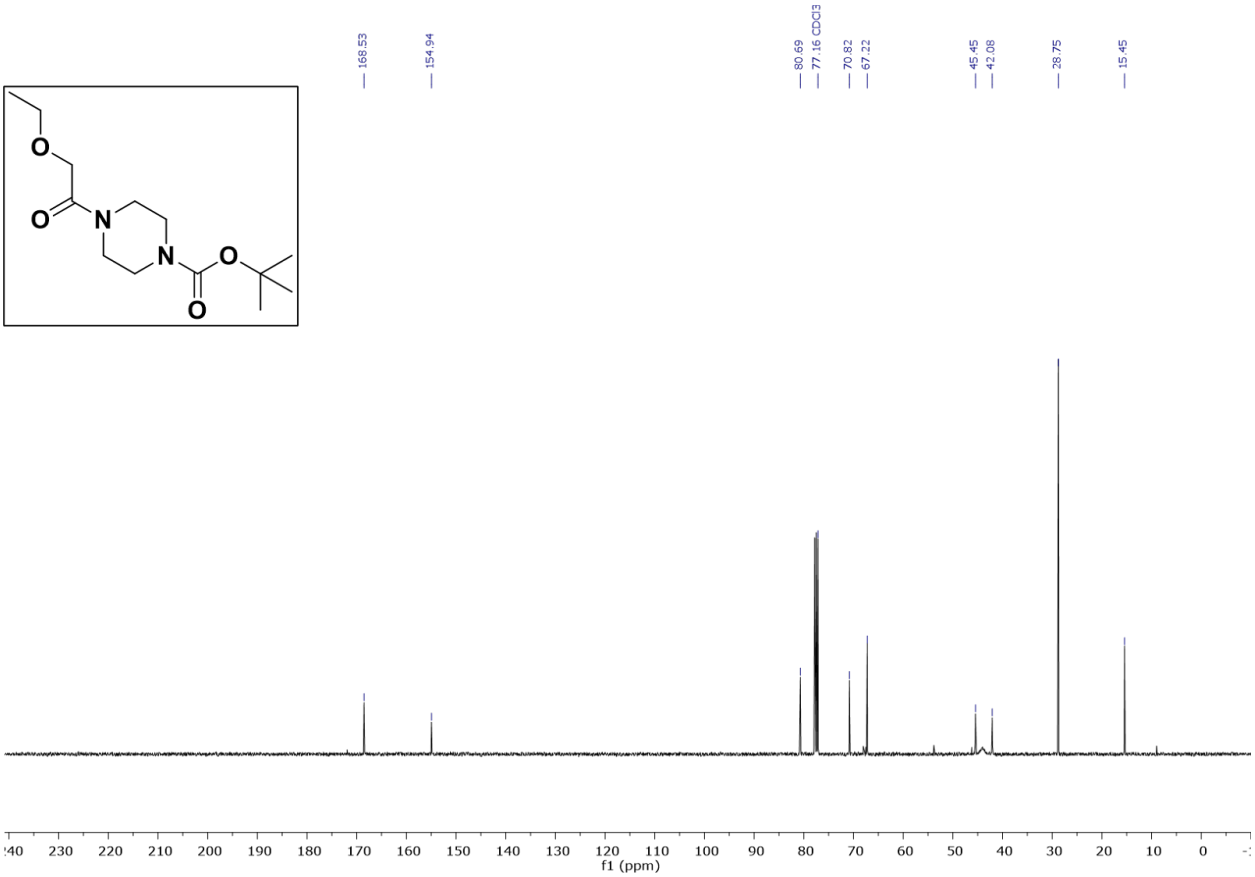

^{13}C NMR of **2-ethoxy-1-(4-(5-phenyl-6H-1,3,4-thiadiazin-2-yl)piperazin-1-yl)ethan-1-one (SO-265-1)** in $CDCl_3$

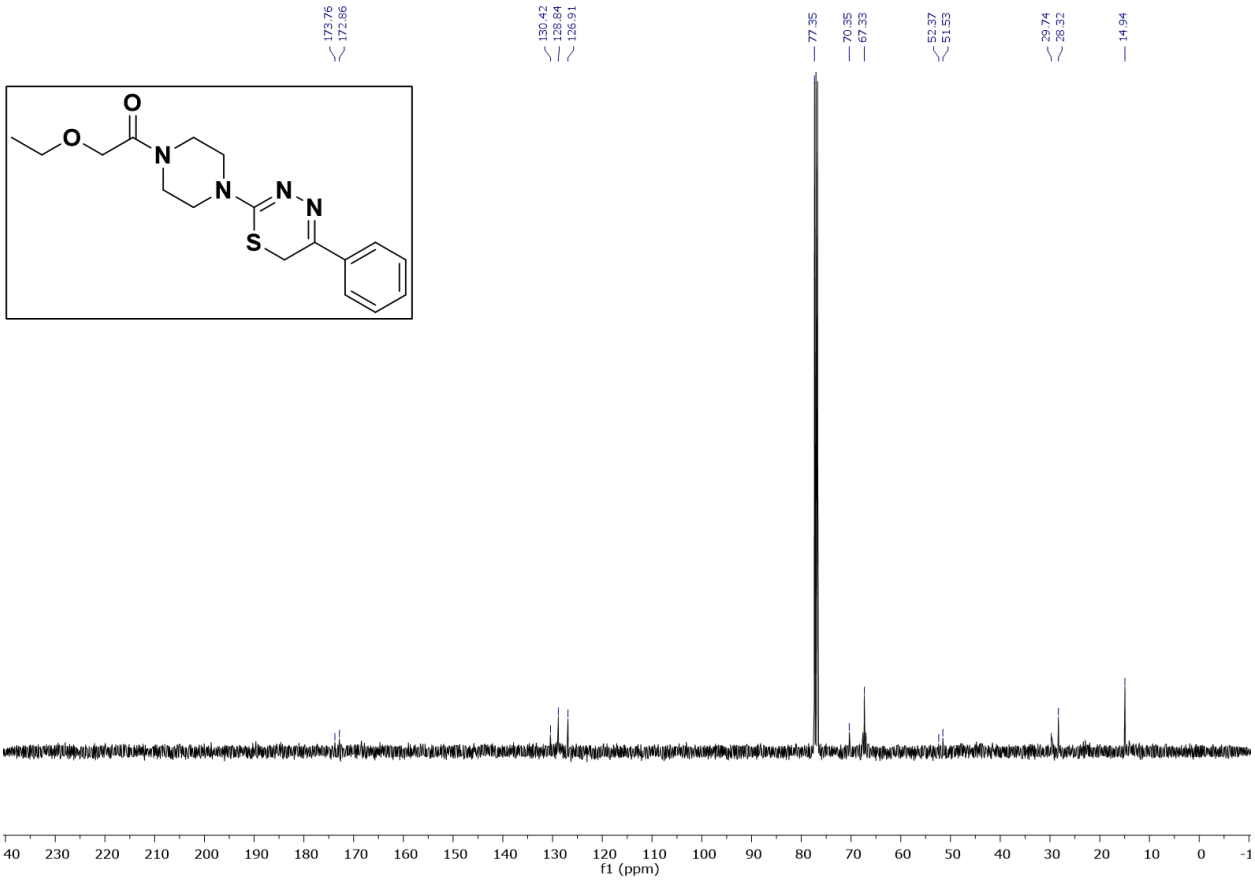

^{1}H NMR of **2-ethoxy-1-(4-(5-phenyl-6H-1,3,4-thiadiazin-2-yl)piperazin-1-yl)ethan-1-one (SO-265-2)** in $CDCl_3$

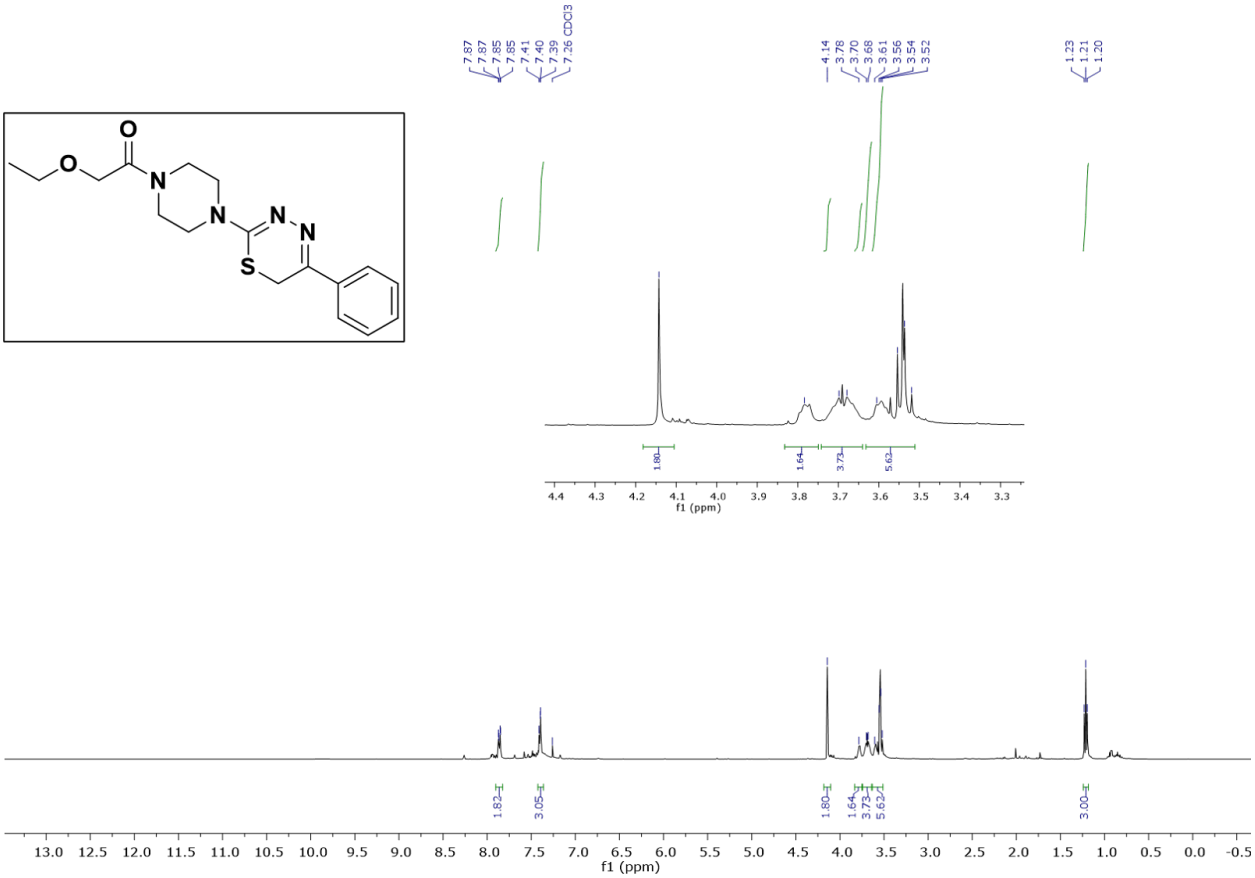

^{13}C NMR of **265-2** in $CDCl_3$ NMR of **2-ethoxy-1-(4-(5-phenyl-6H-1,3,4-thiadiazin-2-yl)piperazin-1-yl)ethan-1-one (SO-265-2)** in $CDCl_3$

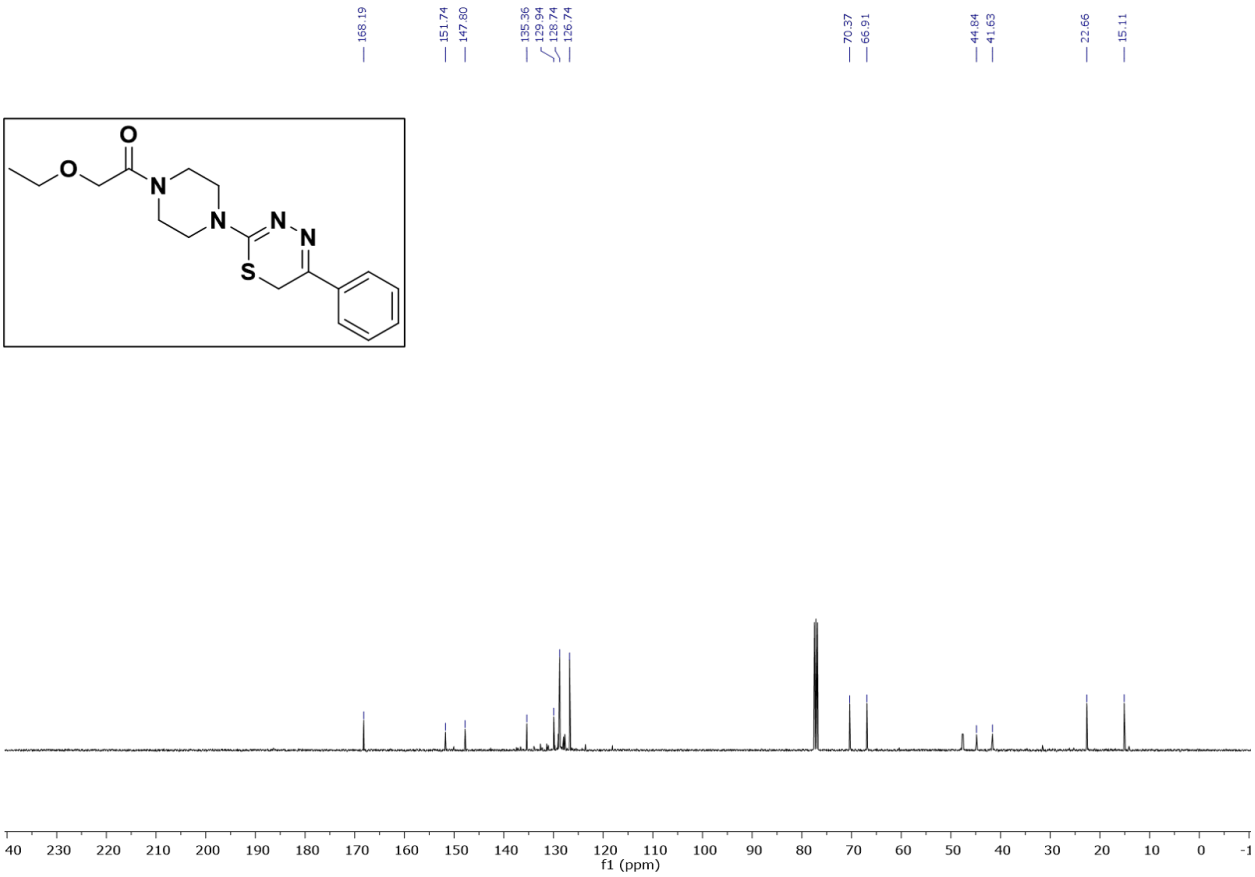

^{1}H NMR of **2-ethoxy-1-(4-(5-phenyl-6H-1,3,4-thiadiazin-2-yl)piperazin-1-yl)ethan-1-one (SO265)** in DMSO-d_6

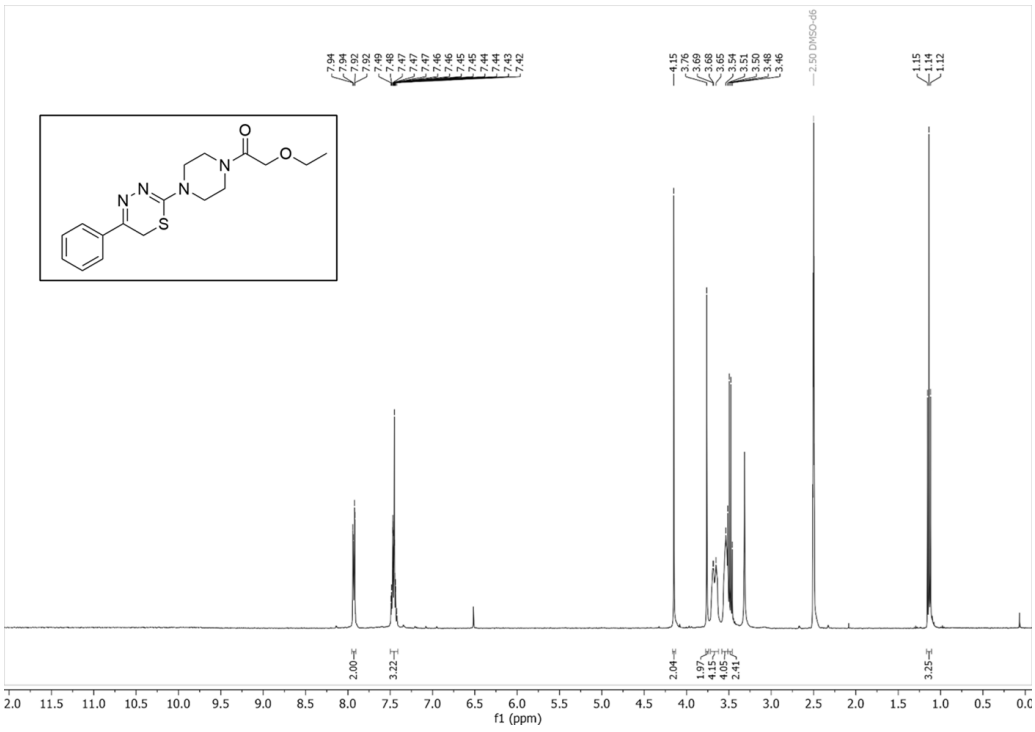

^{13}C NMR of **2-ethoxy-1-(4-(5-phenyl-6H-1,3,4-thiadiazin-2-yl)piperazin-1-yl)ethan-1-one (SO265)** in DMSO

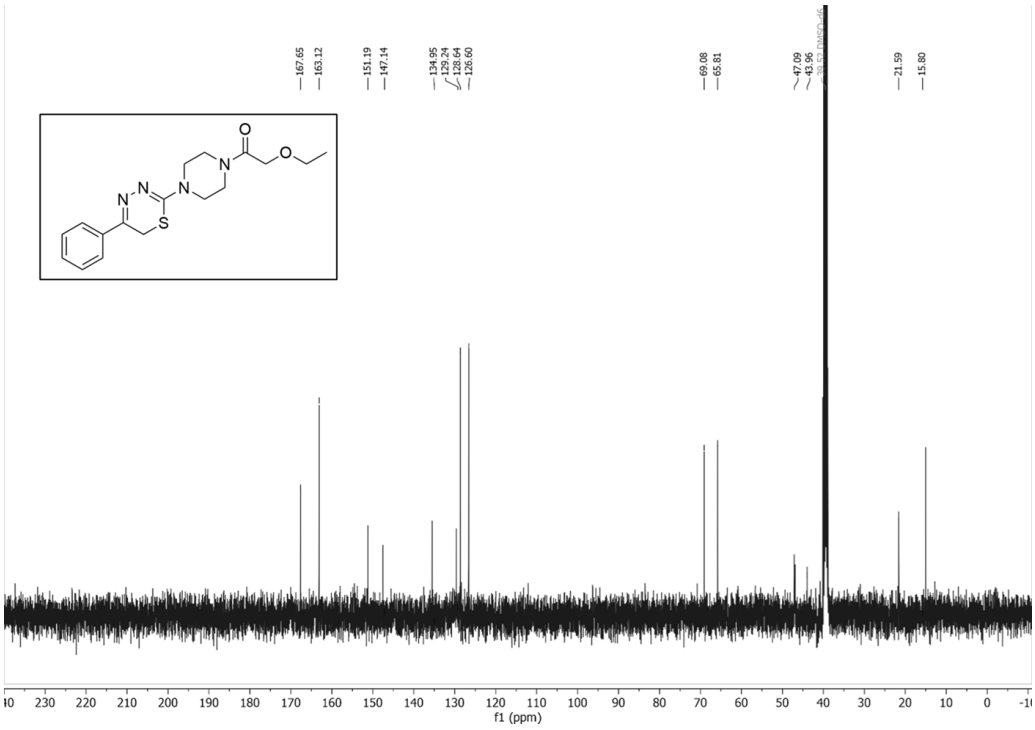

^{1}H NMR of **2-ethoxy-1-(4-(4-mercapto-5-phenyl-1*H*-pyrazol-3-yl)piperazin-1-yl)ethan-1-one (SO265i)** in DMSO-d_6

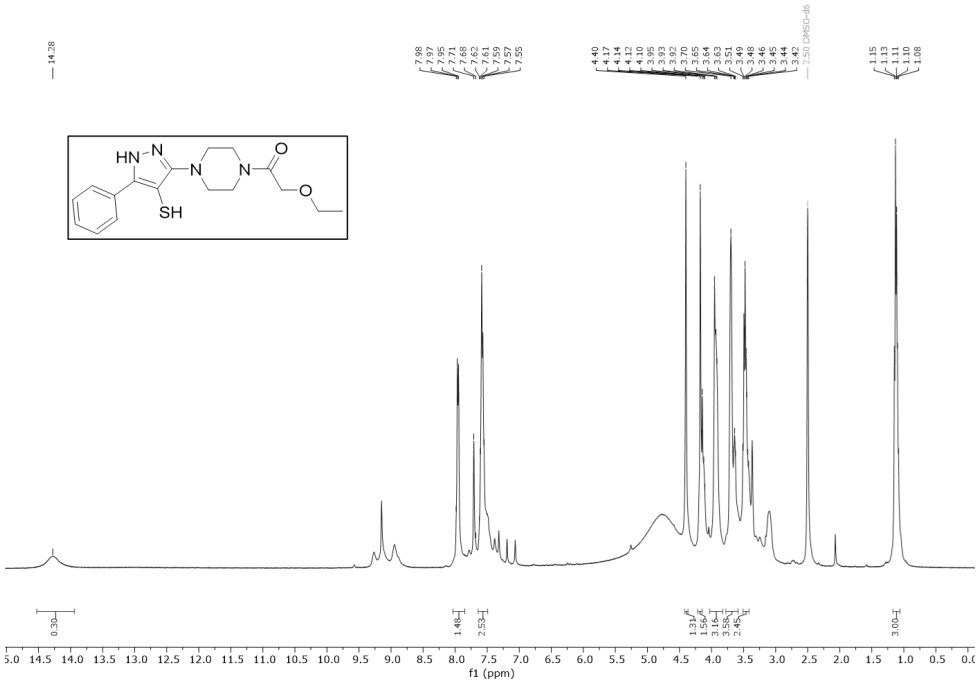

^{13}C NMR of **2-ethoxy-1-(4-(4-mercapto-5-phenyl-1*H*-pyrazol-3-yl)piperazin-1-yl)ethan-1-one (SO265i)** in DMSO-d_6

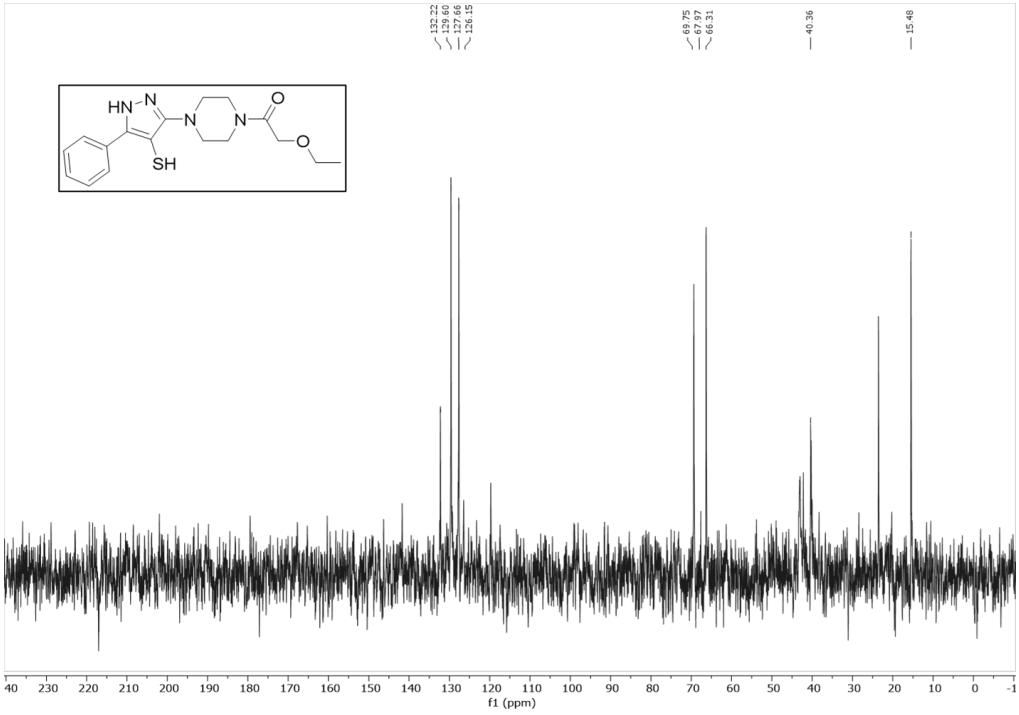

HMBC of **2-ethoxy-1-(4-(4-mercapto-5-phenyl-1*H*-pyrazol-3-yl)piperazin-1-yl)ethan-1-one (SO265i)** in DMSO-d_6

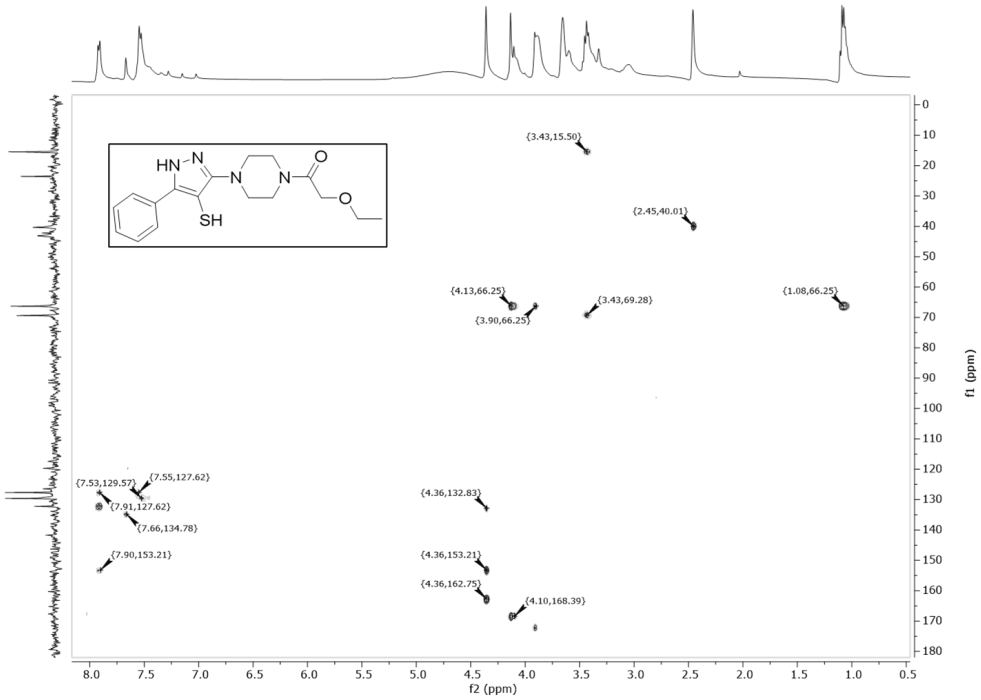

^{1}H NMR of **1,1'-((disulfanediylbis(5-phenyl-1*H*-pyrazole-4,3-diyl))bis(piperazine-4,1-diyl))bis(2-ethoxyethan-1-one) (SO265d)** in DMSO-d_6

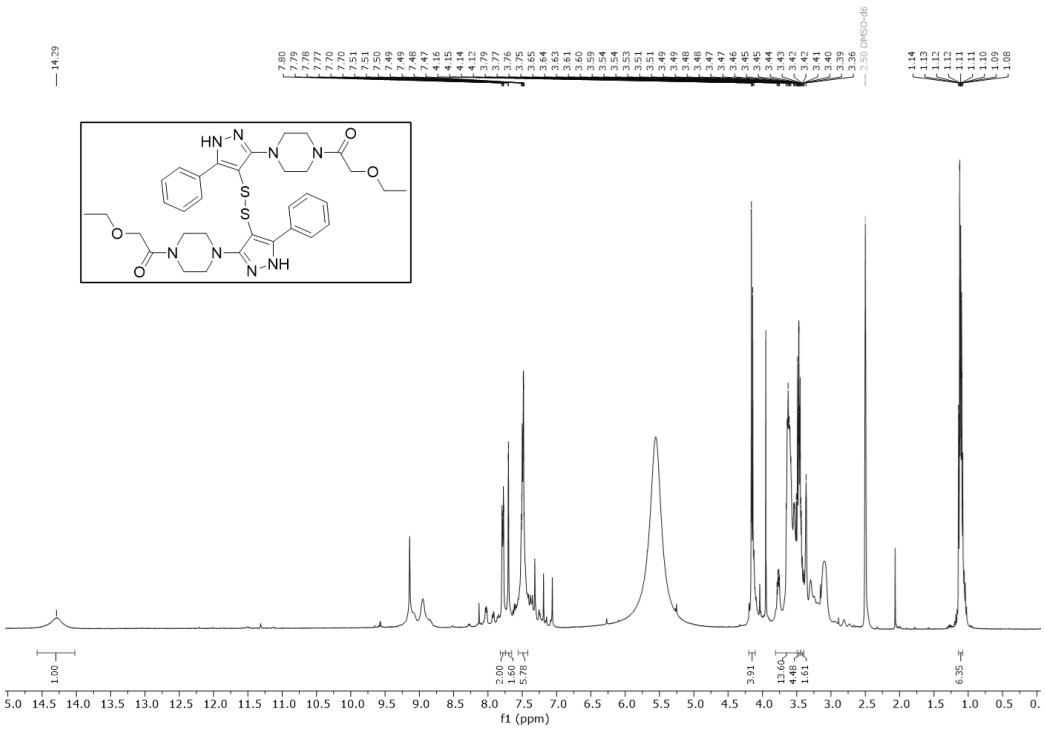

^{13}C NMR of **1,1'-((disulfanediylbis(5-phenyl-1*H*-pyrazole-4,3-diyl))bis(piperazine-4,1-diyl))bis(2-ethoxyethan-1-one) (SO265d)** in DMSO-d_6

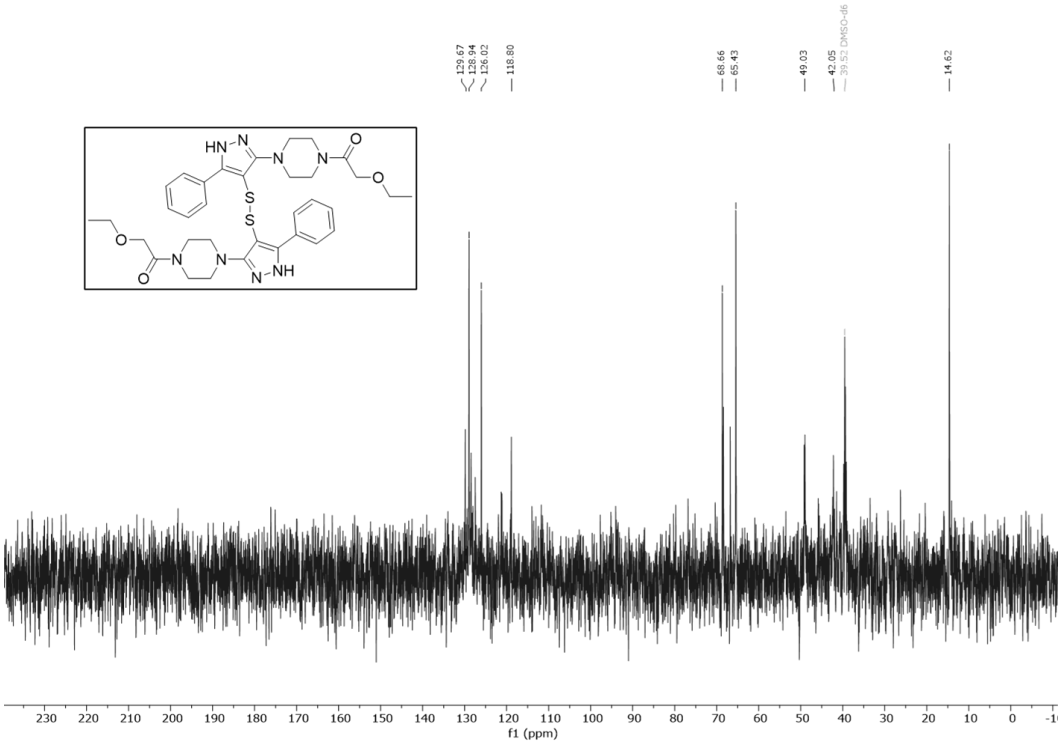

HMBC of **1,1'-((disulfanediylbis(5-phenyl-1*H*-pyrazole-4,3-diyl))bis(piperazine-4,1-diyl))bis(2-ethoxyethan-1-one) (SO265d)** in DMSO-d_6

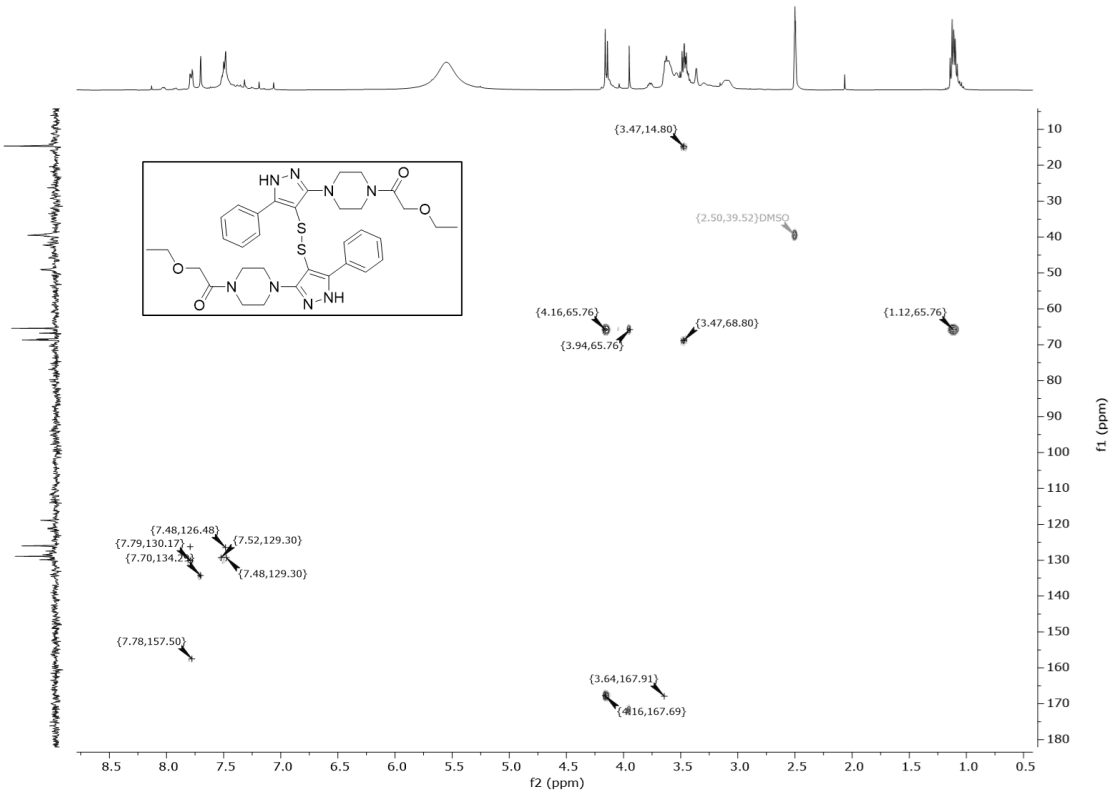

(G) Chemistry Methods

References

1. Backus, K.M., et al., *Proteome-wide covalent ligand discovery in native biological systems.* Nature, 2016. **534**(7608): p. 570-574.

2. Sander, T., et al., *DataWarrior: an open-source program for chemistry aware data visualization and analysis.* J Chem Inf Model, 2015. **55**(2): p. 460-73.

3. Castellón, J.O., et al., *Chemoproteomics Identifies State-Dependent and Proteoform-Selective Caspase-2 Inhibitors.* Journal of the American Chemical Society, 2024. **146**(22): p. 14972-14988.

4. Kedersha, N., et al., *G3BP–Caprin1–USP10 complexes mediate stress granule condensation and associate with 40S subunits.* Journal of Cell Biology, 2016. **212**(7): p. 845-860.

5. Shikwana, F., et al., *CySP3-96 enables scalable, streamlined, and low-cost sample preparation for cysteine chemoproteomic applications*. 2024, American Chemical Society (ACS).

6. Yan, T., et al., *SP3-FAIMS Chemoproteomics for High-Coverage Profiling of the Human Cysteinome***.* ChemBioChem, 2021. **22**(10): p. 1841-1851.

7. Desai, H.S., et al., *SP3-Enabled Rapid and High Coverage Chemoproteomic Identification of Cell-State–Dependent Redox-Sensitive Cysteines.* Molecular & Cellular Proteomics, 2022. **21**(4): p. 100218.

8. Hughes, C.S., et al., *Single-pot, solid-phase-enhanced sample preparation for proteomics experiments.* Nature Protocols, 2019. **14**(1): p. 68-85.

9. Hughes, C.S., et al., *Ultrasensitive proteome analysis using paramagnetic bead technology.* Molecular Systems Biology, 2014. **10**(10): p. 757.

Chapter 4. Conclusion

In this study, I employed multidisciplinary approaches integrating engineered activatable caspase constructs, chemoproteomics, high-throughput screening, and molecular biology techniques to discover selective inhibitors for procaspase-2 and new pan-caspase inhibitors.

In Chapter 2, I first used a mass spectrometry-based chemoproteomics workflow termed isoTOP-ABPP to assess the reactivity of caspase cysteines towards a pan-cysteine reactive probe, iodoacetamide alkyne. I found caspase-2 harbors a unique, noncatalytic, and non-conserved cysteine residue specific to caspase-2, C370. I was initially surprised to observe that the activity of this non-catalytic residue was significantly higher than the catalytic residue, C320. As IAA reactivity can indicate cysteine functionality, I hypothesized that this reactive non-catalytic residue plays an essential role in the activity of procaspase-2. To test this hypothesis, I utilized an engineered TEV cleavable procaspase-2 to assay the activity of the zymogen or inactive form of caspase-2.

I developed irreversible covalent inhibitors that targeted C370 and showed that selectively targeting this noncatalytic residue inhibits caspase-2 activity. Covalent modification of C370 demonstrated selective labeling of the caspase-2 zymogen and monomeric forms. I also found the methylphenylpropiolate scaffold, **P01**, to broadly react with cysteines, highlighting its potential as a versatile scout electrophile. While selective lead compounds showed caspase-2 engagement, only broader caspase inhibitors, such as **P01**, effectively protected against staurosporine and Fas ligand-mediated apoptosis, suggesting inhibition of caspase-2 alone is not sufficient to protect Jurkat cells from

apoptosis. I suspect that the activity of other initiator caspases, like caspase-9, compensates for the lack of caspase-2 activity. Thus, we only see protection against apoptosis after treatment with the broader caspase inhibitors. My findings underscore the potential for creating proteoform selective inhibitors targeting noncatalytic cysteine residues, which could offer new avenues for studying and modulating caspase activity in various disease contexts.

In Chapter 3, I aimed to identify selective procaspase-10 inhibitors that can be used to help elucidate its role in the apoptotic pathway. I used a high-throughput screening (HTS) approach combined with an engineered TEV cleavable activatable caspase-10 construct, proCASP10TEV Linker, to facilitate the discovery of inhibitors that specifically target the inactive form of caspase-10. I performed a large-scale screen of approximately 120,000 compounds using this engineered system, yielding 237 hits. I found several TEV protease inhibitors and inhibitors of active caspase-10. As part of the procaspase-10 hits, I identified a thiadiazine chemotype prone to isomerization.

Interestingly, I found the isomer was inactive until it was stored at ambient conditions for more than 24 hours in DMSO. The isomer further rearranges to a disulfide reactive species responsible for inhibiting procaspase-10. Additionally, the HTS identified PFTμ, a reported p53 inhibitor, as a potent procaspase-10 inhibitor with broader activity across several caspases. This suggests that PFTμ's anti-apoptotic effects may be driven by caspase inhibition rather than p53 targeting. My findings demonstrate the potential of the combined screening platform with the TEV-controlled activity assays for discovering inhibitors that target precursor enzymes, extending beyond caspase-10 inhibitor discovery.

This study used a multidisciplinary approach to discover proteoforms, selective caspase-2 inhibitors, and broad caspase inhibitors. By employing a mass spectrometry chemoproteomics approach and an engineered TEV activatable caspase construct, I identified a unique, highly reactive non-catalytic cysteine residue, C370, in caspase-2 which plays a vital role in procaspase-2 activity. Additionally, HTS was employed to discover procaspase-10 inhibitors, leading to the identification of broad caspase inhibitors, including a thiadiazine chemotype, SO265, and PFTμ. Future directions could involve exploring the biological function of the non-catalytic cysteine residue of caspase-2, as it has been implicated in neurodegenerative diseases and cancers, to explore its therapeutic potential for disease treatment using small chemical probes. Investigating the broader role of pan-caspase inhibition in apoptosis and compensatory mechanisms between caspases will be important to elucidate caspase-regulated programmed cell death.